

**RELAXATION PHENOMENA IN THERMOSETS**

**By**

**MICHEL BERNARD MARIE MANGION**

**A Thesis**

**Submitted to the School of Graduate Studies**

**in Partial Fulfilment of the Requirements**

**for the Degree**

**Doctor of Philosophy**

**McMaster University**

**(c) Copyright by Michel Bernard Marie Mangion, January 1990.**

# RELAXATION PHENOMENA IN THERMOSETS

to: Claire,  
Matthieu,  
Geoffroy,  
and Clothilde,

A mes Parents.

"If I have the gift of prophecy, and  
can fathom all mysteries and all  
knowledge, and If I have a faith that  
can move mountains, but have not love,  
I am nothing." 1 Co 13, 2

DOCTOR OF PHILOSOPHY (1990)  
(Materials Science)

MCMASTER UNIVERSITY  
Hamilton, Ontario

**TITLE:** Relaxation Phenomena In Thermosets

**AUTHOR:** Michel Bernard Marie Mangion, Ingenieur (Ecole  
Centrale des Arts et Manufactures de Paris, Paris,  
France)

D.E.A. (ibid, France)

M.Sc. (McMaster University)

**SUPERVISOR:** Professor G.P. Johari

**NUMBER OF PAGES:** xxiii, 238

## ABSTRACT

Two aspects of the electrical and light scattering properties of various epoxide based thermosets have been studied. In the first, the isothermal curing kinetics of the thermosets have been measured at several temperatures by dielectric spectroscopy and Brillouin scattering measurements. During the process of curing, the dc conductivity decreases according to a scaling law,  $\sigma_0 \propto (t_g - t)^x$ , or equivalently to a new equation,  $\sigma_0 \propto \exp[-B/(t_g - t)]$ , and approaches zero on gel-formation. Concomitantly, the time for the dipolar relaxation process becomes progressively longer and the dielectric permittivity becomes dominated by dipolar relaxation processes. The time dependence of the complex permittivity follows the formalism,  $\phi(t) = \exp-(t/\tau_{cure})^\gamma$  with  $\gamma < 0.4$ .  $\gamma$  decreases as the curing temperature is increased and tends towards a limiting value at a high curing temperature. The relaxation time increases on curing and the rate of its increase with respect to curing time first reaches a maximum and then decreases towards zero. This phenomenon is a manifestation of the rates of chemical processes which control the extent of cure. The initially broad Brillouin peak becomes narrow and shifts towards higher frequencies with the curing. The changes in the hypersonic velocity and attenuation during the curing of a thermoset correspond to the changes observed in the dielectric studies.

In the second, both the sub- $T_g$  and main relaxation processes of the thermosets were measured by dielectric spectrometry and their dependence on the curing and ageing were investigated. Amongst the two sub- $T_g$  relaxation processes, the low temperature process is initially prominent and its strength decreases on both curing and ageing of a thermoset. The strength of the high temperature sub- $T_g$  process initially increases, reaches a maximum value and then decreases on further ageing. A concept of accumulated equivalent curing time is introduced and theoretically justified for use in the investigation of the curing of thermosets, and a general method for obtaining the asymmetric distribution of relaxation times parameter from limited relaxation data is developed. For the sub- $T_g$  relaxations, the calculated parameter remains constant during the curing process, but for the main relaxation it monotonically decreases towards a limiting value. The theoretical analysis developed here is generally applicable to phenomena where molecular diffusion allows a chemical reaction to occur, which in turn retards molecular diffusion which slows the chemical reactions, until a material reaches its vitreous state and both the diffusion and chemical reactions cease to occur over ones experimental time scale.

## ACKNOWLEDGEMENTS

The author wishes to express his sincere gratitude to the following individuals and organizations:

First and foremost, to Dr. G.P. Johari, for the expert guidance, communicative enthusiasm, and unfailing encouragements that he provided throughout the course of this work. This thesis would not be in its present form without the benefit of his numerous criticisms and valuable suggestions. To work and learn under his leadership was most enjoyable and will have a profound influence on the author's future scientific endeavours.

To Dr. G.R. Purdy, Dr. D. Walton and Dr. J. Vlachopoulos who accepted to serve on the supervisory committee. Their interest and comments were greatly appreciated.

To Dr. D. Walton who allowed the use of the Brillouin light scattering equipment and to Jake Vanderwal who generously shared his knowledge of the technique and obtained most of the Brillouin spectra.

To Ms. Linda Palmer, for her careful and conscientious work in typing this dissertation.

To my colleagues Dr. D.L. Sidebottom and Matthew Parthun who accepted to read part of the manuscript and made helpful suggestions, and to Manli Wang for her help in the preparation of the dielectric cells used during the study of the effects of composition on the dielectric properties of the DGEBA-DDM thermoset.

To the Ontario Government, McMaster University and the Department of Materials Science and Engineering for their financial assistance in the form of scholarships to the author.

To the Natural Sciences and Engineering Research Council for its financial support in the form of a research grant to Dr. G.P. Johari.

Above all, to Claire, my wife, who surrounded me with the security and love that allowed me to progress peacefully and bring this work to completion.

## TABLE OF CONTENTS

|                                                       | <u>PAGE</u> |
|-------------------------------------------------------|-------------|
| Chapter 1: Introduction and Basic Concepts            | 1           |
| 1.1 Introduction                                      | 1           |
| 1.2 The Curing Process                                | 1           |
| 1.2.1 Definitions                                     | 5           |
| 1.2.2 Phase Diagrams                                  | 8           |
| 1.2.3 The chemical structures of thermoset precursors | 12          |
| 1.3 Dielectric relaxation spectroscopy                | 14          |
| 1.3.1 The relaxation function                         | 14          |
| 1.3.2 The relaxation times                            | 16          |
| 1.3.3 The conductivity relaxation                     | 21          |
| 1.4 Dielectric spectroscopy of thermoset curing       | 26          |
| 1.4.1 The ionic conductivity                          | 26          |
| 1.4.2 The dielectric relaxation                       | 28          |
| 1.4.3 The sub- $T_g$ relaxations                      | 29          |
| <br>                                                  |             |
| Chapter 2: The experimental procedures                | 31          |
| 2.1 Dielectric spectroscopy                           | 31          |
| 2.1.1 Principles                                      | 31          |
| 2.1.2 The transformer ratio-arm bridge                | 32          |
| 2.1.3 The automatic Genrad digibridge 1689            | 34          |
| 2.1.4 The temperature control assembly                | 34          |
| 2.1.5. The dielectric cells                           | 37          |
| 2.2 Brillouin light scattering measurement            | 41          |
| 2.2.1. Principles                                     | 41          |

|                                                                     | <u>PAGE</u> |
|---------------------------------------------------------------------|-------------|
| 2.2.2 Experimental arrangement                                      | 44          |
| 2.2.3 Procedure                                                     | 45          |
| 2.3 The precursors and thermosets preparation                       | 48          |
| Chapter 3: Results of isothermal curing of<br>thermosets            | 50          |
| 3.1 Dielectric relaxation behaviour                                 | 50          |
| 3.1.1 Isochronal or fixed frequency studies                         | 50          |
| 3.1.2 Isothermal spectrum studies                                   | 58          |
| 3.2 Brillouin scattering study                                      | 65          |
| 3.3 The effects of substitution of amines on the<br>curing kinetics | 76          |
| 3.4 The effects of varying the thermosets composition               | 81          |
| 3.5 The electrical modulus and its analysis                         | 82          |
| Chapter 4: Dielectric characterization of the cure<br>of thermosets | 99          |
| 4.1 Chemical and physical effects                                   | 99          |
| 4.2 The time dependence of the conductivity                         | 101         |
| 4.3 The dipolar relaxation                                          | 110         |
| 4.3.1 The time dependence of $\epsilon^*$                           | 110         |
| 4.3.2 The curing parameter, $\gamma$                                | 118         |
| 4.3.3 The time dependence of the relaxation<br>time                 | 124         |
| 4.4 Changes in the Brillouin spectra                                | 129         |
| 4.4.1 The hypersonic velocity                                       | 129         |

|            | <u>PAGE</u>                                                                                    |
|------------|------------------------------------------------------------------------------------------------|
| 4.4.2      | The attenuation and loss factor 133                                                            |
| 4.4.3      | The curing time and temperature behaviour 134                                                  |
| 4.5        | Effect of substitution of the amines. 136                                                      |
| <br>       |                                                                                                |
| Chapter 5: | The Sub-T <sub>g</sub> relaxations in thermosets 143                                           |
| 5.1        | Characterization of the Sub-T <sub>g</sub> relaxations 143                                     |
| 5.1.1      | Experimental procedures 143                                                                    |
| 5.1.2      | Cured DGEBA-DDM and DGEBA-DDS thermosets 145                                                   |
| 5.1.3      | Effect of curing on the dielectric<br>relaxation of thermosets 150                             |
| 5.2        | Dielectric effects of cross-linking in thermosets 152                                          |
| 5.2.1      | Experimental details 152                                                                       |
| 5.2.2      | DGEBA-DDM and DGEBA-DDS thermosets 155                                                         |
| 5.2.3      | DGEBA cured with a mixture of 70% DDS and<br>30% DDM 165                                       |
| 5.3        | Effects of composition on the sub-T <sub>g</sub> relaxations of<br>the DGEBA-DDM Thermoset 168 |
| <br>       |                                                                                                |
| Chapter 6: | Dielectric relaxation phenomena in<br>thermosets 174                                           |
| 6.1        | Introduction 174                                                                               |
| 6.1.1      | Mechanisms of sub-T <sub>g</sub> relaxations in polymers 174                                   |
| 6.1.2      | Physical ageing effects in thermosets 175                                                      |
| 6.2        | The concept of accumulated equivalent curing time 177                                          |
| 6.2.1      | Definition 177                                                                                 |
| 6.2.2      | theoretical basis 178                                                                          |

|                                                                         | <u>PAGE</u> |
|-------------------------------------------------------------------------|-------------|
| 6.3 Evolutions of the dielectric relaxations features                   | 182         |
| 6.3.1 The relaxations peak height and temperature                       | 182         |
| 6.3.2 Effect of substitution of amines on the<br>sub- $T_g$ relaxations | 188         |
| 6.3.3 Effect of the thermoset's composition                             | 198         |
| 6.4 The distribution of relaxation times and curing<br>effects          | 195         |
| 6.4.1 Isothermal spectra                                                | 195         |
| 6.4.2 Theoretical formalism                                             | 197         |
| 6.4.3 Data analysis                                                     | 202         |
| 6.4.4 Results and Discussion                                            | 206         |
| 6.5 Mechanisms of dielectric relaxations in thermosets                  | 210         |
| 6.5.1 The main or $\alpha$ -relaxation                                  | 210         |
| 6.5.2 The $\beta$ -relaxation                                           | 211         |
| 6.5.3 The $\gamma$ -relaxation                                          | 215         |
| 6.5.4 Physical ageing effects                                           | 216         |
| <br>CHAPTER 7: Conclusions                                              | <br>217     |
| <br>APPENDIX                                                            | <br>222     |
| <br>BIBLIOGRAPHY                                                        | <br>229     |

## LIST OF ILLUSTRATIONS

|                                                                                                         | <u>PAGE</u> |
|---------------------------------------------------------------------------------------------------------|-------------|
| 1.1 The two chemical reactions during the curing of thermosets.                                         | 7           |
| 1.2 Phase diagram for the curing of a thermoset.                                                        | 9           |
| 1.3 Time-Temperature-Transformation diagram.                                                            | 11          |
| 1.4 Chemical structures of the thermosetting systems.                                                   | 13          |
| 1.5 The Debye single relaxation model.                                                                  | 18          |
| 1.6 The complex plane diagram of the Cole-Cole model.                                                   | 20          |
| 1.7 Comparison between the Cole-Davidson and the Kohlrausch-Williams-Watts functions.                   | 22          |
| 1.8 The angular frequency dependence of $\text{Log}(\epsilon^*)$ and $M^*$ for a conducting medium.     | 24          |
| 2.1 The transformer ratio-arm bridge.                                                                   | 33          |
| 2.2 The Genrad Digibridge 1689.                                                                         | 33          |
| 2.3 The dielectric capacitors.                                                                          | 38          |
| 2.4 The experimental arrangement for the dielectric measurements.                                       | 42          |
| 2.5 The experimental arrangement for the Brillouin light scattering measurements.                       | 46          |
| 3.1 The dielectric permittivity, loss and loss tangent of the DGEBA-DDM thermoset plotted against time. | 51          |
| 3.2 The dielectric permittivity, loss and loss tangent of the DGEBA-DDS thermoset plotted against time. | 52          |

|      | <u>PAGE</u>                                                                                                                             |    |
|------|-----------------------------------------------------------------------------------------------------------------------------------------|----|
| 3.3  | The complex plane plots of the dielectric permittivity for the DGEBA-DDM and DGEBA-DDS thermosets.                                      | 54 |
| 3.4  | (a) $t(\epsilon''_m)$ , and (b) $\Delta\epsilon$ , $\epsilon''_m$ and $\epsilon'(0)$ plotted against the reciprocal curing temperature. | 57 |
| 3.5  | The time dependence of the dielectric permittivity of the DGEBA-DDM thermoset cured at 340.9K, measured at several frequencies.         | 60 |
| 3.6  | The time dependence of the dielectric loss of the DGEBA-DDM thermoset cured at 340.9K, measured at several frequencies.                 | 61 |
| 3.7  | The time dependence of the dielectric permittivity and loss of the DGEBA-DDM thermoset cured at 331K, measured at several frequencies.  | 63 |
| 3.8  | A plot of the curing time to achieve half of the total decrease in $\epsilon'$ against frequency for the DGEBA-DDM thermoset at 331K.   | 64 |
| 3.9  | The time dependence of the dielectric permittivity of the DGEBA-DDS thermoset cured at 448.3K, measured at several frequencies.         | 66 |
| 3.10 | The time dependence of the dielectric loss of the DGEBA-DDS thermoset cured at 448.3K, measured at several frequencies.                 | 67 |
| 3.11 | The Brillouin intensity spectrum of the DGEBA-DDM thermoset during its curing.                                                          | 68 |

|      | <u>PAGE</u>                                                                                                                                  |    |
|------|----------------------------------------------------------------------------------------------------------------------------------------------|----|
| 3.12 | The product of the refractive index and velocity of hypersonic waves in the DGEBA-DDM thermoset plotted against the curing time.             | 70 |
| 3.13 | The attenuation of hypersonic waves to refractive index ratio in the DGEBA-DDM thermoset plotted against the curing time.                    | 71 |
| 3.14 | The Brillouin intensity spectrum of the DGEBA-DDS thermoset during its curing.                                                               | 72 |
| 3.15 | The product of the refractive index and velocity of hypersonic waves in the DGEBA-DDS thermoset plotted against the curing time.             | 73 |
| 3.16 | The attenuation of hypersonic waves to refractive index ratio in the DGEBA-DDS plotted against the curing time.                              | 74 |
| 3.17 | The Arrhenius plots of the time for the velocity to reach half its maximum value.                                                            | 75 |
| 3.18 | The dielectric permittivity, loss and loss tangent of the DGEBA-based thermosets cured with mixed amines at 377K.                            | 77 |
| 3.19 | The complex plane plots of the dielectric permittivity for the DGEBA-based thermosets during their curing at 377K.                           | 79 |
| 3.20 | (a) $t(\epsilon''_{min})$ and $t(\epsilon''_m)$ , and (b) $\epsilon''_{min}$ and $\epsilon''_m$ against the composition of the curing agent. | 80 |

- 3.21 The dielectric permittivity, loss and loss tangent of the DGEBA-DDM thermosets of various compositions, during their curing at 341K, plotted against time. 83
- 3.22 The complex plane plots of the dielectric permittivity for DGEBA-DDM thermosets of various compositions during their curing at 341K. 84
- 3.23 The real and imaginary parts of the electrical modulus and the ac conductivity plotted against time during the curing of the DGEBA-based thermosets with pure DDM and pure DDS. 86
- 3.24 The real and imaginary parts of the electrical modulus and the ac conductivity plotted against time during the curing of the DGEBA-based thermosets with mixed amines. 88
- 3.25 The real and imaginary parts of the electrical modulus and the ac conductivity plotted against time during the curing of the DGEBA-DDM thermosets of various compositions. 89
- 3.26 The complex plane plots of the electrical modulus during the curing of the DGEBA-based thermosets with pure DDM and pure DDS. 90
- 3.27 The complex plane plots of the electrical modulus during the curing of the DGEBA-based thermosets with mixed amines. 91

- 3.28 The complex plant plots of the electrical modulus during the curing of the DGEBA-DDM thermosets of various compositions. 92
- 3.29 The real part of the electrical modulus of the DGEBA-DDM thermoset measured at nine frequencies plotted against time of cure at 340.9K. 94
- 3.30 The imaginary part of the electrical modulus of the DGEBA-DDM thermoset measured at nine frequencies plotted against time of cure at 340.9K. 95
- 3.31 The real part of the electric modulus of the DGEBA-DDS thermoset measured at 10 frequencies plotted against time of cure at 448.3K. 96
- 3.32 The imaginary part of the electrical modulus of the DGEBA-DDS thermoset measured at 10 frequencies plotted against time of cure at 448.3K. 97
- 3.33 The complex plane plots of the electrical modulus measured at different frequencies during the curing of the DGEBA-DDM and DGEBA-DDS thermosets. 98

|     |                                                                                                                                                                                      |     |
|-----|--------------------------------------------------------------------------------------------------------------------------------------------------------------------------------------|-----|
| 4.1 | Comparison between the experimental and calculated values of the dc conductivity of the DGEBA-DDM thermoset during its cure at several temperatures.                                 | 104 |
| 4.2 | Comparison between the experimental and calculated values of the dc conductivity of the DGEBA-DDS thermoset during its cure at several temperatures.                                 | 105 |
| 4.3 | Comparison between the experimental and calculated values of the dc conductivity of the DGEBA-based thermosets during their cure with mixed amines at 377K.                          | 106 |
| 4.4 | Comparison between the descriptions of the dielectric relaxation data by various formalisms.                                                                                         | 113 |
| 4.5 | Comparison between the experimental and calculated values of the dielectric permittivity of the(a) DGEBA-DDM and (b) DGEBA-DDS thermosets during their cure at several temperatures. | 115 |
| 4.6 | Comparison between the experimental and calculated values of the dielectric permittivity of the DGEBA based thermosets during their cure with mixed amines at 377K.                  | 116 |

|      | <u>PAGE</u>                                                                                                                                                            |
|------|------------------------------------------------------------------------------------------------------------------------------------------------------------------------|
| 4.7  | Comparison between the experimental and calculated values of the dielectric permittivity of DGEBA-DDM thermosets of various composition during their cure at 341K. 117 |
| 4.8  | The temperature and composition dependence of the curing parameter, $\gamma$ , for the DGEBA-based thermosets. 119                                                     |
| 4.9  | Comparison between the experimental and calculated values of the dielectric permittivity and loss of the DGEBA-DDM thermosets. 120                                     |
| 4.10 | Comparison between the experimental and calculated values of the dielectric permittivity and loss of the DGEBA-DDS thermosets. 127                                     |
| 4.11 | The relaxation time in the DGEBA-DDM and DGEBA-DDS thermosets plotted against the curing time. 128                                                                     |
| 4.12 | The relaxation time in the DGEBA-based thermosets cured at 377K with mixed amines against the curing time. 130                                                         |
| 4.13 | Comparison between the changes in the electrical modulus, sound wave velocity and mechanical modulus during the cure of thermosets. 132                                |
| 4.14 | The extent of reaction of DGEBA-based thermosets plotted against the molar ratio of DDS in the DDM-DDS amine mixture. 140                                              |

|      |                                                                                                                                                                                                                                                |     |
|------|------------------------------------------------------------------------------------------------------------------------------------------------------------------------------------------------------------------------------------------------|-----|
| 4.15 | $d\alpha/d\log t$ measured for $\alpha=0.5$ and $\alpha=0.7$ plotted against the molar ratio of DDS in the DDM-DDS amine mixture.                                                                                                              | 141 |
| 5.1  | (a) The dielectric loss tangent of the DGEBA-DDM thermoset plotted against the temperature (b) The dielectric loss tangent of the fully cured and aged DGEBA-DDM thermoset plotted against the temperature.                                    | 146 |
| 5.2  | The dielectric permittivity and loss spectra of sub- $T_g$ relaxations in the (a) fully cured, and (b) aged DGEBA-DDM thermoset.                                                                                                               | 148 |
| 5.3  | The frequency maximum of $\epsilon''$ against the reciprocal temperature for the DGEBA-DDM thermoset.                                                                                                                                          | 149 |
| 5.4  | (a) The dielectric loss tangent of the DGEBA-DDS thermoset plotted against the temperature for various times of cure at 418K. (b) The dielectric loss tangent of the fully cured and aged DGEBA-DDS thermoset plotted against the temperature. | 151 |
| 5.5  | The dielectric permittivity, loss and loss tangent of the as-prepared mixtures of DGEBA-DDM and DGEBA-DDS, plotted against temperature.                                                                                                        | 153 |
| 5.6  | The peak value of the dielectric loss tangent for (a) the $\beta$ -process and (b) the $\gamma$ -process in the DGEBA-DDM and DGEBA-DDS thermosets.                                                                                            | 154 |

- 5.7 The dielectric loss tangent, permittivity and loss of the DGEBA-DDM thermoset plotted against the temperature for various times of cure at 363K. 159
- 5.8 The dielectric loss tangent, permittivity and loss of the sub- $T_g$  relaxations region of the DGEBA-DDM thermoset plotted against the temperature for various times of cure at 363K. 161
- 5.9 The dielectric loss tangent, permittivity and loss of the sub- $T_g$  relaxations region of the DGEBA-DDM thermoset plotted against the temperature for various times of cure at 403K. 162
- 5.10 The dielectric loss tangent, permittivity and loss of the DGEBA-DDS thermoset plotted against the temperature for various times of cure at 398K. 163
- 5.11 The dielectric loss tangent, permittivity and loss of the sub- $T_g$  relaxations region of the DGEBA-DDS thermoset plotted against the temperature for various times of cure at 398K. 164
- 5.12 The dielectric loss tangent, permittivity and loss of the DGEBA-(0.7 DDS, 0.3 DDM) thermoset plotted against the temperature for various times of cure at 363K. 165

- 5.13 The dielectric loss tangent, permittivity and loss of the sub- $T_g$  relaxations region of the DGEBA-(0.7 DDS -0.3 DDM) thermoset plotted against temperature for various times of cure at 363K. 167
- 5.14 The dielectric loss, permittivity and loss tangent of the as - prepared DGEBA-DDM mixtures of various compositions plotted against temperature. 169
- 5.15 The dielectric loss, permittivity and loss tangent of the saturated DGEBA-DDM thermoset plotted against temperature for various times of cure at 408K. 171
- 5.16 The dielectric loss, permittivity and loss tangent of the starved DGEBA-DDM thermoset plotted against temperature for various times of cure at 408K. 172
- 6.1 The change in temperatures of the  $\gamma$ -,  $\beta$ - and  $\alpha$ -relaxation processes during the curing and post-curing of the DGEBA-DDM and DGEBA-DDS thermosets. 183
- 6.2 The change in the temperatures of the  $\gamma$ -,  $\beta$ -, and  $\alpha$ -relaxation processes during the curing of the DGEBA-(0.7 DDS, 0.3 DDM) thermoset. 184

- 6.3 The change in the  $\epsilon''_m$  value for the  $\gamma$ -,  $\beta$ - and  $\alpha$ -relaxation processes during the curing of the DGEBA-DDM and DGEBA-DDS thermosets. 186
- 6.4 The change in the  $\epsilon''_m$  values for the  $\gamma$ -,  $\beta$ - and  $\alpha$ -relaxation processes during the curing of the DGEBA-(0.7 DDS, 0.3 DDM) thermoset. 187
- 6.5 The loss tangent of the DGEBA-(xDDS, (1-X)DDM) thermosets, measured after their curing at 377K and ageing at 298K, plotted against temperature. 191
- 6.6 (a) The normalized strengths of the  $\gamma$ - and  $\beta$ -relaxation peaks and (b) the corresponding dielectric permittivity plotted against the composition of the curing agent. 192
- 6.7 The change in (a) the temperature of the  $\beta$ -relaxation and (b) the  $\epsilon''_m$  of the  $\gamma$ - and  $\beta$ -relaxation processes during the curing at 403K of the DGEBA-DDM thermosets of various composition. 194
- 6.8 Fitting of a non-exponential decay function to the  $\gamma$ - and  $\beta$ -relaxation peaks of the DGEBA-DDS thermoset cured 15ks at 398K. 205
- 6.9 The changes in the characteristic ratios for the sub- $T_g$  and  $\alpha$ -relaxation processes in the DGEBA-DDM and DGEBA-DDS thermosets. 207
- 6.10 The changes in the characteristic ratios for the dielectric relaxation processes in the DGEBA-(0.7 DDS, 0.3 DDM) thermoset. 208

## LIST OF TABLES

|                                                                                                                                              | <u>PAGE</u> |
|----------------------------------------------------------------------------------------------------------------------------------------------|-------------|
| 3.1 The features of the dielectric behaviour of the DGEBA-DDM and DGEBA-DDS thermosets during their isothermal cure at several temperatures. | 56          |
| 3.2 The features of the dielectric behaviour of mixed amine thermosets during their isothermal curing at 377K.                               | 56          |
| 3.3 The feature of the dielectric behaviour of non-stoichiometric DGEBA-DDM thermosets during their isothermal curing at 341K.               | 84          |
| 4.1 The parameters used for fitting the conductivity of the DGEBA-DDM and DGEBA-DDS thermosets at several temperatures.                      | 107         |
| 4.2 The parameters used for fitting the conductivity of the DGEBA-based thermosets during their cure with mixed amines at 377K.              | 108         |
| 4.3 The parameters used for fitting the dielectric permittivity data of the thermosets.                                                      |             |
| 5.1 The curing conditions of DGEBA-DDM thermoset and the features of the observed dielectric behaviour.                                      | 156         |
| 5.2 The curing conditions of the DGEBA-DDS thermoset and the features of the observed dielectric behaviour.                                  | 157         |
| 5.3 The curing conditions of the DGEBA-(0.7 DDS - 0.3 DDM) thermoset and the features of the observed dielectric behaviour.                  | 158         |

|     |                                                                                                                             |     |
|-----|-----------------------------------------------------------------------------------------------------------------------------|-----|
| 5.4 | The curing conditions of the non-stoichiometric DGEBA-DDM thermosets and the features of the observed dielectric behaviour. | 173 |
| 6.1 | The features of the dielectric sub- $T_g$ relaxations of the mixed amine thermosets after their curing and post curing.     | 189 |
| 6.2 | The parameters used for determining the KWW parameter for sub- $T_g$ relaxations.                                           | 199 |

## CHAPTER 1

### INTRODUCTION AND BASIC CONCEPTS

#### 1.1 INTRODUCTION

The main characteristic of thermosetting polymers, which distinguishes them from other classes of organic polymers, such as thermoplastics and elastomers, is their densely cross-linked molecular structure. The existence of an "infinite" molecular network with covalently bonded junction points, or crosslinks, having functionality greater than two leads to superior properties, such as a high glass transition temperature, high modulus and fracture resistance and excellent electrically insulating characteristics. Thermosets constitute the major class of advanced materials in the fields of tooling, encapsulation, adhesives, laminates and coatings and are widely used as high strength structural parts and low loss, stable, electronic components.

Research on thermosets has been traditionally dominated by attempts to understand the chemical processes that lead to their formation. Nevertheless, over the past two decades, a materials science approach to their study has grown. This approach promises a further understanding of the relationship between the structure and the physical properties of thermosets. Since the molecular structure of a thermoset greatly depends upon its preparation conditions, these conditions have recently become the focus of increased research. These aspects of preparation have been ably reviewed



continuous occurrence of a change in the properties has rendered a detailed and complete study of the curing process of thermosets particularly difficult by conventional methods which require a significant time period for data collection. For this reason, dielectric spectroscopy was selected as our main experimental technique since it allowed the investigation of the entire cross-linking process which converts a sol to a gel and a gel to a glass from measurements that required time periods too small to cause errors due to change in the physical state of thermosets. A parallel study by Brillouin light scattering to investigate the gelation and vitrification phenomenon was further carried out. The work described in this thesis is part of this systematic study of the cross-linking kinetics of epoxide thermosets, the effects of chemical and physical ageing on their electrical properties after their glass formation, and a theoretical description of their dielectric and Brillouin light scattering effects.

The thesis is divided into seven chapters. This chapter also introduces the various definitions and concepts related to the curing of thermosets, continues with a presentation of the dielectric theories, and ends with a survey of the most important results related to our work. The preparation of the various samples as well as the experimental techniques used for this study are described in Chapter 2.

The results obtained during the isothermal cure of several thermosets at various temperatures are subsequently presented in Chapter 3. Here, the change in both their dielectric

properties and their phonons properties, as measured by Brillouin scattering techniques, has been determined from their sol to gel to glass formation regions. The effects of mixing the two selected amines in various ratios on the thermoset dielectric behaviour is also analyzed in this Chapter.

The effects of isothermal curing during the early period of the cure on the electrical and dielectric properties of thermosets are analyzed in terms of both the percolation concepts, and an empirical equation similar to the classical Vogel-Fulcher-Tamman approach in Chapter 4. The dielectric features observed at longer periods of the isothermal cure are in turn described in terms of a stretched exponential decay function formalism and its theoretical implications are discussed.

The sub- $T_g$  relaxations of both the uncured and cured thermosets were characterized by dielectric measurements over a wide frequency and temperature range and these are presented in Chapter 5. The evolution of the features of both the sub- $T_g$  and the primary relaxations as the curing proceeded is further analysed. New experiments on the effects of progressive substitution of one diamine by the other and the relaxation behaviour of nonstoichiometric thermosets have been investigated and are also reported in this chapter.

The results presented in Chapter 5 are discussed in detail in Chapter 6 where the parameters characterizing the dielectric relaxations are analyzed in terms of the concept of accumulated equivalent curing time, which has been developed for a general

application in the curing of thermosets. A formalism which allowed the determination of the value of the distribution of relaxation times parameter from our fixed frequency measurements is also presented in this Chapter and mechanisms for the dielectric relaxations in thermosets are proposed and discussed.

The conclusions of this work are given in Chapter 7.

Since October 1987, when this study began, several papers on the calorimetric, mechanical and electrical properties of a variety of thermosets have appeared including a special issue of Polymer Science and Engineering (29(5) 1989) which contained exclusively papers on the cure monitoring and cure modelling of thermosets. Therefore it was necessary to submit for publication an account of this study prior to writing the thesis. This was done, and four papers based on part of the work described in this thesis have been accepted for publication in the Journal of Polymer Science: Polymer Physics Edition and Macromolecules and one of them appeared in J. Polym. Sci. Polym. Phys. 28, 71 (1990). Two further papers are under consideration for publication in the Journal of Polymer Science: Polymer Physics Edition.

## **1.2 THE CURING PROCESS**

### **1.2.1 DEFINITIONS**

In the curing of an epoxy resin, two low molecular weight reactants cross-link to form a three dimensional molecular network structure as a result of their chemical reactions. The

chemically additive reactions of an epoxide resin with a primary amine, which acts as a curing or cross-linking molecule, occur in two stages. The first is the reaction of the epoxide group with the primary amine which forms a secondary amine as is illustrated in Figure 1.1. The secondary amine then chemically combines with a second molecule containing the epoxide group, and forms a junction or branch point as also illustrated in Figure 1.1. The rates of both the linear and branched growths of a chain or network depend upon the relative rates of reaction of the epoxide with the primary or secondary amines. This aspect of the curing has been ably reviewed by Dusek (1985). As the reactions reach near-completion, the molecular chains ultimately become linked into a network structure of a formally infinite molecular weight. During the process of its cure, the specific volume of the liquid thermoset decreases as a result of the replacement of Van der Waals "bonds" by shorter covalent bonds which in turn increases the viscoelastic relaxation time. Thus, the glass transition temperature,  $T_g$ , of the liquid continually increases until its value reaches the temperature of isothermal cure and, the liquid thermoset becomes a rigid solid.

The time period during the cure when an irreversible transformation from a viscoelastic liquid to an elastic (solid) gel occurs is known as the gel point,  $t_g$ . At this instant, a covalently bonded molecular network extends throughout the bulk or volume of the polymer, its viscosity approaches infinity and the polymer behaves as a Bingham solid. It has been shown by

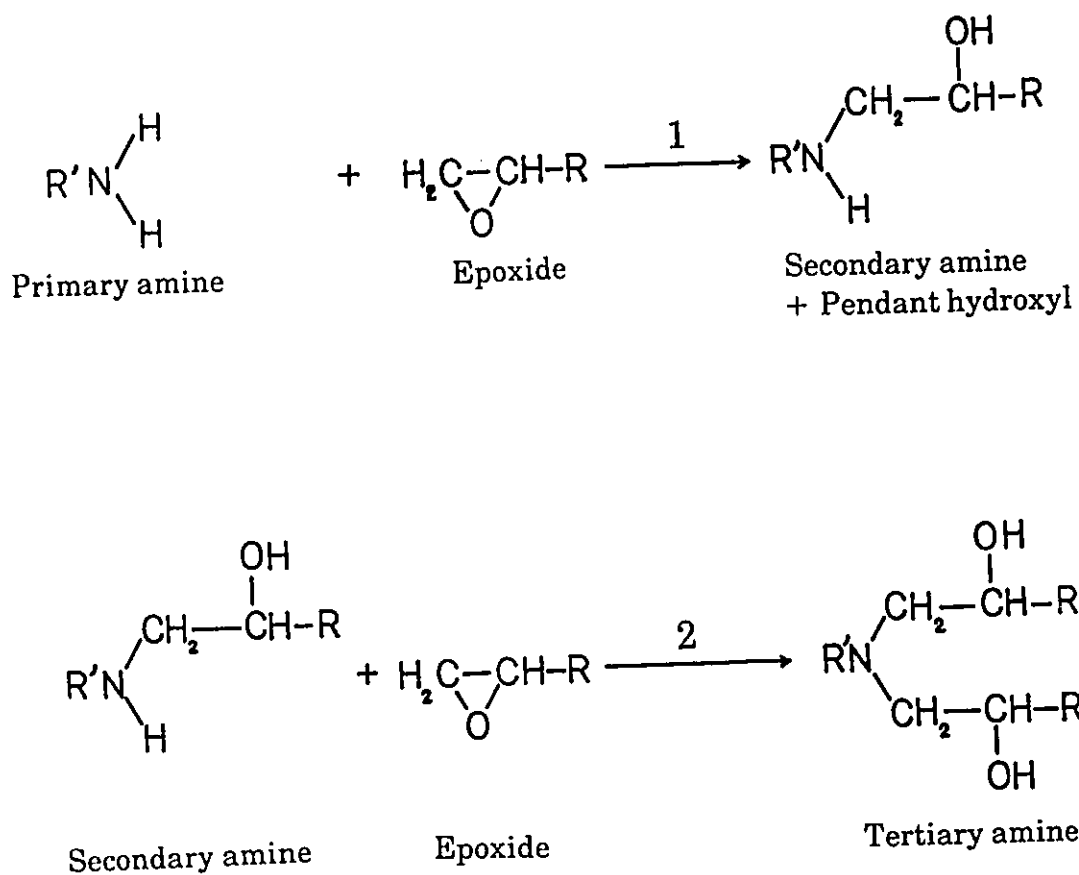


**Figure 1.1:** The two chemical reactions during the cross-linking of an epoxide resin with a diamine: (1) The conversion of a primary amine to a secondary amine, and (2) the conversion of a secondary amine to a tertiary amine.

Oleinik (1985) that the extent of chemical reactions at the instant of gelation depends upon the chemical functionality of the cross-linking agent, its reactivity and the relative amounts of the reactants. Gelation typically occurs at 55% to 80% conversion of the epoxide groups, i.e., when mole fraction of the reacted epoxide groups,  $\alpha$ , is in the range 0.55 to 0.80.

Quite distinct from gelation, vitrification of a thermoset may occur at any stage of the isothermal reactions. This vitrification, or transformation from a viscous liquid or elastic gel to a glass, occurs when the increasing glass transition temperature of the thermosetting liquid reaches the curing temperature,  $T_{\text{cure}}$ . Further chemical reactions or cure in the glassy state continue and occur extremely slowly. As Kaiser (1989) has discussed in a comprehensive review, these reactions become diffusion controlled.

### 1.2.2 PHASE DIAGRAMS

Owing to the difficulties in determining the various transformation times and temperatures and their interdependence, quantitative phase diagrams for thermosets have not as yet been constructed. But qualitative and general descriptions of the various transformations are available in the literature. Figure 1.2 illustrates a simplified phase diagram originally given by Williams (1985) which is helpful in illustrating the main phases and transitions that occur during the curing process. Williams has assumed that the extent of reactions for gelation,  $\alpha_g$ , is independent of temperature, and

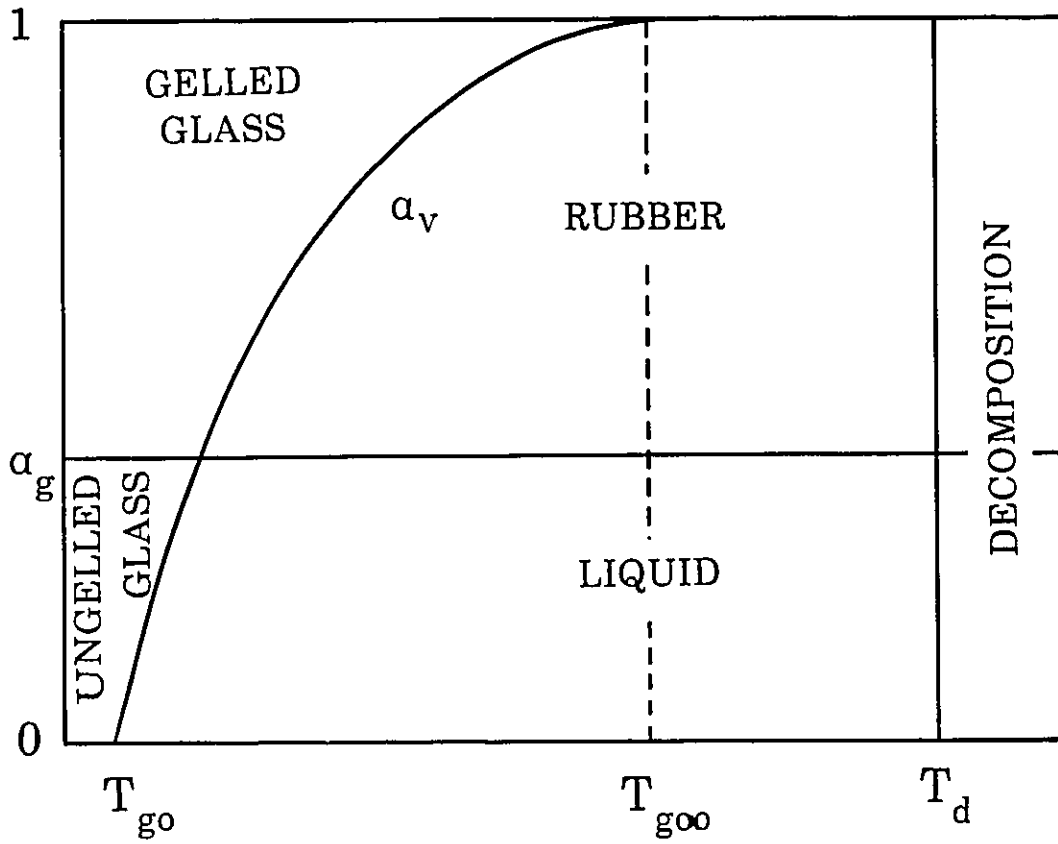


**Figure 1.2:** The extent of epoxide conversion against the curing temperature phase diagram for the isothermal curing of a thermoset polymer (Williams 1985).

further, that the thermoset's decomposition reactions are independent of this extent of reactions in this diagram.  $T_{g0}$  is the glass transition temperature of the unreacted mixture, and  $T_{g\infty}$  is that of the fully reacted thermoset. At  $T \leq T_{g0}$ , chemical reactions formally do not occur and a complete stoichiometric reaction occurs only when  $T \geq T_{g\infty}$ . For temperatures between  $T_{g0}$  and  $T_{g\infty}$ , the maximum chemical conversion in the thermoset is limited by the vitrification curve,  $\alpha_v$ , of Figure 1.2. At  $\alpha_v$ , the curing reaction becomes dramatically slow and consequently the ultimate glass transition temperature of the resulting thermoset is usually about 20-30K higher than the isothermal curing temperature, as has been observed by Peng and Gillham (1985).

A comprehensive diagram, which is known as the isothermal Time-Temperature-Transformation diagram for a thermosetting material was developed by Gillham and co-workers (Enns and Gillham 1983, (a) and (b), Chan and Gillham 1984, Aronhime and Gillham 1986, Gillham 1986). This diagram is shown in Figure 1.3 where the horizontal trajectories alone have a physical meaning. The diagram indicates the various distinct regions of the phases that can appear in the thermosetting material which include liquid, sol/gel rubber, gel rubber, sol/gel glass, gel glass and sol glass phases. In addition to  $T_{g0}$  and  $T_{g\infty}$ , which have already been defined, the diagram includes a third temperature,  $T_{gg}$ , which is defined as the temperature at which gelation and vitrification coincide.

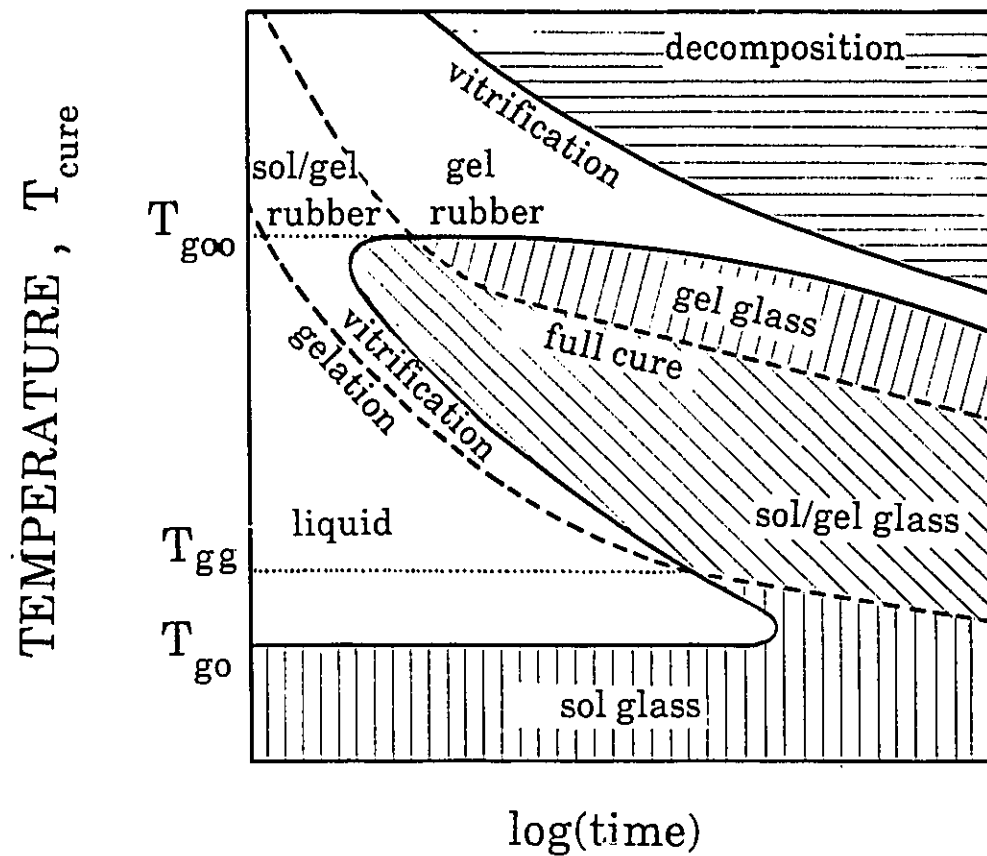
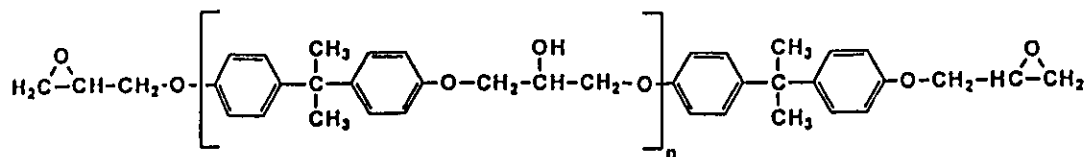


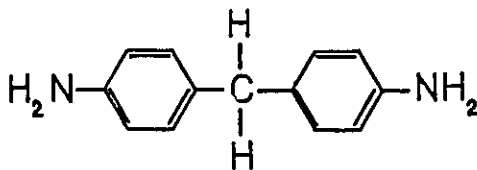
**Figure 1.3:** Schematic Time-Temperature-Transformation (TTT) isothermal diagram for the curing of a thermosetting system (Gillham 1986).

### 1.2.3 THE CHEMICAL STRUCTURES OF THERMOSET PRECURSORS

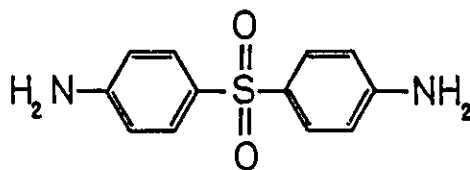
The chemical structures of the diglycidyl ether of bisphenol-A resin, abbreviated as DGEBA, and of the two curing agents diaminodiphenyl methane and diaminodiphenyl sulfone abbreviated as DDM and DDS, respectively, which were selected for this investigation are illustrated in Figure 1.4. During the cross-linking reaction, illustrated in Figure 1.1, one hydrogen atom associated with the primary amine dissociates, the original epoxy group of the resin opens, and its oxygen atom forms a hydroxyl group with the hydrogen from the amine. This is equivalent to an irreversible proton transfer from  $\text{-NH}_2$  to  $\text{-O-}$  atom. The nitrogen atom thus links with the end carbon atom of the newly formed hydroxyether group of the DGEBA molecule. This event, which is illustrated in Figure 1.1, creates a secondary amine. The remaining hydrogen of this secondary amine may in turn react with the epoxy group of another DGEBA molecule to form a tertiary amine. The molecular entities that are removed or formed during the cross-linking reaction are all highly polar groups. These are (1) the hydroxyether groups as have been identified by Blyakhman et al (1970(a) and (b)), and Ochi et al (1982), (2) the epoxy groups as discussed by Huraux and Sellaimia (1973) and Soualmia et al (1982), and (3), both the reacted and unreacted diamines, as was shown by Sheppard and Senturia (1985). Therefore, it seems natural to choose dielectric relaxation spectroscopy as a technique for both the monitoring of the curing process of and the study of molecular diffusion processes in thermosets. The



DGEBA



DDM



DDS

**Figure 1.4:** Chemical structures of the thermosetting systems used in this study. From top to bottom, diglycidyl ether of bisphenol-A (DGEBA), 4,4'-diaminodiphenylmethane (DDM) and 4,4'-diaminodiphenylsulfone.

technique has a further advantage by virtue of the extreme sensitivity of the dielectric properties to any change in the average dipole moment and dipolar reorientation rate, the latter as a result of change in the steric hindrance of the reorienting dipoles. Furthermore, dielectric relaxation spectroscopy can serve as a nondestructive technique which can be used with equal ease for in situ study of both liquid and solid states of thermosets with considerable reliability ensured by its well established principles.

### 1.3 DIELECTRIC RELAXATION SPECTROSCOPY

#### 1.3.1 THE RELAXATION FUNCTION

When a constant electric field,  $E_0$ , is applied across two parallel conducting plates separated by a narrow gap filled with a dielectric medium, both instantaneous and time dependent charges build up on the plates. This build-up of charges occurs at a rate controlled by the polarization of the dielectric. The dielectric response to a step voltage experiment is thus expressed as:

$$P(t) = P_0 + P_1 (1-\phi(t)) \quad (1.1)$$

where  $P$  represents the polarization,  $P_0$  the instantaneous or distortion polarization which arises from the displacement of electrons with respect to their nuclei and the displacement of atoms relative to each other, and  $P_1$ , the time dependent polarization due to the angular rotation of a dipole vector. The normalized decay function,  $\phi$ , also known as the relaxation function (McCrum et al 1967), describes the approach of  $P(t)$  to

an equilibrium value. The total charge density on the plate, or the electric displacement,  $D$ , is related to  $P$  and  $E_0$  according to:

$$D(t) = e_0 E_0 + P(t) = \epsilon(t) e_0 E_0 \quad (1.2)$$

where  $\epsilon$  is the permittivity of the dielectric medium, and  $e_0$  that of vacuum or free space ( $e_0 = 8.854 \times 10^{-12} \text{ Fm}^{-1}$ ). When the electric field is not constant, the superposition principle (Hopkinson 1877, Curie, 1888) is generally applicable and the value of the electric displacement at any instant of time,  $t$ , due to a complex electric field history becomes the sum of displacements arising from the incremental fields applied at previous times,  $\mu$  when  $\mu \leq t$ :

$$D(t)/e_0 = \epsilon_\infty E(t) + (\epsilon_0 - \epsilon_\infty) \int_0^t [1 - \phi(t-\mu)] dE(\mu) \quad (1.3)$$

where  $\epsilon_\infty$  and  $\epsilon_0$  are the instantaneous and long time (or static) permittivities, respectively. Integrating by parts, and replacing  $(t-\mu)$  by  $\theta$  gives:

$$D(t)/e_0 = \epsilon_\infty E(t) + (\epsilon_0 - \epsilon_\infty) \int_0^\infty E(t-\theta) (-d\phi/d\theta) d\theta \quad (1.4)$$

In the special case of dynamic experiments when the applied electric field is periodic:

$$E^* = E_0 \exp(j\omega t), \quad (1.5)$$

where  $\omega$  is the angular frequency and  $j$  the square root of  $(-1)$ . In such a case, the phase of the corresponding displacement lags behind that of  $E^*$  according to equation,

$$D^* = D_0 \exp(j(\omega t - \delta)), \quad (1.6)$$

where  $\delta$  represents this phase difference. Equation (1.2) becomes

$$D^* = \epsilon^* e_0 E^* \quad (1.7)$$

where  $\epsilon^*$  is a complex dielectric permittivity. By combining eqns. (1.5) to (1.7) one obtains,

$$\epsilon^* = (D_0/e_0 E_0) (\cos\delta - j\sin\delta) = \epsilon' - j\epsilon'' \quad (1.8)$$

$$\text{where, } \epsilon' = (D_0/e_0 E_0) \cos\delta \quad (1.9)$$

$$\text{and, } \epsilon'' = \epsilon' \tan\delta \quad (1.10)$$

$\tan\delta$  is known as the loss tangent or dissipation factor.

Combining eqns (1.5) and (1.7) with eqn (1.4) yields the frequency dependence of the dielectric permittivity:

$$\epsilon^* = \epsilon_\infty + (\epsilon_0 - \epsilon_\infty) \int_0^\infty \exp(-j\omega t) (-d\phi/dt) dt \quad (1.11)$$

or

$$(\epsilon^* - \epsilon_\infty) / (\epsilon_0 - \epsilon_\infty) = N^* = \lambda(-d\phi/dt) \quad (1.12)$$

where  $N^*$  is the normalized complex dielectric permittivity, and  $\lambda(y)$  represents a one sided Fourier or pure imaginary Laplace transform of a function  $y$ .

### 1.3.2 THE RELAXATION TIMES

In cases where  $P_1$  in eqn (1.1) varies at a rate proportional to its displacement from the equilibrium value, with a proportionality constant equal to  $1/\tau_0$ , the relaxation function is given as a simple exponential of the form (Fröhlich 1949):

$$\phi(t) = \exp(-t/\tau_0). \quad (1.13)$$

This behaviour is observed only for a limited number of cases, such as dilute solutions of polar molecules in a nonpolar solvent and substances at high-temperatures. The main

advantage of eqn (1.13) lies in its mathematical simplicity which leads to the classical Debye equation (Debye 1929) which is obtained by combining eqns (1.12) and (1.13):

$$(\epsilon^* - \epsilon_\infty) / (\epsilon_0 - \epsilon_\infty) = 1 / (1 + j\omega\tau_0) \quad (1.14)$$

or, equivalently:

$$\epsilon' = \epsilon_0 + (\epsilon_0 - \epsilon_\infty) / (1 + \omega^2\tau_0^2) \quad (1.15)$$

$$\epsilon'' = (\epsilon_0 - \epsilon_\infty)\omega\tau_0 / (1 + \omega^2\tau_0^2) \quad (1.16)$$

$\tau_0$  is the single relaxation time and represents the time required for the total dipolar polarization to decrease by a factor of  $e^{-1}$  after the removal of the electric field. The expected frequency dependence of  $\epsilon'$ ,  $\epsilon''$  and  $\tan\delta$  for such cases, which is known as the Debye behaviour is illustrated in Figure 1.5.

Most solids, and liquids of high viscosity do not exhibit the Debye behaviour (Davidson and Cole 1951, Davidson 1961, Williams 1984). The relaxation function observed for these cases is often considered to arise from a superposition of exponential relaxation functions according to:

$$\phi(t) = \int_0^\infty \exp(-t/\tau)g(\tau)d\tau \quad (1.17)$$

with  $\int_0^\infty g(\tau)d\tau = 1 \quad (1.18)$

where  $g(\tau)$  is the relaxation time distribution function. Several attempts have been made by different groups (Wagner 1913, Whitehead and Banos 1932, Yager 1936, Fuoss and Kirkwood 1941, Cole and Cole 1941, Davidson and Cole 1950 and 1951, Hamon 1952, Havriliak and Negami 1966, Williams and Watts 1970) to empirically determine  $g(\tau)$  that would best describe the experimentally observed dielectric relaxation features of

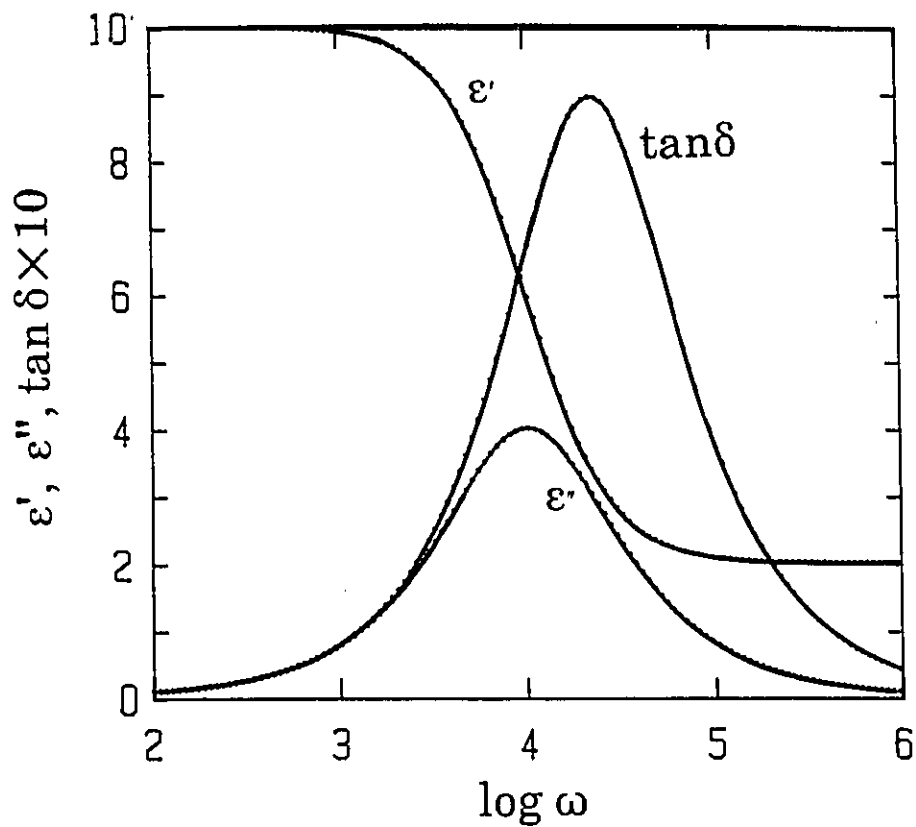


**Figure 1.5:** The angular frequency dependence of the dielectric permittivity, loss and loss tangent using the Debye single relaxation model with  $\epsilon_{\infty}=2$ ,  $\epsilon_0=10$  and  $\tau=10^{-4}$ s.

materials. A comparison between the most frequently used amongst these is briefly given as follows:

The differences between the various relaxation functions can be easily seen by plotting the measured dielectric loss against the dielectric permittivity in complex plane plots which are named after K.S. Cole and R.H. Cole who first proposed its use in 1941. A Debye behaviour represented in a Cole-Cole diagram is a semi-circle of diameter  $(\epsilon_0 - \epsilon_\infty)$  with its centre on the  $\epsilon'$ -axis. When the  $(j\omega\tau_0)$  term in eqn (1.14) is raised to the power  $\alpha$  where  $0 \leq \alpha \leq 1$ , Cole and Cole (1941) showed that the corresponding diagram becomes an arc of circle whose center lies in the half plane below the  $\epsilon'$  axis as shown in Figure 1.6. Both the Debye and Cole-Cole equations give complex plane plots of  $\epsilon''$  and  $\epsilon'$  which are symmetrical about  $\omega\tau_0 = 1$ , and therefore  $\tau_0$  represents the average relaxation time. However, complex plane plots of  $\epsilon''$  and  $\epsilon'$  for a variety of liquids and solids are found to be semicircle at low frequencies and skewed at high frequencies, an observation first made and considered by Davidson and Cole (1950, 1951) who proposed an empirical fit to the data by raising  $(1 + j\omega\tau_0)$  in eqn (1.14) to the power  $\beta_{CD}$  where  $0 \leq \beta_{CD} \leq 1$ . In a complex plane plot, this equation gives a semicircle on the low frequency side, but approaches the  $\epsilon'$ -axis linearly at an angle  $(\beta_{CD}\pi/2)$  on the high frequency side. Alternatively, Williams and Watts (1970) have found that the stretched exponential decay function

$$\phi(t) = \exp-(t/\tau_0)^\beta \quad (1.19)$$

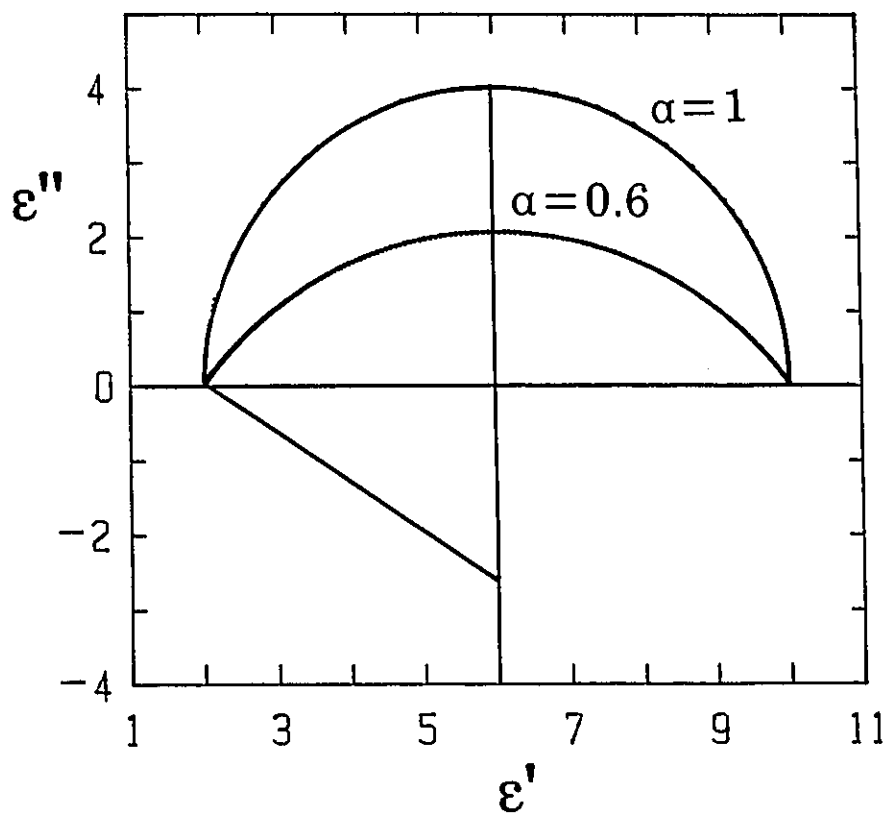


**Figure 1.6:** The complex plane diagram of the dielectric permittivity using both the Cole-Cole model with  $\alpha=0.6$  and the Debye model ( $\alpha=1$ ).

which was earlier used by Kohlrausch (1854) for the time-domain measurement of creep adequately describes the dielectric behaviour of a variety of materials. This function is now referred to as the Kohlrausch-Williams-Watts (KWW) function and  $\beta$  as the KWW parameter. For both the Cole-Davidson and KWW representations, the curves obtained are asymmetric, and  $\tau_0$  is related to the average relaxation time,  $\langle\tau\rangle$ , according to:

$$\langle\tau\rangle = \beta_{CD}\tau_0 \quad (1.20)$$

in the Cole-Davidson formalism. In the KWW formalism,

$$\langle\tau\rangle = (\tau_0/\beta)\Gamma(1/\beta) \quad (1.21)$$

where  $\Gamma(y)$  represents the gamma function of  $y$ . A comparison between the complex plane plots of  $\epsilon''$  and  $\epsilon'$  obtained by using the Cole-Davidson and the KWW function has been discussed by Lindsey and Patterson (1980), and the plots of  $\epsilon''$  against  $\epsilon'$  derived by them are given in Figure 1.7.

### 1.3.3 THE CONDUCTIVITY RELAXATION

The derivations of the final equations in the previous section have been based on the assumption that the dielectric material under study does not conduct electricity for a steady electric field or that its dc conductivity is zero. When both the thermally activated motion of dipoles and diffusion of ions occur in a material, one needs to consider further the value of the finite leakage current which is given by:

$$I_o^* = G_o V^* = G_o \ell E^* \quad (1.22)$$

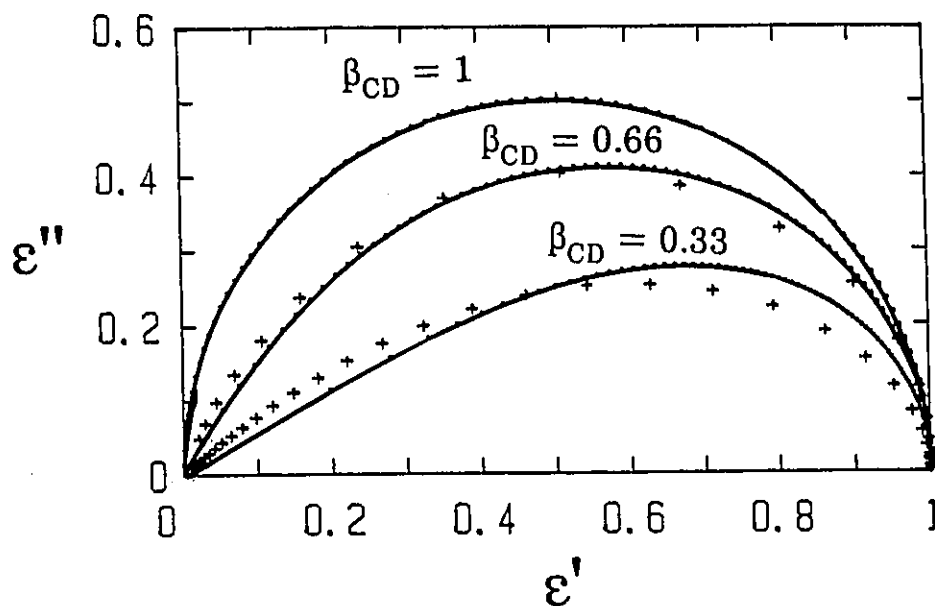


**Figure 1.7:** A graphical comparison between the Cole-Davidon (solid line) and the Kohlrausch-Williams-Watts (crosses) functions plotted in the complex plane. The numbers next to the curves refer to the values of  $\beta_{CD}$ . Parameter values are  $\beta_{CD}=0.33$  and  $\beta=0.46$ ,  $\beta_{CD}=0.66$  and  $\beta=0.77$ , and  $\beta=\beta_{CD}=1$  for the Debye model. (Lindsey and Patterson 1980).

where  $V^*$  and  $E^*$  are the applied sinusoidal voltage and electric field, respectively,  $G_0$  is the dc conductance and  $\ell$  is the distance between the electrodes. Since the current flowing across the dielectric medium is defined by,

$$I^* = A(dD^*/dt), \quad (1.23)$$

where  $A$  represents the total area of the electrodes, the additional displacement term,  $D_\sigma^*$ , due to the dc conductivity of the material is given by:

$$D_\sigma^* = (\sigma_0/j\omega)E^*, \quad (1.24)$$

where  $\sigma_0$  is the dc conductivity. According to the definition of  $\epsilon^*$  given in eqn (1.7), the dc conductivity contributes only to the imaginary part of the complex permittivity by an amount,  $\epsilon_\sigma^*$ , which is given by,

$$\epsilon^* = \epsilon_{\text{dip}}^* + \epsilon_\sigma^* \quad (1.25)$$

with

$$\epsilon_\sigma^* = \sigma_0/j\omega\epsilon_0 \quad (1.26)$$

where  $\epsilon_{\text{dip}}^*$  is the complex permittivity due to the dipolar reorientation alone, which has been dealt with in detail in Section 1.3.2, and  $\epsilon_\sigma^*$  that due to the dc conductivity alone.

For both the frequency and temperature ranges over which a dielectric material does not exhibit a dispersion,  $\epsilon_0$  is equal to  $\epsilon_\infty$ , and the dielectric permittivity is accordingly given by:

$$\epsilon^* = \epsilon_\infty - i(\sigma_0/\epsilon_0\omega). \quad (1.27)$$

The corresponding plots of  $\epsilon'$  and  $\epsilon''$  against  $\log\omega$  are shown in Figure 1.8(a). By analogy with mechanical relaxations spectroscopy, a new representation in terms of complex

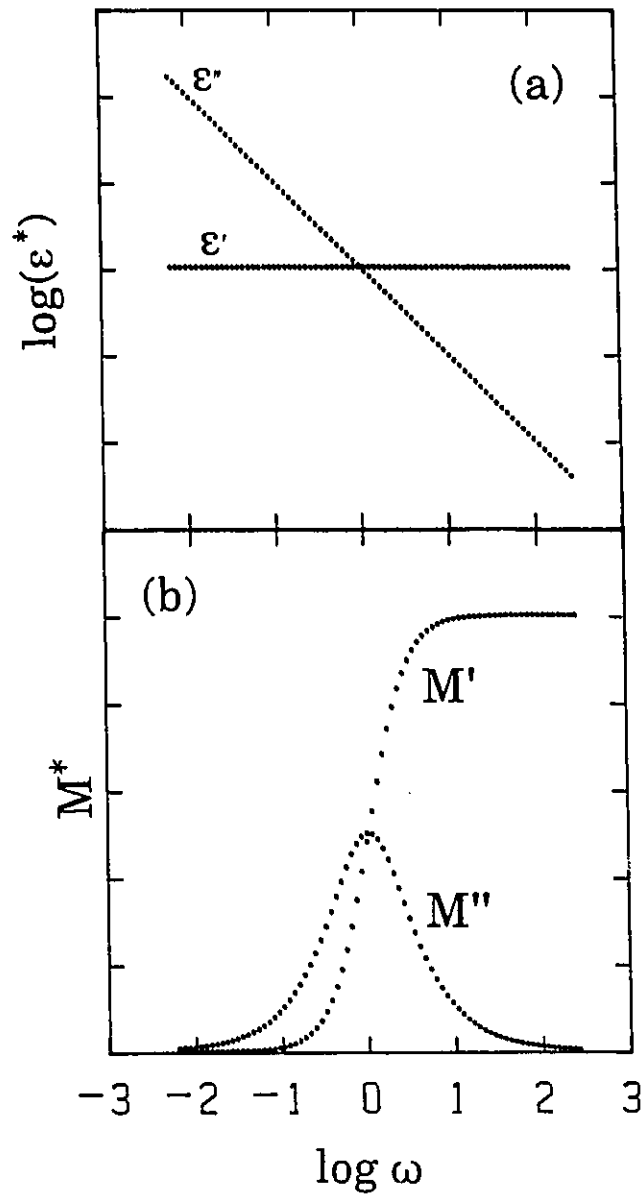


**Figure 1.8:** The angular frequency dependence of  $\text{Log}(\epsilon^*)$  and  $M^*$  for a conducting medium with frequency independent dielectric permittivity and conductivity.

electrical modulus  $M^*$  was provided for such cases by Macedo et al (1972) as,

$$M^* = 1/\epsilon^* = M' + iM'' \quad (1.28)$$

where  $M'$  and  $M''$  are respectively the real and imaginary components of  $M^*$ , which are defined by:

$$M' = \epsilon' / (\epsilon'^2 + \epsilon''^2) \quad (1.30)$$

$$M'' = \epsilon'' / (\epsilon'^2 + \epsilon''^2). \quad (1.31)$$

By combining eqns. (1.30) and (1.31) with eqn. (1.27) one obtains,

$$M' = M_\infty (\omega\tau_\sigma)^2 / (1 + \omega^2\tau_\sigma^2) \quad (1.32)$$

$$M'' = M_\infty \omega\tau_\sigma / (1 + \omega^2\tau_\sigma^2) \quad (1.33)$$

$$\text{or } M^* = M_\infty j\omega\tau_\sigma / (1 + j\omega\tau_\sigma) \quad (1.34)$$

where  $M_\infty = (\epsilon_\infty)^{-1}$  is the unrelaxed electrical modulus, and  $\tau_\sigma$ , the (single) conductivity relaxation time similar to that given by Maxwell for an RC circuit and is defined by,

$$\tau_\sigma = e_0 \epsilon_\infty / \sigma_0. \quad (1.35)$$

A significant feature of the  $M^*$  representation is that it exhibits a dispersion which is symmetric about  $\omega\tau_\sigma = 1$ , as is illustrated in Figure 1.8(b). When  $M''$  is plotted against  $M'$  in a complex plane, the plot is a semicircle of diameter  $M_\infty$ , with its center on the  $M'$ -axis. This formalism has been further extended by Moynihan et al (1973), Hodge et al (1975, 1976) and Grant et al (1977), who introduced the concept of distributions of conductivity relaxation times in order to account for the deviations in the shape of the  $M^*$  spectra from those given by eqns (1.32) to (1.34) and Figure 1.8 exhibited by ion-

containing materials. The basis for the representation in terms of the distribution of conductivity relaxation times has recently become questionable in the light of observations by Johari and Pathmanathan (1988), Cole (1989) and Elliott and Owen (1989), and the theoretical aspects of this debate would be of much interest in the future studies of the conduction phenomenon in ionic materials.

#### 1.4 DIELECTRIC SPECTROSCOPY OF THERMOSET CURING

##### 1.4.1 THE IONIC CONDUCTIVITY

Organic liquid precursors used for the preparation of thermosets often contain free impurity ions as residuals of their processing conditions. Their concentration does not change appreciably during the cross-linking as a result of chemical reactions as was originally found by Fava and Horsfield (1968). The dc conductivity due to the diffusion of ions can be expressed as,

$$\sigma_0 = \sum q_i N_i \mu_i \quad (1.36)$$

where  $q_i$  is the electronic charge,  $N_i$ , is the number of atoms of the  $i$ th charge carrying species per unit volume, and  $\mu_i$  is their mobility. The decrease observed in the dc conductivity during the cross-linking of precursors has therefore been interpreted in terms of a decrease in the ionic mobility of impurities. The relationship between the ionic mobility and the viscosity can be qualitatively examined by using a variation derived by Bockris and Reddy (1975) of Stokes-Einstein equation for the drift of spherical particles of

radius  $r$  in a viscous medium when subjected to a force  $q_i E$ , according to:

$$\mu_i = q_i / 6\pi\eta r \quad (1.37)$$

where  $\eta$  is the viscosity of the medium. Lawless (1980), Tajima and Crozier (1983), Kranbuehl et al (1985) and Lane et al (1986), have found that the dc conductivity of a thermoset is approximately inversely proportional to its viscosity prior to its gelation. But, this relation becomes less appropriate in the vicinity of the gelation point where the viscosity diverges towards infinity while the dc conductivity remains finite and increases without a discontinuity, as the curing proceeds.

The dc conductivity of ionic substances is necessarily needed to be measured by ac impedance methods so that the electrode polarization effects are avoided. Earlier studies by Acitelli et al (1971) and Tajima and Crozier (1983) of dc conductivity by dc resistance measurements are seen by Senturia and Sheppard (1985) to have been biased by electrode polarization effects due to the large dc conduction of the liquid thermosets. More recent measurements of dc conductivity, have too been affected by the occurrence of significant electrode polarization effects in thermosets during their cure, particularly at short curing times. These effects gradually decrease as the curing proceeds and the conductivity concomitantly decreases. Whether this decrease in conductivity is a consequence of the gelation or of an approach to the vitrification of the thermoset, is still unclear and presently debated.

The dc conductivity remains a particularly useful quantity for probing the extent of thermosets cure since its value becomes increasingly more sensitive to the curing time near  $T_g$ . Therefore, several groups (Kranbuehl et al 1989, Nass and Seferis 1989, Bidstrup et al 1989, Lane et al 1989) are currently engaged in studying the conductivity behaviour of curing thermosets with the motivation towards determining the parameters necessary for the process controls.

#### 1.4.2 THE DIELECTRIC RELAXATION

Several research groups (Huraux and Sellaimia 1973, Soualmia et al 1982, Lane et al 1986) have observed that the dipolar relaxation time remains directly proportional to the viscosity. Since the viscosity of a thermoset, diverges to infinity at the gelation point, several authors (Delmonte 1959 and Haran 1965) have associated the occurrence of the dielectric dipolar relaxation peak with the onset of the gelation process. But, more recently, Sheppard et al (1984) have shown that the dielectric relaxation peak is not associated with the gelation process. They have compared the time required to reach the dipolar loss peak, measured at two frequencies of 10Hz and 10KHz, for the DGEBA (whose number of repeat unit,  $n$ , in figure 1.4 is equal to zero) cured with DDS, and compared it against the gelation and vitrification times obtained independently by Enns and Gillham (1983 (b)). The parallel trend found between the time at which the dielectric loss peak appeared and the time for vitrification demonstrated that the dielectric

relaxation peak was associated with the glass transition and not gelation of the thermoset.

#### 1.4.3 THE SUB- $T_g$ RELAXATIONS

All amorphous solids retain a certain degree of molecular motion in their rigid matrix, which appears as a sub- $T_g$  relaxation. The existence of these relaxations is attributed to local high energy, low density, regions in which localized molecular motions persists (McCrum et al 1967). Since an amorphous solid's effectiveness as an electrically insulating and mechanically tough material is also determined by the degree of localized molecular motions or sub- $T_g$  relaxations in it, the occurrence of these relaxations is now regarded as technologically important.

Epoxide thermosets show two sub- $T_g$  relaxations in their dynamic mechanical spectra. The low temperature or  $\gamma$ -relaxation and the high temperature or  $\beta$ -relaxation of the cured thermosets have been extensively characterized by dynamic mechanical measurements and the effect of physical ageing on these mechanical relaxations has been investigated (Chai & McCrum 1980, Plazek et al 1981, Aherne et al 1982, Choy & Plazek 1986, Mikolajczak et al 1987 and Cavallé et al 1987). The  $\gamma$ -relaxation has not been dielectrically characterized but, the mechanically analogous peak has been attributed by Ochi et al (1982) to the localized motions of polymeric sequences consisting of at least four carbon atoms in the network. The  $\beta$ -relaxation has been dielectrically characterized and

molecular mechanisms have been proposed by several workers who studied it also by varying the chain length of the cross-linking component (Ochi et al 1982, Shimbo et al 1984, Ochi et al 1986 and 1987). They have attributed the  $\beta$ -relaxation process to the motions of hydroxyl-ether groups and to other (unspecified) parts of the network. Keenan et al (1979) have attributed the same process to a crankshaft rotational motion of the glycidyl portion of the glycidyl ether within the thermoset network. In general, therefore, these relaxations have been attributed to the thermally activated motion of specific groups or network segments. In view of the findings (Johari and Goldstein 1970, Johari 1973) that amorphous solids in which molecules lack internal degrees of freedom also show sub- $T_g$  relaxations, it became necessary to examine whether the assignment of these relaxations to the motion of specific polymer groups is satisfactory. To this end, a study of the effects of a variation in the composition of the thermoset and the time dependence of the strength of sub- $T_g$  relaxations were necessary.

## CHAPTER 2

### THE EXPERIMENTAL PROCEDURES

#### 2.1 DIELECTRIC SPECTROSCOPY

##### 2.1.1 PRINCIPLES

When a sinusoidal voltage of the form,

$$V^* = V_0 \exp(j\omega t), \quad (2.1)$$

is applied across the dielectric sample of thickness  $\ell$  placed between two plates each of area  $A$ , the current  $I^*$  flowing across the dielectric sample is obtained by combining eqns (2.1), (1.23) and (1.7) to give,

$$I^* = j\omega C_0 \epsilon^* V^* \quad (2.2)$$

where  $C_0 = e_0 (A/\ell)$  (2.3)

$C_0$  is called the geometric capacitance and  $e_0$  is the permittivity of free space defined in eqn. (1.2). The admittance  $Y^*$  of the dielectric is given by

$$Y^* = I^*/V^* = C_0 (\epsilon'' + j\epsilon') \quad (2.4)$$

The equipment used for the determination of the dielectric relaxation spectra is designed to measure the equivalent admittance,  $Y$ , of the dielectric sample. When the sample is electrically equivalent to a capacitance,  $C_p$  in parallel with a resistance,  $R_p$ , the real and imaginary components of dielectric permittivity are given by:

$$\epsilon' = C_p/C_0 \quad (2.5)$$

$$\epsilon'' = 1/R_p \omega C_0 = G_p/\omega C_0 \quad (2.6)$$

$$\tan \delta = 1/R_p C_p \omega = G_p/\omega C_p \quad (2.7)$$

But, when the equivalent circuit is in series, i.e.  $R_s$  and  $C_s$  in series,  $\epsilon'$  and  $\epsilon''$  of the sample are related to  $R_s$  and  $C_s$  by equations

$$\epsilon' = C_s/C_o(1 + \tan\delta) \quad (2.8)$$

$$\epsilon'' = R_s C_s^2 \omega / C_o (1 + \tan^2 \delta) \quad (2.9)$$

$$\tan\delta = R_s C_s \omega \quad (2.10)$$

### 2.1.2 THE TRANSFORMER RATIO-ARM BRIDGE

Cole and Gross (1949), Thompson (1956) and Lynch (1957) have described impedance measurement bridges in which the ratio arms comprise closely coupled transformers. The advantage of these ratio-arm bridges over conventional equipment is that the residual impedance and guard circuit impedance are eliminated under the bridge balance conditions. In addition, the transformer's arms can be wound to give an accuracy of a few parts in  $10^6$  in transformer output voltage ratios. As a result, the capacitance and loss tangent are measured with a very high accuracy over an extremely large range of capacitance and loss tangent values.

A transformer ratio-arm bridge model GR1615A purchased from General Radio Corporation was used for part of these measurements. Its schematic diagram is given in Figure 2.1. The transformer in the measuring arm has electrical taps along its length at  $1/10^{\text{th}}$  intervals. The measuring arm contains eight fixed capacitors,  $C_n$ , ranging in capacitance from 1000 pF to 0.0001 pF in decade intervals.

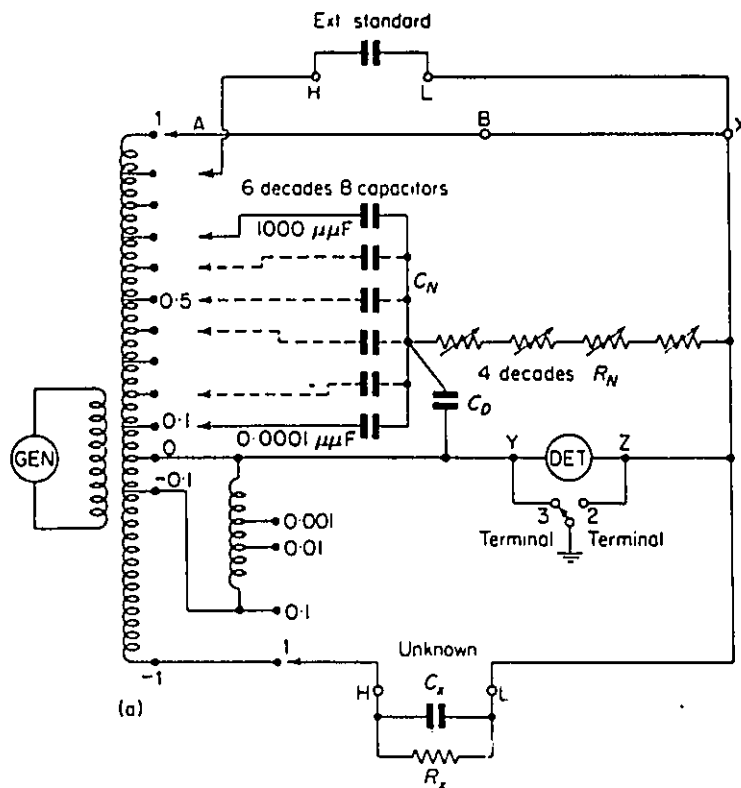


Figure 2.1: Schematic diagram of the transformer ratio-arm bridge, model General Radio 1615A.

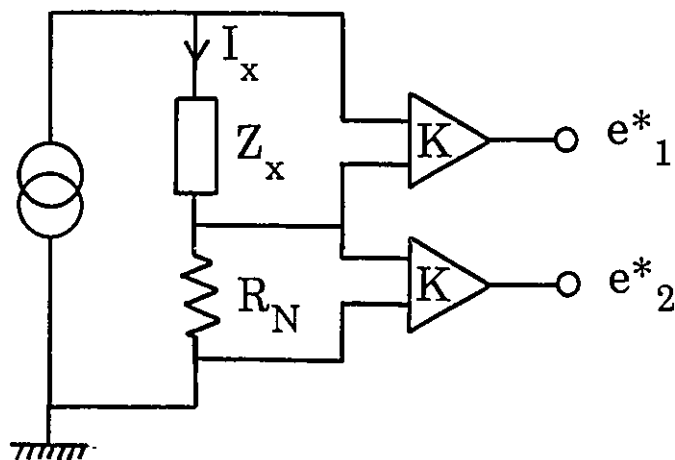


Figure 2.2: The elementary measurement circuit of the Genrad Digibridge 1689 model.

The capacitors  $C_n$  are connected at a common point to decade resistors  $R_n$  which cover the range  $100\Omega$  to  $0.1\Omega$  in 4 decades. The standard capacitors  $C_n$  may tap the transformer in any desired combination. The bridge is balanced when the current flowing through the detector is zero. This is achieved at a particular value for  $C_n$  and  $R_n$ , which correspond to an equivalent series capacitance and resistance value for the sample.

The sinusoidal voltage was supplied by a test oscillator purchased from Hewlett Packard Model 651B. The maximum voltage was 0.1V and its frequency was between  $10^2$  and  $10^6$ Hz. The voltage frequency was determined using a Hewlett Packard model HP3450A multifunction meter. The current detected in the balancing arm of the bridge was amplified by a tunable amplifier purchased from Rohde and Schwarz type UBM and sent to the Y channel of an oscilloscope. The X channel received the applied voltage and balancing conditions were satisfied when the Lissajous figure on the oscilloscope coincided with the X-axis.

### 2.1.3 THE AUTOMATIC GENRAD DIGIBRIDGE 1689

Most of the dielectric measurements for this study were carried out using a microprocessor-controlled automatic impedance meter known as Genrad Digibridge 1689 which is manufactured by General Radio Corporation. This equipment uses a measurement technique in which a microprocessor is used to calculate the impedance of the sample from a series of eight

voltage measurements. These measurements include quadrature ( $\pi/2$ ) and inverse ( $\pi$ ) vector components of the voltage across a standard resistor  $R_N$  carrying the same current as the unknown impedance,  $Z_x$ . Each set of voltage measurements is made in rapid sequence with the same phase-sensitive detector and an analog-to-digital converter. Therefore, properly chosen differences between these measurements subtract out the fixed offset errors, and ratios between the differences cancel out the values of the common current and the scale factor of the detector-converter.

The simplified diagram of the measurements method is given in Figure 2.2. A sine-wave generator sends a current  $I_x$  through the unknown impedance  $Z_x$  and a standard resistor  $R_N$  in series. Two differential amplifiers with the same gain  $K$  produce voltages  $e_1^*$  and  $e_2^*$ . Therefore, the unknown complex impedance is given by

$$Z_x = R_N(e_1^*/e_2^*) \quad (2.11)$$

from which two values,  $C_p$  and  $\tan\delta$ , are automatically calculated by the microprocessor for a given frequency. The precision components in this instrument are four standard resistors and one quartz-crystal stabilized oscillator which has zero standard reactance.

In order to facilitate the use of Digibridge 1689 for our studies, it was necessary to incorporate into it an automatic data acquisition system. The digibridge was therefore interfaced with a personal computer. Part of the procedure for interfacing is described in my Master's Thesis (Mangion

1987). The present study required the development of software for the collection of data at a fixed ac frequency but in the time domain at increasing intervals of time. This software was developed and incorporated in the data collection system. The data acquisition system was further developed by designing and incorporating into it a software that allowed the display on the monitor of the dielectric relaxation spectra in real time during the course of the measurements.

#### 2.1.4 THE TEMPERATURE CONTROL ASSEMBLY

A 16cm long, 6cm diameter brass or aluminum block having a concentric, 3cm wide, 12cm deep bore acted as a thermostat. It was coated with an electrically insulating  $\text{Al}_2\text{O}_3$  ceramic. A high resistance nichrome wire was wound around the entire length of the block to provide a 600W heater. The assembly was concentrically placed inside a 13cm diameter, 17cm long, metal can with uniformly thick silica fiber insulation in the annular space. The assembly was immersed in a metal dewar flask containing liquid nitrogen. The temperature of the block was controlled by means of a temperature programmer model Tempstar II, purchased from Thermoelectric Inc., which regulated the power supply of the heating coil. The relatively large thermal capacity of the metal block facilitated a stable and uniform temperature in the sample, and temperatures could be controlled to better than  $\pm 0.4\text{K}$  for a period of several days, and  $\pm 0.1\text{K}$  for several hours.

The temperature was determined by means of a copper-constantan thermocouple placed in thermal contact with the thermoset sample, with its second junction placed in ice at 273.16K. The emf was measured by means of an HP3478A multimeter, purchased from Hewlett Packard, which was also interfaced with the data acquisition system. The measured emf was converted into temperature using a sixth degree polynomial approximation accurate to within  $\pm 0.2\text{K}$ .

#### 2.1.5 THE DIELECTRIC CELLS

The reacted epoxy polymer strongly adhered to metal, polymer and glass parts of the containers used for the construction of a dielectric cell. This prevented the re-use of the dielectric cell for further studies. Therefore, disposable dielectric cells were designed which could be easily constructed and could provide data with the desired degree of accuracy. Parallel plate dielectric cells illustrated in Figure 2.3(a) and (b) were used for isothermal measurements and concentric electrode capacitors shown in Figure 2.3(c) and (d) were used for measurements at different temperatures. Except for the fourth type of cell, shown in Figure 2.3(d), where copper tubes acted as electrodes, the electrodes were in all cases made out of aluminum.

The parallel plate dielectric cell, shown in Figure 2.3(a), which was used for the study of the isothermal curing kinetics of the thermosets, at temperatures lower than 363K consisted of two aluminum pistons whose flat faces acted as

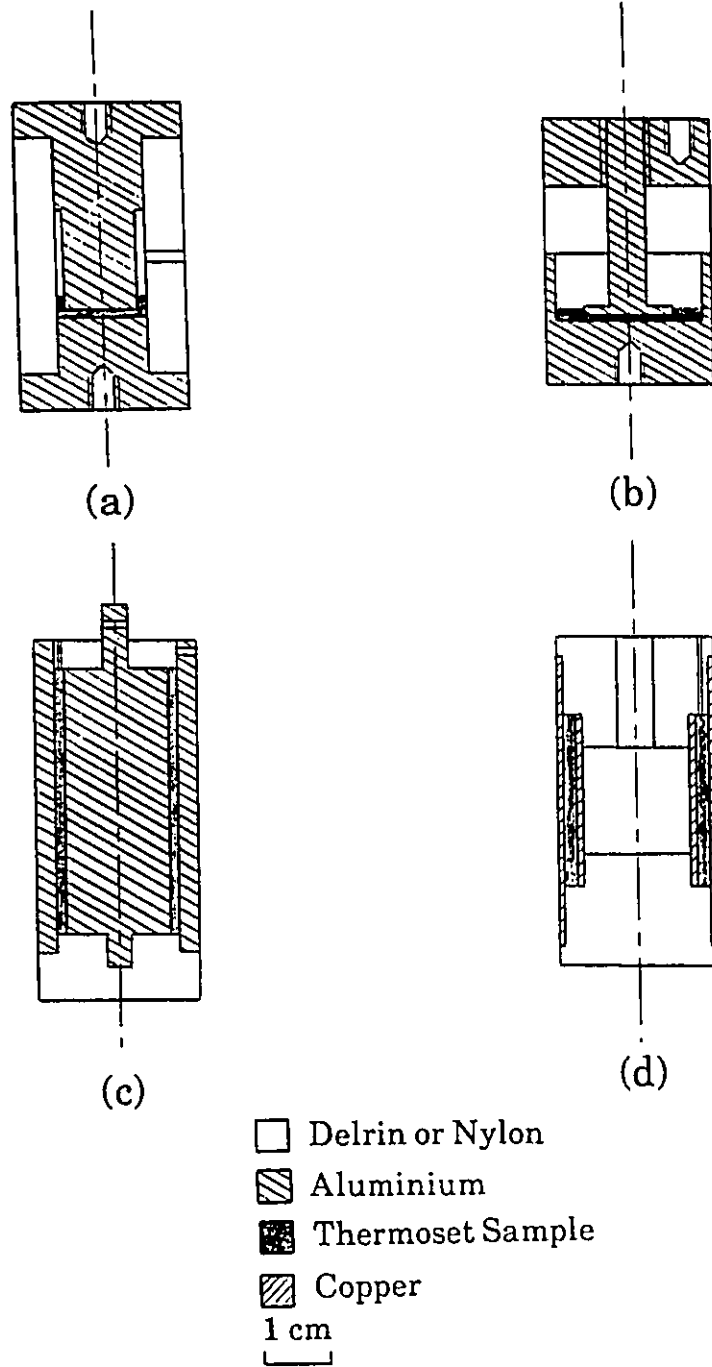


Figure 2.3: Diagram of the four disposable dielectric capacitors used in this study.

electrodes. These were snugly fitted inside either a delrin or a nylon tube. The diameter of the upper electrode was slightly smaller than the tube's inner diameter to allow the liquid sample to overflow through a hole in the tube's wall. Electrical leads were connected to the electrodes by means of screws. For curing temperatures higher than 363K, dilation of the delrin or nylon tube of dielectric cell (a) caused the liquid thermoset sample to flow out of the measuring cell. In this case, the dielectric cell shown in Figure 2.3(b) was preferred. Its lower electrode is the flat surface of an aluminum cup, and a piston acts as the upper electrode. The cell constant,  $C_0$ , was determined by measuring the capacitance of the empty cell at the temperature where isothermal curing was done. The value of  $C_0$  was typically about 5pF for both the parallel plate dielectric cells. The  $C_0$  value of the measuring cell was further corrected by taking the dielectric permittivity,  $\epsilon'$ , value after a long curing time of the same types of thermosets at all curing temperatures to be the same and equal to the limiting high frequency permittivity of the cured thermoset. Measurements were repeated with various cells and these gave values of the  $\epsilon'$  and  $\tan\delta$  within a few percent of each other. We regard this variation to be well within the uncertainty of our measurements.

The dielectric cell shown in Figure 2.3(c) was a concentric electrode assembly which was used for measurements as a function of temperature because its geometric capacitance was less sensitive to changes in the temperature. The internal

diameter of the outer cylindrical electrode of the dielectric cell was 16mm. The diameter of the central rod electrode was nominally 15mm and its length 30mm. The ends of the rod were machined out to reduce its diameter to about 4mm. The concentricity of the two electrodes in the dielectric cell was ensured by placing two concentric separator rings made from delrin or nylon at each end of the electrodes. These delrin, or in some cases nylon, rings tightly fitted the annular spaces provided at both ends of the cell. The thickness of each separator was less than 5% of the length of the inner electrode which ensured that the stray capacitance was minimum. Electrical leads were held in contact with the electrodes by friction between delrin and the metal cylinders. The capacitance of the empty cell which was nominally 20pF and its loss factor were measured over the temperature range 90-400K. This capacitance increased by less than  $\pm 2.5\%$  over the entire temperature range while the loss factor was less than 0.002 over the temperature range 90-300K. These introduced an error of less than  $\pm 1.5\%$  in our dielectric loss data.

The dielectric cell shown in Figure 2.3(d) was used for the study of the effects of composition change of several thermosets on its dielectric relaxation spectra. The design of this cell eliminated the errors in the measurement of both the loss factor and stray capacitance through its delrin or nylon parts.

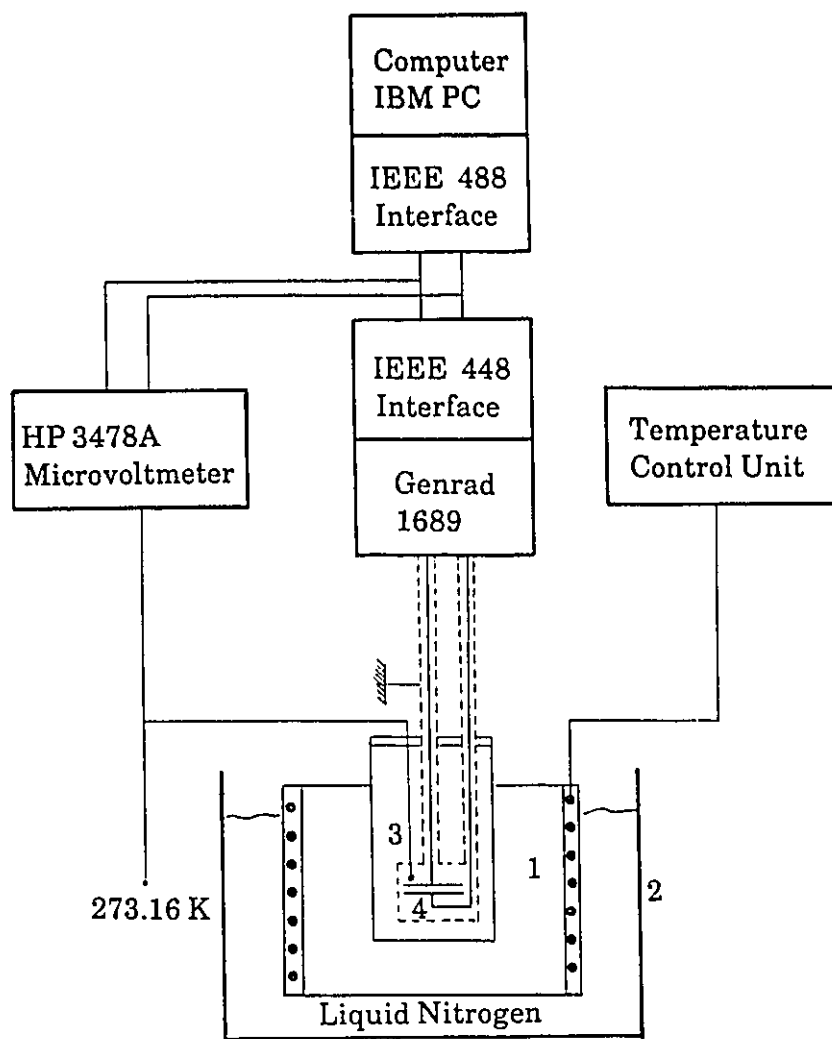
Before measurements were made, an insulating teflon tape was wound around the dielectric cell and its copper connectors, and a shield of aluminum foil was wrapped around the cell and electrically grounded. One cm lengths of copper wires attached to the electrodes were spliced with coaxial cables which, in turn, were used to connect the dielectric cell assembly to the measuring equipment. The dielectric cell assembly was designed such as to remain hermetically sealed during the measurement in order to prevent exchange of gas during the cooling and heating cycles. The diagram of the experimental set up used in this study is shown in Figure 2.4 which is self explanatory.

## **2.2 BRILLOUIN LIGHT SCATTERING MEASUREMENT**

### **2.2.1 PRINCIPLES**

A successful technique for studying the high frequency mechanical behaviour of polymer materials is to measure the velocity of sound waves and its attenuation in the polymer. The use of this technique has been reviewed by Patterson (1980). In the ultrasonic frequency or MHz range, the generally used procedure is to observe the propagation of externally excited sound waves through the medium. In the hypersonic frequency or GHz range, it is more convenient to study the intrinsic thermal acoustic phonons by light scattering.

Laser light is generally scattered by fluctuations in the dielectric tensor,  $\vec{\epsilon}$ , of a material. For organic liquids and glasses, the primary sources of light scattering that couple



1. Thermostat Block
2. Dewar Flask
3. Thermocouple
4. Dielectric Cell

**Figure 2.4:** Diagram of the experimental arrangement for the dielectric measurements.

with the dielectric tensor are fluctuations in density, mechanical shear, and optical anisotropy. Dynamic fluctuations, due to thermally activated phonons, which inelastically scatter light produce Brillouin scattering.

Phonons are defined as the material's quantized vibrational modes in analogy with the photon of the electromagnetic wave. An incident laser light of wave vector  $\vec{k}^i$ , with

$$|\vec{k}^i| = n(\omega_i/c) \quad (2.12)$$

where  $n$  is the sample's refractive index,  $c$  the speed of light, and  $\omega_i$  the angular frequency of the incident light beam, is scattered into a state  $(\vec{k}^s, \omega_s)$  by a sound wave  $(q, \omega_q)$  propagating through a sample. Such a sound wave is called a hypersonic acoustic phonon when its frequency exceeds  $10^9$  Hz. Conservation equations, as reviewed by Sandercock (1982), require that

$$\vec{k}^s - \vec{k}^i = \pm \vec{q} \quad (2.13)$$

$$\omega_s - \omega_i = \pm \omega_q \quad (2.14)$$

where the positive sign refers to the phonon absorption (anti-Stokes event) and the negative sign to phonon emission (Stokes event). The sound velocity,  $v_q$ , is in most cases negligible in comparison with the speed of light,  $c$ , and it is assumed that:

$$|\vec{k}^s| = |\vec{k}^i| \quad (2.15)$$

Therefore, equations (2.13) and (2.14) yield:

$$q = 2n \sin(\theta/2) \quad (2.16)$$

$$\text{and } \omega_q/\omega_s = (2n v_q/c) \sin(\theta/2) \quad (2.17)$$

where  $\theta$  is the angle between  $\vec{k}^s$  and  $\vec{k}^i$ , known as the scattering

angle. Eqn (2.17), when applied to the Brillouin frequency shift, is known as the Brillouin equation. It is analogous to Bragg's reflection from a grating of spacing  $2\pi/q$  moving with a velocity  $v_q$ .

### 2.2.2 EXPERIMENTAL ARRANGEMENT

An Argon ion laser Innova Model 90-3 purchased from Coherent Corporation was used to provide the excitation radiation at 514.5nm. After a 30 minute period for stabilization, the laser was operated at typically 300mW. Conventional optical elements described by Hu (1988) were used to focus the incident beam and collect the scattered light at a right angle scattering geometry. Frequency analysis was performed by a piezo-electrically scanned tandem Fabry-Perot interferometer with an advanced feedback system which adjusted for any non-linearities of the piezo-elements during a scan as described by Vanderwal et al (1981). Light with a wavelength,  $\lambda$ , will be transmitted if a constructive interference condition is satisfied:

$$d = m(\lambda/2) \quad (2.18)$$

where  $m$  is the order of interference and  $d$  is the distance between the two parallel mirrors. The main advantage of the tandem Fabry-Perot spectrometer which contains two sets of parallel mirrors as designed by Sandercock (1982) is that it eliminates overlapping orders of interference. The frequency separation between the two neighbouring maximum transmissions,

$c/2d$ , is called the free spectral range and this, in our experiment, was set at 15.2GHz.

The optical arrangement of the apparatus is sketched in Figure 2.5. A four beam-pass arrangement was used with the beam passing through each etalon twice. The signal transmitted by the interferometer was then directed onto a photomultiplier and the amplified signal was collected by a personal computer. The computer accumulated the spectra and provided feed-back for alignment voltages to maintain mirror parallelism.

### 2.2.3 PROCEDURE

The liquid thermoset was placed inside a cylindrical glass container which in turn was closely fitted inside a 15mm diameter concentric cavity drilled in a cylindrical aluminum block. This block was wound with a nichrome heating wire and acted as a thermostat. Three 5mm diameter holes drilled in the block allowed the incident light beam to go through the sample and the scattered light to escape at an angle of  $90^\circ$ . The time at which the temperature of the sample reached the preselected value of the curing temperature was taken as the initial curing time.

The number of scans performed to collect one spectrum was selected to be high enough so that the accuracy of measurements remained satisfactory, but this number was low enough so that the time needed for one set of data collection was significantly smaller than the time for a significant change to occur in the chemical and physical states of the thermoset.

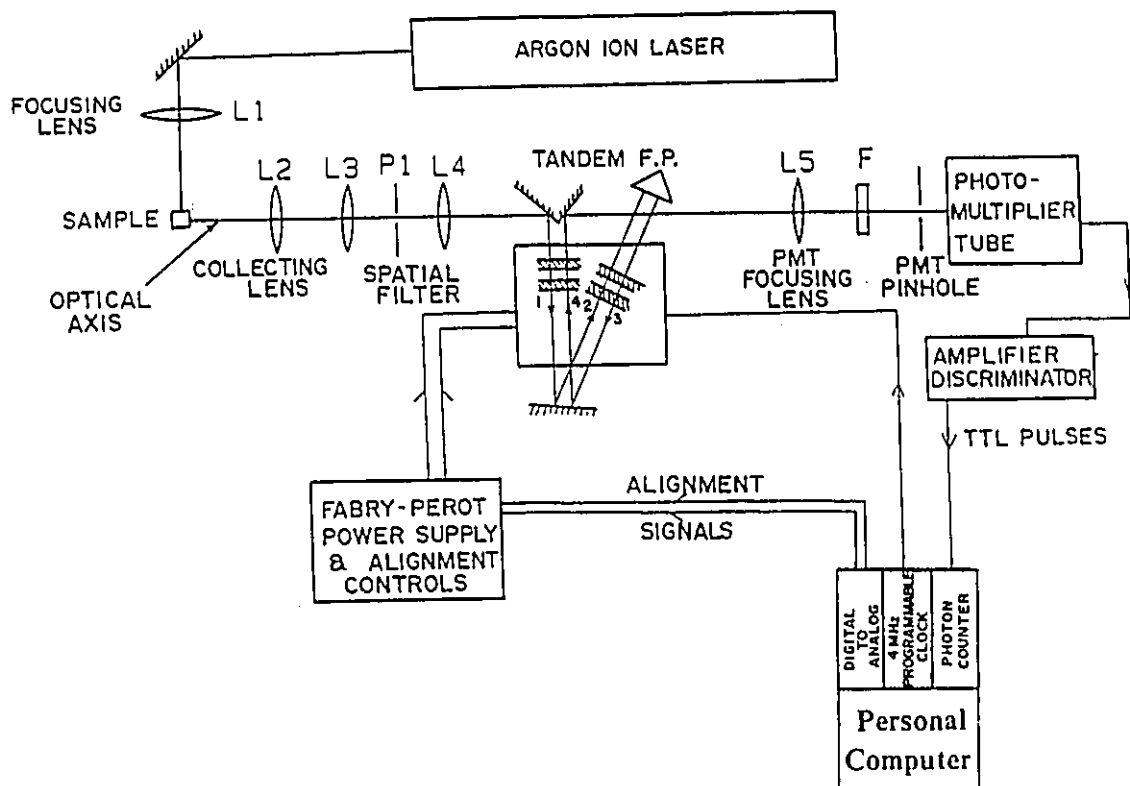


**Figure 2.5:** Diagram of the experimental arrangement for the Brillouin light scattering measurements.

This latter time period depends on the reaction kinetics at the  $T_{\text{cure}}$  of the thermoset, but, because of the continuous, albeit slow, change in the physical state of the thermoset during the measurement, the results are not as accurate as for isothermal measurements on physically and chemically stable liquids.

The temperature of the sample was measured by means of a copper-constantan thermocouple placed inside the liquid sample. During the curing, this temperature remained stable within  $\pm 0.5\text{K}$ . Nevertheless, localized laser heating did occur in the scattering volume of the sample during the measurement. Since the local increase in temperature increases the spontaneous mass convection in the fluid which dissipated this heat, the overall effect due to heating was relatively small in the early stages of the reaction. Near the end of the reaction, when the sample became viscous and almost rigid, mass convection did not occur and the heat dissipation became slow. At this stage, local heating caused an estimated temperature rise by as much as  $3\text{K}$  within the scattering volume.

As the curing reaction neared completion, the incident laser beam was found to become suddenly refracted. Consequently the intensity of the scattered light drastically decreased. When this occurred the glass container was rotated in order to change the location of the scattering volume. This was done periodically near the completion of measurements for each curing temperature. Since the thermal history of the new scattering volume differed slightly from that of the previous one, this additional source of error contributed to the scatter

of the data collected.

### 2.3 THE PRECURSORS AND THERMOSETS PREPARATION

The thermosets studied were prepared from three precursors, diglycidylether of bisphenol-A or DGEBA, 4,4'-diaminodiphenyl methane or DDM, and 4,4'-diaminodiphenyl sulfone or DDS. Diglycidylether of bisphenol-A or DGEBA was obtained from Shell Chemicals. This is supplied to us in the form of a viscous liquid under the trade name EPON 828. LeMay et al (1984) have characterized this as an epoxide with an average molecular weight,  $M$ , of 380g/mol, number of repeat units,  $n$ , of 0.14, and glass transition temperature of 259K. These values were found to be correct in our own studies and were used as such. The two amines, DDM and DDS, of 99+% purity were obtained from Aldrich Chemicals Company. The chemical structures of these compounds are schematically drawn in Figure 1.4. Both DDM and DDS, hereafter referred to as the curing agents, are granular at room temperature, and had melting temperatures of 363K and 448K, respectively.

Each curing agent has four N-H bonds and the DGEBA molecules contain 2 epoxy groups. Therefore, stoichiometric considerations for a chemical reaction require that 2 moles of DGEBA be mixed with one mole of the curing agent. Except when specified, the results reported here were obtained on stoichiometric mixtures. The epoxy thermosetting liquids were prepared by mechanically mixing with a glass rod accurately weighed amounts of DDM or DDS, for two minutes with a weighed

amount of liquid DGEBA at 360K and 420K, respectively. The resulting homogeneous mixtures were then directly poured into the dielectric cells . For Brillouin light scattering studies the precursor mixtures were kept in their transparent container.

For part of this study, the two amine curing agents together were mixed with the DGEBA resin. In these cases, an appropriately weighed amount of granular DDS was first mechanically mixed with the required amount of liquid DGEBA using a glass rod for two minutes at 420K. The resulting homogeneous liquid was quenched to 360K and the required weight of granular DDM was added. The mixture was mechanically mixed further with a glass rod for two minutes and allowed to cool to room temperature, and thereafter poured into the dielectric cell.

## CHAPTER 3

### RESULTS OF ISOTHERMAL CURING OF THERMOSETS

#### 3.1 DIELECTRIC RELAXATION BEHAVIOUR

##### 3.1.1 ISOCHRONAL OR FIXED FREQUENCY STUDIES

The dielectric permittivity,  $\epsilon'$ , loss,  $\epsilon''$ , and loss tangent,  $\tan\delta$ , of the DGEBA-DDM thermoset during its isothermal curing were measured for a fixed frequency of 1kHz. These data are plotted against the curing time in Figure 3.1 for three different  $T_{\text{cure}}$ s, the temperatures of curing, from 303K to 341K. The plots show that  $\epsilon'$  monotonically decreases on curing and that  $\epsilon''$  and  $\tan\delta$  initially decrease, and then go through a minimum value which is followed by a peak. All the three quantities ultimately decrease to low values characteristic of an amorphous polymer. The plots also show that as the curing temperature is increased, the permittivity at the beginning of the cure, or at  $t \approx 0$ , decreases, and  $\epsilon''$  and  $\tan\delta$  increase. The increase in the latter two quantities correspond to an increase in the dc conductivity,  $\sigma_0$ . Furthermore, the increase in the  $T_{\text{cure}}$  causes the  $\epsilon''$  and  $\tan\delta$  peaks to decrease and the peak positions to shift to shorter times.

The corresponding plots for the DGEBA-DDS thermoset are shown in Figure 3.2. As evident, in the plots, the dielectric features observed for this thermoset are qualitatively similar to those observed with the DGEBA-DDM thermoset as shown in Figure 3.1, but they differ in that the  $\epsilon''$  and  $\tan\delta$  peaks are

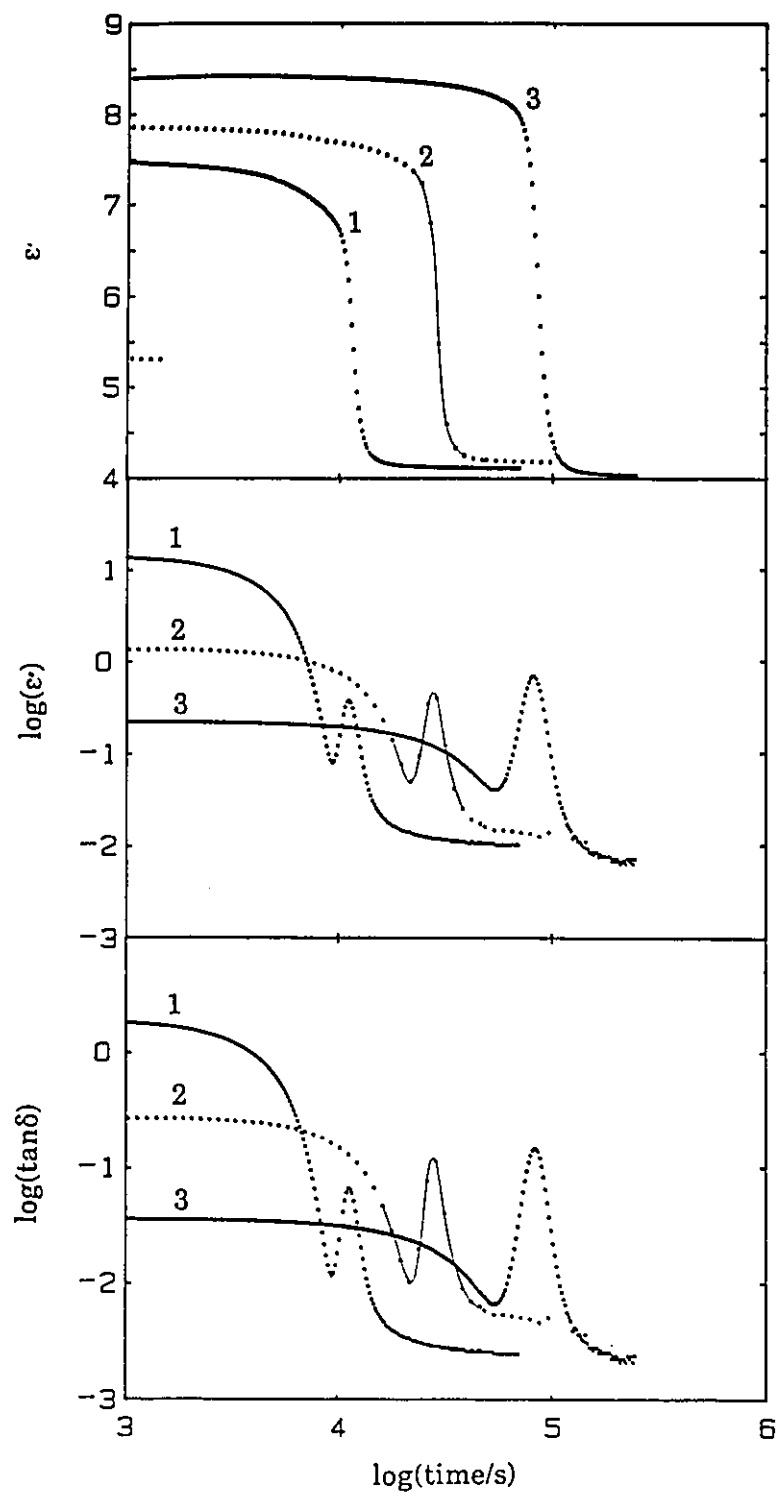


**Figure 3.1:** The dielectric permittivity, loss and loss tangent of the DGEBA-DDM thermoset measured at 1kHz are plotted against time.  $T_{cure}$  for curves labelled 1, 2 and 3 are 340.9K, 322.0K and 303.5K, respectively.

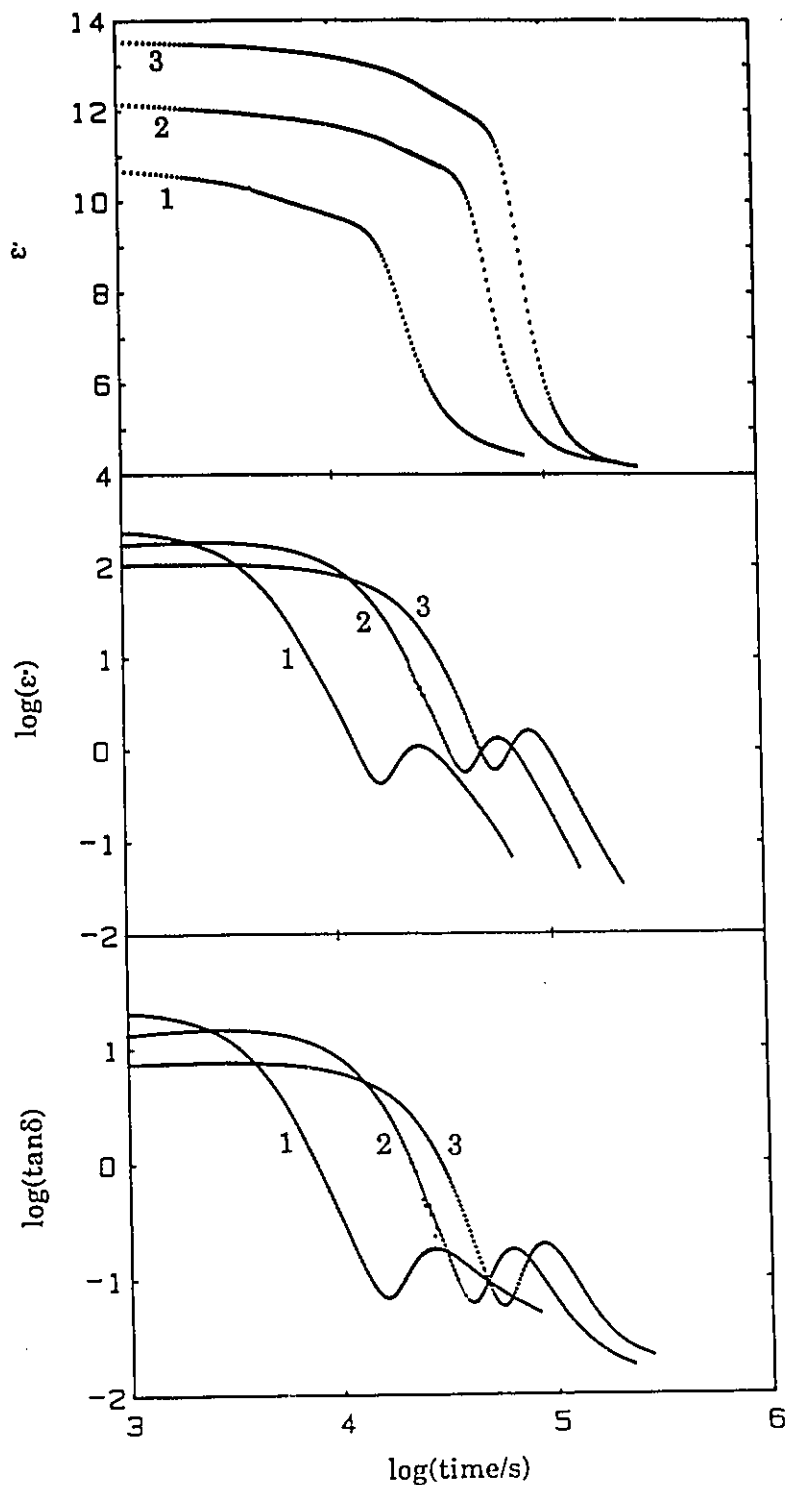


**Figure 3.2:** The dielectric permittivity, loss and loss tangent of the DGEBA-DDS thermoset measured at 1kHz are plotted against time.  $T_{\text{cure}}$  for curves labelled 1, 2 and 3 are 412.0K, 387.2K and 377.3K, respectively.

significantly broader and the values of  $\epsilon'$ ,  $\epsilon''$  and  $\tan\delta$  at the beginning of the cure are all higher than the corresponding values observed in Figure 3.1 for the DGEBA-DDM thermoset. Furthermore, in contrast with the observations for the DGEBA-DDM thermoset, the DGEBA-DDS thermoset shows a second dispersion or a step like decrease in  $\epsilon'(t)$  at short curing times, or early during the cure.

Electrode polarization effects responsible for the large decrease in  $\epsilon'$  with time near the beginning of the curing process at  $T_{\text{cure}}$  and the concomitant peak in  $\epsilon''$  that have been observed by earlier workers (Sheppard, Jr., et al 1984 and Figure 21 in Senturia and Sheppard 1986), were not observed in this study. Electrode polarization effects may account for the small dispersion in  $\epsilon'$  observed at shorter times only in our study of the DGEBA-DDS thermoset, which exhibits a higher dc conductivity than DGEBA-DDM, as is evident from a comparison of their respective  $\epsilon''$  values in Figures 3.1 and 3.2. Nevertheless, this dispersion in  $\epsilon'$  is insignificantly small in comparison with the large dispersion observed at longer times and therefore is not considered further here.

The  $\epsilon'$  and  $\epsilon''$  values, which were measured for a fixed frequency of 1kHz during the curing process at a given  $T_{\text{cure}}$ , are plotted in a complex plane in Figure 3.3. The figure includes data for both the DGEBA-DDM and DGEBA-DDS thermosets. These plots show the changes with time in the  $\epsilon'$  and  $\epsilon''$  which occur during the process of isothermal curing at longer curing times. The shape of the complex plane plots in Figure

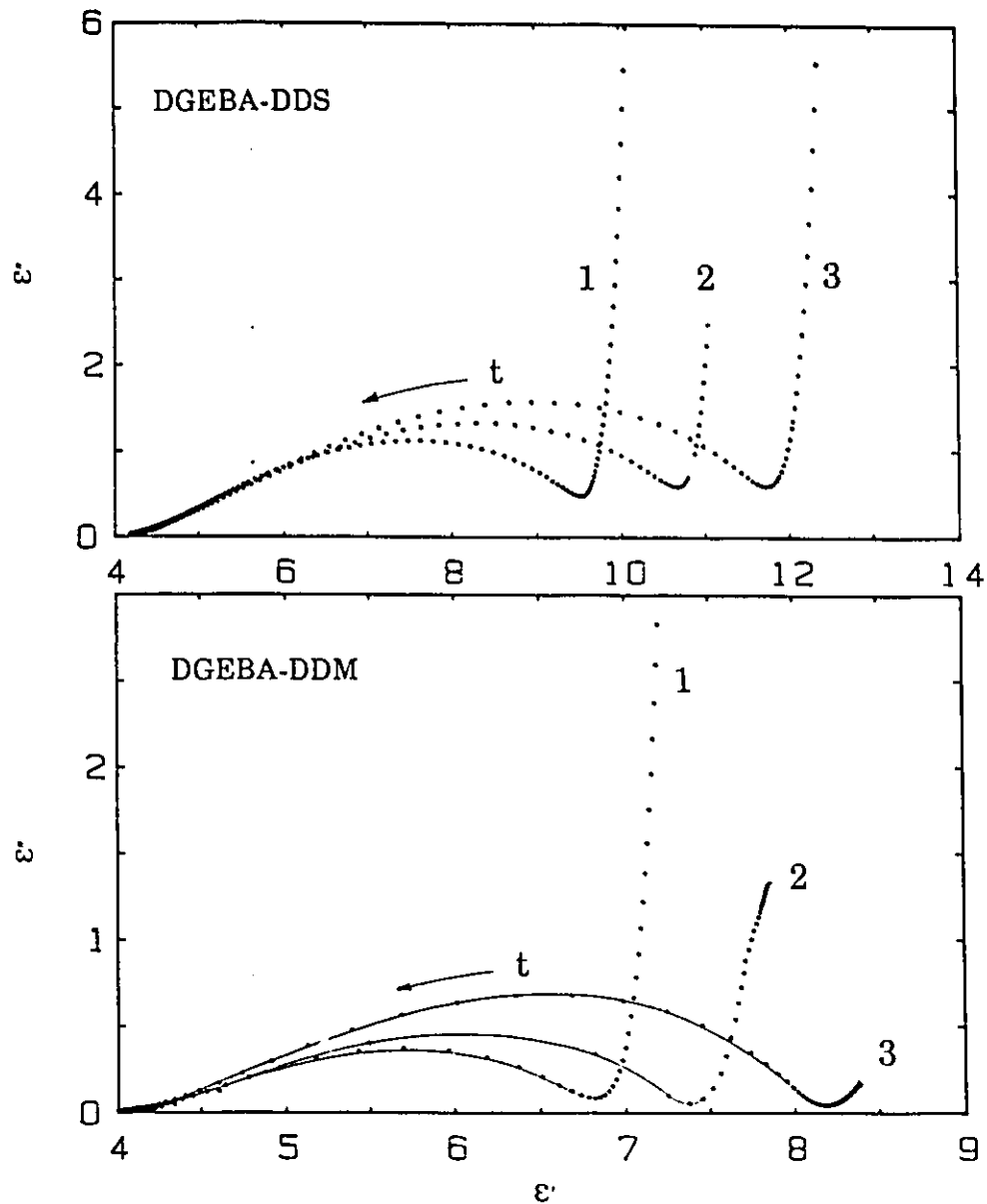


**Figure 3.3:** The complex plane plots of  $\epsilon'(t)$  and  $\epsilon''(t)$  measured at a frequency of 1kHz at different temperatures for the DGEBA-DDM and DGEBA-DDS thermosets.  $T_{\text{cure}}$  for curves labelled 1, 2 and 3 are the same as in Figures 3.1 and 3.2.

3.3 is skewed (from the shape of a circular arc) at both the short and the long curing time regions, with a greater skew at longer times where  $\epsilon'$  approaches  $\epsilon'(\infty)$ , the infinite time limit of  $\epsilon'$  during the cure.

The curing time at which  $\epsilon''$  reaches its peak value for a fixed frequency of 1kHz,  $t_{\text{cure}}(\epsilon''_m)$ , was determined from the plots in Figures 3.1 and 3.2 and its value given in Table 3.1 is plotted against the reciprocal  $T_{\text{cure}}$  for the two thermosets in Figure 3.4. The plots are linear for the two sets of data, each of which was obtained on a separate sample of the thermoset. The consistency of these observations confirms the essential correctness of our experimental procedure and the reproducibility of the data, but more importantly, the plots in Figure 3.4 show that  $t_{\text{cure}}(\epsilon''_m)$  linearly increases with an increase in  $T_{\text{cure}}^{-1}$ . Since  $t_{\text{cure}}(\epsilon''_m)$  in this plot represents the time at which the relaxation rate of the thermoset corresponds to 1kHz, it can be regarded as the time of cure for which the occurrence of chemical reactions has produced, in each thermoset, cross-linked networks which are indistinguishable in their average dielectric relaxation rates. Therefore, the slope of the plots represents an activation energy for that chemical reaction whose products control the features of the dipolar relaxation process through an increase in the chain length or the number of cross-links. The plots, shown in Figure 3.4(a), follow an equation  $t(\epsilon''_m) = t_0 \exp(E/RT)$  which seems analogous to an Arrhenius equation. The plots in Figure 3.4 were thus used to calculate the values of  $t_0$  and  $E$ , which

Table 3.1: The features of the dielectric behaviour of the DGEBA-DDM and DGEBA-DDS thermosets during their isothermal cure at several temperatures.

| thermosets | T/K   | $t(\epsilon''_m)/ks$ | $\epsilon'(0)$ | $\Delta\epsilon$ | $\epsilon''_m$ | $M_w \times 100$ |
|------------|-------|----------------------|----------------|------------------|----------------|------------------|
| DGEBA-DDM  | 303.5 | 83                   | 8.42           | 3.80             | .670           |                  |
|            | 312.6 | 54                   | 8.39           | 3.65             | .597           |                  |
|            | 322.0 | 28                   | 7.78           | 2.95             | .420           |                  |
|            | 331.0 | 18                   | 7.57           | 2.70             | .400           |                  |
|            | 340.9 | 11.2                 | 7.50           | 2.50             | .365           | 13.8             |
| DGEBA-DDS  | 377.3 | 79.4                 | 13.7           | 7.30             | 1.56           | 8.1              |
|            | 387.2 | 57.0                 | 12.3           | 6.30             | 1.31           | 8.8              |
|            | 400.6 | 34.7                 | 11.0           | 5.80             | 1.30           |                  |
|            | 412.9 | 24.4                 | 11.6           | 5.20             | 1.10           | 9.9              |

Table 3.2: The features of the dielectric behaviour of the DGEBA-(xDDS, (1-x)DDM) thermosets during their isothermal curing at  $377 \pm 2K$ .

| x   | $\epsilon''_{min}$ | $t_{min}(ks)$ | $\epsilon''_{max}$ | $t_{max}(ks)$ | T/K   | $M_w \times 10_2$ |
|-----|--------------------|---------------|--------------------|---------------|-------|-------------------|
| 0   | 0.353              | 2.08          | 0.495              | 2.50          | 375.0 | 15.1              |
| 0.1 | 0.426              | 2.50          | 0.636              | 3.02          | 377.3 | 14.2              |
| 0.3 | 0.455              | 2.60          | 0.807              | 4.20          | 379.7 | 12.1              |
| 0.5 | 0.544              | 6.00          | 0.978              | 13.7          | 376.4 | 11.1              |
| 0.7 | 0.625              | 18.9          | 1.297              | 33.5          | 375.6 | 9.5               |
| 0.9 | 0.966              | 40.6          | 1.526              | 57.0          | 377.8 | 8.8               |
| 1.0 | 0.654              | 55.0          | 1.560              | 79.4          | 377.3 | 8.0               |

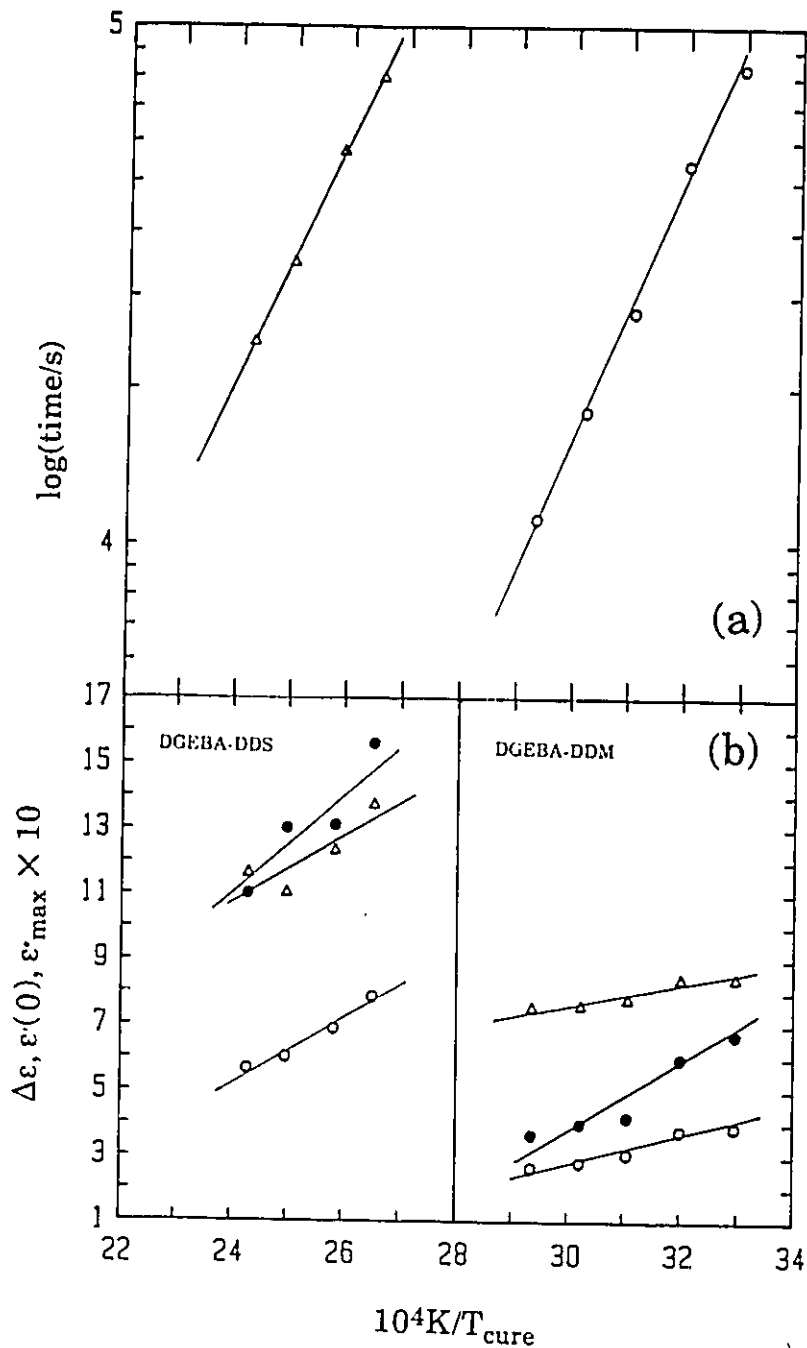


Figure 3.4: (a) The curing time at which  $\epsilon''$  measured at 1kHz reaches a maximum value is plotted against the reciprocal curing temperature for the (o) DGEBA-DDM and ( $\Delta$ ) DGEBA-DDS thermosets. (b) A plot of (o)  $\Delta\epsilon$ , ( $\bullet$ )  $\epsilon''_{\text{max}}$  and ( $\Delta$ )  $\epsilon'(0)$  against the reciprocal temperature for the DGEBA-DDM and DGEBA-DDS thermosets.

gave  $t_0=668\mu\text{s}$  and  $E=47.1\text{kJ/mole}$  for the DGEBA-DDM thermoset and  $t_0=56.4\text{ms}$  and  $E=44.5\text{kJ/mole}$  for the DGEBA-DDS thermoset.

In order to determine the changes in the dielectric relaxation parameters with changing temperature of the isothermal cure,  $\epsilon'(0)$ , the decrease in  $\epsilon'$  on curing or  $\Delta\epsilon$ , and the height of the  $\epsilon''$  peak for both thermosets are given in Table 3.1 and are plotted against the reciprocal curing temperature in Figure 3.4(b). Within experimental uncertainty, these plots are also linear, and show that the decrease in  $\epsilon'(0)$ ,  $\Delta\epsilon$  and  $\epsilon''_m$  with increasing  $T_{\text{cure}}$  follows a general relationship of the type  $p \propto T_{\text{cure}}^{-1}$ , where  $p$  denotes the values of  $\epsilon'(0)$ ,  $\Delta\epsilon$  or  $\epsilon''_m$ .

### 3.1.2 ISOTHERMAL SPECTRUM STUDIES

In an attempt to obtain the isothermal spectra of dielectric relaxation, or the frequency dependence of  $\epsilon^*$ , at several predetermined curing times, the  $\epsilon'$  and  $\epsilon''$  of the thermoset samples were measured at various frequencies at fixed intervals during the isothermal curing process at a selected  $T_{\text{cure}}$ . For these measurements, the equipment required calibration for each frequency of measurements and this procedure raised the time needed to complete a full scan in frequency to about 15 minutes. The requirements for accuracy in such measurements therefore restricted the frequency range measurements to about three decades from 30Hz to 20kHz. Since the thermosetting reactions continuously occur, it was necessary to seek a compromise between selecting

closely spaced measuring frequencies, so as to obtain data points, in the frequency plane, which could provide a well-defined spectrum, and fewer frequencies so as to obtain for each frequency more data points in the time plane. It was decided to obtain spectra for nineteen frequencies. So, although the  $\epsilon'$  and  $\epsilon''$  for the DGEBA-DDM thermoset were measured at nineteen different frequencies during its curing at 340.9K, for the sake of clarity, data for only six of these frequencies are plotted in Figures 3.5 and 3.6. These plots show that the time required for the dielectric loss to reach its maximum value decreases with an increase in the ac frequency of the dielectric measurement. Furthermore, the plots show that  $\epsilon'$  undergoes, at short curing times, a second dispersion, and the low frequency value of  $\epsilon'$  increase with the decrease in the frequency of measurement. This initial dispersion in  $\epsilon'$  remains small as compared with the prominent dipolar dispersion which is observed at longer curing times. The value of  $\epsilon''$  at  $t_{\text{cure}} = 0$  also increases with a decrease in frequency. Since, early in the cure, the dielectric loss is only due to the dc conductivity, its value is expected to increase in proportion to the reciprocal frequency according to eqn. (1.25). This agrees with our observation in Figure 3.6 where  $\epsilon''$  increases with decreasing frequency.

The time during which the dipolar peak at 340.9K appeared was too short to allow measurements for more than four data points per frequency. A lower curing temperature of 331.0K

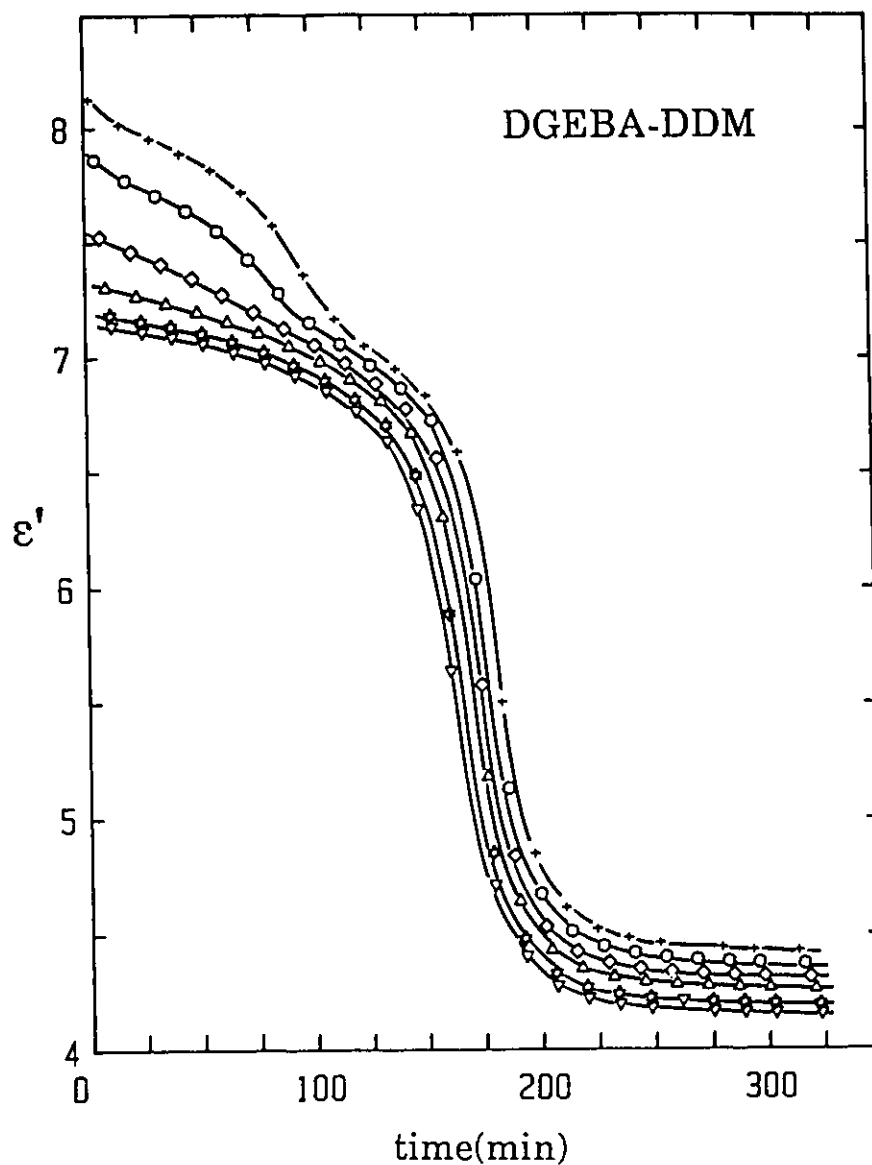


**Figure 3.5:** The dielectric permittivity of the DGEBA-DDM thermoset measured at ( $\nabla$ )20, ( $*$ )10, ( $\Delta$ )3, ( $\diamond$ )1, ( $\circ$ )0.3 and ( $+$ )0.1kHz is plotted against the time of cure at 340.9K.

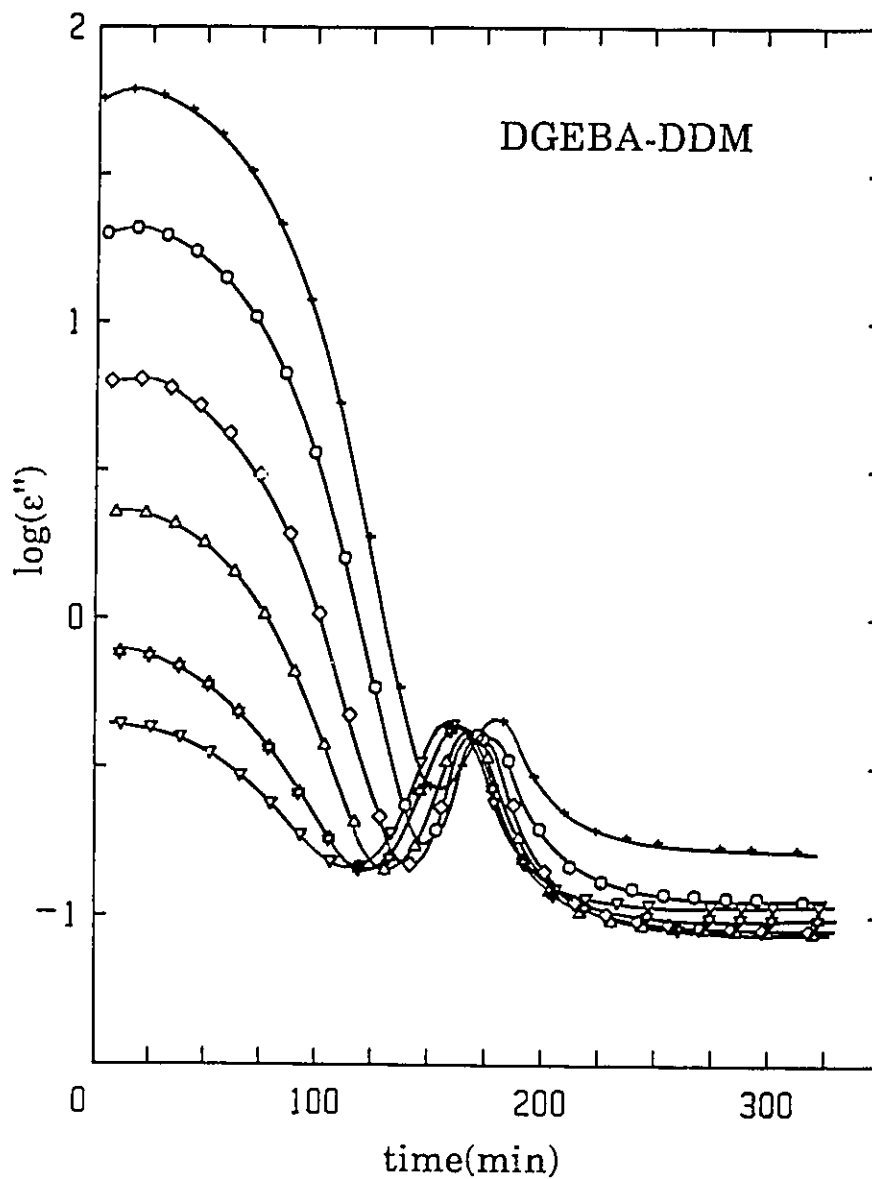


**Figure 3.6:** The dielectric loss of the DGEBA-DDM thermoset measured at ( $\nabla$ )20, ( $\odot$ )10, ( $\Delta$ )3, ( $\circ$ )0.3 and (+)0.1kHz is plotted against the time of cure at 340.9K.

was therefore selected, and the measurements of  $\epsilon'$  and  $\epsilon''$  were repeated. The frequency was kept constant at 1kHz for the first 200 minutes and thereafter measurements for the isothermal spectra were made. The results of the measurements are plotted against time in Figure 3.7. Although the data for each frequency in Figure 3.7 are not closely spaced, the number of points corresponding to the dipolar dispersion seems adequate and this allows us to obtain isothermal dielectric loss spectra of the DGEBA-DDM thermoset at a "fixed time" by interpolating the  $\epsilon''$  values along a vertical cut near the  $\epsilon''$  peak. The procedure allows the determination of the  $\epsilon^*(\omega)$  only at limited number of measurement frequencies, at a fixed interval of isothermal cure, and therefore the time-dependence of the complete shape of the Cole-Cole plot of  $\epsilon^*(\omega)$  can not be determined. Instead, we have chosen to plot, in Figure 3.8, logarithmically the frequency,  $f_{\frac{1}{2}}(t)$  at which the measurements were made at the curing temperature of 331K against that time during the cure when the decrease in  $\epsilon'$  reached half of its total decrease. An analysis of this plot showed that the frequency  $f_{\frac{1}{2}}$ , can be described by the equation:

$$f_{\frac{1}{2}}(t) = f_{\frac{1}{2}}(0)\exp(-kt_{\text{cure}}) \quad (3.1)$$

where  $f_{\frac{1}{2}}(0)$  and  $k$  are constants and  $t_{\text{cure}}$  is the curing time.

Similar measurements were obtained with the DGEBA-DDS thermoset which was cured at 448.3K. The  $\epsilon'$  and  $\epsilon''$  for this thermoset were also measured at nineteen frequencies but, for the sake of clarity, only five of these frequencies are

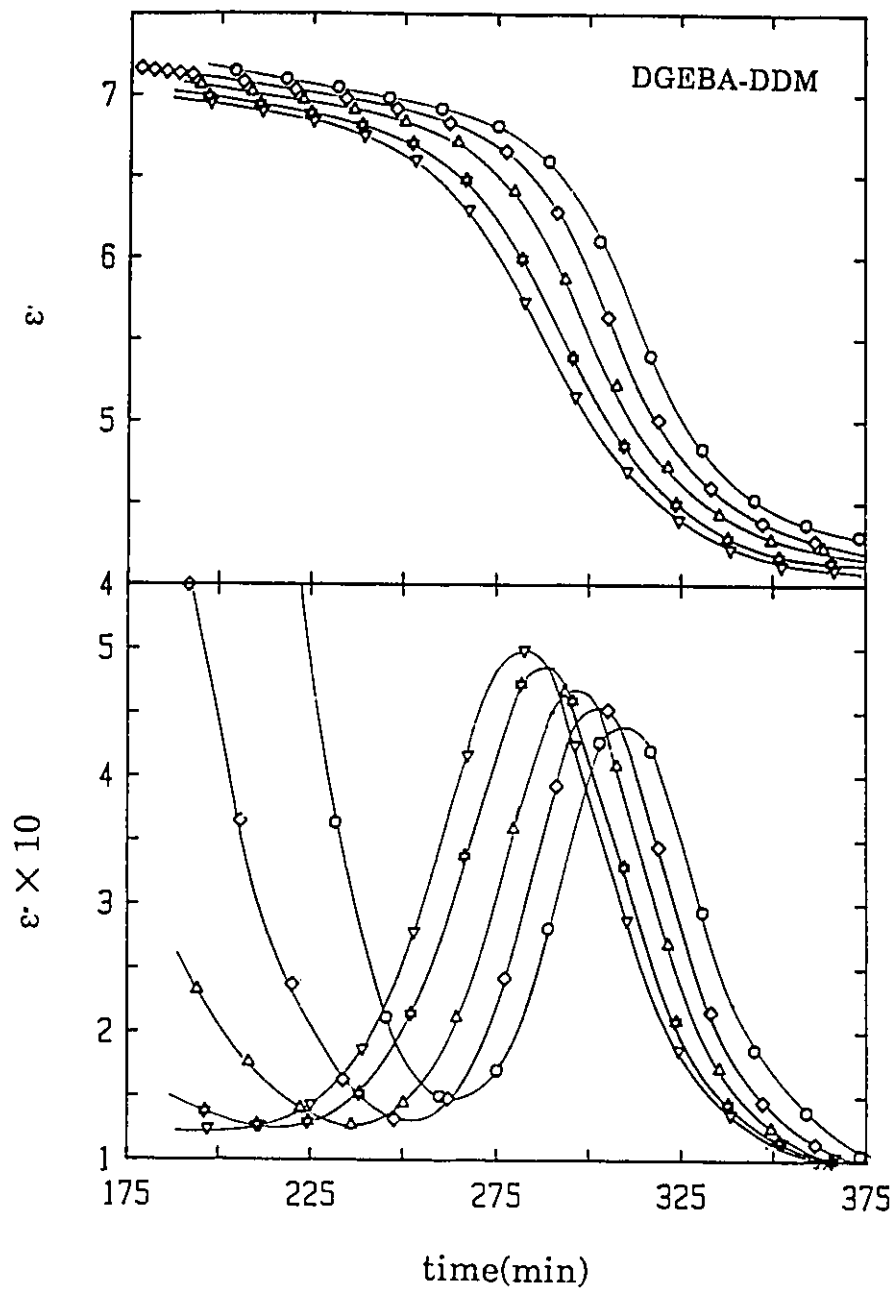


**Figure 3.7:** The dielectric permittivity and loss of the DGEBA-DDM thermoset measured at ( $\nabla$ ) 20, ( $\otimes$ ) 10, ( $\Delta$ ) 3, ( $\diamond$ ) 1 and (o) 0.3 kHz are plotted against the time of cure at 331K.

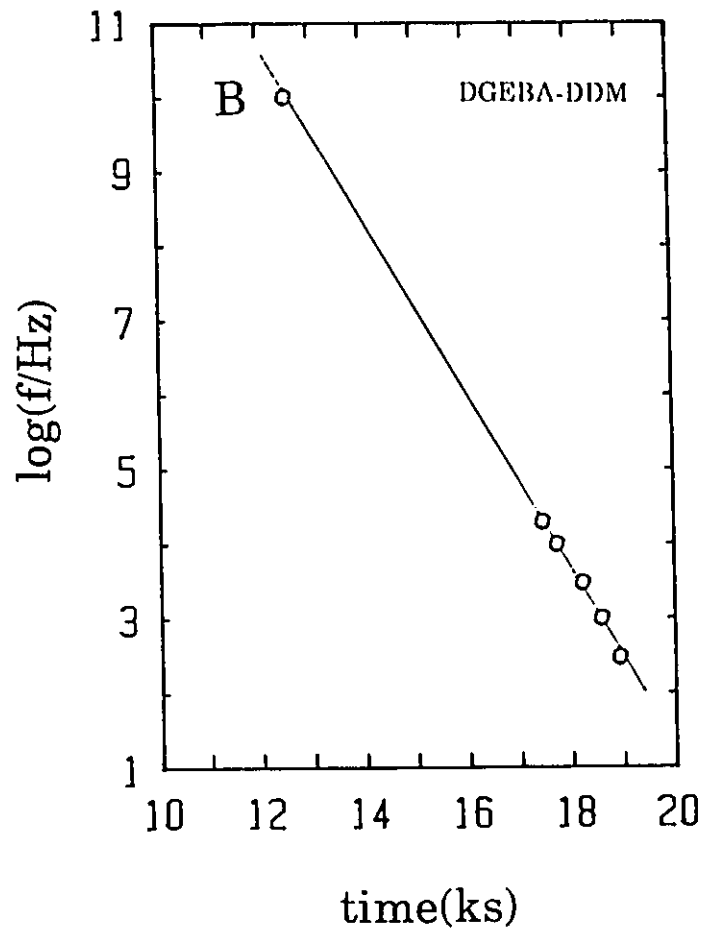


**Figure 3.8:** A plot of the curing time to achieve half of the total decrease in  $\epsilon'$  for the DGEBA-DDM thermoset at 331K. The data labelled B is obtained from Brillouin scattering and refers to the corresponding time for an increase in the velocity of sound.

plotted against time in Figures 3.9 and 3.10. In these plots, the curves obtained at higher frequencies are qualitatively similar to those observed for the DGEBA-DDM thermoset. However, at lower frequencies, the  $\epsilon''$  peak is seen to diminish gradually and merge into an increasing background level. Correspondingly,  $\epsilon'$  is seen to increase and then decrease in the time range corresponding to the  $\epsilon''$  peak. These features are due to a high level of ionic conduction which causes the space charge polarization to contribute at low frequencies. These effects seemed too large and prevented us from performing a further analysis of the dipolar relaxation behaviour on the DGEBA-DDS thermoset.

### 3.2 BRILLOUIN SCATTERING STUDY

Typical isothermal frequency spectra of the DGEBA-DDM thermoset cured at 324K which were measured after eight different periods of cure are shown in Figure 3.11. The figure shows that during the period of 27.45h, the Brillouin frequency shift,  $f_B$ , increases with time from 8 to 12GHz while its linewidth,  $\Gamma_B$ , decreases from 2.0 to 0.7GHz. Using the Rayleigh peak of the last spectrum recorded (corresponding to an almost fully cured thermoset) as a resolution function, the Brillouin frequencies and widths of all the spectra were obtained by least-square fitting of the Lorentzian profiles.

The values of the measured Brillouin frequency shift,  $f_B$ , and the full width at half height,  $\Gamma_B$ , were used to obtain the sound velocity,  $v$ , and absorption coefficient,  $\alpha$ , according to

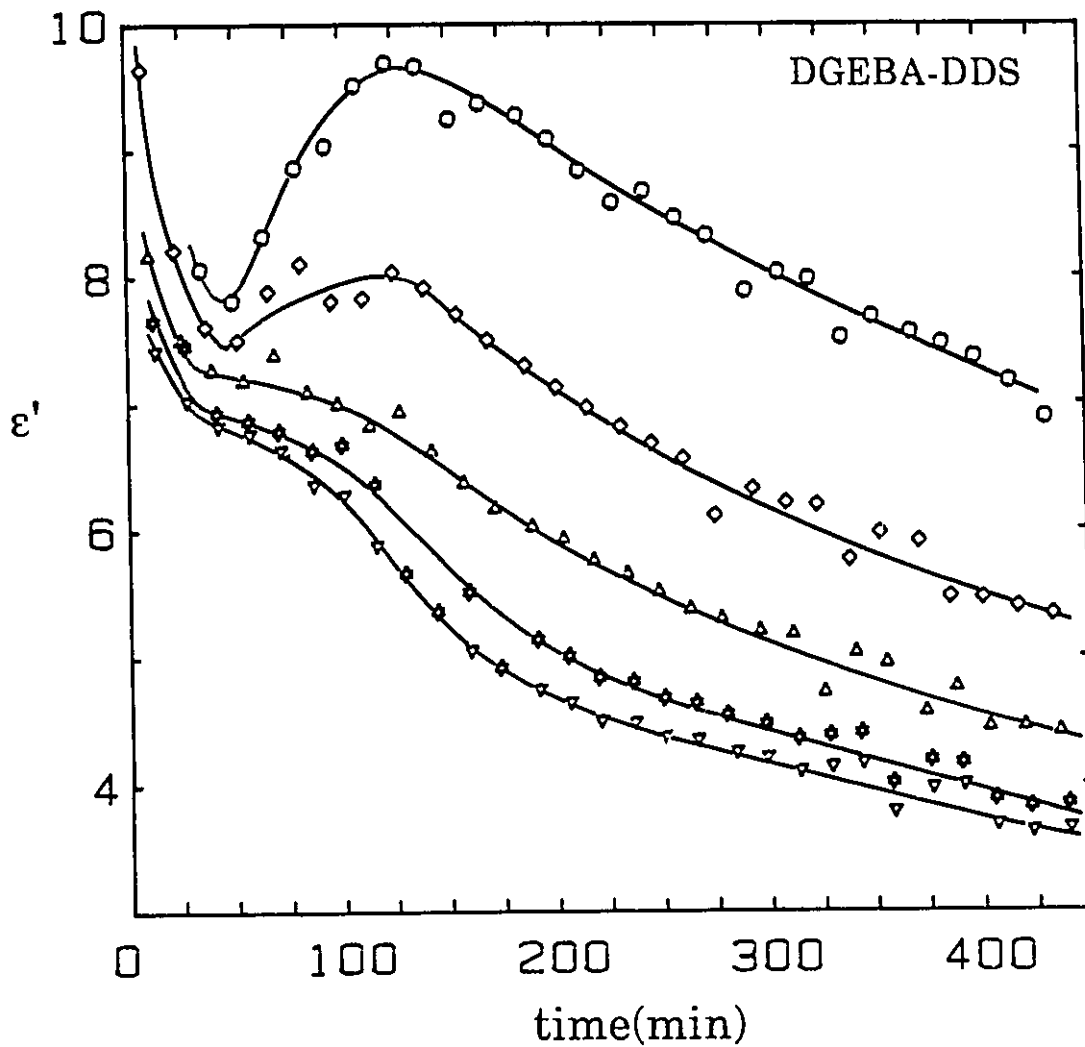


Figure 3.9: The dielectric permittivity of the DGEBA-DDS thermoset measured at ( $\nabla$ )20, ( $\ast$ )10, ( $\Delta$ )3, ( $\diamond$ )1 and ( $\circ$ )0.3kHz is plotted against the time of cure at 448.3K.

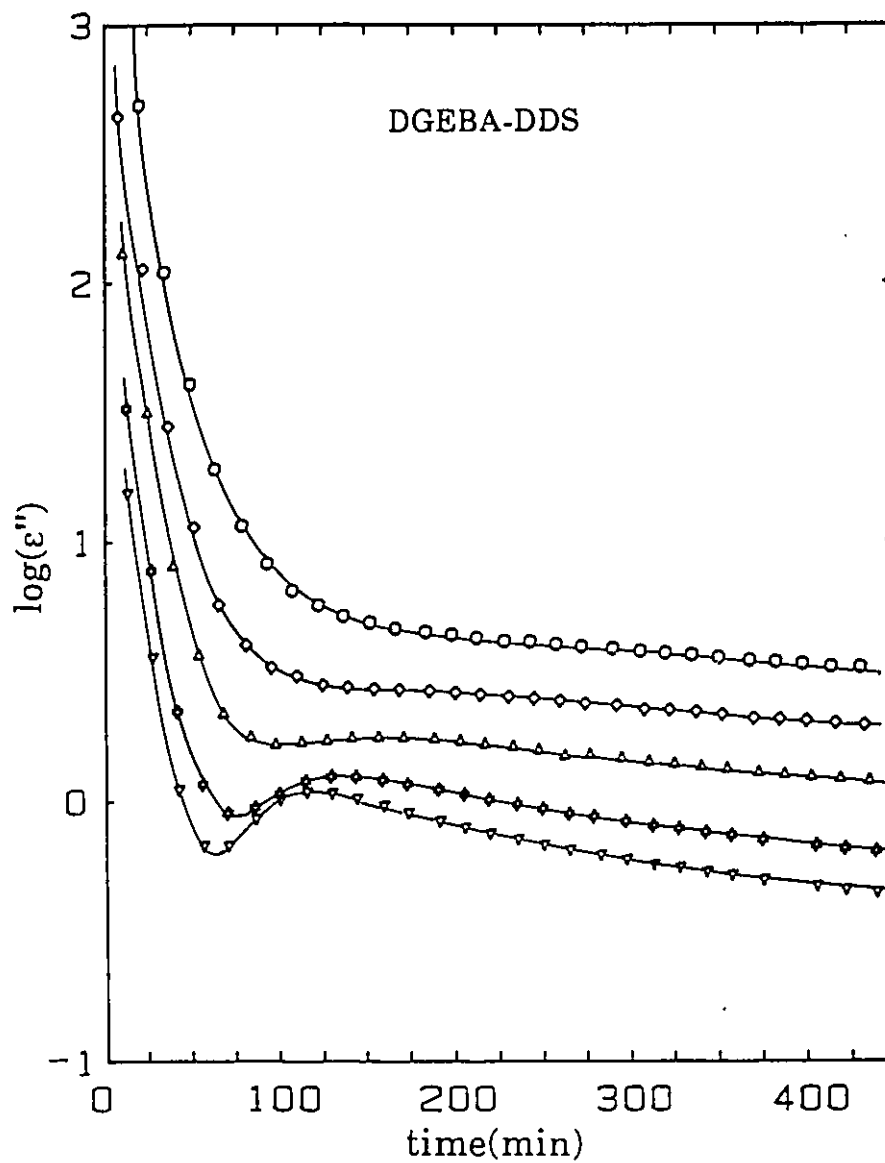
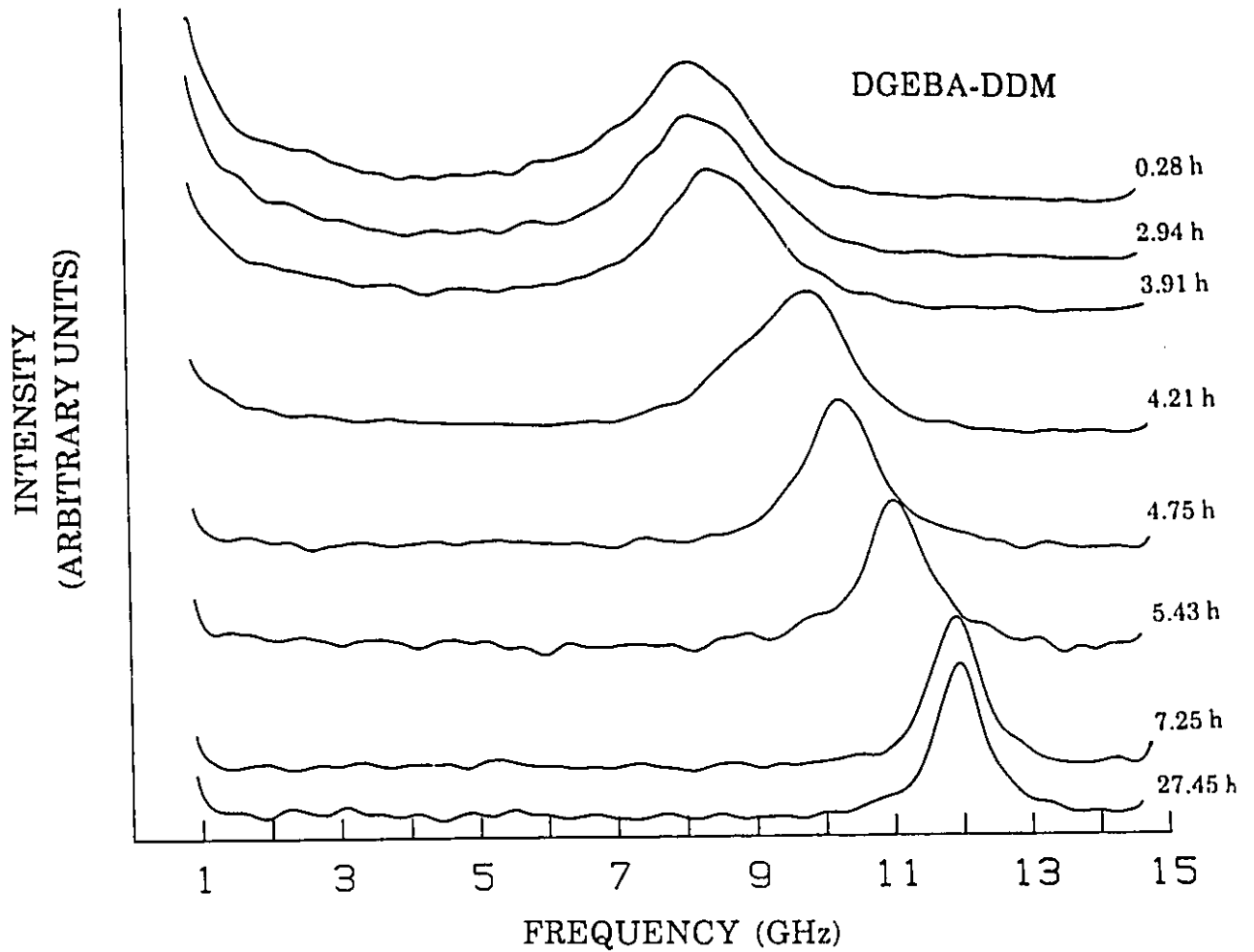


Figure 3.10: The dielectric loss of the DGEBA-DDS thermoset measured at ( $\nabla$ )20, ( $\diamond$ )10, ( $\Delta$ )3, ( $\diamond$ )1 and ( $\circ$ )0.3kHz is plotted against the time of cure at 448.3K.



**Figure 3.11:** The Brillouin intensity spectrum during the curing or crosslinking of the DGEBA-DDM thermoset at 324K. Legends next to the curves are the times after which the spectrum was measured.

the following relationships (Sandercock 1982):

$$v = f_b \lambda_o / 2n \sin(\theta/2) \quad (3.2)$$

$$\alpha = 2\pi\Gamma_b/v \quad (3.3)$$

where  $\lambda_o$  is the wavelength of the incident light ( $\lambda_o=514.5\text{nm}=c/f_o$ , see eqn. (2.12)),  $\theta$  the scattering angle ( $\theta=90^\circ$ ) and  $n$  the refractive index of the medium. Values of  $n$  for the thermosets studied are not known but the index of refraction of DGEBA mixed with *m*-phenylenediamine was found by Dannenberg (1959) to increase from a value of 1.5635 to 1.6055 on curing. This represents a change of less than 3% on curing. Therefore, we chose to plot the values of  $nv$  and  $\alpha/n$  as a function of logarithmic time of cure in Figures 3.12 and 3.13, respectively, for the DGEBA-DDM thermoset during its curing at different temperatures. The corresponding Brillouin spectra and plots of  $nv$  and  $\alpha/n$  during the curing of DGEBA-DDS thermoset at different temperatures are shown in Figures 3.14, 3.15 and 3.16, respectively. In figures 3.12, 3.13, 3.15 and 3.16, both a decrease in  $\alpha/n$  and increase of  $nv$  become detectable after a certain time  $t_1$ , from the beginning of the curing process, and thereafter both  $\alpha/n$  and  $nv$  reach a stable value after a certain time  $t_2$ . The curing time  $t_{1/2}$  at which the product  $nv$  reaches half its total change is logarithmically plotted against the reciprocal temperature in Figure 3.17. The figures show that the data lie on a straight line of an Arrhenius-type equation

$$t_{1/2} = t_o \exp(E/RT) \quad (3.4)$$

for both systems. The values of  $t_o$  and  $E$  are 2.95ms and

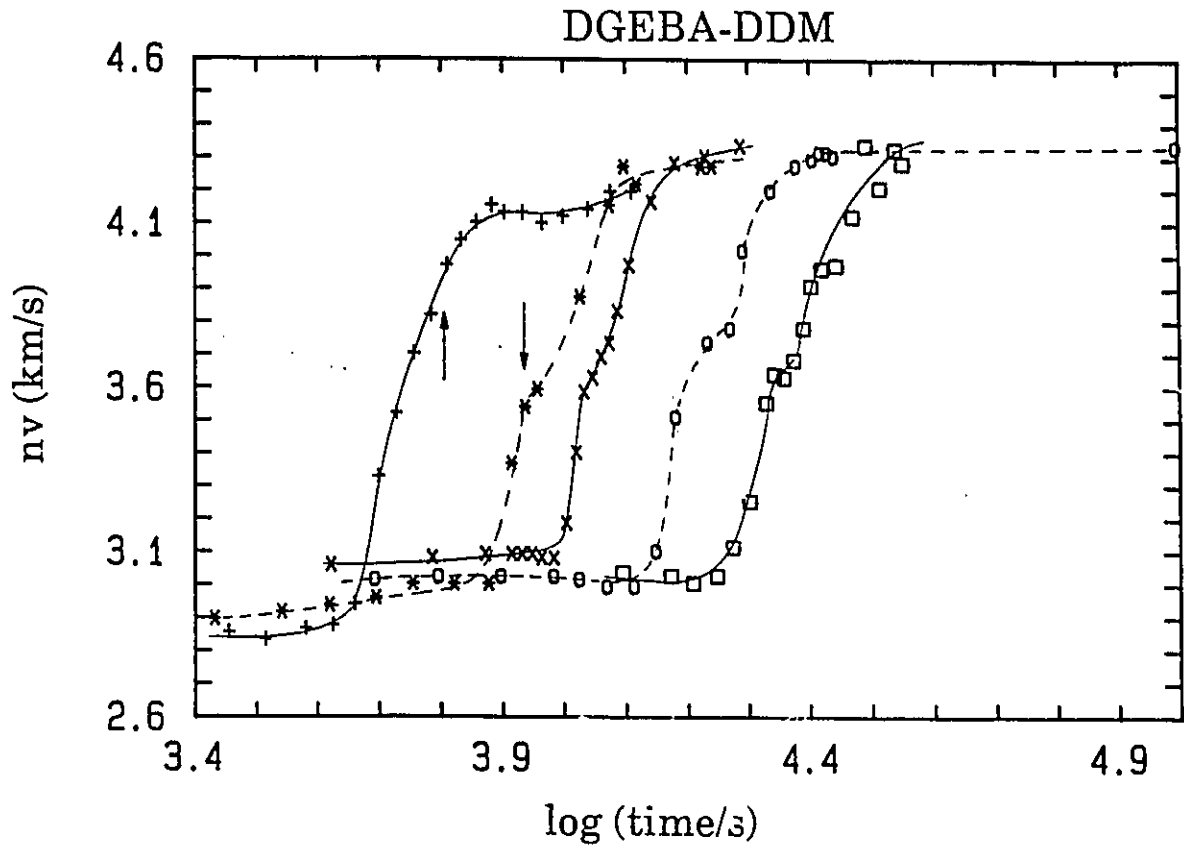


**Figure 3.12:** The product of the refractive index and velocity of hypersonic waves in the DGEBA-DDM thermoset plotted against the curing time. The curing temperatures are: (+)349K; (\*)339K; (X)334K; (O)324K; and (□)319K.

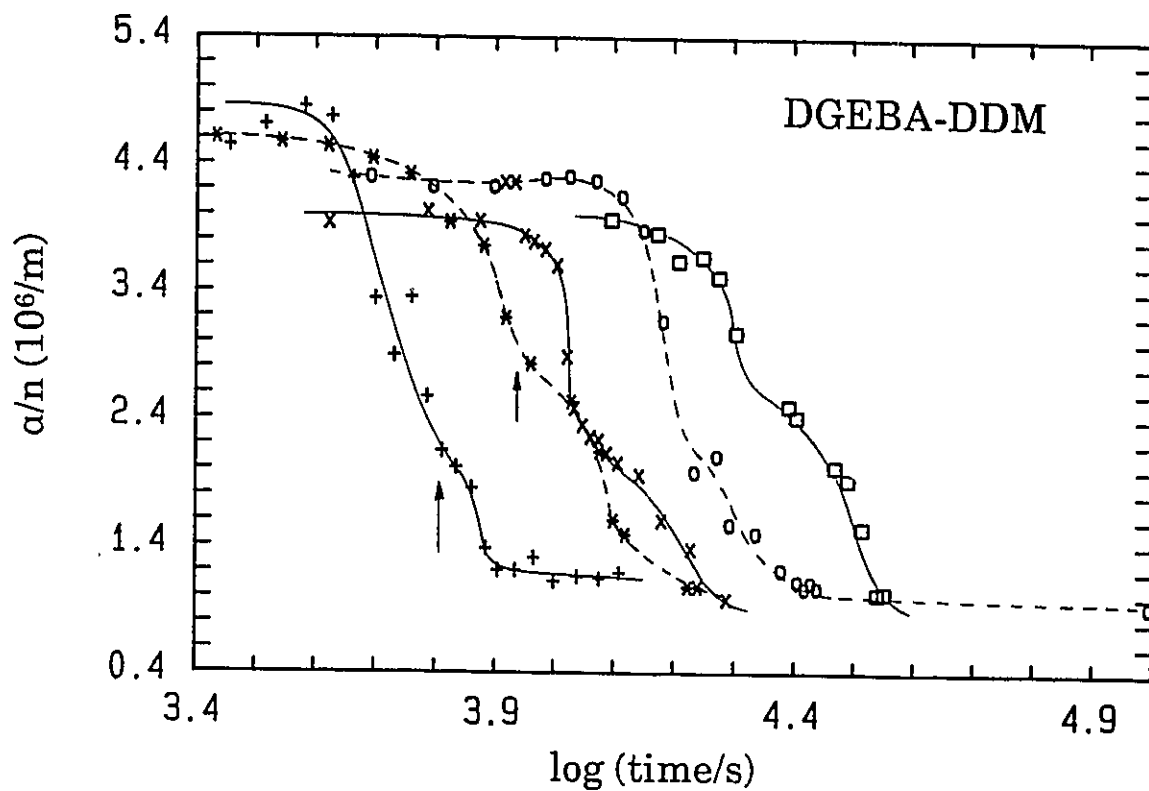
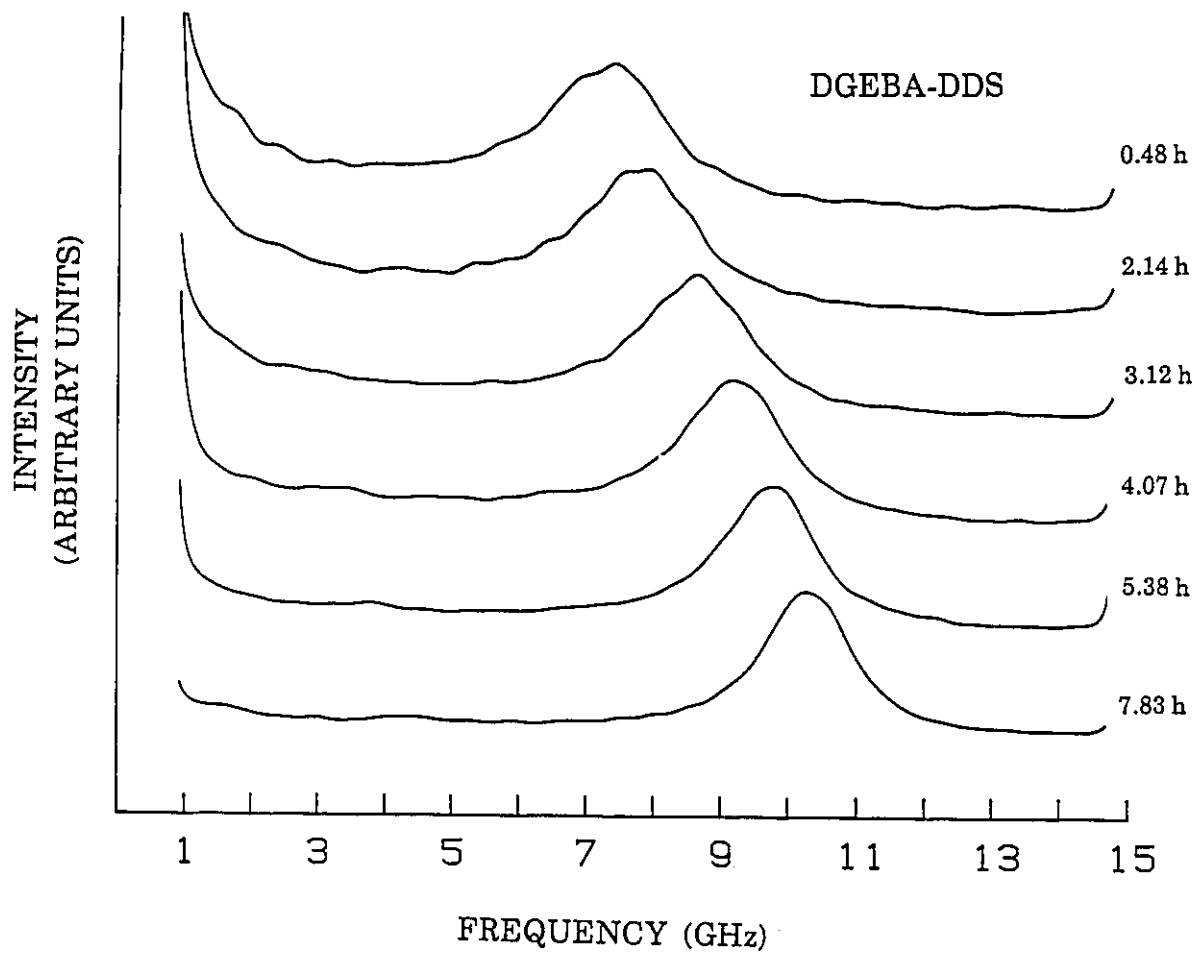
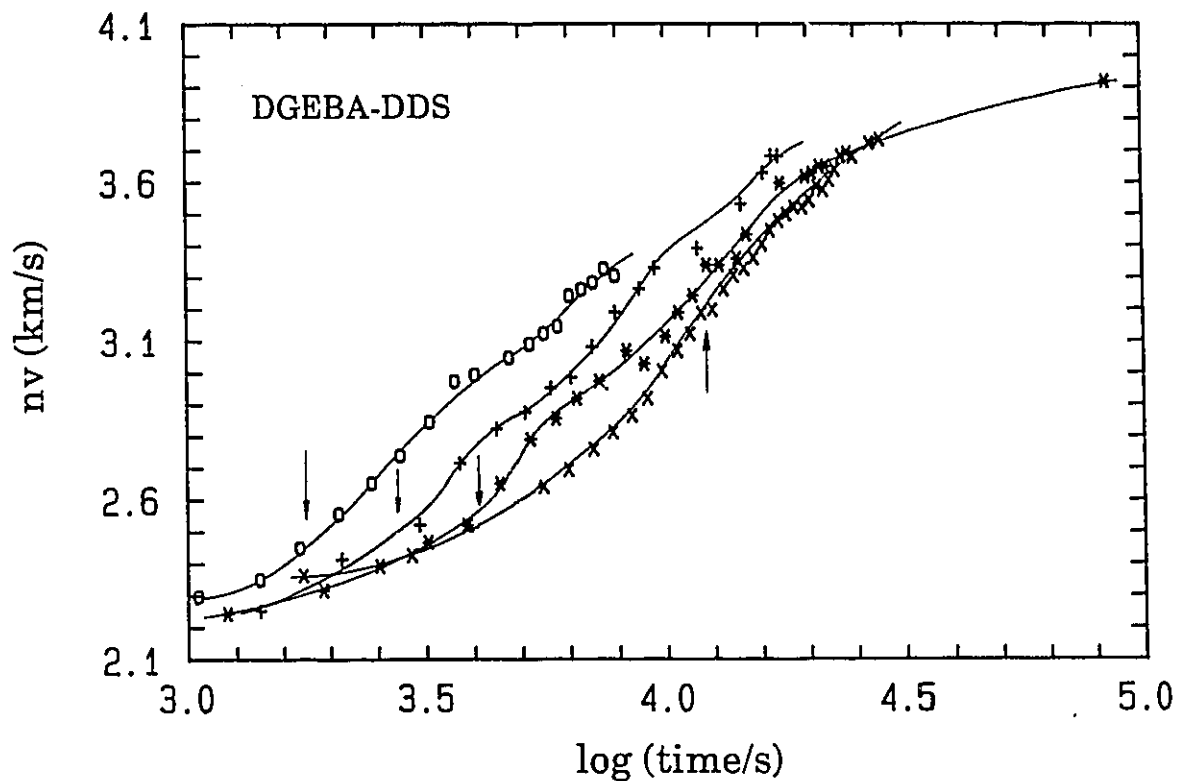


Figure 3.13: The ratio ( $\alpha/n$ ) of the attenuation to refractive index of hypersonic waves in the DGEBA-DDM thermoset plotted against the curing time. The curing temperature and notations are the same as in Figure 3.12.



**Figure 3.14:** The Brillouin intensity spectrum during the curing or cross-linking of the DGEBA-DDS thermoset at 401K. Legends next to the curves are the times after which the spectrum was measured.



**Figure 3.15:** The product of the refractive index and velocity of hypersonic waves in the DGEBA-DDS thermoset plotted against the curing time. The curing temperatures are: (O)444K; (+)433K; (\*)423K; and (X)401K.

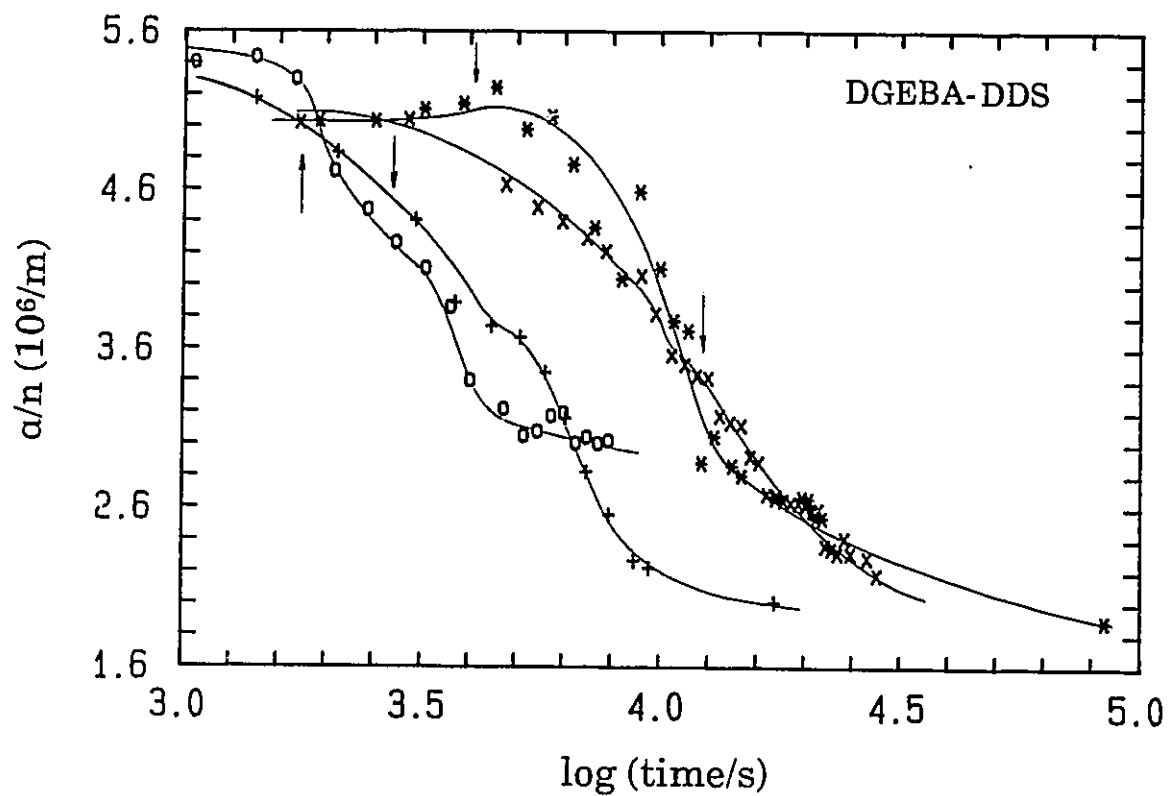
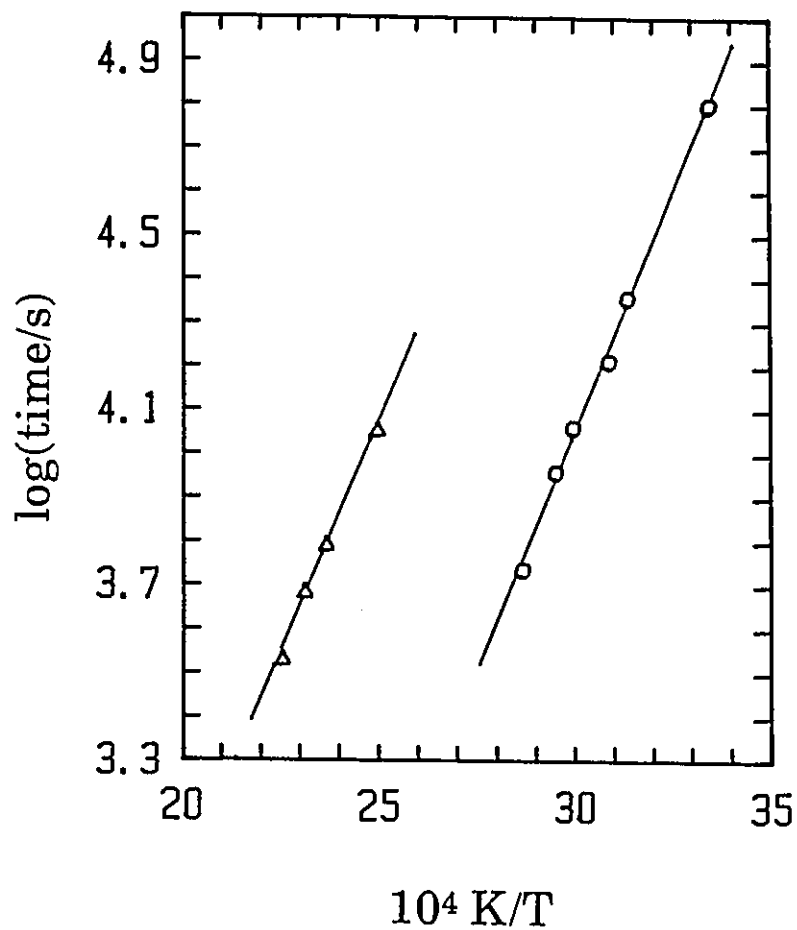


Figure 3.16: The ratio ( $\alpha/n$ ) of the attenuation to refractive index of hypersonic waves in the DGEBA-DDS thermoset plotted against the curing time. The curing temperatures and notations are the same as in Figure 3.15.



**Figure 3.17:** The Arrhenius plots of the time for the velocity (from Figures 3.12 and 3.15) to reach half its maximum value,  $t_{1/2}$ , for the (O) DGEBA-DDM and ( $\Delta$ ) DGEBA-DDS thermosets.

42.0kJ/mole, respectively, for the DGEBA-DDM thermoset, and 57.1ms and 40.7kJ/mol, respectively for the DGEBA-DDS thermoset.

### 3.3 THE EFFECTS OF SUBSTITUTION OF AMINES ON THE CURING KINETICS

The chemical kinetics of the curing of DGEBA-DDM and DGEBA-DDS thermosets are expected to be very different, as of course was shown by Dobas et al (1975). This is due to the differences between their  $k_1/k_2$  ratios where  $k_1$  and  $k_2$  are the chemical rate constants for the formation of secondary and tertiary amines, respectively, according to the reactions given in Figure 1.1. As evident in Figures 3.1 to 3.10, the dielectric behaviour of these thermosets during their curing process differs significantly, and these differences made it necessary to study the curing behaviour of DGEBA by systematically substituting DDM by DDS as the curing agent. Samples of thermosets were therefore prepared by mixing one mole of the mixed amines ( $x$  DDS,  $(1-x)$  DDM) with two moles of DGEBA, where the value of  $x$  was fixed as 0, 0.1, 0.3, 0.5, 0.7, 0.9 and 1.

The dielectric permittivity, loss, and loss tangent, which were measured for a fixed frequency of 1kHz at increasing intervals of time during the isothermal curing of the seven thermosets are plotted against the time of cure in Figure 3.18. The temperatures of the isothermal cure could not be exactly matched because of the time constraint and the

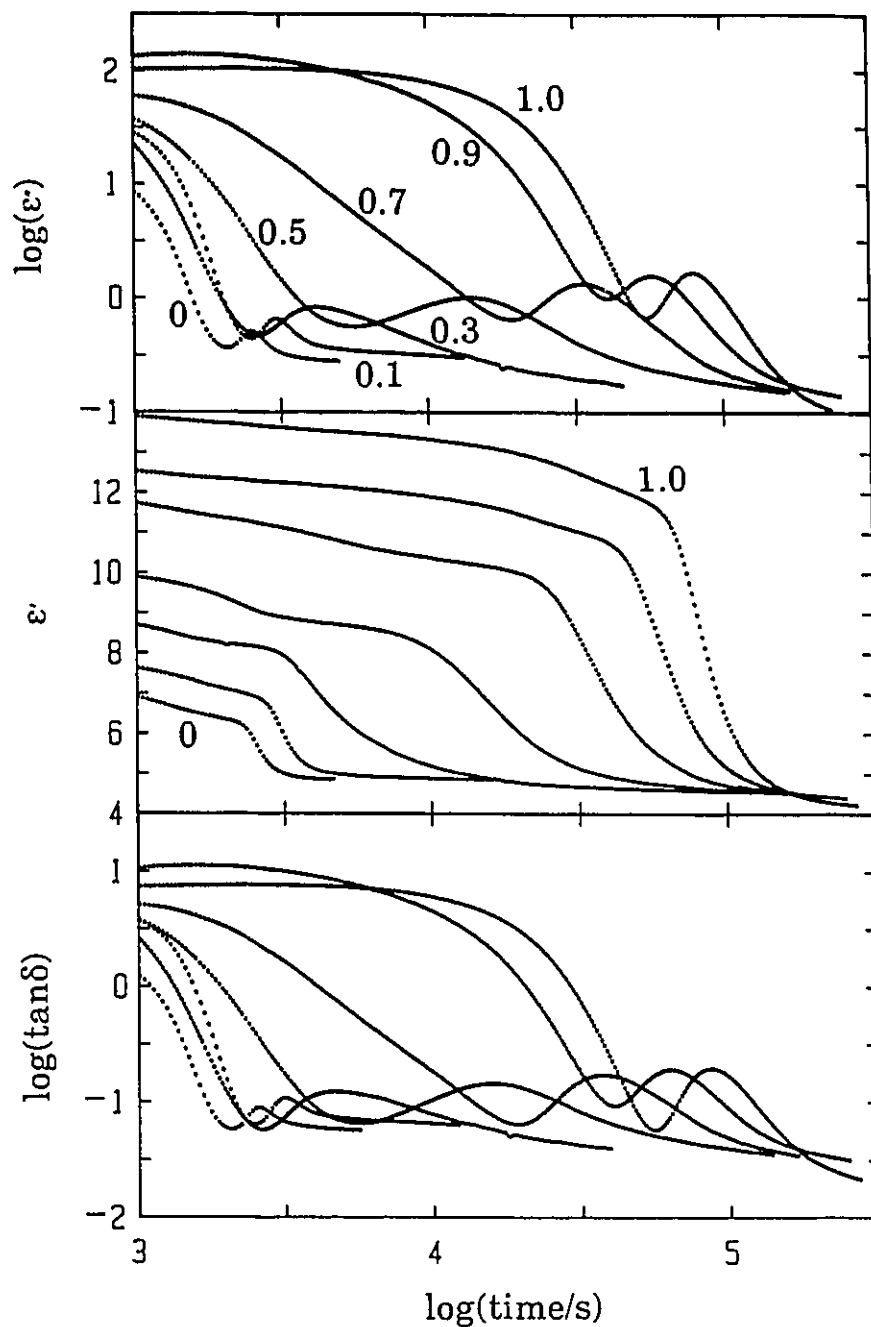


**Figure 3.18:** The dielectric permittivity, loss and loss tangent of the DGEBA-based thermosets measured for a fixed frequency of 1kHz during their curing at 377K. The number next to the curves is the mole fraction of DDS in the DDM-DDS amine mixture.

occurrence of continuous curing. Therefore, its value varies between 375K and 379K for the various thermosets, but this variation is considered insignificant for our purpose here and the data are regarded as corresponding to a curing temperature of  $377 \pm 2\text{K}$  for all cases. This caused an absolute error of not more than 2% in the  $\epsilon'$  and  $\epsilon''$  values, which was calculated from the data in Figure 3.4(b). This error is within the overall errors of the measurements. The plots in Figure 3.18 show that the value of  $\epsilon'$  monotonically decreases on curing for all the seven thermosets, and both  $\epsilon''$  and  $\tan\delta$  initially decrease, reach a minimum value after a certain period of cure, which is then followed by a peak before the ultimate decrease to a value of  $10^{-2}$ . The time at which  $\epsilon''$  reaches its minimum and its peak values for the various thermosets are listed in Table 3.2, along with the minimum and peak values of  $\epsilon''$  themselves in page 56.

The  $\epsilon'$  and  $\epsilon''$  data shown in Figure 3.18 are plotted in a complex plane in Figure 3.19. These plots show changes in  $\epsilon'$  and  $\epsilon''$  that occur as the liquid thermoset cures and ultimately becomes rigid. The shape of the plots is skewed at both extremes of the short and the long curing times, with a greater skew of the circular arc at longer times, when  $\epsilon'$  approaches its infinite time limit.

The curing times at which  $\epsilon''$  reaches its minimum and its peak values for a fixed frequency of 1kHz are plotted in Figure 3.20(a) against the composition which is represented by the mole fraction,  $x$ , of DDS in the curing agent. The values

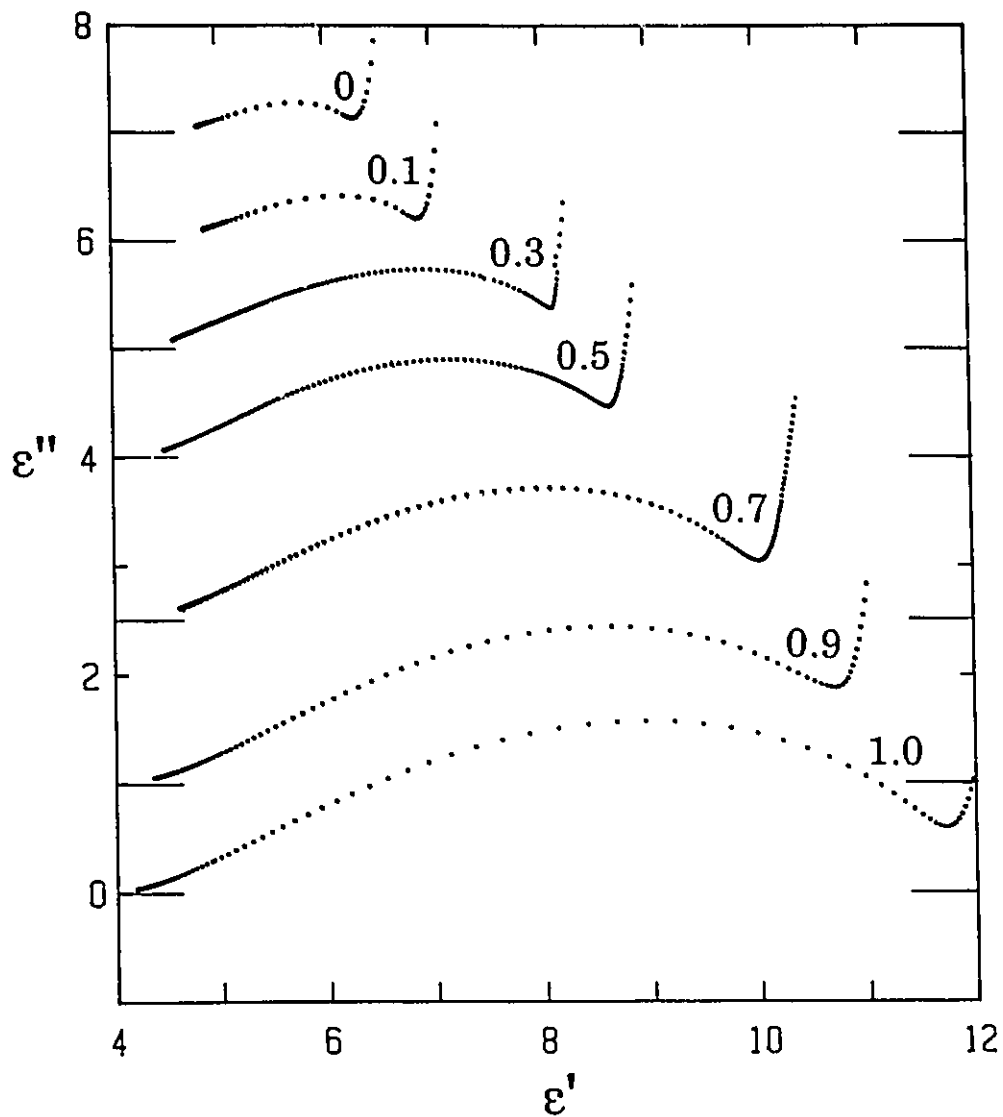


**Figure 3.19:** The complex plane plots of  $\epsilon^*$  of the DGEBA-based thermosets measured for a fixed frequency of 1kHz during their curing at 377K. The number next to the plots represents the same as in Figure 3.18.

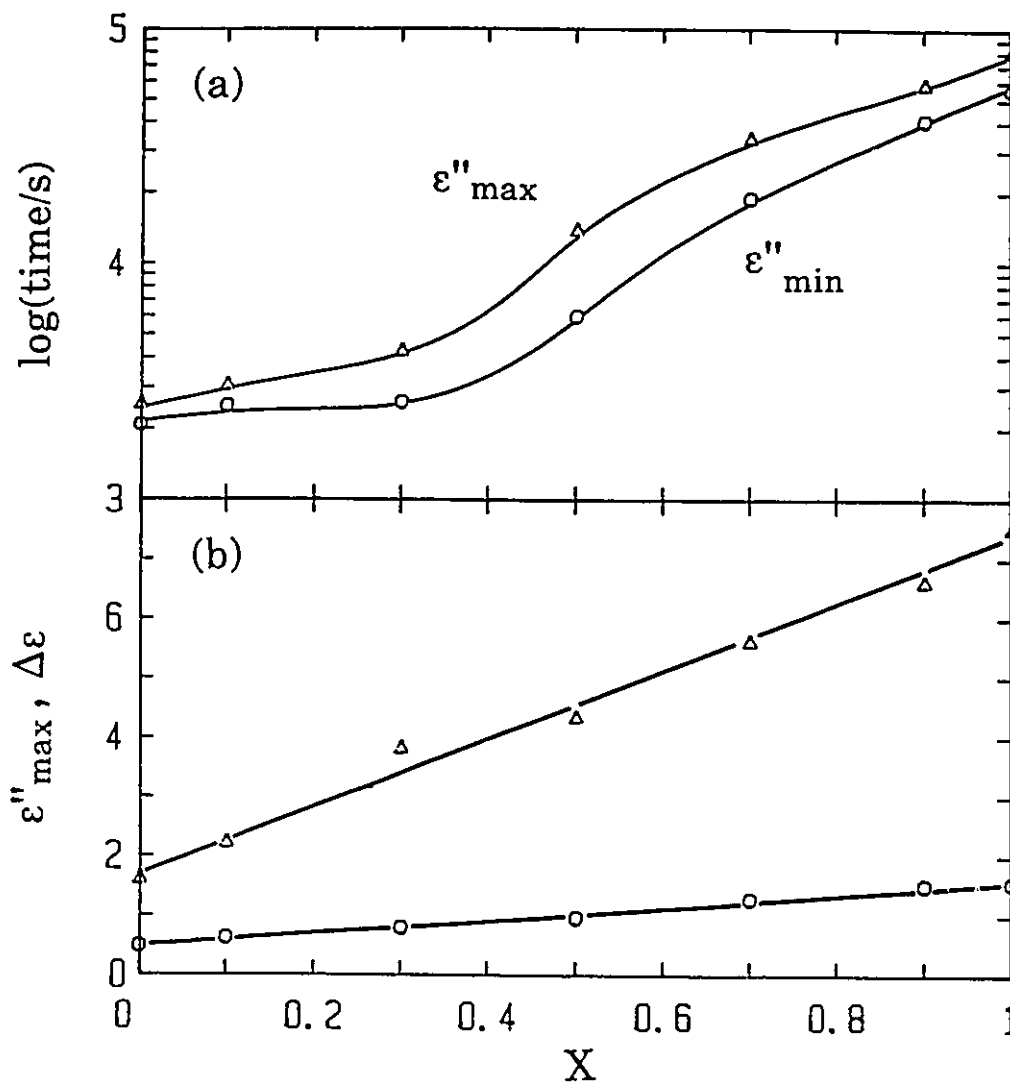


Figure 3.20: (a) The plots of the time during the curing process when  $\epsilon''$  reaches its minimum value,  $t(\epsilon''_{\text{min}})$ , and its peak value,  $t(\epsilon''_{\text{m}})$ , against the composition of the curing agent. (b) The plots of  $\Delta\epsilon$  and  $\epsilon''_{\text{m}}$  at 377K against the composition of the curing agent.

of  $\epsilon''_m$  and  $\Delta\epsilon$  obtained from Figure 3.19 for the seven thermosets are plotted against  $x$  in Figure 3.20(b). These plots show that  $\log[t(\epsilon''_{\min})]$ ,  $\log[t(\epsilon''_m)]$ ,  $\epsilon''_m$  and  $\Delta\epsilon$  all increase with the increase in the mole fraction of DDS in the DDS-DDM mixtures of curing agent.

The curves of  $\log\epsilon''$  against  $\log(t)$  in Figure 3.18 show in each case a point of inflexion, and further that as  $x$  increases, the value of  $[d\log\epsilon''/d\log t]$  at the point of inflexion initially decreases, reaching a minimum at  $x=0.7$  and then increases as  $x$  approaches unity. Figure 3.20 further shows that the logarithmic separation in time between the  $\epsilon''$  maximum and the  $\epsilon''$  minimum initially increases up to  $x=0.5$  where it reaches a maximum, and then decreases.

#### 3.4 THE EFFECTS OF VARYING THE THERMOSET'S COMPOSITION

In an attempt to determine the specific effects associated with the presence of each precursor on the dielectric behaviour of thermosets during their isothermal cure, two non-stoichiometric samples of the DGEBA-DDM were also prepared. The first sample, hereafter referred to as the 'starved' sample, was prepared by mixing 2 moles of DGEBA with 0.75 moles of DDM. The second sample, hereafter referred to as the 'saturated' sample, was prepared by mixing 2 moles of DGEBA with 1.25 moles of DDM. These samples are 'starved' or 'saturated' with respect to the stoichiometric amount of curing agent, DDM, necessary to develop a completely cross-linked network.

The data of dielectric permittivity, loss, and loss tangent, were measured with the dielectric cell 2.3(d) for a fixed frequency of 1kHz at increasing intervals of time during the isothermal cure at 341K of both the starved and saturated thermosets. These are plotted against time in Figure 3.21. The features of the curves shown in Figure 3.21 are generally similar to the features seen in Figures 3.1, 3.2 and 3.3, and described in Section 3.1 and 3.3 for the dielectric behaviour of stoichiometric mixtures of DGEBA-(x DDS, (1-x)DDM) thermosets, but the time of cure required to reach the  $\epsilon''$  peak is less for the saturated sample than it is for the starved sample. These similarities and the differences are also evident in the complex plane plots of  $\epsilon'$  and  $\epsilon''$  data which are shown in Figure 3.22.

The curing times at which  $\epsilon''$  reaches its peak, the peak values for a fixed frequency of measurement of 1kHz, the values of  $\epsilon'$  at the beginning of cure,  $\epsilon'(0)$ , and the values of  $\epsilon''(0)$  are listed in Table 3.3.

### **3.5 THE ELECTRICAL MODULUS AND ITS ANALYSIS**

As reviewed in Section 1.3.3, the electrical modulus formalism and the method for the transformation of the dielectric data into this formalism were originally developed by Macedo et al (1972) and Moynihan et al (1973) for the analysis of the conductivity data in predominantly ionically conducting networks and ionic glasses. We concur that the electrical modulus representation of dielectric data offers a

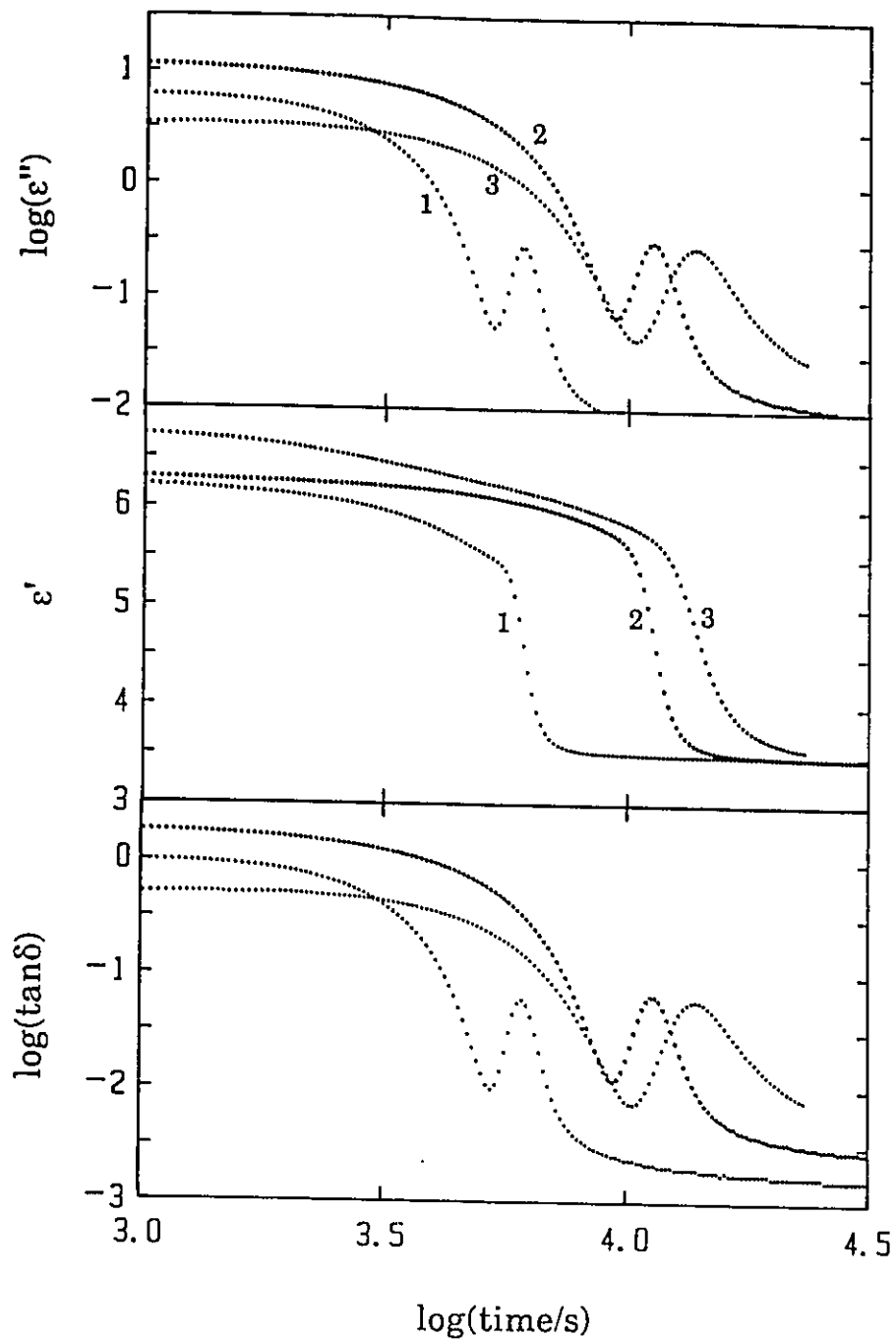


**Figure 3.21:** The dielectric permittivity, loss and loss tangent of the DGEBA-DDM thermosets measured at 1kHz against the time of cure at 341K. Curves 1, 2 and 3 are for the saturated, stoichiometric and starved mixtures, respectively.

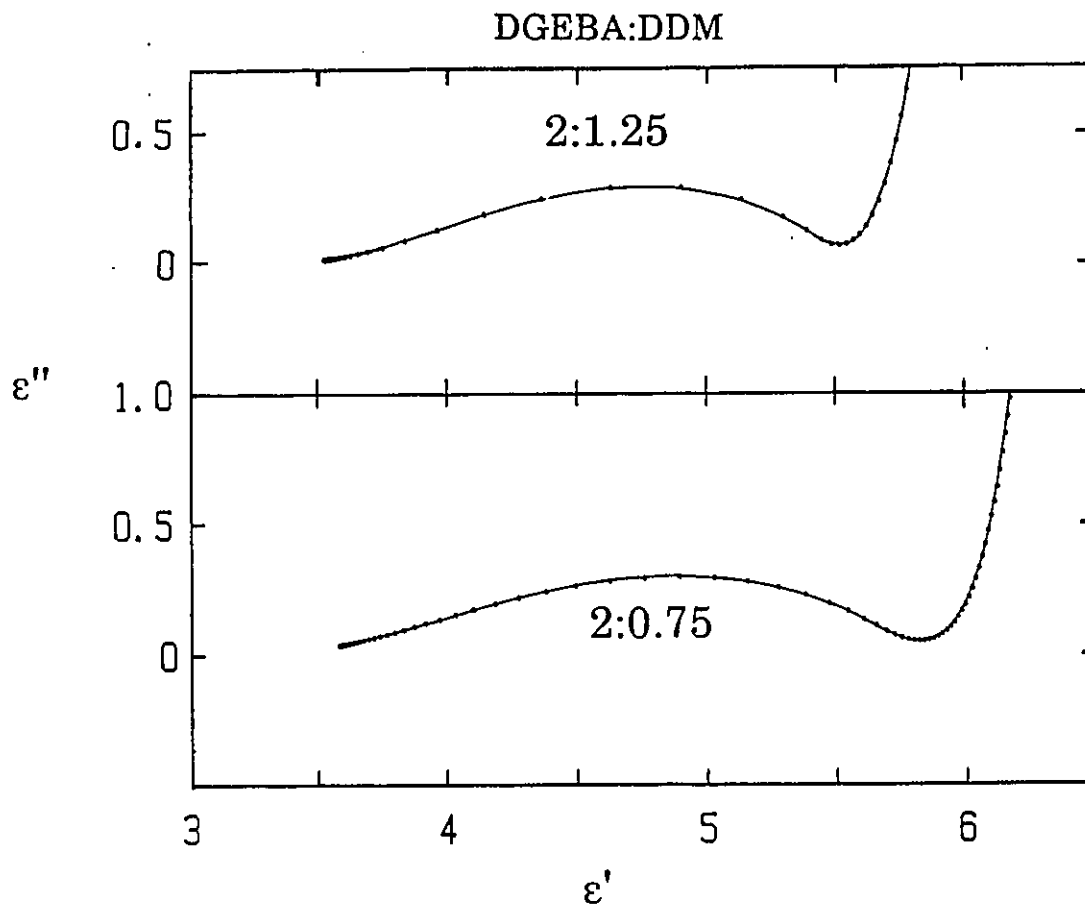


**Figure 3.22:** The complex plane plots of  $\epsilon^*$  of the DGEBA-DDM thermosets cured at 341K measured at 1kHz. The top and bottom curves are for the saturated and starved mixtures, respectively.

**Table 3.3:** The features of the dielectric behaviour of the non stoichiometric DGEBA-DDM thermosets during their curing at 341K.

|           | $\epsilon'(o)$ | $\epsilon''(o)$ | $\epsilon''_{max}$ | $t_{max}(ks)$ | T/K   | $M_w \times 10^2$ |
|-----------|----------------|-----------------|--------------------|---------------|-------|-------------------|
| starved   | 6.70           | 3.51            | 0.291              | 13.6          | 340.8 |                   |
| saturated | 6.22           | 6.19            | 0.281              | 6.00          | 340.0 | 16.8              |

major advantage over other types of analysis in that it almost entirely suppresses the effects of electrode polarization, as can be seen from a cursory analysis of eqn (1.28) (see also Hodge et al 1976, Doi 1988). We extend this approach and show it to be useful also in determining the conductivity of a thermoset at any instant during its curing. The dielectric permittivity data presented in Sections 3.1, 3.3 and 3.4 are accordingly cast in the electrical modulus representation and reanalysed as follows.

The measured values of the permittivity and loss are converted into  $M'$  and  $M''$  using eqns (1.30) and (1.31). These  $M'$  and  $M''$  values, which were measured for a fixed frequency of 1 kHz, for stoichiometric compositions of DGEBA-DDM and DGEBA-DDS thermosets, at various temperatures, are plotted against the isothermal curing time in Figure 3.23. As has been described in Section 1.3.3, the dc conduction contributes partly to the dielectric loss value according to eqn (1.25), and the remaining part of the dielectric loss,  $\epsilon''_{dip}$ , is caused by the reorientation of dipoles. By analogy with eqn (1.26),  $\epsilon''_{dip}$  is related to the ac conductivity according to:

$$\epsilon''_{dip} = \sigma_{ac} / \omega \epsilon_0 \quad (3.6)$$

Hence the total conductivity of a dielectric material measured at an ac frequency  $\omega$  is given by:

$$\sigma = \sigma_0 + \sigma_{ac} = \omega \epsilon_0 \epsilon'' \quad (3.7)$$

The values of  $\sigma(t)$  thus obtained at a fixed frequency of 1kHz are also plotted against the isothermal curing time in Figure 3.23. The corresponding plots of  $M'$ ,  $M''$  and  $\sigma$  for the DGEBA-

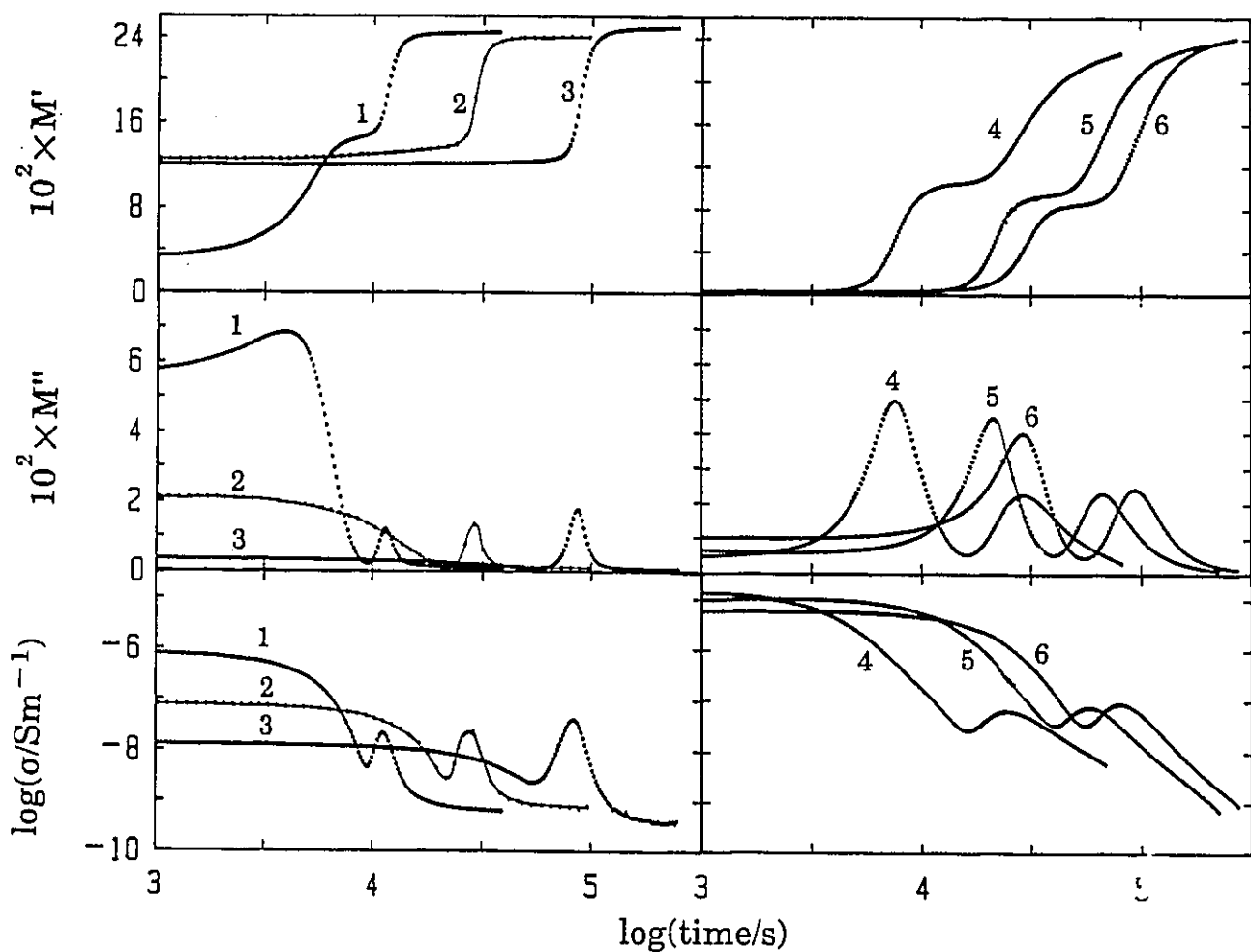


**Figure 3.23:** The real and imaginary parts of the electrical modulus,  $M'$  and  $M''$ , and the measured ac conductivity at a fixed frequency of 1kHz are plotted against time during the curing of the DGEBA-based thermosets with pure DDM and pure DDS. The isothermal curing temperatures are 340.9K, 322.0K and 303.5K for the plots labelled 1, 2 and 3, respectively, and are 412.9K, 387.2K and 377.3K for the plots labelled 4, 5 and 6, respectively.

based thermosets cured with the mixed amines, i.e. DDM and DDS, are shown in Figure 3.24. The corresponding plots for the saturated and starved DGEBA-DDM thermosets are shown in Figure 3.25. The values of  $M'$  and  $M''$  for the thermosets whose behaviours are seen in Figures 3.23, 3.24 and 3.25 are plotted in a complex plane in Figures 3.26, 3.27 and 3.28, respectively.

The two relaxation peaks in the  $M''$  plots, and the corresponding plateaus in the  $M'$  plots observed with increase in the period of isothermal curing, as seen in Figures 3.23 to 3.25, are due to conductivity and dipolar relaxations, respectively. The semicircle centered on the  $M'$ -axis, which is shown by dashes, represents the best fit to the conductivity relaxation arc which appears as a semicircle for the  $M''$  data. The fit of the data is generally good except at long times where contributions from the dielectric relaxation process begin to become significant. This means that the  $M'$  representation of the conductivity relaxation during the curing of thermosets follows the Maxwell's equation with formally a single relaxation time. The diameter of the dashed circles in Figures 3.23 to 3.25, which is equal to  $M_{\infty}$ , is given in Tables 3.1 and 3.2. The second arc, which is skewed at both ends with a greater skew at longer times, corresponds to that obtained in a Cole-Cole representation of the data in Figures 3.3, 3.19 and 3.22, and is due to dipolar relaxation.

The  $\epsilon'$  and  $\epsilon''$  value for the DGEBA-DDM and DGEBA-DDS thermosets cured at 340.9K and 448.3K, respectively, and

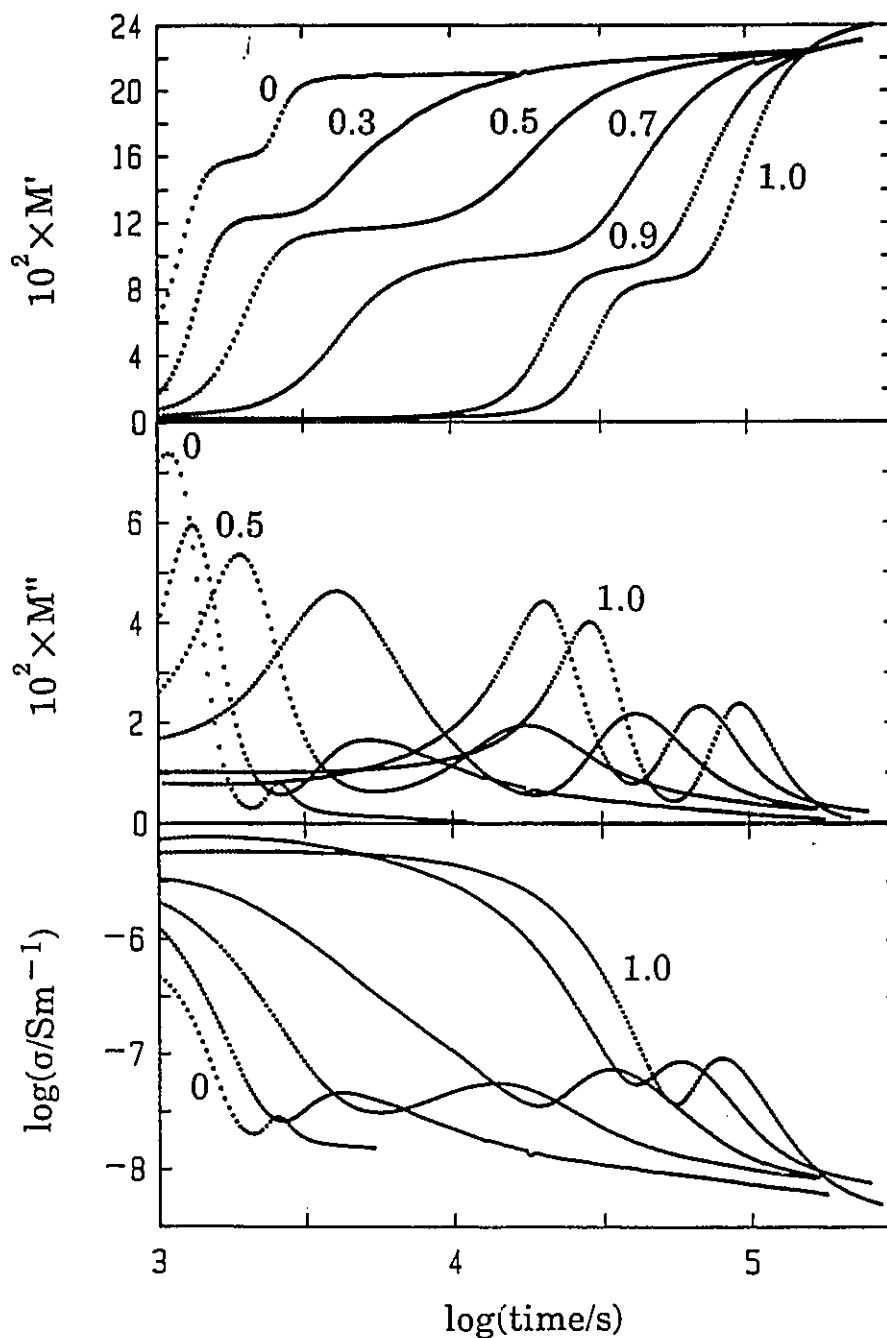


**Figure 3.24:** The real and imaginary parts of the electrical modulus,  $M'$  and  $M''$ , and the measured ac conductivity at a fixed frequency of 1kHz are plotted against time during the curing of the DGEBA-based thermosets with mixed amines. The number next to the curves represents the mole fraction of DDS in the DDM-DDS amine mixtures. The temperature of cure is 377K.

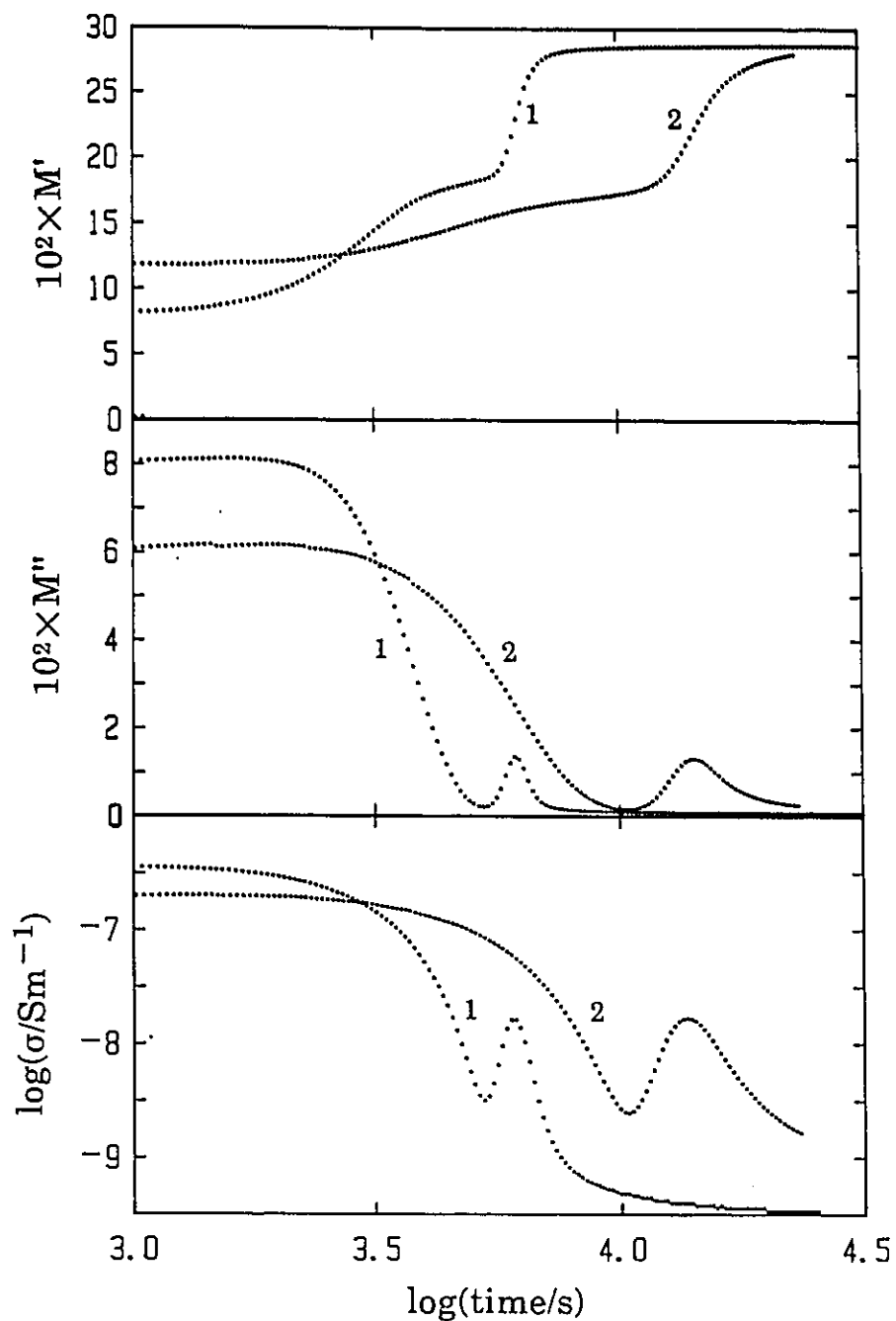


**Figure 3.25:** The real and imaginary parts of the electrical modulus, and the measured ac conductivity at a fixed frequency of 1kHz are plotted against time during the curing of the DGEBA-DDM thermosets at 341K. Curves labelled 1 and 2 are for the saturated, and starved samples.

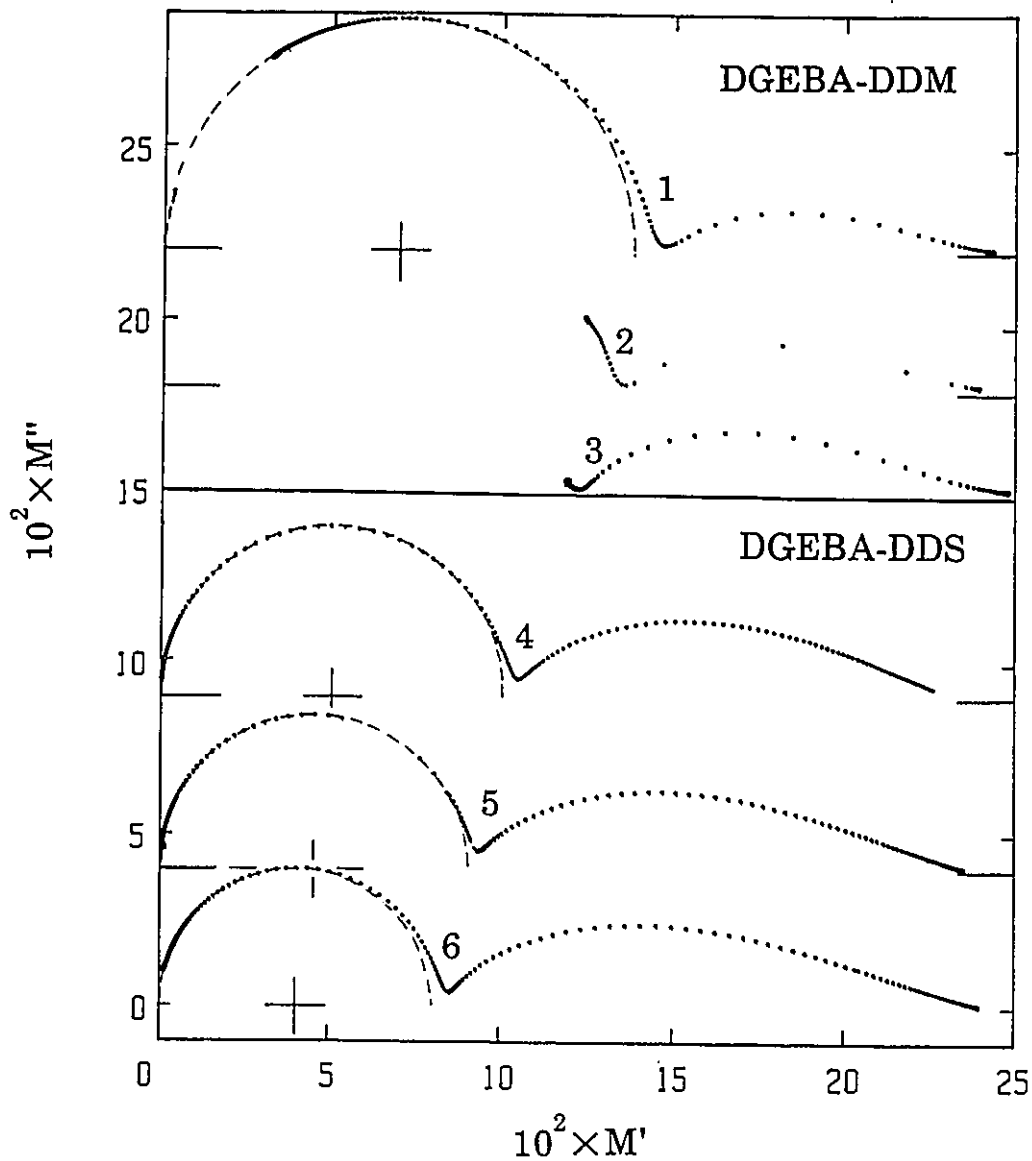


**Figure 3.26:** The complex plane plots of the electrical modulus  $M^*$  measured at a fixed frequency of 1kHz during the curing of the DGEBA-based thermosets with pure DDM and pure DDS. The isothermal cure temperatures are 340.9K, 322.0K and 303.5K for the plots labelled 1, 2 and 3, respectively, and are 412.9K, 387.2K and 377.3K for the plots labelled 4, 5 and 6, respectively.

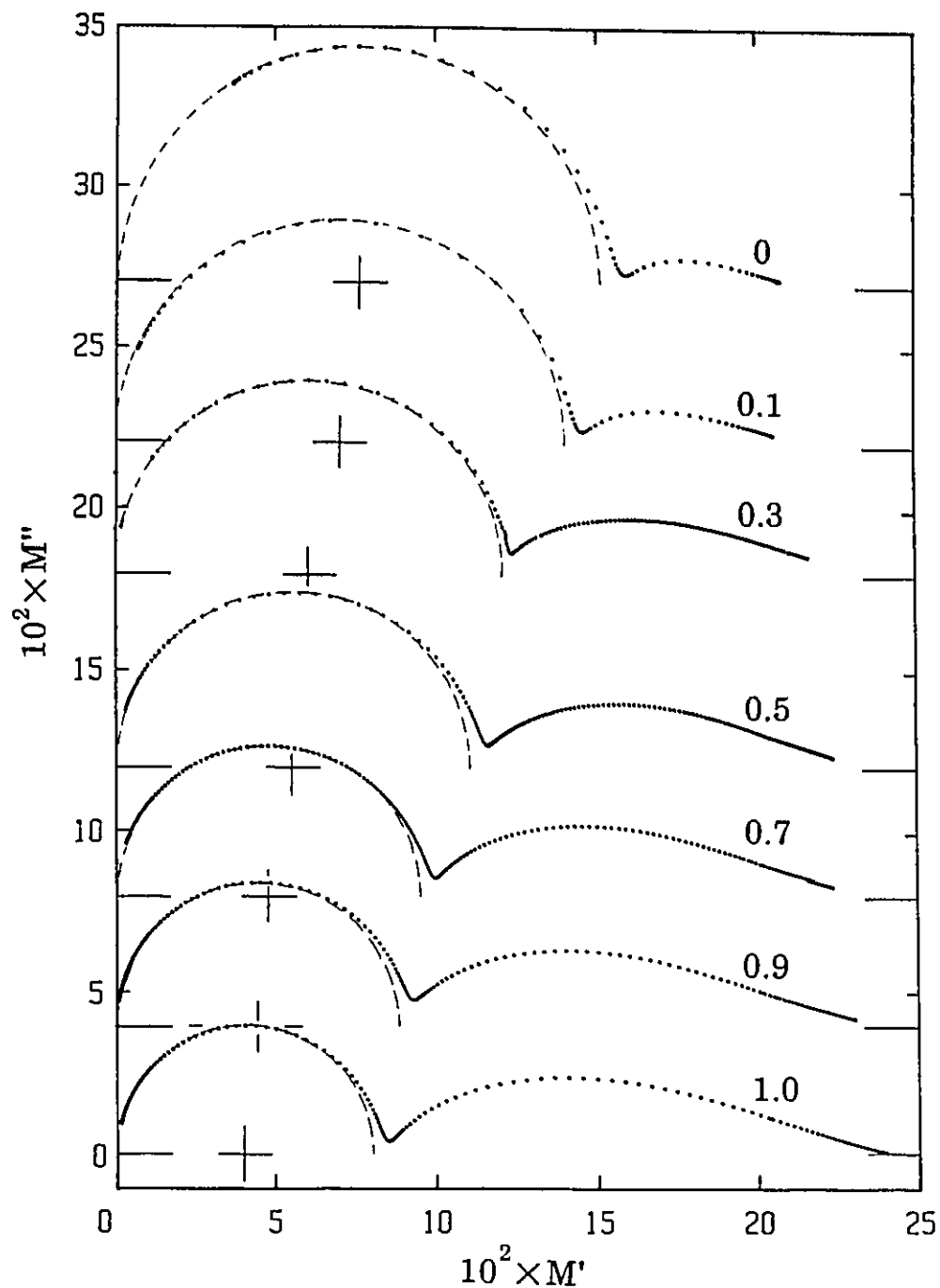


**Figure 3.27:** The complex plane plots of the electrical modulus  $M^*$  measured at a fixed frequency of 1 kHz during the curing of the DGEBA-based thermosets with mixed amines. The number next to the curves represents the mole fraction of DDS in the amine mixtures.

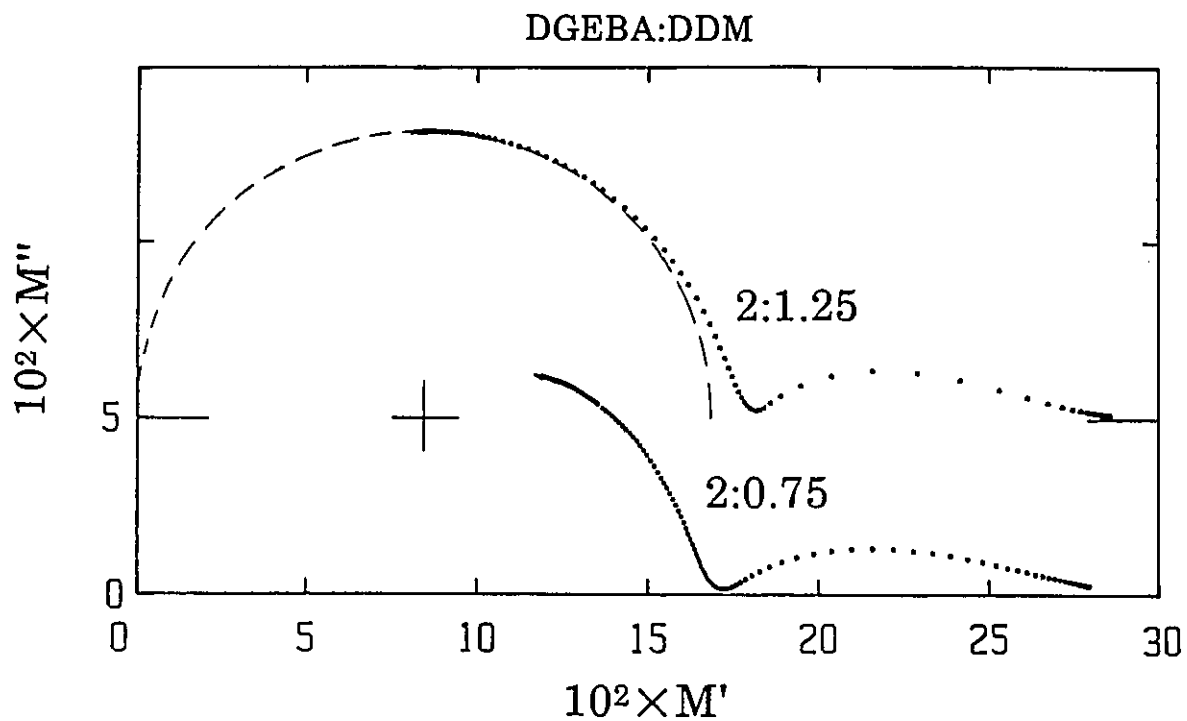


**Figure 3.28:** The complex plane plots of the electrical modulus  $M^*$  measured at a fixed frequency of 1kHz during the curing of DGEBA-DDM thermosets at 341K. Top and bottom curves are for the saturated and starved mixtures, respectively.

measured at several frequencies, which are shown in Figures 3.5, 3.6, 3.9, and 3.10, were also converted into the  $M'$  and  $M''$  values. The values of  $M'$  and  $M''$  for the DGEBA-DDM and DGEBA-DDS thermosets are plotted against time in Figure 3.29 to 3.32, respectively, where only those frequencies for which the  $M''$  conductivity relaxation peak is well-separated from the  $M''$  dipolar relaxation peak are presented. Frequencies above 700Hz are not shown in the  $M'$  and  $M''$  plots of Figures 3.29 and 3.30 for the DGEBA-DDM thermoset because at those frequencies the value of  $M''$  did not show a peak. The data at frequencies lower than 300Hz are not included in the  $M'$  and  $M''$  plots of the DGEBA-DDS thermoset shown in Figures 3.31 and 3.32 because the two relaxation peaks are seen to merge at these frequencies. These features become clearly evident in the complex plane plots of  $M^*$  which are shown in Figure 3.33 for both the DGEBA-DDM and DGEBA-DDS thermosets at the measurement frequencies used in Figures 3.29 to 3.32, where the measured data at various frequencies superpose for the DGEBA-DDM thermoset while only the data obtained at the four highest frequencies, i.e. 15, 10, 6.67 and 4.62kHz, superpose for the DGEBA-DDS thermoset because of the increasing proximity of the conductivity and dipolar relaxation peaks with decreasing frequency.

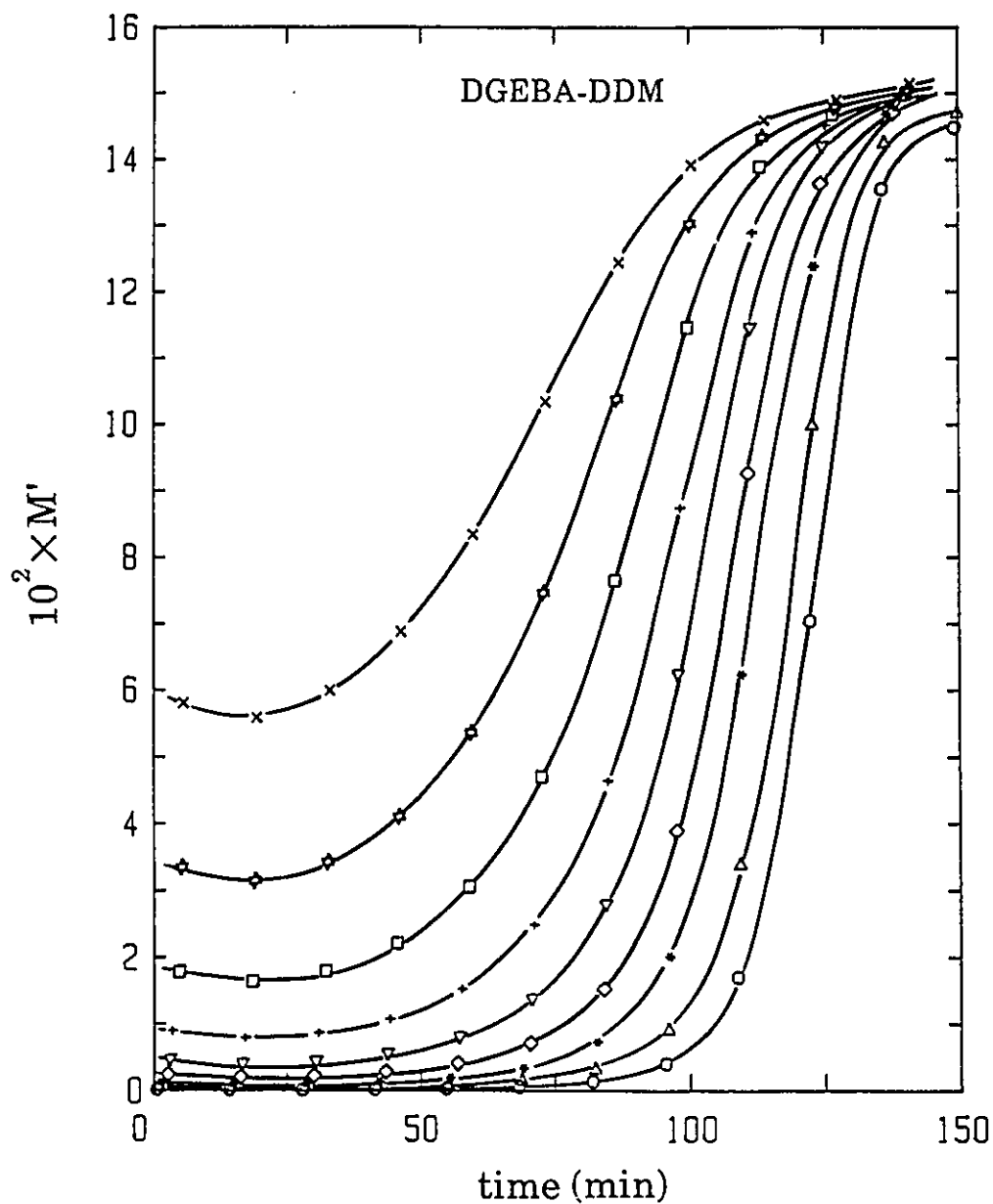


**Figure 3.29:** The real part of the electrical modulus,  $M'$ , of the DGEBA-DDM thermoset measured at nine frequencies is plotted against time of cure at 340.9K. Curves are for data measured at (x) 697, ( $\phi$ ) 451, ( $\square$ ) 300, (+) 200, ( $\nabla$ ) 140, ( $\diamond$ ) 100, (\*) 69.8, ( $\triangle$ ) 44.8 and (o) 30Hz.

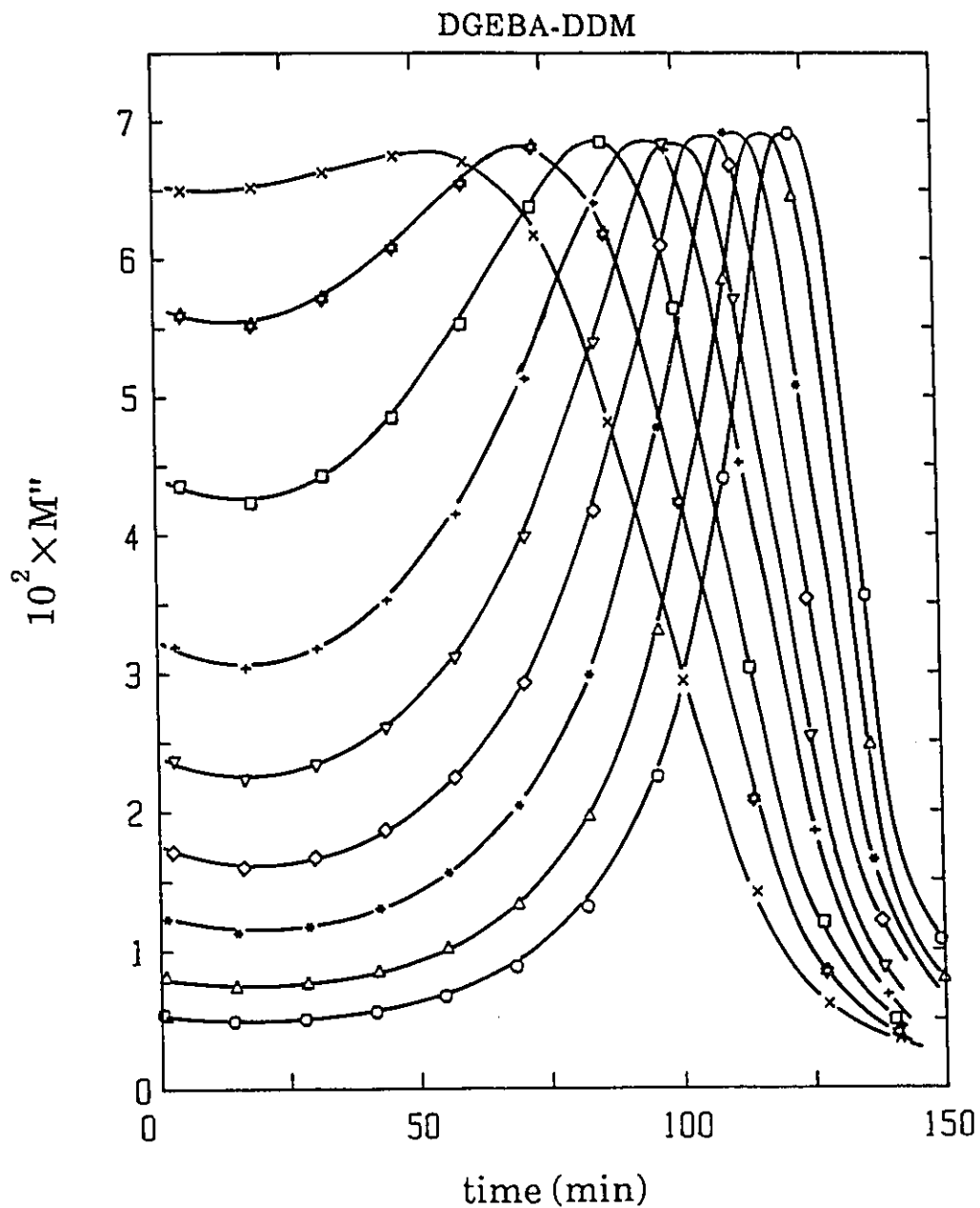


**Figure 3.30:** The imaginary part of the electrical modulus,  $M''$ , of the DGEBA-DDM thermoset measured at nine frequencies plotted against time of cure at 340.9K. Curves are for data measured at (X) 697, ( $\phi$ ) 451, ( $\square$ ) 300, (+) 200, ( $\nabla$ ) 140, ( $\diamond$ ) 100, (\*) 69.8, ( $\Delta$ ) 44.8 and (O) 30Hz.

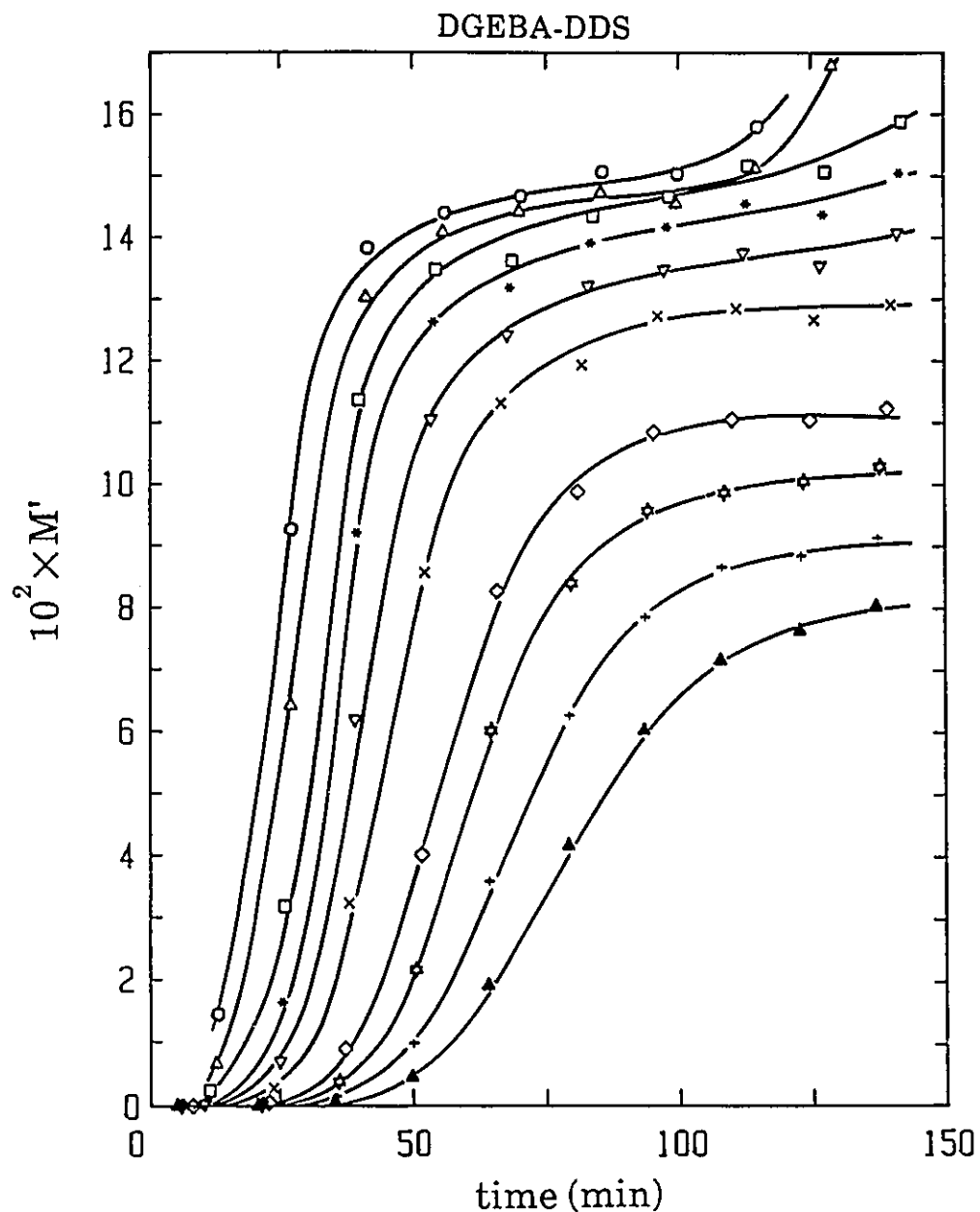


**Figure 3:31:** The real part fo the electrical modulus,  $M'$ , of the DGEBA-DDS thermoset measured at 10 frequencies plotted against time of cure at 448.3K. Curves are for data measured at (O)15, ( $\Delta$ )10, ( $\diamond$ )6.667, (\*)4.6154, ( $\nabla$ )3, (X)2, ( $\diamond$ )1, ( )0.697, (+)0.4511 and ( $\Delta$ )0.3kHz.

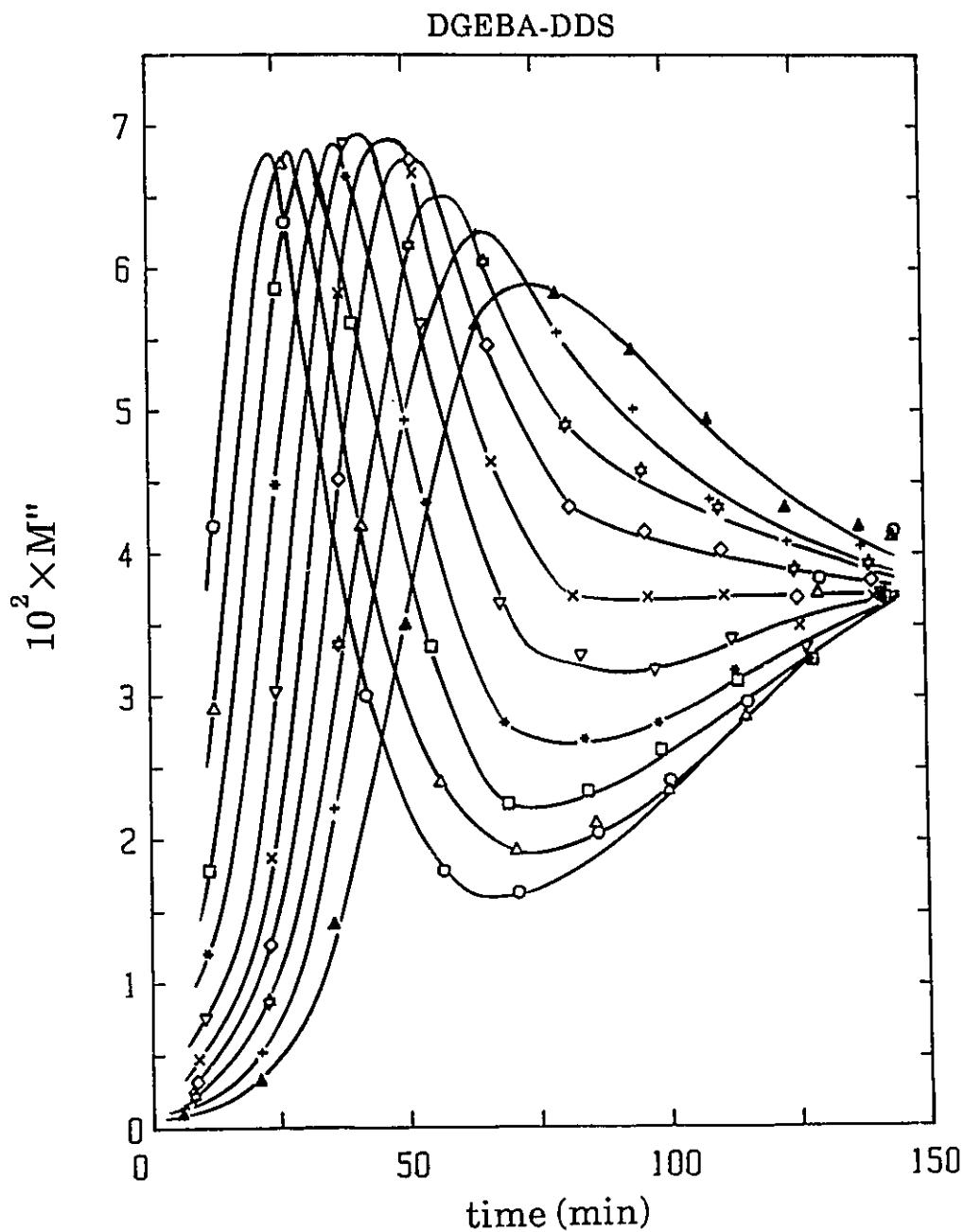


**Figure 3.32:** The imaginary part of the electrical modulus,  $M''$ , of the DGEBA-DDS thermoset measured at 10 frequencies plotted against time of cure at 448.3K. Curves are for data measured at (O)15, ( $\Delta$ )10, ( $\diamond$ )6.667, (\*)4.6154, ( $\nabla$ )3, (X)2, ( $\square$ )1, ( )0.697, (+)0.4511 and ( $\triangle$ )0.3kHz.

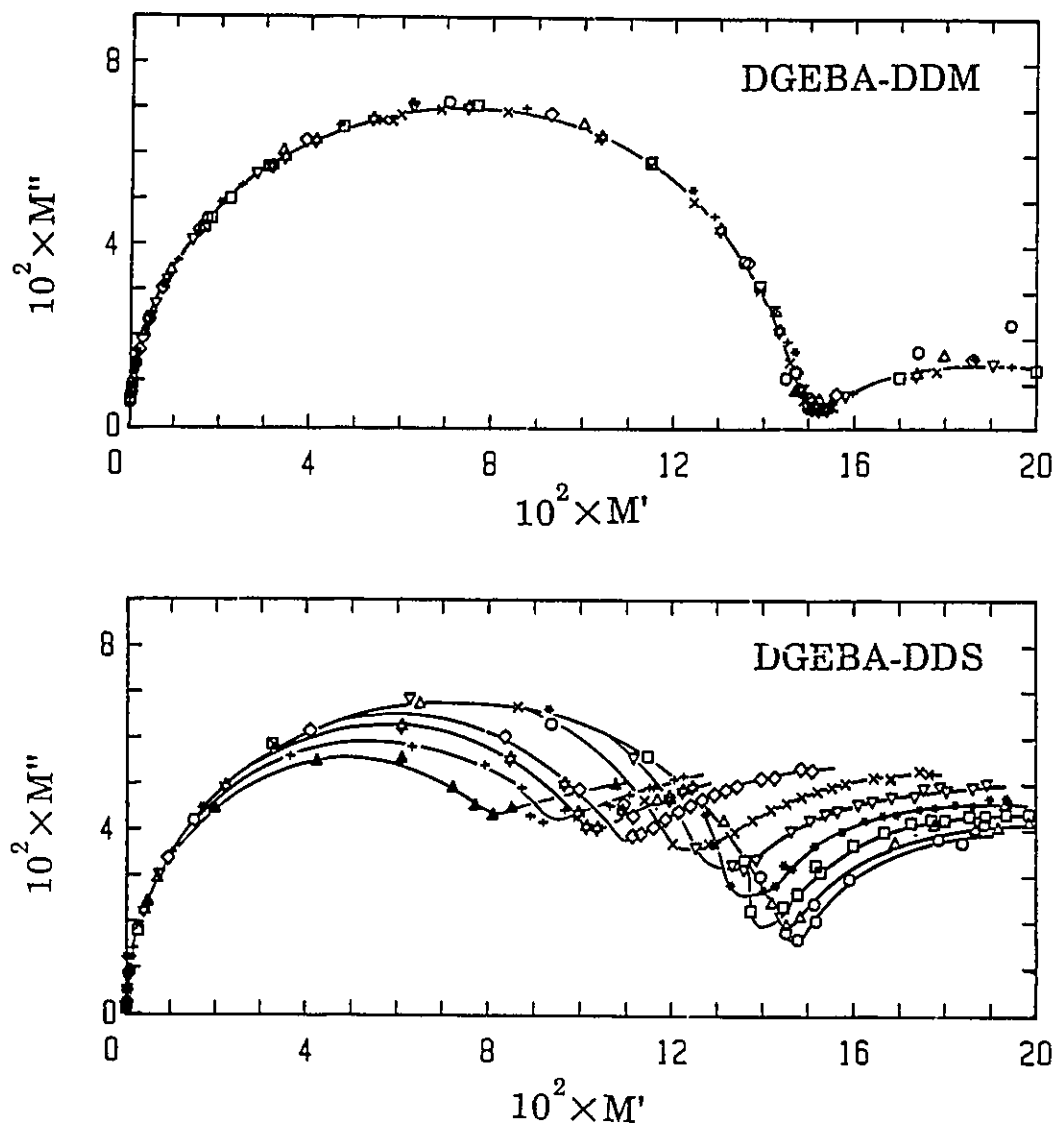


Figure 3.33: The complex plane plots of the electrical modulus,  $M^*$ , measured at different frequencies during the curing of the DGEBA-DDM and DGEBA-DDS thermosets at 340.9K and 448.3K, respectively. The symbols used have the same meaning as those in Figures 3.29 and 3.32.

## CHAPTER 4

### DIELECTRIC CHARACTERIZATION OF THE CURE OF THERMOSETS

#### 4.1 CHEMICAL AND PHYSICAL EFFECTS

The dielectric properties of a thermoset during its curing process are determined by its changing chemical composition as a result of the chemical reactions which decrease the concentration of certain molecular segments and increase the concentration of others. This change in the chemical composition also causes a decrease in the diffusivity or increase in its viscosity, which in turn decreases the probability of the occurrence of further chemical reactions. The auto-catalytic reactions thus become self-retarding as the increase in the viscosity increases the thermoset's  $T_g$  towards the  $T_{cure}$  value. At high viscosities encountered near  $T_g$ , the rate of chemical changes becomes controlled by the rate of molecular diffusion instead of by the law of mass action, although at relatively low viscosities the latter has been regarded as the controlling factor. The frequency of 1kHz at which the dielectric loss peak is observed here corresponds to a relaxation time of  $159\mu\text{sec}$  which, according to the Maxwell equation (1863),  $\tau = \eta/G$ , corresponds to a viscosity of about  $10^5\text{P}$ , if the shear modulus  $G$  is assumed to be  $10^8\text{Pa}$ , and at curing times prior to the appearance of the  $\epsilon''$  peak, this viscosity is even less. Therefore, at low viscosities or at short curing times, the observed changes in  $\epsilon''$ , which are mainly attributable to changes in the dc conductivity, are

controlled by the chemical reactions, and the observed decrease in both  $\epsilon'$  and  $\epsilon''$ , during the period of curing after the appearance of the  $\epsilon''$  peak, indicates a mechanism that is predominantly diffusion controlled.

From a physical point of view, cross-linking that ultimately forms a network causes the translational and rotational diffusion of individual molecules in the thermoset to become more sterically hindered. As in the case of linear-chain polymerization, the changes that occur during the densification of the network as a result of increased cross-linking are (1) a decrease in the mobility of the impurity ions, and a decrease in the concentration and mobility of protons which are produced by partial dissociation of amine groups, (2) a decrease in the contribution to the static dielectric permittivity per unit molecule as a result of increased chain length (Huraux and Sellaimia 1973, Sheppard and Senturia 1986), (3) a general decrease of the dipolar reorientation rate caused by an increased steric hindrance and (4) an increase in the distribution of relaxation times (as evident from the work of Soualmia et al (1982)). Although these changes continuously occur with time, their relative magnitudes differ with the time of curing. In view of the observed dielectric properties, which have been described in Chapter 3, it is appropriate therefore to consider two different regions of the curing period during which these changes dominate. First the period prior to the appearance of the minimum in  $\epsilon''$  in Figures 3.1, 3.2, 3.5, 3.6 and 3.7 where  $\epsilon''$  is principally

affected by a large decrease in the dc conductivity of the thermoset, and second the period past this  $\epsilon''$  minimum where the  $\epsilon''$  due to dc conductivity has decreased to a negligibly small value and when the dielectric properties are mainly affected by the dipolar relaxation of the network segments. The former is predominantly affected by the decrease in the ionic conductivity and the latter by the decrease in the rate of diffusion of dipolar segments. These two effects are now discussed separately in the following Sections:

#### 4.2 THE TIME DEPENDENCE OF THE CONDUCTIVITY

We now consider how the dc conductivity or  $\sigma_0$  can be determined from our results. The measured conductivity at 1kHz of a curing thermoset is equal to its dc conductivity under conditions when dipolar contributions to  $\sigma$  are zero. This condition is not strictly fulfilled at all times of the cure as the dipolar contributions to the measured  $\sigma$  are finite. Nevertheless, at  $t < t_{\min}$ , where  $t_{\min}$  is the time of the appearance of the minimum in  $\sigma$ , the dipolar contribution to  $\sigma$  is negligibly small and at  $t_{\min}$ , the decrease in contributions from the ionic conductivity is compensated for by an increase in the dipolar contributions. Therefore the measured conductivity  $\sigma(t)$ , at a time,  $t$ , is equal to the dc conductivity when  $t < t_{\min}$  but exceeds the true  $\sigma_0$  as  $t$  approaches  $t_{\min}$ . An analysis of the dc conductivity in terms of kinetic effects during the curing must be restricted to data obtained for times less than  $t_{\min}$ .

The value of  $\sigma_0(t)$  and its decrease during the curing process is now used to examine, as follows, whether or not the sol to gel conversion of a thermoset can be described in terms of a critical phenomenon based on scaling concepts. The conversion of a sol, or liquid, to a gel has been theoretically considered by Stauffer (1976) and De Gennes (1976), and reviewed by Stauffer et al (1982) and Djabourov (1988). In general terms of a critical phenomenon, an equation which is widely known as power law,

$$p \propto [(t_g - t)/t_g]^x \quad (4.1)$$

is used to describe the temporal variation of a kinetic or transport property,  $p$ , with the gelling time  $t_g$  and an empirical parameter known as critical exponent,  $x$ . In order to examine the applicability of scaling concepts to the conductivity behaviour of thermosets, the value of  $t_g$  must be known. Since the value of  $t_g$  depends on the method of preparation of the thermoset and its conditions of cure, and is subjective to the techniques used (Haran and Laudouard 1985) in determining  $t_g$ , the values of  $t_g$  given in the literature cannot be directly used in Eqn (4.1). Therefore, it seemed suitable to follow a reiterative procedure in which  $t_g$  was initially selected as the time during the curing process at which  $\epsilon''$  reached a minimum. This value of  $t_g$  was then adjusted until the equation,

$$\sigma_0 = \Sigma_0 [(t_g - t)/t_g]^x, \quad (4.2)$$

fitted the  $\sigma_0$  values with a minimum in the sum of square deviations. A software was developed to enable us to (1)

determine the mean square deviations of the calculated and experimental  $\sigma_0(t)$  values, (2) minimize the mean square deviations by changing the value of the gelling time,  $t_g$ , and (3) graphically display the resulting fit on the monitor with the corresponding value of the fitting parameters. A comparison between the experimental and calculated values is shown in Figures 4.1 to 4.3. The experimental values of  $\sigma_0$  determined from  $t=1ks$ , to a time slightly larger than  $t_{min}$  is shown by the data points and the calculated fit is shown as the dashed curve. The parameters,  $t_g$ ,  $x$ , and  $\Sigma_0$ , used for the fit to the data obtained for the various thermosets at different temperatures are given in Tables 4.1 and 4.2. The calculated and the experimental values in Figures 4.1 to 4.3 clearly show that the decrease in conductivity can be adequately described by the power law or Eqn (4.2).

It is useful to also examine another representation of the decrease of dc conductivity, which is an alternative to the use of the power law description and whose plausibility lies in recognizing that the increase in viscosity during the early stages of the curing process controls the ionic diffusion according to the Stokes-Einstein equation. This is particularly so in view of Anderson's (1986) and Johari and Pathmanathan's (1990) arguments that the power law of eqns (4.1) and (4.2) when applied to temperature dependence of relaxation time is equivalent to the well known Vogel-Fulcher-Tamman equation over a narrow range of measurements. We propose an alternative equation which also implies an approach

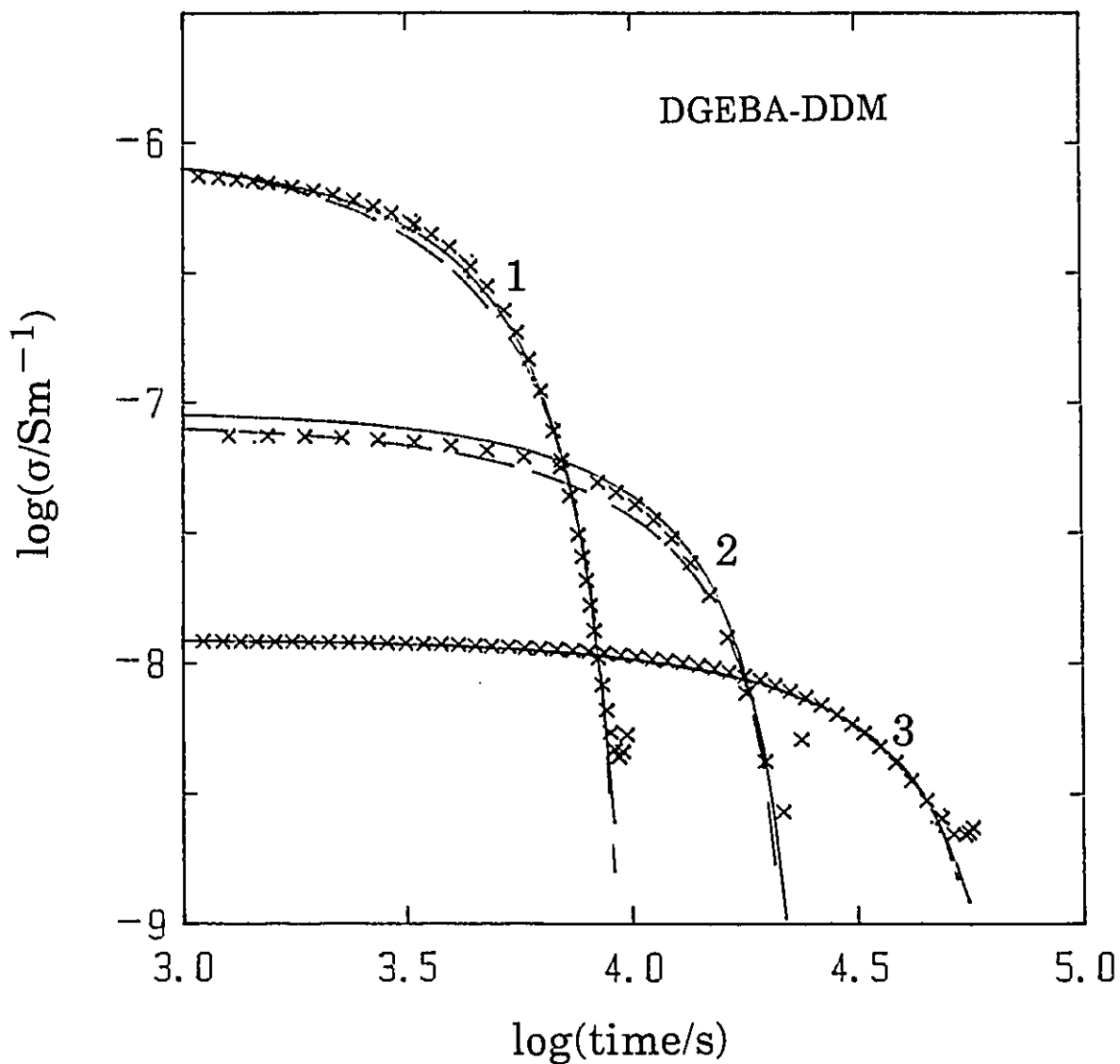


**Figure 4.1:** The plots of the measured conductivity against the curing time for the DGEBA-DDM thermoset cured at (1) 340.9K, (2) 322.0K and (3) 303.5K. The dashed line was calculated from eqn (4.2) and the continuous line from eqn (4.3).

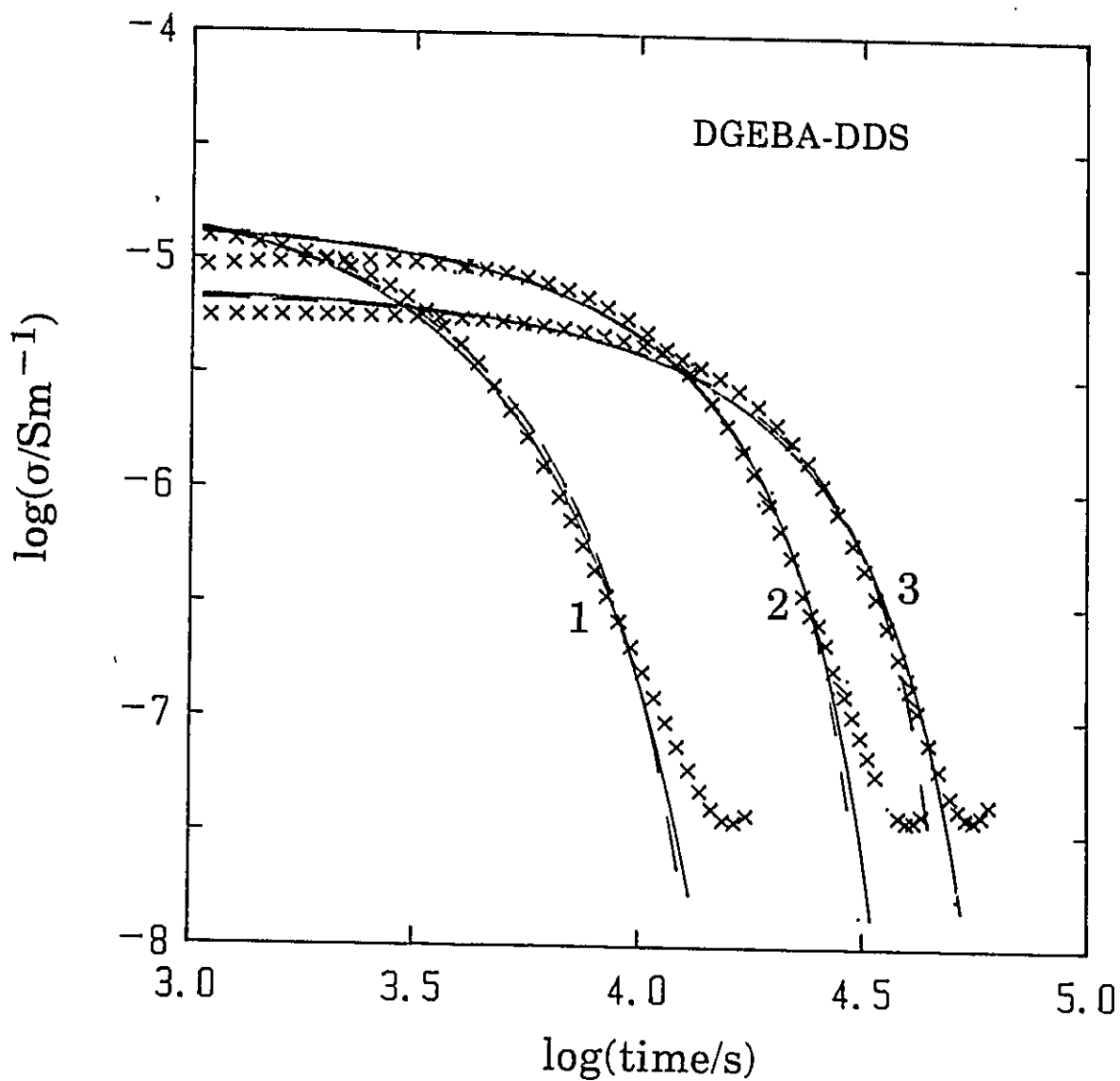


**Figure 4.2:** The plots of the measured conductivity against the curing time for the DGEBA-DDS thermoset cured at (1) 412.9K, (2) 387.2K and (3) 377.3K. The dashed line was calculated from eqn (4.2) and the continuous line from eqn (4.3).

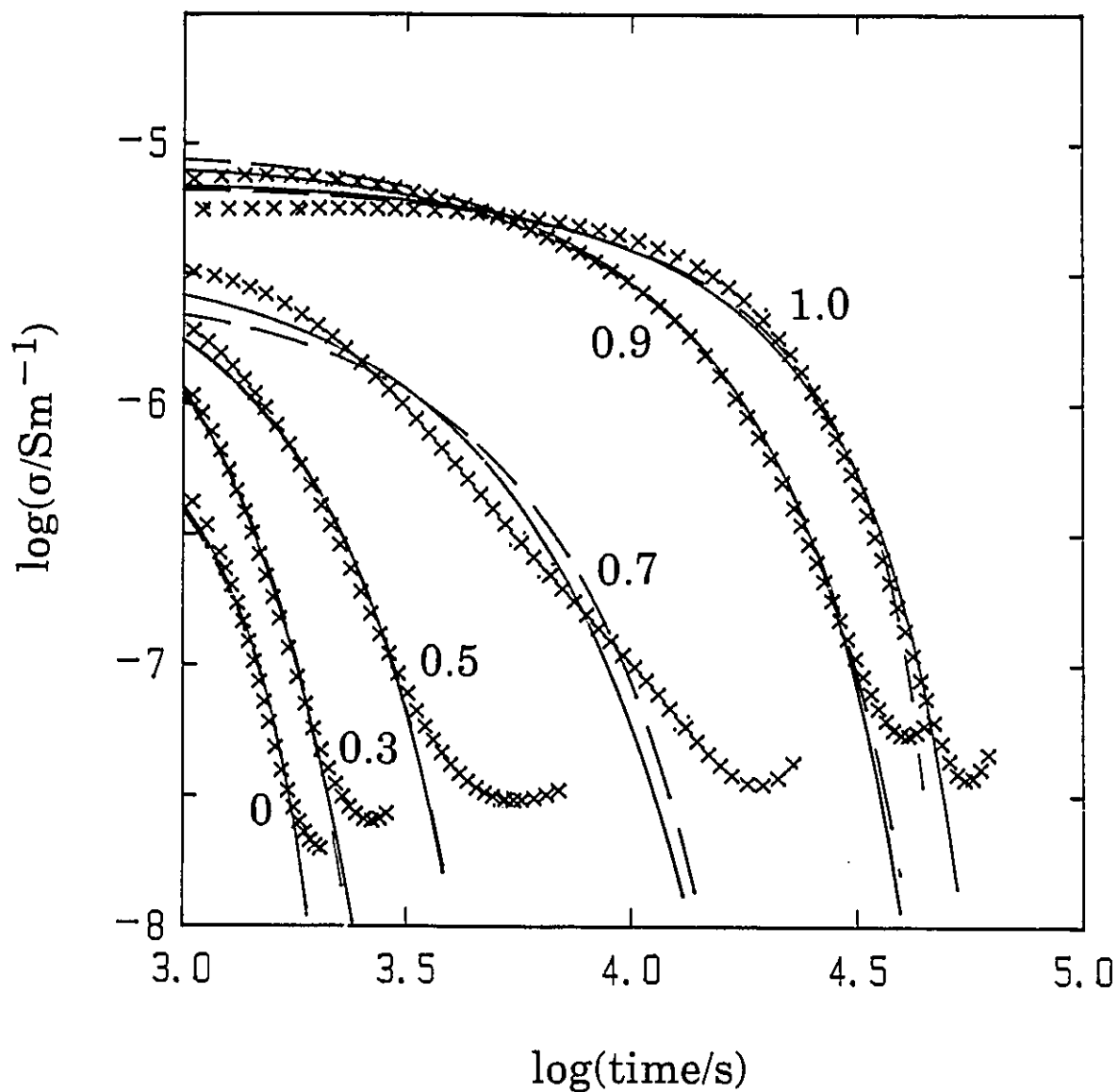


**Figure 4.3:** The plots of the measured conductivity against the curing time for the DGEBA-based thermosets during their cure with mixed amines. The dashed line was calculated from eqn (4.2) and the continuous line from eqn (4.3). The number next to the curves is the mole fraction of DDS in the DDM-DDS amine mixtures.

Table 4.1: The parameters of Eqns. (4.2) and (4.3) used for fitting the measured conductivity of DGEBA-based thermosets during their curing with DDM and DDS at several temperatures.

DGEBA-DDM THERMOSET

| T/K   | $t_0/s$ | x    | $\Sigma_0/S_m^{-1}$   | A/ $S m^{-1}$         | B/s                 | $t_0/s$ |
|-------|---------|------|-----------------------|-----------------------|---------------------|---------|
| 303.5 | 61,000  | 1.07 | $1.24 \times 10^{-8}$ | $5.35 \times 10^{-8}$ | $1.355 \times 10^5$ | 91,000  |
| 322.0 | 22,000  | 1.38 | $8.75 \times 10^{-8}$ | $4.00 \times 10^{-7}$ | $4.201 \times 10^4$ | 29,000  |
| 340.9 | 9,600   | 2.10 | $1.00 \times 10^{-6}$ | $6.80 \times 10^{-6}$ | $2.416 \times 10^4$ | 12,200  |

DGEBA-DDS THERMOSET

| T/K   | $t_0/s$ | x    | $\Sigma_0/S_m^{-1}$   | A/ $S m^{-1}$         | B/s                 | $t_0/s$ |
|-------|---------|------|-----------------------|-----------------------|---------------------|---------|
| 377.3 | 51,000  | 2.65 | $7.04 \times 10^{-6}$ | $2.04 \times 10^{-3}$ | $5.635 \times 10^5$ | 100,000 |
| 387.2 | 36,000  | 3.48 | $1.46 \times 10^{-5}$ | $3.43 \times 10^{-3}$ | $3.237 \times 10^5$ | 59,000  |
| 412.9 | 19,000  | 6.59 | $1.97 \times 10^{-5}$ | $2.77 \times 10^{-2}$ | $7.057 \times 10^5$ | 43,000  |

Table 4.2: The parameters of Eqns. (4.2) and (4.3) used for fitting the conductivity measured during the curing of DGEBA thermosets with mixed DDM and DDS at  $377 \pm 2\text{K}$ .

| DDM:DDS ratio | $t_g/s$ | $x$  | $\Sigma_0/Sm^{-1}$    | $A/Sm^{-1}$           | $B/s$              | $t_0/s$ |
|---------------|---------|------|-----------------------|-----------------------|--------------------|---------|
| 1.0:0         | 2,300   | 3.04 | $2.21 \times 10^{-6}$ | $4.79 \times 10^{-5}$ | $1.00 \times 10^4$ | 3,100   |
| 0.9:0.1       | 2,650   | 3.21 | $6.22 \times 10^{-6}$ | $1.51 \times 10^{-4}$ | $1.20 \times 10^4$ | 3,550   |
| 0.7:0.3       | 3,500   | 6.20 | $8.89 \times 10^{-6}$ | $5.93 \times 10^3$    | $1.79 \times 10^4$ | 9,000   |
| 0.5:0.5       | 7,000   | 7.31 | $5.43 \times 10^{-6}$ | $2.76 \times 10^{-1}$ | $1.20 \times 10^5$ | 11,000  |
| 0.3:0.7       | 30,000  | 8.76 | $2.96 \times 10^{-6}$ | $1.83 \times 10^7$    | $2.34 \times 10^6$ | 80,000  |
| 0.1:0.9       | 70,000  | 7.78 | $9.74 \times 10^{-6}$ | $1.06 \times 10^{-1}$ | $8.94 \times 10^5$ | 95,000  |
| 0:1.0         | 51,000  | 2.65 | $7.04 \times 10^{-6}$ | $2.04 \times 10^{-3}$ | $5.64 \times 10^5$ | 100,000 |

Table 4.3: The parameters used for fitting the dielectric permittivity data of the thermosets.

| Thermosets                    | $T, K$ | $\epsilon_\infty$ | $\Delta\epsilon$ | $\gamma$ | $x$ |
|-------------------------------|--------|-------------------|------------------|----------|-----|
| DGEBA-DDM                     | 303.5  | 4.20              | 3.80             | 0.31     |     |
|                               | 312.6  | 4.25              | 3.65             | 0.28     |     |
|                               | 322.0  | 4.30              | 2.95             | 0.27     |     |
|                               | 331.0  | 4.20              | 2.70             | 0.27     |     |
|                               | 340.9  | 4.20              | 2.50             | 0.26     |     |
| DGEBA-DDS                     | 377.3  | 4.50              | 7.30             | 0.38     |     |
|                               | 387.2  | 4.50              | 6.30             | 0.38     |     |
|                               | 400.6  | 4.30              | 5.80             | 0.39     |     |
|                               | 412.0  | 4.40              | 5.20             | 0.38     |     |
| DGEBA-( $x$ DDS, $(1-x)$ DDM) | 375.0  | 4.40              | 1.59             | 0.27     | 0   |
|                               | 377.3  | 4.40              | 2.20             | 0.30     | 0.1 |
|                               | 379.7  | 4.50              | 3.80             | 0.33     | 0.3 |
|                               | 376.4  | 4.50              | 4.32             | 0.36     | 0.5 |
|                               | 375.6  | 4.55              | 5.60             | 0.38     | 0.7 |
|                               | 377.8  | 4.60              | 6.60             | 0.38     | 0.9 |
|                               | 377.3  | 4.50              | 7.50             | 0.38     | 1.0 |
| DGEBA:DDM=2:0.75<br>3:1.25    | 341    | 3.60              | 2.10             | 0.25     |     |
|                               | 341    | 3.62              | 1.85             | 0.27     |     |

to singularity during the curing process, according to which the variation of  $\sigma_0$  with the curing time up to the time of singularity  $t_0$ , may be given by,

$$\sigma_0(t) = A \exp[-B/(t_0-t)] \quad (4.3)$$

where A and B are empirical constants whose values vary with the curing temperature. In eqn (4.3), as t approaches  $t_0$ , the conductivity approaches zero. Therefore, eqn (4.3) represents a progressively rapid decrease in  $\sigma_0$  as  $t_0$  is reached in much the same manner as does eqn (4.2), when  $t_g$  is reached. Eqn (4.3) was fitted to the data given in Figures 4.1 to 4.3 using a reiterative procedure, similar to that described for the fitting of the power law, during which the value of  $t_0$  was adjusted until the sum of mean square deviations became minimum. The calculated data are shown as solid lines in Figures 4.1 to 4.3. The corresponding values of the parameters used for fitting eqn (4.3) are also listed in Tables 4.1 and 4.2. The time of singularity,  $t_0$ , is located near the  $\epsilon''$  peak position which is thus relatively close to  $t_v$ .

Over the limited range of the conductivity values, the fit to the data which is shown in Figures 4.1 to 4.3 seems equally good for both eqns (4.2) and (4.3), except for one set of data, obtained for the DGEBA cured with (0.7 DDS, 0.3 DDM) thermoset which is poorly described by both equations (explanations for this will be discussed in Section 4.5). Based on the fit of our data in Figures 4.1 to 4.3, it is thus difficult to unequivocally determine whether the rapid decrease in the dc conductivity is caused by the network formation, or by the

increase in the viscosity associated with the approach to the glass transition temperature. In physical terms, it means that, although the viscosity approaches infinity at  $t_g$ , the  $\sigma_0$  may or may not approach zero at  $t_g$  and a preference for either of two mechanisms for dc conduction in thermosets remains subjective.

### 4.3 THE DIPOLAR RELAXATION

#### 4.3.1 THE TIME DEPENDENCE OF $\epsilon^*$

We now discuss the changes of  $\epsilon^*$  of a thermoset during its curing and focus our discussion on those changes that occur after the dc conductivity's contribution to  $\epsilon''$  has become negligible. The change in  $\epsilon'$  and  $\epsilon''$ , beyond the time of the appearance of a minimum in  $\epsilon''$ ,  $t_{min}$ , measured for a 1kHz frequency during the isothermal curing are shown in the plots of Figures 3.1, 3.2, 3.5 3.6 and 3.7. These plots resemble the plots of the frequency dependence of  $\epsilon'$  and  $\epsilon''$  of chemically and physically stable dipolar liquids or solids measured at a fixed temperature, an example of which is shown in figure 1.5 (see also Smyth 1955, McCrum et al 1967, Johari and Dannhauser 1969, Johari and Smyth 1972). The resemblance becomes further evident when a comparison of their complex plane plots shown in Figures 3.3, 3.19 and 3.22 is made against the corresponding plots illustrated in Figures 1.6 and 1.7 for chemically and physically stable liquids and solids. This resemblance underscores a phenomenological equivalence between the dielectric effects of a continuously occurring chemically and

physically irreversible change with time in the structure of the thermosets and the corresponding effects of an increase in the measurement frequency during the isothermal study of a chemically and physically stable dipolar liquid or solid.

For establishing a theoretical basis for this phenomenological equivalence, we consider that, at any instant of cure after the  $t_{min}$ , the  $\epsilon^*$  data are represented by eqn (1.11) which we adapt to explicitly include the  $t_{cure}$  conditions as follows:

$$\epsilon^*(t_{cure}) = \epsilon_{\infty}(t_{cure}) + [\epsilon_0(t_{cure}) - \epsilon_{\infty}(t_{cure})] \int_0^{\infty} e^{-j\omega t} (-d\phi(t)/dt) dt \quad (4.4)$$

where  $\phi(t)$  is the dielectric relaxation function at the instant  $t_{cure}$ , and  $t$  is the time for the observation of the decay of the response to an electrical field. For a measurement frequency of 1kHz,  $t$  is of the order of 1ms during which the effect due to a change in the state of the thermoset is assumed to be justifiably negligible at the selected curing temperatures.

Several empirical expressions for the time dependence of  $\phi$  have been found to describe the dielectric properties of thermosets during their cure. Soualmia et al (1982) and Lane et al (1986) have used the Cole-Cole formalism and Lane and Seferis (1986) and Nass and Seferis (1989) have used the Havriliak-Negami (1966) formalism which involves an additional fitting parameter for the shape of the plot. However, the frequency or time range covered by the previous authors were not large enough to allow them to accurately determine which, if any, formalism best described their results. In the results of Soualmia et al (1982), we observe that the distribution of

relaxation time parameter decreases early during the cure, which indicates that the distribution of relaxation times became broader as the chain length increases with the curing time or as the structural network forms. Further to this, we propose that, once the gel is formed, or as the thermoset's viscosity has reached a high enough value, the distribution of relaxation times reaches a limiting value and, therefore, the distribution of relaxation times parameter becomes constant over the period of further curing. These ideas, when incorporated in eqn (4.4), give,

$$\epsilon^*(t_{\text{cure}}) = \epsilon_{\infty}(t_{\text{cure}}) + [\epsilon_0(t_{\text{cure}}) - \epsilon_{\infty}(t_{\text{cure}})]N^*(\omega\tau_{\text{cure}}) \quad (4.5)$$

where  $\tau_{\text{cure}}$  represents the dipolar relaxation time of the structural state of the thermoset at a given instant,  $t_{\text{cure}}$ , and  $N^*$ , as defined in eqn (1.12), is independent of the time during the further cure. The values of  $\epsilon_0(t_{\text{cure}})$  and  $\epsilon_{\infty}(t_{\text{cure}})$  are expected to decrease by a relatively small amount during the curing and Soualmia et al (1982) have indeed found marginal decrease early during the cure. Since this decrease could not be accurately measured here, as a first approximation, the  $\epsilon_0(t_{\text{cure}})$  and  $\epsilon_{\infty}(t_{\text{cure}})$  are assumed to remain constant and their values can be regarded as equal to  $\epsilon_0$  and  $\epsilon_{\infty}$ , respectively.

Attempts were then made to fit the  $\epsilon^*$  data in Figures 3.3, 3.19 and 3.22 to the Cole-Cole, Cole-Davidson and Kolbrausch-Williams-Watts relaxation functions using eqn (4.5). Figure 4.4, where a comparison of the various relaxation functions is made, shows that the KWW formalism was most suitable for describing our results over a wide range of curing times.

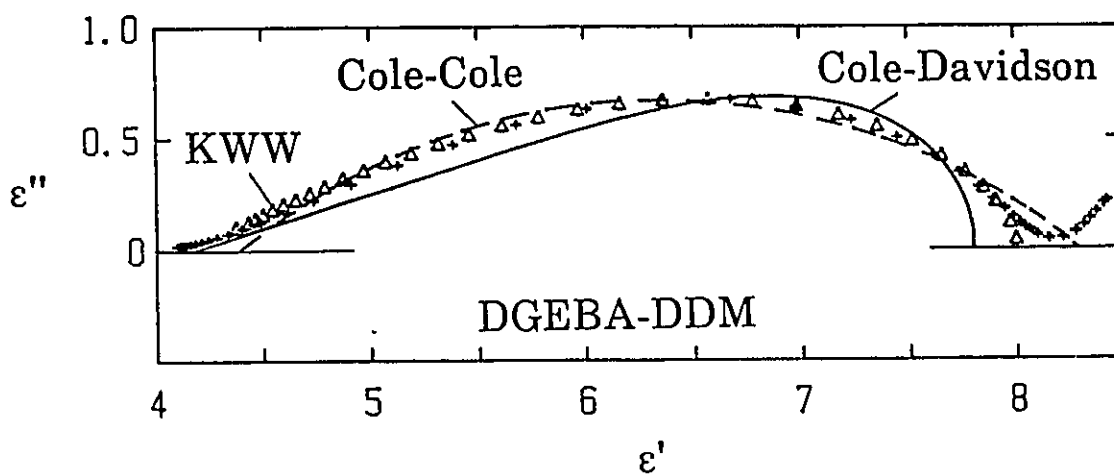


**Figure 4.4:** Comparison between the experimental data (+) obtained during the curing of the DGEBA-DDM thermoset at 303.5K and the theoretical behaviour calculated using the Cole-Cole (dashed line), Cole-Davidson (solid line) and Kohlrausch-Williams-Watts ( $\Delta$ ) functions. The parameters used for the Cole-Cole fit are  $\epsilon_{\infty}=4.4$ ,  $\Delta\epsilon=3.9$  and  $\alpha=0.42$ , for the Cole-Davidson fit;  $\epsilon_{\infty}=4.2$ ,  $\Delta\epsilon=3.6$  and  $\beta_{CD}=0.19$  and for the Kohlrausch-Williams-Watts fit;  $\epsilon_{\infty}=4.2$ ,  $\Delta\epsilon=3.8$  and  $\beta=0.31$ .

Therefore all data analysis were based on this formalism, but, we adapt the relaxation function of eqn (1.19) and rewrite it as:

$$\phi(t) = \exp-(t/\tau_{\text{cure}})^{\gamma} \quad (4.6)$$

where  $\gamma$  is referred to as the curing parameter. Our preference for a different notation, namely, the parameter  $\gamma$  rather than the KWW parameter  $\beta$ , is necessary here to help avoid any confusion between our new parameter with the parameter  $\beta$ , since  $\beta$  is used only for the description of a physically and chemically stable material.

We now proceed to calculate the curing parameter from our data for the thermosets. The values of  $N^*(\omega\tau)$  corresponding to the relaxation function of eqn (4.6) have been tabulated by Moynihan et al (1973) for the equivalent  $\beta$  values between 0.3 and 1 and  $\omega\tau$  values between  $10^{-3}$  and  $10^4$ . For values of  $\beta$ , or as in our case  $\gamma$ , lower than 0.3, we used the  $(\omega\tau)$ -dependence of  $N^*$  derived from the formalism and tables developed by Bendler and coworkers (Montroll and Bendler 1984, Dishon et al 1985 and Weiss et al 1985) as described in the Appendix. From the values  $N^*(\omega\tau)$ , we calculate  $\epsilon'$  and  $\epsilon''$  from eqn (4.5), and plot the calculated values in Figures 4.5, 4.6 and 4.7 together with the experimental data and list the parameters used for the calculation in Table 4.3 (p.108). The agreement between the calculated and experimental values seen in Figures 4.5 to 4.7 is satisfactory and demonstrates the adequacy of the use of our formalism for the curing of thermosets.

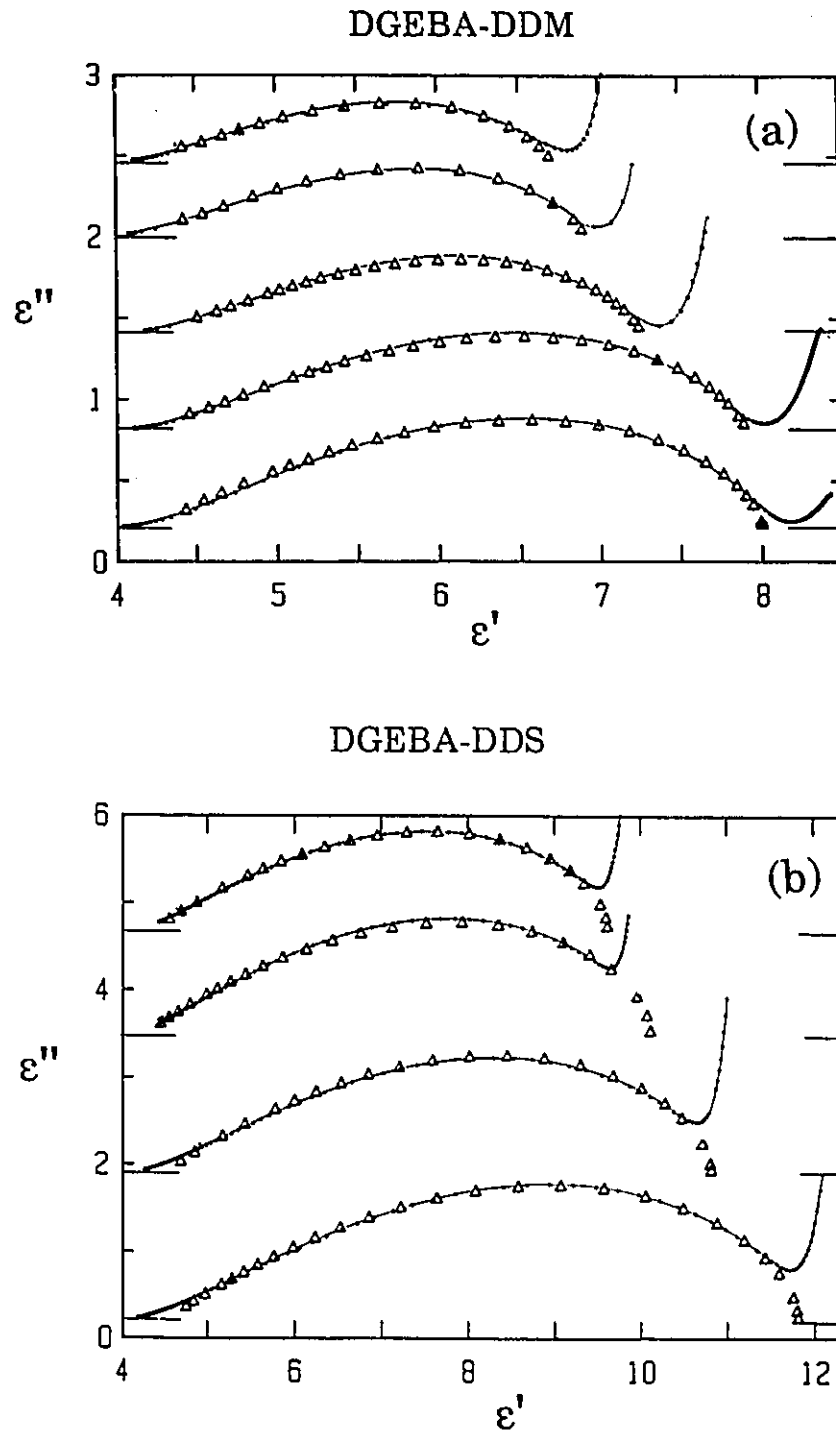


**Figure 4.5:** The complex plane plots of  $\epsilon^*$  for the (a) DGEBA-DDM and (b) DGEBA-DDS thermosets measured at a frequency of 1kHz. The triangles were calculated using eqn (4.5) and the parameters given in Tables 4.3. The  $T_{\text{cure}}$  for the curves are from top to bottom: (a) 340.9K, 331.0K, 322.0K, 312.6K and 303.5K, (b) 412.0K, 400.6K, 387.2K and 377.3K.

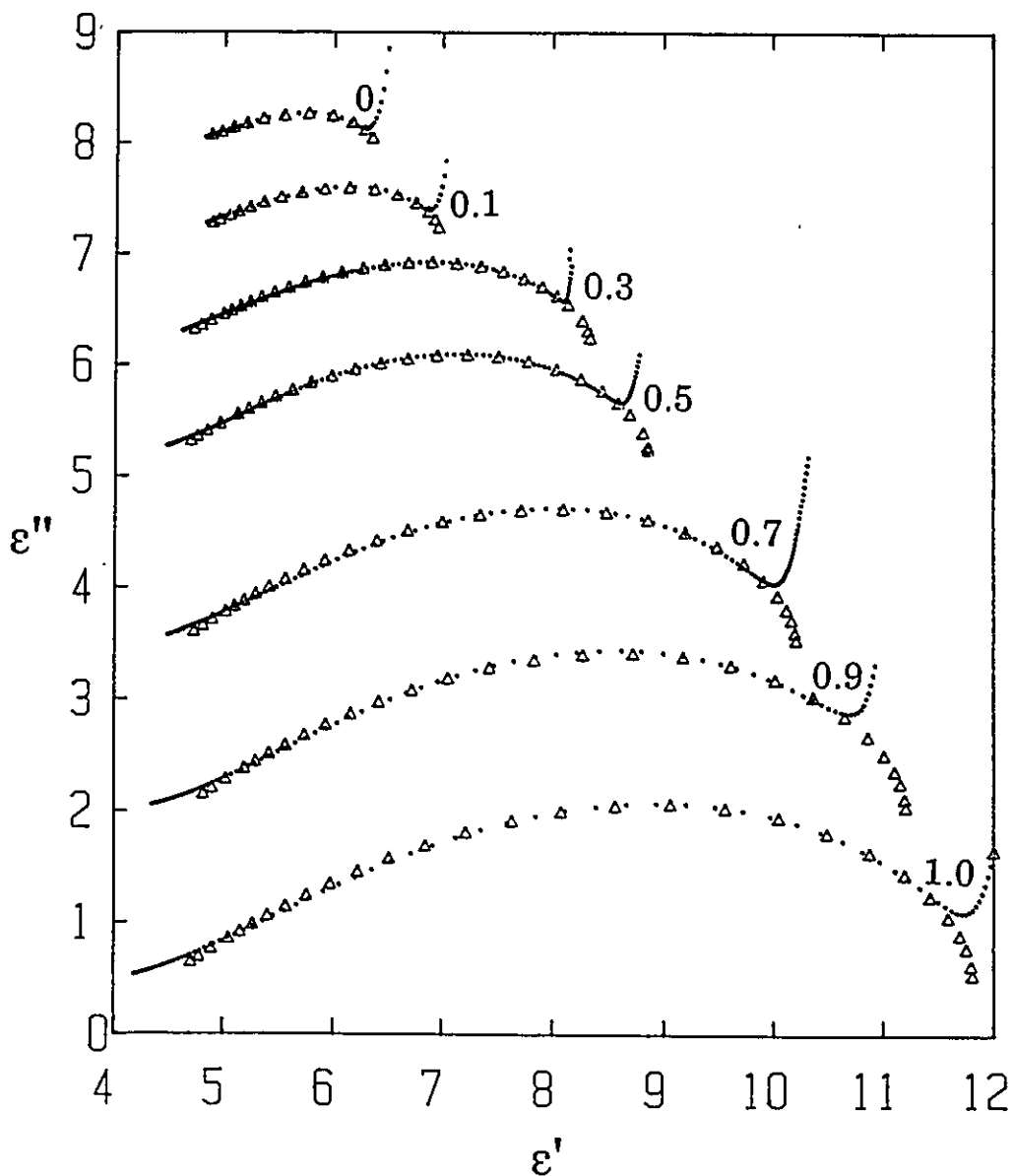


**Figure 4.6:** The complex plane plots of  $\epsilon^*$  for the DGEBA-based thermosets cured with mixed amines at 377K. The triangles were calculated using eqn (4.5) and the parameters given in Table 4.3. The number next to the curves is the mole fraction of DDS in the amine mixture.

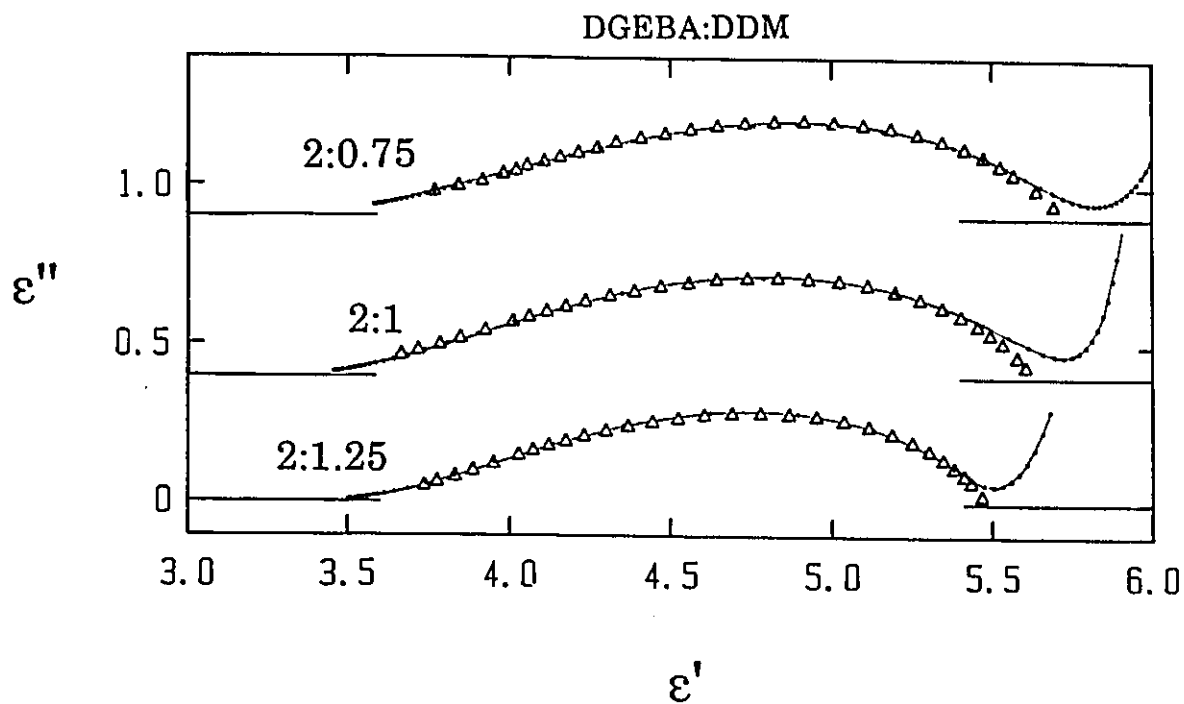


**Figure 4.7:** The complex plane plots of  $\epsilon^*$  for the DGEBA-DDM thermosets of various compositions as they cure at 341K. The triangles were calculated using eqn (4.5) and the parameters given in table 4.3. The ratio next to the curves represent the molar amount of DGEBA over that of DDM.

We further point out that the phenomenological equation for  $\epsilon^*$ , i.e. eqn (4.5), is invariant with respect to one's choice of a change in either  $\omega$  or  $\tau$ . That is that the various shapes of the complex plane plots of  $\epsilon^*$  can be obtained by varying either  $\omega$  or  $\tau$ . Whereas in chemically stable materials, these shapes are obtained by varying the frequency or the temperature and pressure of measurement, here, it is obtained by a spontaneous increase in  $\tau$  which occurs as a result of an increase in the steric hindrance caused by an increase in the chain length or number density of cross-links in a curing thermoset. This statement will be examined in further detail in Section 4.3.3.

#### 4.3.2 THE CURING PARAMETER, $\gamma$

The values of  $\epsilon_\infty$ ,  $(\epsilon_0 - \epsilon_\infty)$ , or  $\Delta\epsilon$ , and  $\gamma$  which were used for the fitting of the  $\epsilon^*$  data to eqn (4.5) and which are listed in Table 4.3 can now be examined for their dependence upon the temperature and composition of the thermosets. For this, we have plotted the curing parameter against the reciprocal temperature and composition in Figure 4.8.

It is seen that the parameter  $\gamma$  in Figure 4.8(a) decreases with an increase in the temperature of isothermal curing of DGEBA-DDM and tends towards a constant value at higher temperatures. This indicates that for the curing period of relevance of the DGEBA-DDM thermoset the value of  $\gamma$  is high, and the distribution of dipolar relaxation times is narrower, when cross-linking occurs at a lower temperature. It means

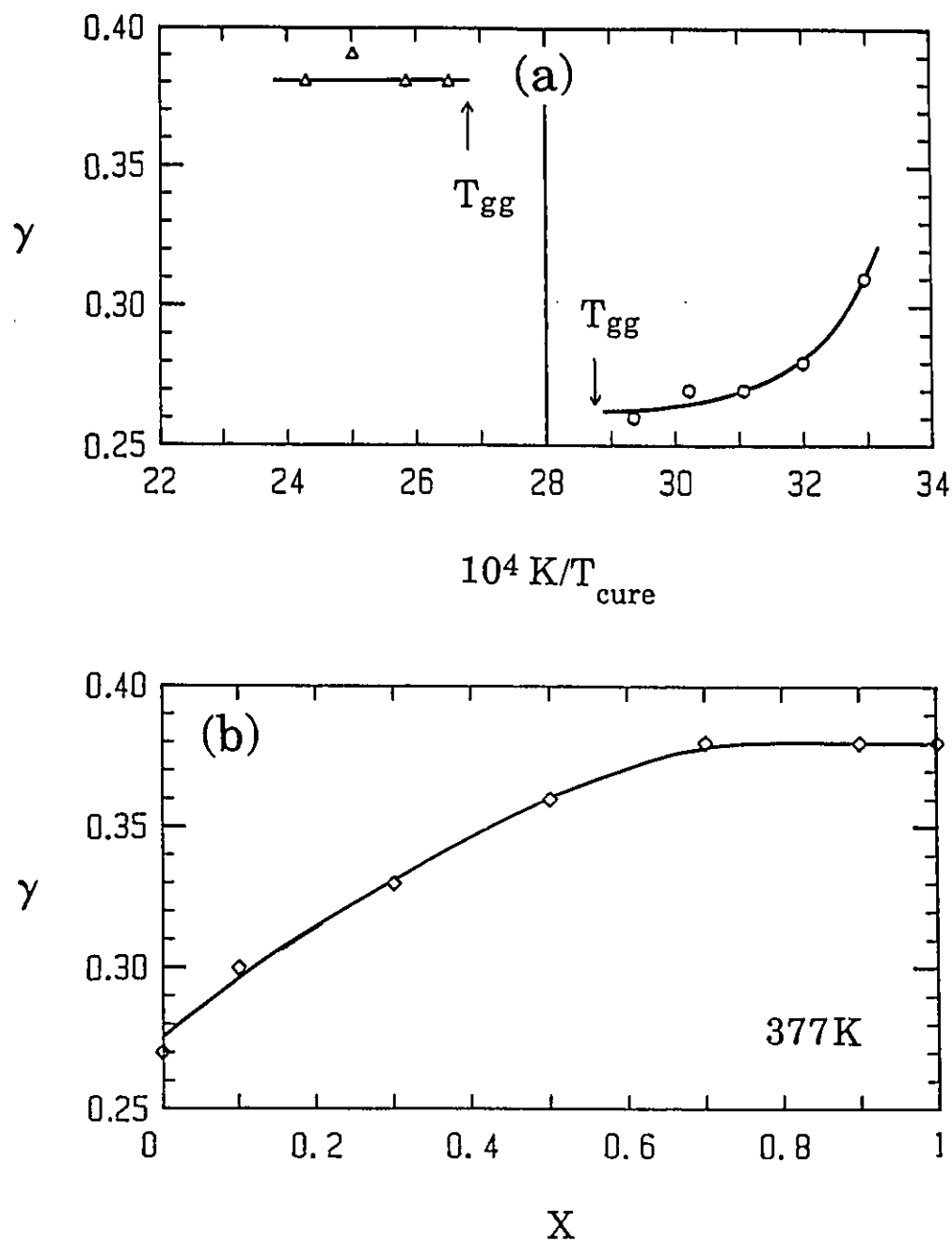


**Figure 4.8** The curing parameter  $\gamma$  plotted against (a) the reciprocal temperature for the DGEBA-DDM and DGEBA-DDS thermosets and (b) the molar ratio of DDS in the curing amine for the DGEBA-based thermosets cured at 377K.

that, in its structurally arrested state at the end of the cure, the main relaxation spectra is narrower when the thermoset is cured at a low temperature. This also, of course, implies that the achieved chemical and physical structures of the DGEBA-DDM thermoset largely depend on the selected curing temperature, especially at lower curing temperatures. But at high temperatures of curing the distribution parameter in the cured thermoset is lowered and beyond a certain temperature its value remains unchanged.

The above given observations of the variation of  $\gamma$  with temperature can be rationalized in the following manner: Enns and Gillham (1983a) have provided partial TTT diagrams for the curing of several thermosets, including DGEBA-DDM and DGEBA-DDS. These were obtained from measurements of the dynamic mechanical behaviour using a torsional braid analysis technique. From their Figure 22, the  $T_{gg}$  value for the DGEBA-DDM thermoset is estimated to lie between 343K and 363K, where  $T_{gg}$  represents the curing temperature at which the gel point of the thermoset coincides with its vitrification point. Since the curing temperatures selected here for the dielectric study of the DGEBA-DDM thermoset are less than 341K as is seen in Table 4.3, the thermoset's structure is not likely to have formed a gel before its vitrification. Since the extent of reaction,  $\alpha_v$ , at the time for vitrification,  $t_v$ , increases with an increase in  $T_{cure}$ , as shown in Figure 1.2, the average chain length of the ungelled structure at  $t_v$  is increased. The progressively rapid increase of  $\gamma$  with a decrease in the

temperature observed in Figure 4.8(a) is thus an indication of a strong dependence of the distribution of relaxation times on the length of the polymer molecular chain. As the curing temperature is raised towards the estimated value of  $T_{gg}$ , the DGEBA-DDM thermoset acquires at its vitrification point an increasingly more network structure. Thus, the value of its  $\gamma$  depends less and less on the curing temperature. The value of  $\gamma$  in Figure 4.8(a) becomes constant at about 0.27 at 322K. This value is the same as the  $\gamma$  value of 0.27 determined for the DGEBA-DDM thermoset, cured at  $377 \pm 2K$ , in our independent study of the mixed amine cured thermosets for which the values of  $\gamma$  are plotted against the composition in Figure 4.8(b). This agreement is a further confirmation of the interpretation given here.

The  $\gamma$  value of the DGEBA-DDS thermoset in Figure 4.8(a) remains constant with temperature. This is in contrast with the corresponding temperature dependence of  $\gamma$  in the DGEBA-DDM thermoset. Enns and Gillham (1983a) did report a  $T_{gg}$  value of 373K for the DGEBA-DDS thermoset. This means that for curing temperatures higher than 373K, the molecular structure of the DGEBA-DDS thermoset has reached its gelled state before vitrification. Since the curing temperatures selected for the dielectric study of the DGEBA-DDS thermoset are higher than 373K, the constant value of  $\gamma$  in Figure 4.8(a) indicates that, after the DGEBA-DDS thermoset has gelled, the distribution of relaxation times becomes insensitive to a further increase in its cross-link density which in turn ultimately vitrifies it.

The above given discussion has an important consequence for our preference of  $\gamma$  over the distribution parameter  $\beta$  and this relies upon the distinction between the generally observed temperature dependence of the two parameters. Although, as mentioned earlier,  $\gamma$  is phenomenologically equivalent to  $\beta$  as implied by eqns (1.19) and (4.6), the value of the parameter  $\gamma$  increases with decreasing temperature in contrast with the value of the KWW parameter which either remains constant or instead generally increases with an increase in temperature, as observed by Williams (1984), Mangion and Johari (1988) and Boese et al (1989), and as evident in the loss spectrum of polymers discussed by McCrum, Read and Williams (1967). This distinction justifies our preference for  $\gamma$  as the curing parameter for thermosets.

The foregoing discussion can now also be extended to determine the time dependence of  $\gamma$  during a thermoset cure. Before the gelation of a thermoset, its value of  $\gamma$  decreases rapidly as the polymerization increases the chain length, and reaches a limiting value at a time just before the gel point. This confirms the validity of our earlier assumption that  $\gamma$  remains constant with time after gelation.

As seen in Figure 4.8 and Table 4.3, the  $\gamma$  value of 0.38 observed for the curing of the DGEBA-DDS thermoset is significantly higher than that of about 0.27 corresponding to the DGEBA-DDM thermoset. The curing temperatures for the DGEBA-DDS are about 50K higher than those for the DGEBA-DDM thermoset, which is comparable with the difference in their  $T_g$ .

values of 485K and 442K, respectively, as measured by Choy and Plazek (1986). The large difference between the  $\gamma$  values of DGEBA-DDM and DGEBA-DDS thermosets thus cannot be explained by the difference between their curing temperatures alone. We suggest that this difference is a reflection of the dissimilar kinetics of the cross-linking reactions in the two thermosets which produce differences in their network topology. In this respect, it is useful to recall that Dobas et al (1975) have also reported differences between the rate constant ratio,  $k_1/k_2$ , for the primary amine to the secondary amine reactions in the two types of thermosets. This ratio is in the range 2-3 for the DGEBA-DDM thermoset and in the range 4-6 for the DGEBA-DDS thermoset, which suggests that the network structures resulting from the cross-linking reactions with DDM and DDS, respectively, would be dissimilar. The different distributions of relaxation times in DDM and DDS cured DGEBA may be related to this dissimilarity of kinetics.

An important aspect of the change in the  $\gamma$  values with the change in composition of the curing agent in the thermoset can be seen in Figure 4.8(b) and Table 4.3 where  $\gamma$  increases non linearly from 0.27 to 0.38, as the molar ratio of DDS in the (DDS, DDM) mixture,  $x$ , is increased from 0 to 1, and tends towards a constant value of 0.38 when  $x \geq 0.7$ .

Further information on the dependence of  $\gamma$  on the network formation in thermoset may be obtained from a comparison between the behaviours of the starved and saturated thermosets. The  $\gamma$  value of 0.25 observed for the stoichiometrically starved

DGEBA-DDM thermoset as seen in Table 4.3 is comparable with the value of 0.27 for the saturated thermoset which in turn is comparable with the corresponding  $\gamma$  value of 0.26 for the stoichiometric thermoset. All these observations suggest, in a self-consistent manner, that once the network structure has formed, further increase in the cross-link density has no effect on the curing parameter.

#### 4.3.3 THE TIME DEPENDENCE OF THE RELAXATION TIME

We now develop a method for determining the time-dependence of the relaxation time during the curing of thermosets. In the complex plane plot of the dielectric permittivity in Figure 4.6, the points are the values measured at a time  $t$  during the curing and the triangles are the values calculated using the KWW formalism. Each calculated value corresponds to a value of  $(\omega\tau_{cure})$  in eqn (4.5), where  $\tau_{cure}$  is the relaxation time that appears in the expression of the relaxation function,  $\phi$ , in eqn (4.6). Although the  $\epsilon'$  and  $\epsilon''$  calculated from eqn (4.5) could be temporally matched with the experimental ones in some cases, in others it was necessary to interpolate the time at which the values were calculated. This procedure made it possible to associate a curing time value to almost every value of  $(\omega\tau_{cure})$  for each of the isothermal curing experiments on the various thermosets. Since a value of  $(\omega\tau_{cure})$  uniquely corresponds to a value for  $N'$  and  $N''$ , as seen in the tables given in the Appendix, it becomes possible to calculate the time dependence of  $\epsilon^*$ .

The adequacy of this method can be tested by comparing the time dependence of the calculated  $\epsilon^*$  with the experimental results. This comparison is shown in Figures 4.9 and 4.10, where the  $\epsilon'$  and  $\epsilon''$  are plotted on a linear scale against logarithmic time, for the DGEBA-DDM and DGEBA-DDS thermosets, respectively, measured at various curing temperatures. The agreement between the calculated and the experimentally measured values in Figures 4.9 and 4.10 demonstrates that the procedure used here is satisfactory.

From the values of the  $(\omega\tau_{\text{cure}})$  at various times, the variation of  $\tau_{\text{cure}}$  against time is now calculated for  $\omega=2\pi f=6.28\text{kHz}$  and the calculated values of  $\tau_{\text{cure}}$  are plotted against the curing time in Figure 4.11 for both the DGEBA-DDM and DGEBA-DDS thermosets at several temperatures of cure. The range of  $(\omega\tau_{\text{cure}})$  values used for the calculation of the KWW data, as given by Moynihan et al (1973), is available over seven decades from  $10^{-3}$  to  $10^4$ . Therefore, the range of  $\tau_{\text{cure}}$  values characterized in Figure 4.11 becomes limited to seven decades from  $10^{-6}$  to 10 sec. (Although a larger range could be chosen by using the Table given in the Appendix, little accurate information could be further obtained by doing so).

In Figure 4.11(a), the time evolutions of  $\tau$  in the DGEBA-DDM thermoset are seen to remarkably differ from those in the DGEBA-DDS thermoset in figure 4.11(b), even when their curing times are comparable. This difference in the behaviour, is obviously associated with the differences in their molecular size, shape and charge distribution and the consequent

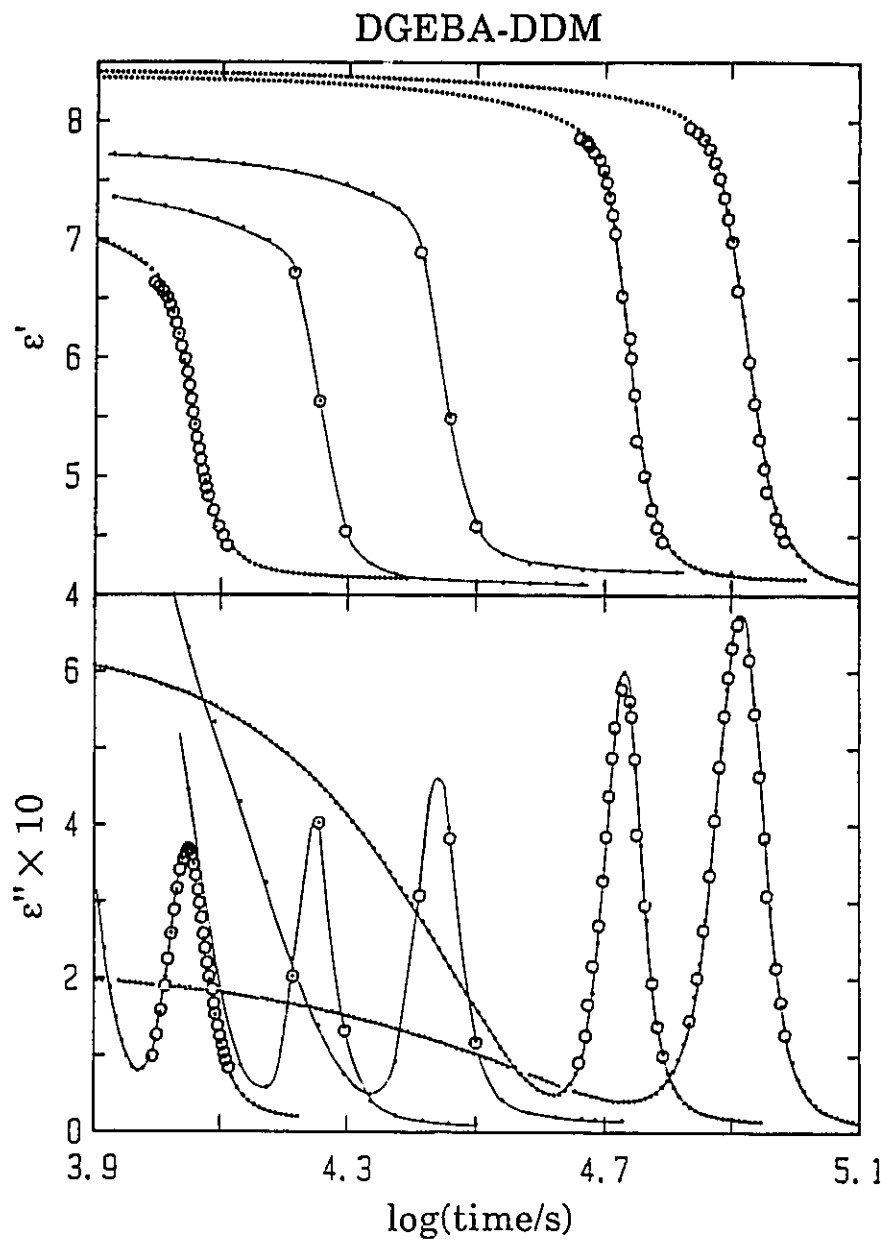


**Figure 4.9:** The dielectric permittivity and loss of the DGEBA-DDM thermoset measured at 1kHz are plotted against the curing time.  $T_{\text{cure}}$  for the curves from left to right is 340.9K, 331.0K, 322.0K, 312.6K and 303.5K. The circles were determined from the fit of Figure 4.5.

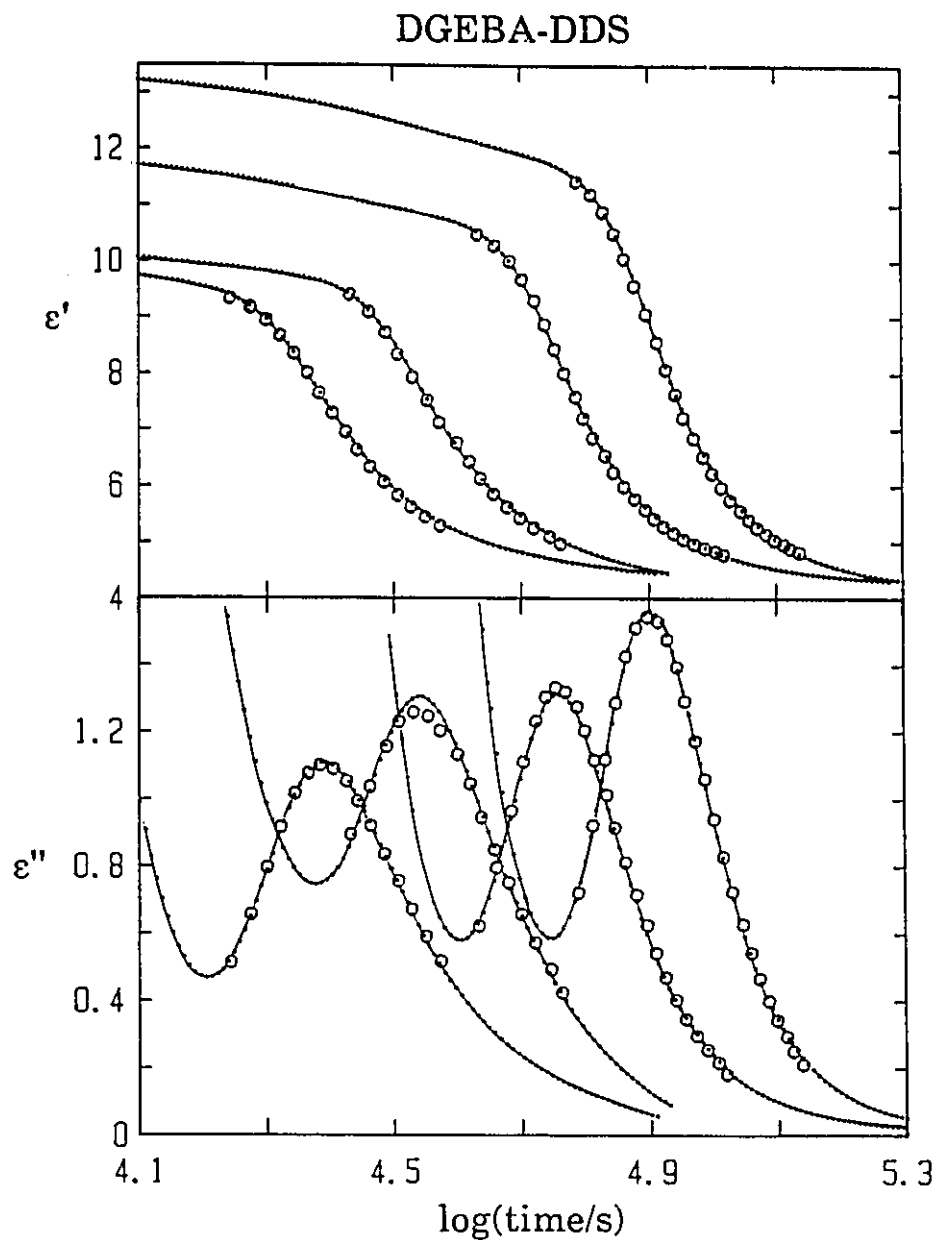


**Figure 4.10** The dielectric permittivity and loss of the DGEBA-DDS thermoset measured at 1kHz are plotted against the curing time.  $T_{\text{cure}}$  for the curves from left to right is 412.0K, 400.6K, 387.2K and 377.3K. The circles were determined from the fit of Figure 4.5.

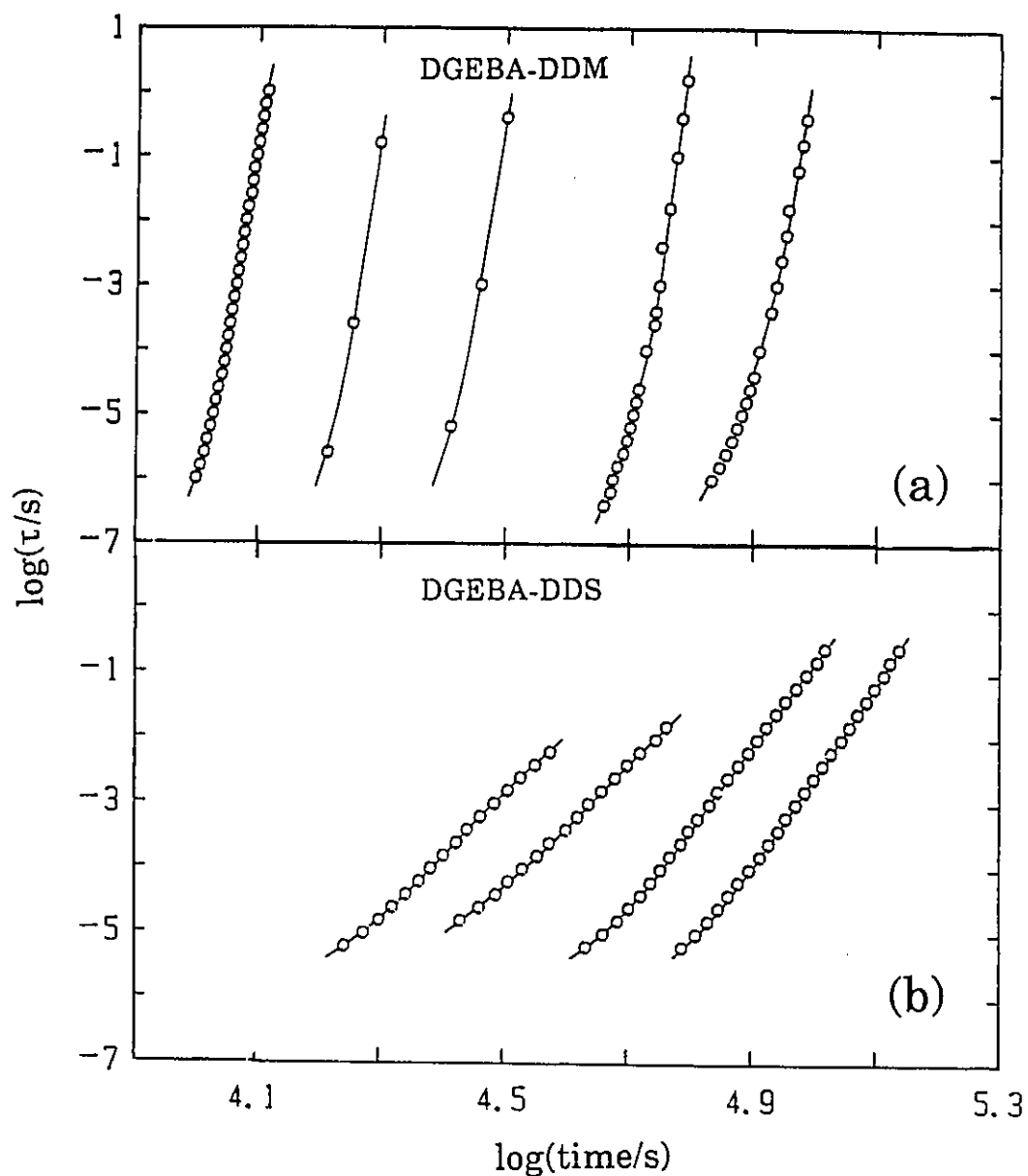


**Figure 4.11** The relaxation time in the (a) DGEBA-DDM and (b) DGEBA-DDS thermosets is plotted against time.  $T_{\text{cure}}$  for the curves from left to right are (a) 340.9K, 331.0K, 322.0K, 312.6K and 303.5K, and (b) 412.0K, 400.6K, 387.2K and 377.3K.

differences in their cross-linking reaction kinetics as discussed in Section 4.3.2.

The formalism derived above for determining the curing time dependence of  $\tau$  is now further used to analyze the data for the DGEBA-based thermosets cured with amine mixtures of different compositions. The data obtained are plotted against time for the seven thermosets in Figure 4.12, which shows that the plots have the shape of an elongated S with a point of inflexion. The value of  $(d\log\tau/d\log t)$  at the point of inflexion in Figure 4.12 first decreases to a minimum value when the molar ratio of DDS in the amine mixture,  $x$ , is 0.5, and then increases. These observations on the dependence of the relaxation time on the curing time would be interpreted in terms of the curing kinetics in Section 4.5.

#### **4.4 CHANGES IN THE BRILLOUIN SPECTRA**

##### **4.4.1 THE HYPERSONIC VELOCITY**

It is well known (Ferry 1980, LeMay and Kelley 1986) that the elastic constants of a polymer increase with increase in its molecular weight. For thermosets, this increase is expected to occur during its curing process. Figures 3.12 and 3.15, where the product of sound wave velocity,  $v$ , and refractive index,  $n$ , is plotted against the curing time of the DGEBA-DDM and DGEBA-DDS thermosets at different temperatures, show a similar behaviour with the increase in the curing time when cross-linking increases the molecular weight. In these figures, the product  $nv$  is seen to continue to increase after

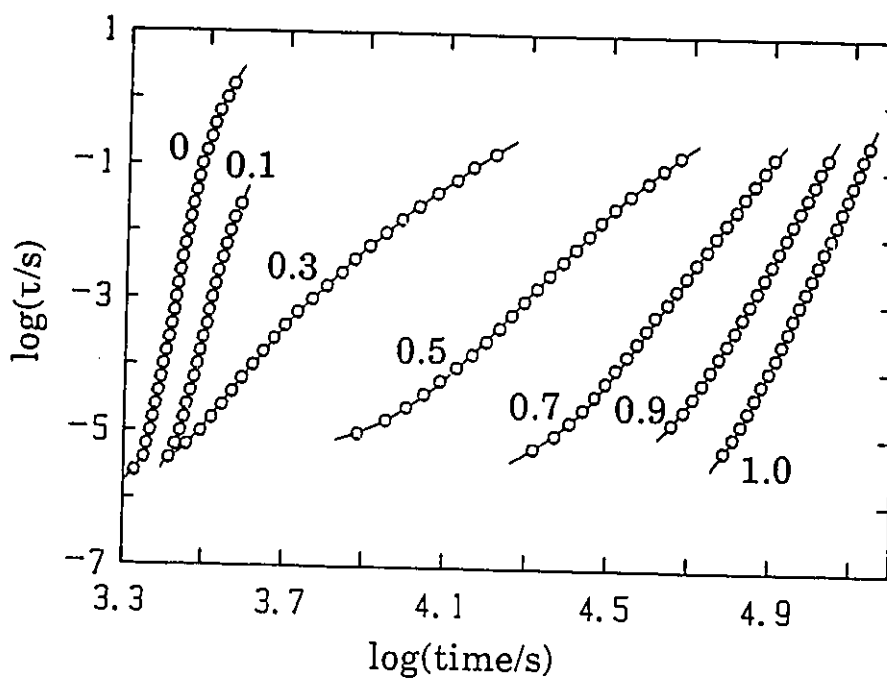


**Figure 4.12:** The relaxation time in the DGEBA-based thermosets cured at 377K with mixed amines is plotted against the curing time. The number next to the curves refers to the mole fraction of DDS in the DDM-DDS amine mixture.

the gelling point despite the fact that, formally speaking, the molecular weight becomes infinite at  $t_g$  and does not increase beyond  $t_g$ . As mentioned in Section 3.2 the change in  $n$  on curing is less than 3% and can be ignored so that further considerations may be made only in terms of the velocity.

One of the remarkable features of the profile of velocity with curing time is that it seems to increase in two steps, or that the profile is divided into two elongated, S-shaped curves. This shape is similar to the shape we observed for the time dependence of the electrical modulus as well as to that observed for the mechanical modulus,  $G'$ , at 1Hz reported by Enns and Gillham (1983(a)), Harran et al (1985, 1986 and 1988) and Gotro and Yandrasits (1989). A comparison of the plots is made in Figure 4.13 where the  $t_g$  values calculated in Section 4.1 and given in Table 4.1 are indicated by arrows. These observations clearly establish that the change in mechanical modulus determined from the velocity of sound by Brillouin scattering is qualitatively equivalent to the change in shear modulus measured at 1Hz and in the electrical modulus measured at 1kHz.

We now examine whether the magnitude of increase in the hypersonic velocity differs in the two thermosets during their curing. In the sol state, the value of  $nv$  in Figures 3.12 and 3.15 is in the range 2.8 to 3.0km/s for the DGEBA-DDM thermoset, which is nearly 20% higher than the corresponding range of 2.2 to 2.4 km/s for the DGEBA-DDS thermoset. The ultimate velocity of hypersonic waves in the glassy state of

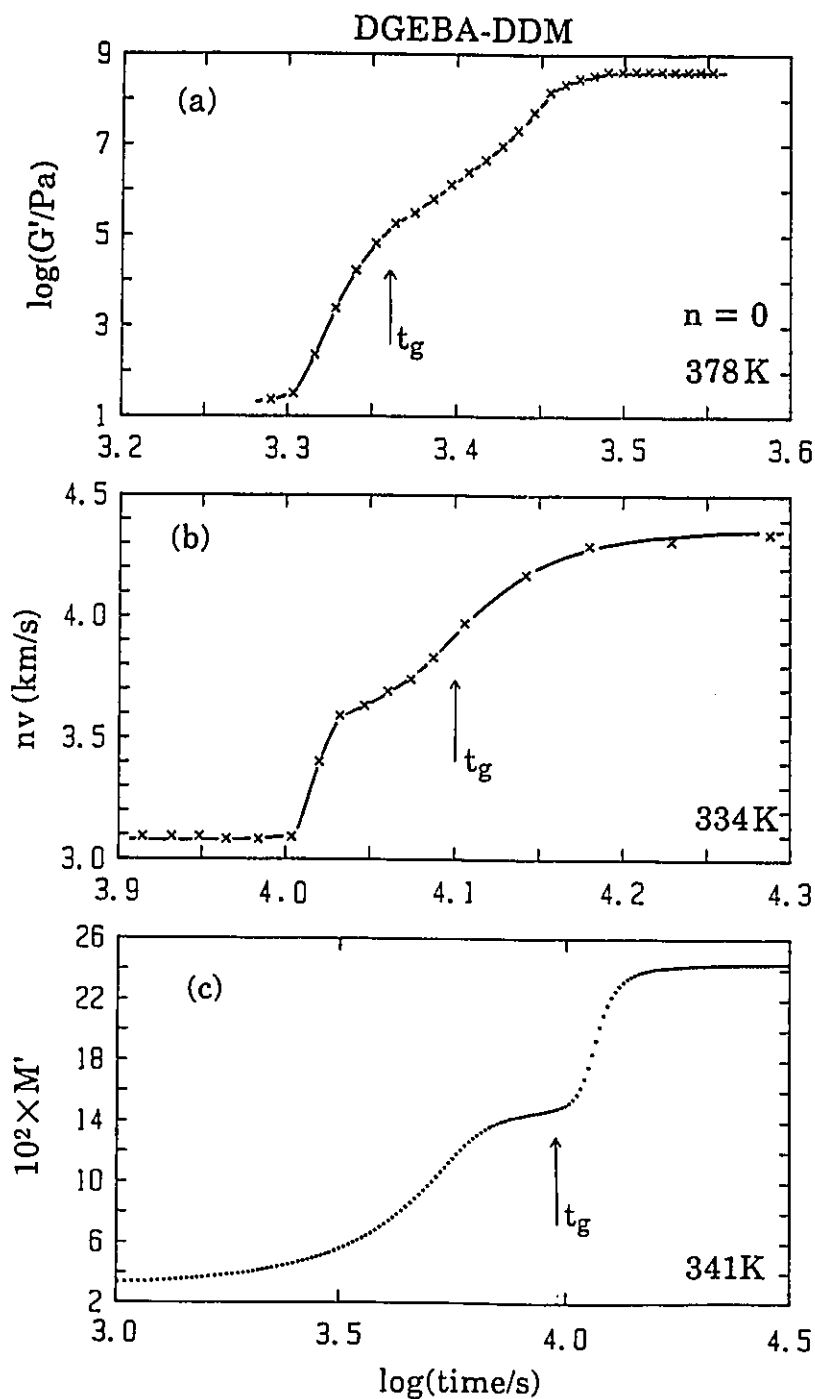


**Figure 4.13:** The curing time dependence of (a) the real part of the elastic modulus (Harran et al 1988), (b) the product of the refractive index and velocity of hypersonic waves (Figure 3.12) and (c) the real part of the electrical modulus (Figure 3.23) of the DGEBA-DDM thermoset. The curing temperatures are indicated on each graph. The arrows represent the values of the gelling time calculated in Section 4.2 and given in Table 4.1.

the former thermoset is  $(4.3/n)$ km/s which is nearly 7% higher than  $(4.0/n)$ km/s in the glassy state of the latter thermoset. These results suggest that the net increase in the value of  $n_v$  is 21% higher for the DGEBA-DDS than for the DGEBA-DDM thermoset under identical conditions of curing.

There is a further point of interest which deals with the rate at which the conversion from sol to gel to glass in the two thermosets occurs. From its initial increase to reach its limiting modulus at 324K, the DGEBA-DDM thermoset takes about 1.3ks while the DGEBA-DDS thermoset reaches its limiting value at 423K in about 3.9ks, indicating that the conversion in the latter occurs more gradually than in the former. As discussed in Section 4.2.3, these observations are again a reflection of the differences between the molecular size, charge density and reactivity of the two curing agents, which cause the chemical kinetics of their curing reactions with the DGEBA to differ.

#### 4.4.2 THE ATTENUATION AND LOSS FACTOR

In Figures 3.13 and 3.16, where the attenuation to refractive index ratio of elastic waves,  $\alpha/n$ , is plotted against time, the curves show that  $\alpha/n$  decreases from values between  $4.2 \times 10^{-6}$  and  $5.0 \times 10^{-6} \text{m}^{-1}$  to  $1.0 \times 10^{-6} \text{m}^{-1}$  for the DGEBA-DDM thermoset and from between  $5.0 \times 10^{-6}$  and  $5.6 \times 10^{-6} \text{m}^{-1}$  to  $1.9 \times 10^{-6} \text{m}^{-1}$  for the DGEBA-DDS thermoset. This is an evidence that the cured DGEBA-DDS thermoset causes a higher damping of the hypersonic waves than the DGEBA-DDM thermoset, and is likely to be a

reflection of the relatively loose structure of the network in the DGEBA-DDS thermoset.

The curves in Figures 3.13 and 3.16 also show a step-decrease at approximately the gel point of the two thermosets, which is qualitatively similar to the corresponding velocity of sound plots in Figures 3.12 and 3.15. Therefore, we suggest that this stepwise decrease in  $(\alpha/n)$  also indicates a transformation of sol to gel during the curing of the thermoset.

#### 4.4.3 THE CURING TIME AND TEMPERATURE BEHAVIOUR

We now consider the correspondence between the curing time and the temperature of cure of the two thermosets in the Brillouin scattering studies. The step-like increase that divides the curves in Figures 3.12, 3.13, 3.15 and 3.16 into two elongated S-shaped curves appears at a curing time which increases with a decrease in the curing temperature. In order to determine the effect of temperature on the position of this step-like increase, the curing time needed to reach half of the total change was determined from Figures 3.12 and 3.15 and the values are logarithmically plotted against reciprocal temperatures in Figure 3.17. The data follow a straight line with an activation energy of 42kJ/mole for the DGEBA-DDM and 41kJ/mole for the DGEBA-DDS thermosets. These values reasonably agree with those of 47 and 45kJ/mole, respectively, obtained from the dielectric measurements in Section 3.1.1, and this agreement substantiates our earlier finding that the

underlying mechanisms for the observed changes in both Brillouin and dielectric properties are the rates of chemical reactions.

It is useful to examine whether the variation of the curing time with curing temperature, as noted above, can be seen in the dependence of the relaxation rate on the curing time. For this we return to our study in Section 3.1.2 of the dielectric properties of the DGEBA-DDM thermoset during its cure at 331K which allowed us to derive the frequency dependence of the time of cure needed to achieve half of the total decrease in  $\epsilon'$ , and to plot it against time in Figure 3.8. In this figure, we have also included one data point for the time needed to achieve half of the total increase in  $n_V$ , which was measured from Brillouin scattering data in Figure 3.12 for the DGEBA-DDM thermoset cured at 334K. Despite the 3 degree difference in the temperature of the dielectric and Brillouin measurements, the dielectric data linearly extrapolates to the Brillouin frequency range according to the equation

$$f(t) = f_0 \exp(-kt_{\text{cure}}) \quad (4.7)$$

where  $f_0$  and  $k$  are constants with values of  $3.5 \times 10^{24} \text{Hz}$  and  $2.66 \times 10^{-3} \text{s}^{-1}$ , respectively. This means that assuming a constant distribution of relaxation times or curing parameter, the average relaxation rate in the thermosets measured by the Brillouin and dielectric method decreases exponentially with the curing time. Similar connections between Brillouin and dielectric data but with changing temperature have been also

noted by Angell (1986) and Angell et al (1986) and Mangion and Johari (1988), for the conductivity and Brillouin relaxation rates in AgI-based ionic glasses.

#### 4.5 EFFECT OF SUBSTITUTION OF THE AMINES

In Section 3.3, we have seen that for the mixed amines cured thermosets, the  $\epsilon''$  goes through a point of inflexion during the curing and that the  $(d\log\epsilon''/d\log t)$  value at that point reaches a minimum at  $x=0.7$ . As deduced in Section 4.1, the decrease in  $\epsilon''$  that occurs within the time range of the inflexion point, is mainly caused by the decrease in the dc conductivity towards its ultimate zero value at the gel point. As discussed in Section 4.1, the rate of decrease in the dc conductivity at the inflexion point is controlled by the rate of increase in viscosity and the network formation which in turn are controlled by the rate of reactions at the corresponding curing time. The extent of reaction at this curing time is expected to be somewhat less than the extent of reaction at gelation, or  $\alpha_g$ , and so this point of inflection occurs in the sol state of the thermoset.

We now seek a connection between the above mentioned behaviour and the time dependence of the relaxation time given in Section 4.1 and Figure 4.12. Here, the relaxation time obtained from our theoretical analysis also seems to go through a point of inflexion, and the value of  $(d\log\tau/d\log t)$  at this point reaches a minimum at a composition,  $x=0.5$ .

Correspondingly, the temporal separation between the  $\epsilon''_{\min}$  and  $\epsilon''_{\max}$  reaches a maximum value at  $x=0.5$ , as is seen in Figure 3.20. The rate of the increase of  $\log r$  is again controlled by the rate of increase in viscosity and of network formation which in turn is controlled by the reaction rates at the corresponding times during curing, from near the gel point to the vitrification point. From the foregoing discussion, it seems that an explanation for the non-monotonic composition dependence of the dielectric features of DGEBA cured with the mixed amines is related to the manner by which the extent of reaction changes with the curing time in each thermoset. Theoretical consideration and justification for these observations are now discussed as follows.

The curing kinetics of thermosets has been ably reviewed by Barton (1985), Prime (1980), and Williams (1985). In general, terms of the fractional degree of conversion,  $\alpha$ , the curing kinetics is written as:

$$d\alpha/dt = f(\alpha) \quad (4.8)$$

where  $f$ , the functional form of  $\alpha$ , varies with the nature of the thermoset. Barton (1980, 1985) found that his calorimetric data obtained during the curing of the DGEBA-DDS thermoset were satisfactorily fitted to the function  $f$  in the form,

$$f(\alpha) = (A_0 + A_1\alpha + A_2\alpha^2)(1-\alpha), \quad (4.9)$$

where the values of the temperature-dependent kinetic constants  $A_0$ ,  $A_1$  and  $A_2$ , extrapolated to 377K From Barton's results (1980), are  $6.40 \times 10^{-6} \text{ s}^{-1}$ ,  $2.6 \times 10^{-4} \text{ s}^{-1}$  and  $4.86 \times 10^{-4} \text{ s}^{-1}$  respectively. Equation (4.9) has been found to account for both the

chemically controlled and the diffusion controlled kinetics for the DGEBA-DDS thermoset. The equivalent expression for the curing kinetics of the DGEBA-DDM thermoset was given by Sourour and Kamal (1976) and Huguenin and Klein (1985) as,

$$f(\alpha) = (k_1 + k_2\alpha)(1-\alpha)(0.99-\alpha) \quad (4.10)$$

where the values of the kinetic constants  $k_1$  and  $k_2$  at 377K are  $1.07 \times 10^{-4} \text{s}^{-1}$  and  $3.35 \times 10^{-3} \text{s}^{-1}$ , respectively.

These functional forms allow us to calculate the time needed to reach a given conversion during the curing of both the DGEBA-DDM and DGEBA-DDS thermosets by a numerical integration of eqn (4.8), as follows:

$$t(\alpha) = \int_0^\alpha d\alpha / f(\alpha) \quad (4.11)$$

Plots of  $\alpha$  against time of cure thus calculated are shown in Figure 4.14, where it is evident that the cure of DGEBA occurs much faster with DDM than with DDS, at the same temperature of 377K. For example, after 2.6ks, the extent of reaction is 80% for the DGEBA-DDM thermoset and only 2.5% for the DGEBA-DDS thermoset. Therefore, it is reasonable to assume that, during the cure of DGEBA with a mixture of amines, the addition reactions of the DDM molecules with the epoxide group occurs preferentially and is completed before those of the DDS molecules begin, in order to allow us to construct the plots of the extent of reaction against time as follows: For a given value of  $\alpha$ , which is less than the amount  $(1-x)$  of DDM in the mixed amine, the plot of  $\alpha$  against time would correspond to the one for pure DGEBA-DDM thermoset. For values of  $\alpha$  higher than  $(1-x)$ , the plot would correspond to that of the pure DGEBA-DDS

mixture but would be shifted along the time axis as is intuitively required for the continuity of the addition reactions. The extent of reaction against time plots were thus constructed. These plots for all mixed amine thermosets except for the DGEBA-(0.1 DDS, 0.9 DDM) thermoset, which has been deleted for the sake of clarity, are shown in Figure 4.14. The lower dashed horizontal line in Figure 4.14, represents conversion from sol to gel and the upper line from gel to glass, which we assume to occur at a fixed value of the extent of reaction, i.e.  $\alpha_g = 0.7$  and  $\alpha_v = 0.85$ , respectively, values which were taken from the work of Enns and Gillham (1983b). We realize that, since the  $T_{gm}$  value of the DGEBA-DDM thermoset is about 40K lower than that of the DGEBA-DDS thermoset (Choy and Plazek 1986), the extent of reaction of DGEBA-(xDDS, (1-x)DDM) thermosets reached at the vitrification point during their cure at 377K is expected to decrease as x increases and that therefore the dashed lines should be composition dependent and not horizontal. However, as would become clear in further discussion, the assumption of composition independence of  $\alpha_g$  and  $\alpha_v$  in Figure 4.14 does not alter the final conclusions of our derivations given as follows:

The slope of the plots of  $\alpha$  against  $\log t$  curve was measured for each thermoset at the point corresponding to a selected constant value of  $\alpha$ . The values of  $(d\alpha/d\log t)$  are plotted against x in Figure 4.15, which shows a minimum at about  $x=0.7$  for  $\alpha=0.5$  and  $x=0.5$  for  $\alpha=0.7$ . The time of cure needed to reach an extent of reaction or  $\alpha$  of 0.5 is shorter

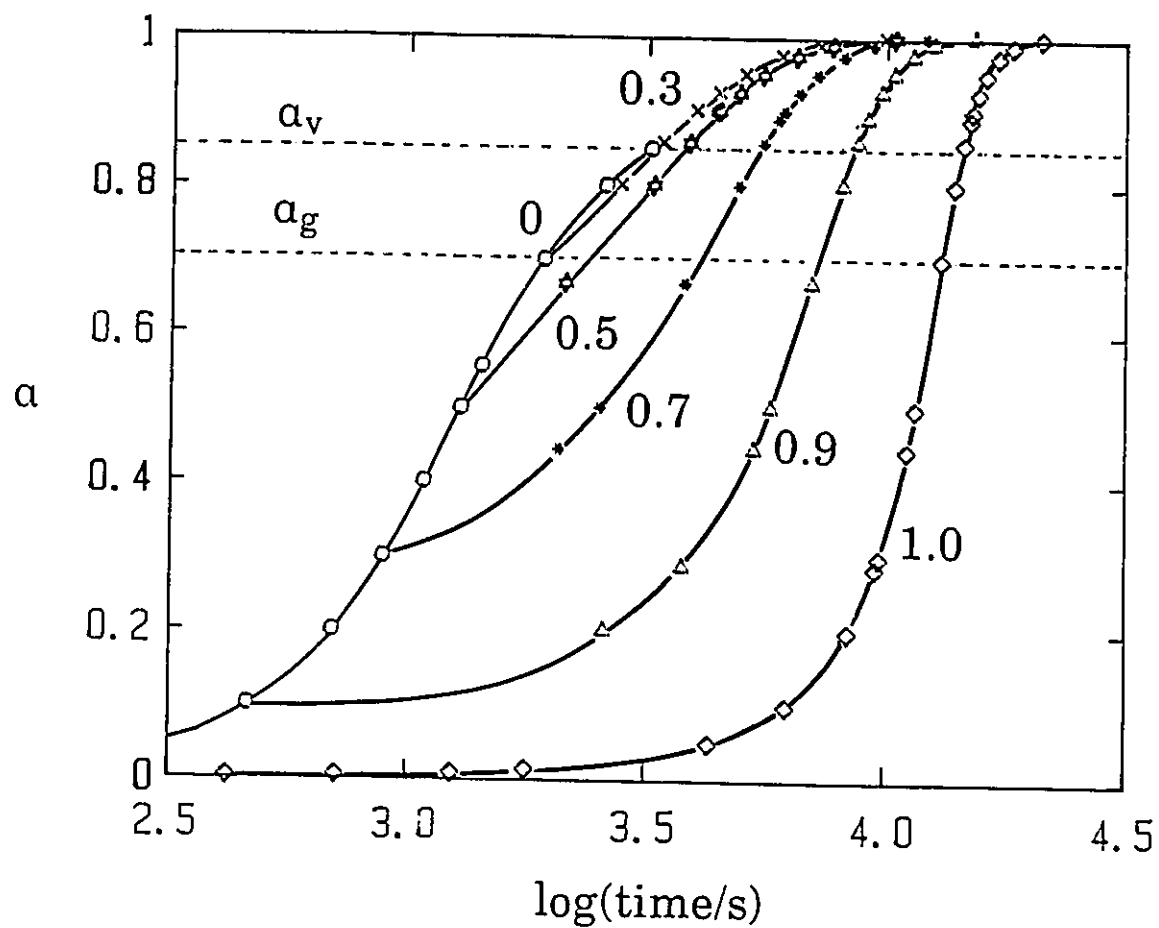


**Figure 4.14:** The extent of reaction of DGEBA with a mixture of amines is plotted against the curing time at 377K. The molar ratio of DDS in the DDM-DDS amine mixture is (o)0, (x)0.3, (✱)0.5, (\*)0.7, (Δ)0.3 and (◇)1.

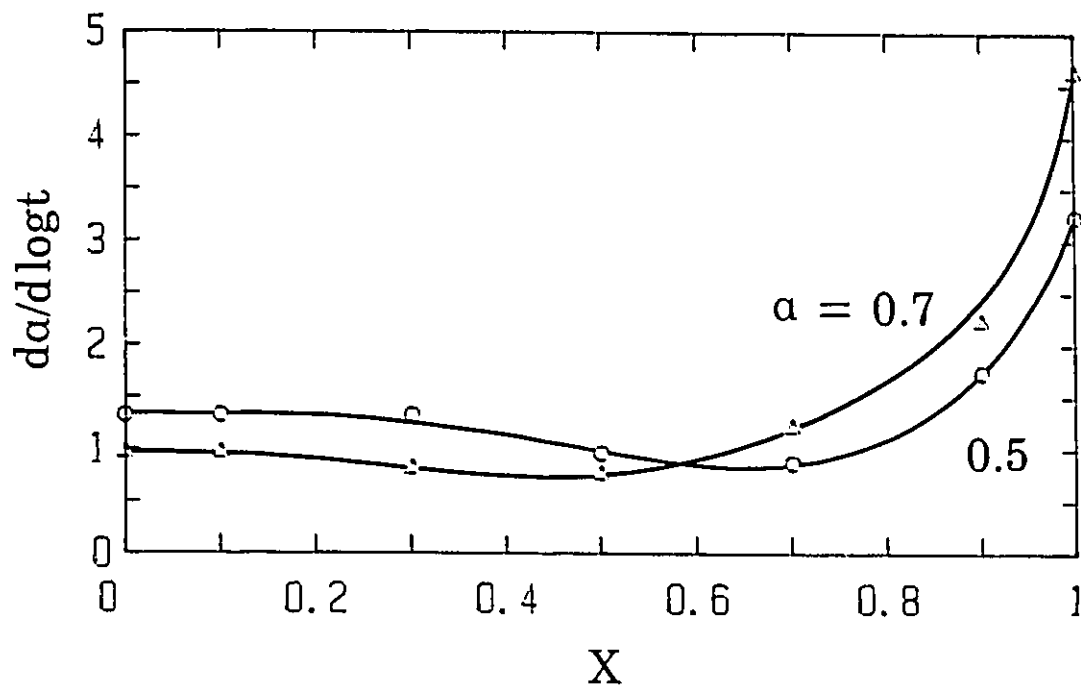


Figure 4.15: The tangent to the curve of Figure 4.14,  $da/d\log t$ , measured for (o) $\alpha=0.5$  and ( $\Delta$ ) $\alpha=0.7$ , is plotted against the molar ratio of DDS in the mixture of DDM-DDS amines.

than  $t_g$ . Therefore, as discussed in the beginning of this section, the values plotted in Figure 4.15 should be related to the rate of the decrease of  $\log\sigma_0$  prior to the gel point which also presents a minimum value at  $x=0.7$ . Therefore, we conclude that considerations in terms of the curing kinetics alone of the thermosets are sufficient to account for both the occurrence of the minimum in the rate of the decrease in  $\sigma_0$  with the composition and its position. The shift in the position of the minimum to  $x=0.5$  when  $\alpha=0.7$ , is also in agreement with our observation, given in the beginning of this Section, that the rate of increase in relaxation time, which corresponds to times near the gel point, is minimum for  $x=0.5$ .

As discussed in Section 4.1, the decrease in the dc conductivity measured during the cure of the DGEBA-(0.7 DDS, 0.3 DDM) thermoset, i.e.  $x=0.7$ , could not be satisfactorily described by either of the two formalisms given in eqns (4.2) and (4.3). This anomalous behaviour, we suggest is related again to the chemical kinetics of the cure. An implication of the above discussed observations is that, near the time of cure which correspond to an extent of conversion of 0.5, the cure kinetics of DGEBA-(0.7 DDS, 0.3 DDM) undergoes a gradual transition from its control by the rate constants of DGEBA-DDM to the rate constants of DGEBA-DDS. Thus, the modelling of the decrease in  $\sigma_0$  for that thermoset would require the use of two sets of equations, one for each amine.

## CHAPTER 5

### THE SUB- $T_g$ RELAXATIONS IN THERMOSETS

#### 5.1 CHARACTERIZATION OF THE SUB- $T_g$ RELAXATIONS

##### 5.1.1 EXPERIMENTAL PROCEDURES

The detailed procedure for the study of sub- $T_g$  relaxations in the DGEBA-DDM and DGEBA-DDS thermosets evolved as the study progressed, and became in this sense specific to the sample studied. Therefore, the procedures for the study differed from the general experimental procedure described in Chapter 2 in several respects, and in view of this, it is necessary to describe in the following the particular procedures used for the study of sub- $T_g$  relaxation in each thermoset.

The stoichiometric mixture of DGEBA and DDM, or DDS, prepared as described in Section 2.3, was poured into a preheated mold and kept at  $T_{cure}$  for a predetermined period for curing,  $t_c$ . In order to prevent any fracture induced by thermal stresses, the samples were then allowed to cool from  $T_{cure}$  to 294K in about 1h. The mold consisted of two aluminum foil-covered, 5mm thick, glass plates which were kept apart by spacers at a distance of 1mm. The foil prevented the thermoset from sticking to the glass, thereby facilitating the removal of the sample from the mold.

Samples of the DGEBA-DDM thermoset were cured for 1h at 357K, kept for one day at 294K and then cooled to 77K. Its dielectric permittivity and loss factor at a fixed frequency of 1kHz were then measured as a function of temperature up to a

temperature of 30K below its  $T_{cure}$ . The procedure was repeated with 2h, 4h, 7h and 8h of additional periods of curing at 357K after which the dielectric properties of the sample had reached a constant value. The sample was then kept for 3 months at 294K and its  $\epsilon'$  and  $\tan\delta$  were measured again as functions of both temperature, at a fixed frequency of 1kHz, and frequency, at several fixed temperatures. It was then further aged for seven days at 413K and any effects of further ageing at a high temperature were studied by measuring again its  $\epsilon'$  and  $\tan\delta$  as a function of both temperature and frequency in a manner similar to above.

Three different samples of DGEBA cross-linked with DDS were studied. These were cured for 1.75h, 3.50h and 5.33h at 418K in each case. Another cured sample was prepared by heating it to 404K for 5h and to 473 for 1h. After the  $\epsilon'$  and  $\tan\delta$  of this sample were measured as a function of temperature, it was further aged for 19.5h at 453K and studied again.

0.1mm thick copper foils which acted as electrodes were pressed onto the opposite sides of the flat rectangular samples of predetermined geometry. The sample with the copper electrodes was then sandwiched between two 1mm glass plates held by a steel pressure clip. The samples dimensions decreased on ageing as more cross-links formed during its post-curing and, as the polymer structure relaxed towards its lower energy, higher density state on physical ageing. From the volumetric study of Choy and Plazek (1986), we estimate that the maximum decrease is about 5% in volume or about 3% in the

thickness of the thermoset sample. Thus, the measured value of the dielectric permittivity and loss should be corrected for these changes. Since the change in the sample dimensions was not measured during or after the post-curing, or physical ageing, the measured  $\epsilon'$  and  $\epsilon''$  values do not have the desired accuracy. Nevertheless, the  $\tan\delta$  value does not depend upon the geometry of a dielectric sample, and therefore, all data given here can be analyzed in terms of the  $\tan\delta$  values (or in terms of  $\epsilon'$  and  $\epsilon''$  values only when the isothermal measurements are reported).

#### 5.1.2 CURED DGEBA-DDM AND DGEBA-DDS THERMOSETS

The  $\tan\delta$  of the DGEBA-DDM thermoset measured at 1kHz is plotted against temperature in Figure 5.1(a). The plot shows one sub- $T_g$  relaxation peak and a shoulder on the low temperature side of the peak. This indicates the presence of two relaxation processes, the high temperature or  $\beta$ -relaxation being the more prominent and the low temperature or  $\gamma$ -relaxation being less prominent. The magnitude of the  $\tan\delta$  peak increased from 0.0098 to 0.0167 after an additional one hour of curing at 357K. A further 2h of curing increased this value to 0.0185, a further 4 h of curing to 0.0196 and an additional 7h to 0.0203. Since the dielectric properties of the sample after 15h of cure showed little change from those of its previous state of cure, the sample thus obtained was taken to have been almost fully cured.

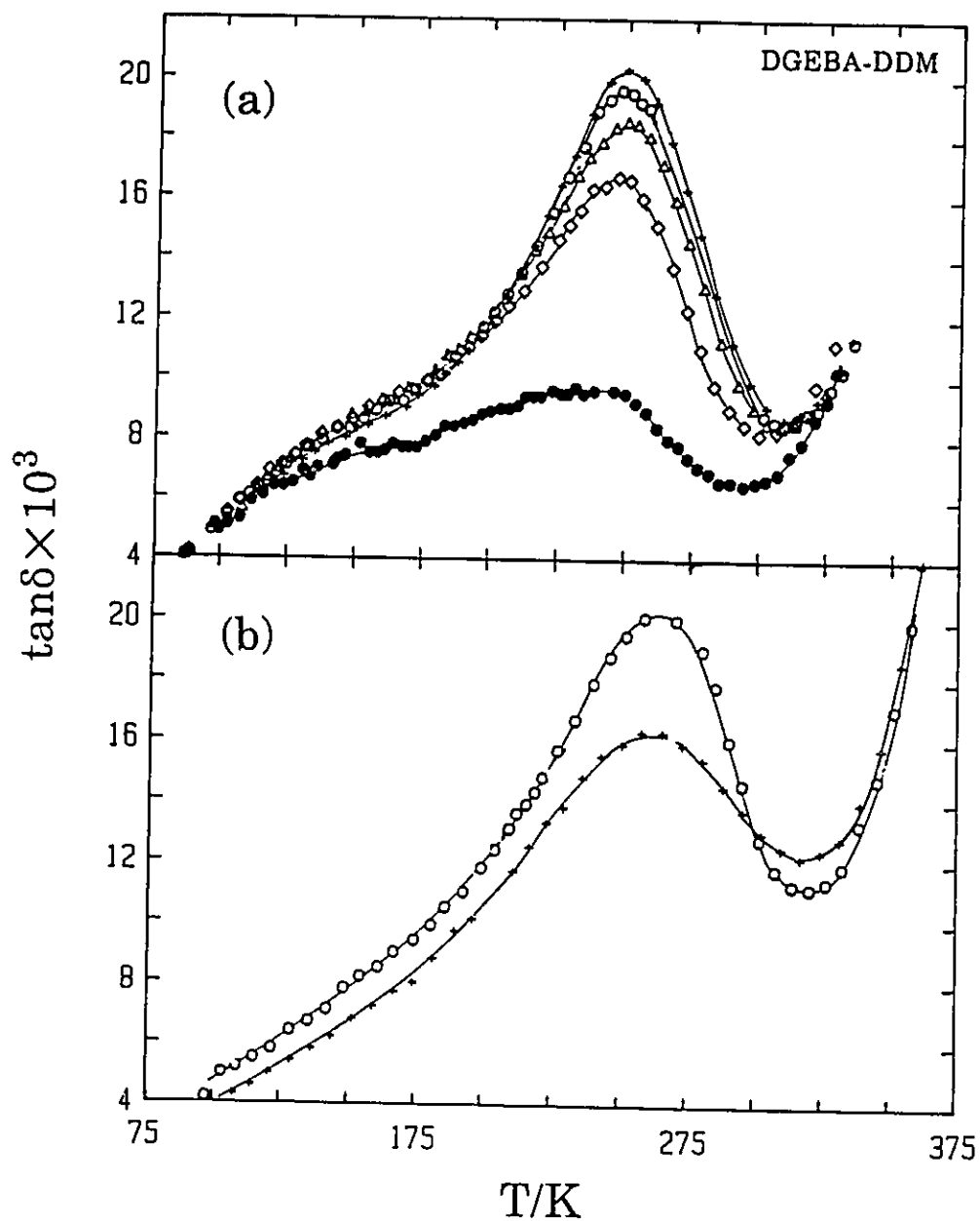


**Figure 5.1:** (a) The dielectric loss tangent plotted against the temperature of the DGEBA-DDM thermoset cured (.)1, ( $\diamond$ )2, ( $\Delta$ )4, (o)8 and (+)15 h at 357K. (b) The dielectric loss tangent plotted against the temperature of the (o) fully cured and (+) aged DGEBA-DDM thermosets.

In order to determine the effects of physical ageing on the DGEBA-DDM thermoset, the fully cured sample which had already been studied, was kept at 357K for an additional 8h and at 294K for 3 months. Thereafter its  $\tan\delta$  was measured for a fixed frequency of 1kHz from 77K to about 320K, and is plotted against temperature in Figure 5.1(b). After the measurements as a function of temperature, the isothermal spectra of  $\epsilon'$  and  $\epsilon''$  of the thermoset were measured at selected temperatures in order to determine the relaxation rate or the peak frequency of the relaxation process. These spectra measured over a temperature range, are shown in Figure 5.2(a). Since the dimensions of the sample changed with temperature by less than 0.1% over this temperature range, the shape of the spectra in Figure 5.2 is more reliable than the values of  $\epsilon'$  and  $\epsilon''$ .

The most fully cured thermoset was then heated to 413K for 7 days (i.e. about 22K below its  $T_g$  of 435K as measured by Choy and Plazek (1986)). After this ageing, its  $\epsilon'$  and  $\tan\delta$  were again measured at 1kHz from 77K to 320K and its  $\epsilon'$  and  $\epsilon''$  spectra measured at several temperatures over the range 220K to 300K. The plots of their  $\tan\delta$  against temperature and of their  $\epsilon'$  and  $\epsilon''$  against frequency at different temperatures are shown in Figures 5.1(b) and 5.2(b), respectively. The rate of sub- $T_g$  relaxation or, equivalently, the frequency  $f_m$  at which the loss reaches a maximum value for both the normal and aged samples is plotted against the reciprocal temperature in Figure 5.3. Two data points taken from the 50Hz and 3kHz fixed frequency measurements made by Ochi et al (1987) included in this figure

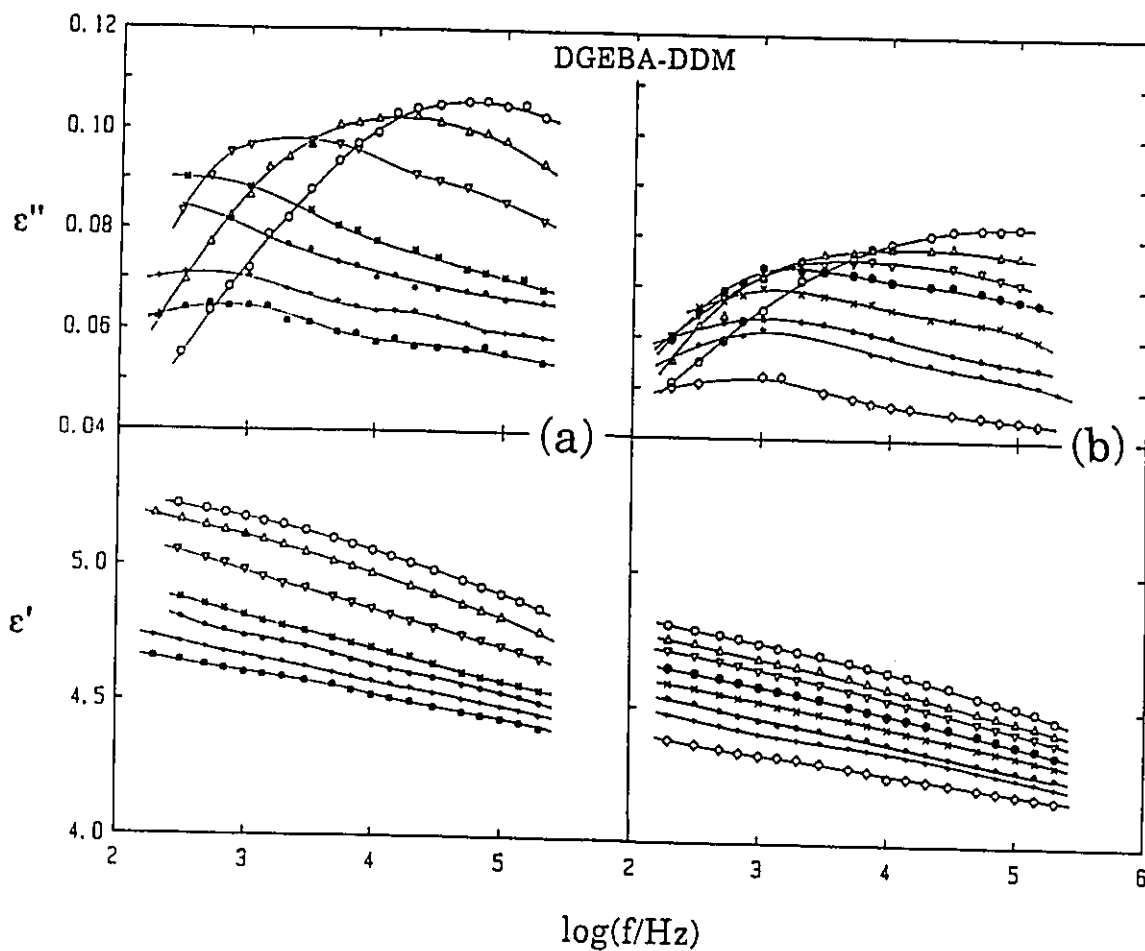


**Figure 5.2:** The dielectric permittivity and loss spectra of sub- $T_g$  relaxations in DGEBA-DDM (a) fully cured measured at (o)221.2, (+)229.2, (\*)238.9, (X)247.2, ( $\nabla$ )266.8, ( $\Delta$ )280.7 and (o)292.5K and (b) aged measured at ( $\diamond$ )220.4, (+)237.8, (\*)245.2, (X)255.3, (.)264.8, ( $\nabla$ )273.0, ( $\Delta$ )281.2 and (o)291.9K.

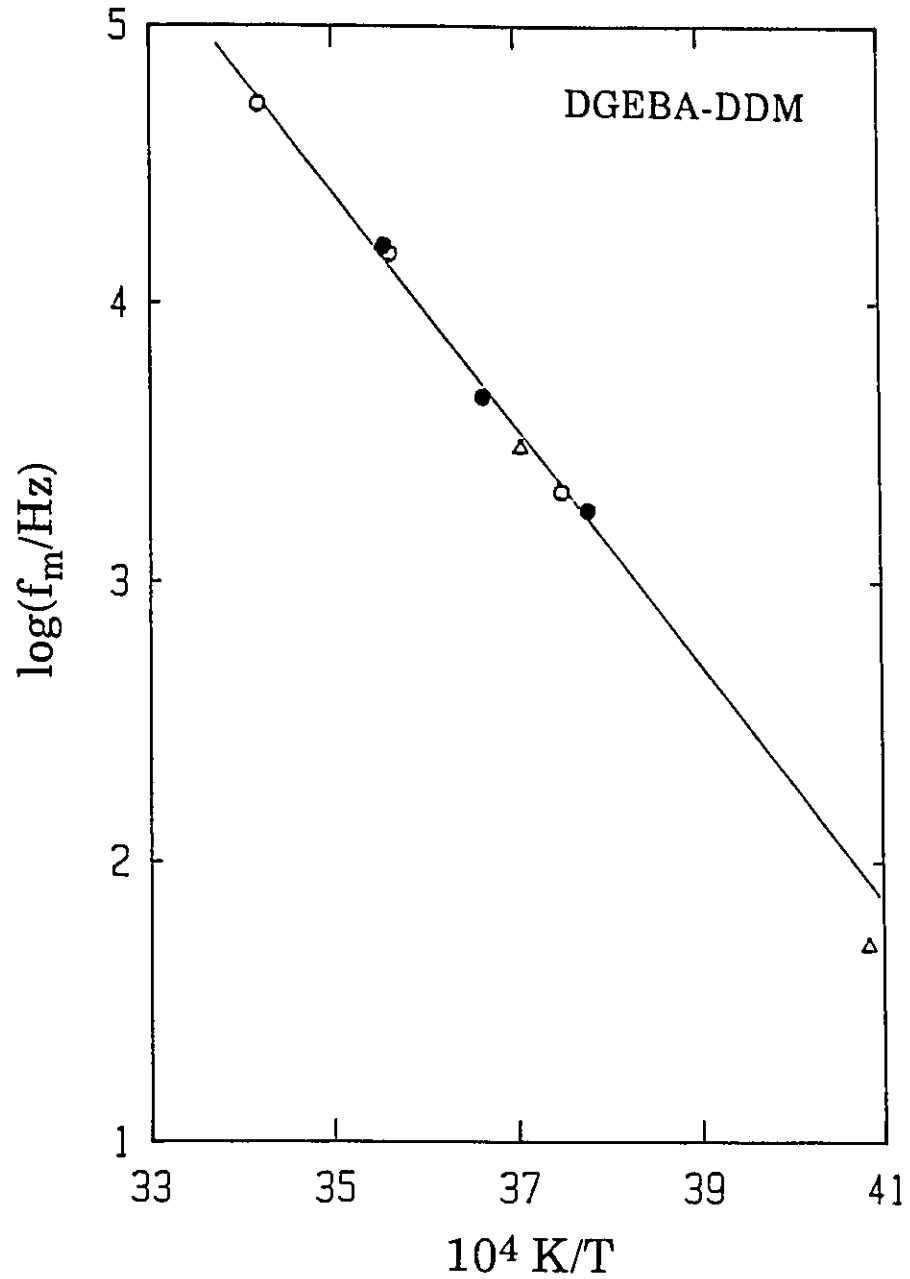


**Figure 5.3:** The frequency maximum of  $c''$  against the reciprocal temperature for the (o) fully cured and (.) aged DGEBA-DDM thermosets. (Δ) were calculated from the isochronal measurements of Ochi et al (1986).

for a comparison show a general agreement within the experimental errors. The data in Figure 5.3 were fitted to the Arrhenius equation

$$f_m = f_0 \exp(-E/RT) \quad (5.1)$$

with  $f_0 = 1.8 \times 10^{19} \text{ Hz}$  and  $E = 81.3 \text{ kJ/mol}$ .

In an attempt to also study the primary, or  $\alpha$ -relaxation process (at  $T > T_g$ ) in the DGEBA-DDS thermoset, several samples of the DGEBA-DDS liquids were prepared for curing at 418K for preselected periods, as mentioned in Section 5.1.1. These samples were subsequently cooled to 77K and their  $\tan\delta$  were measured for a fixed frequency of 1kHz as a function of temperature up to 450K. The plots of  $\tan\delta$  against temperature are shown in Figure 5.4(a). Another sample of the thermoset was then prepared as explained in Section 5.1.1 and its  $\epsilon'$  and  $\tan\delta$  were measured from 77K to 450K, and the  $\tan\delta$  plots are shown in Figure 5.4(b). The sample was then aged for 19h30min at 453K i.e. 32K below its  $T_g$  value as measured by Choy and Plazek (1986), and its  $\tan\delta$  was measured for a fixed frequency of 1kHz. This is plotted against temperature in Figure 5.4(b).

### 5.1.3 EFFECT OF CURING ON THE DIELECTRIC RELAXATION OF THERMOSETS

In order to examine in more detail the effects of the cross-linking reactions on the sub- $T_g$  relaxations, liquid mixtures of DGEBA-DDM and of DGEBA-DDS were poured immediately after their preparation into a dielectric cell suitable for liquids and were vitrified by quenching in liquid  $N_2$ . The  $\epsilon'$ ,

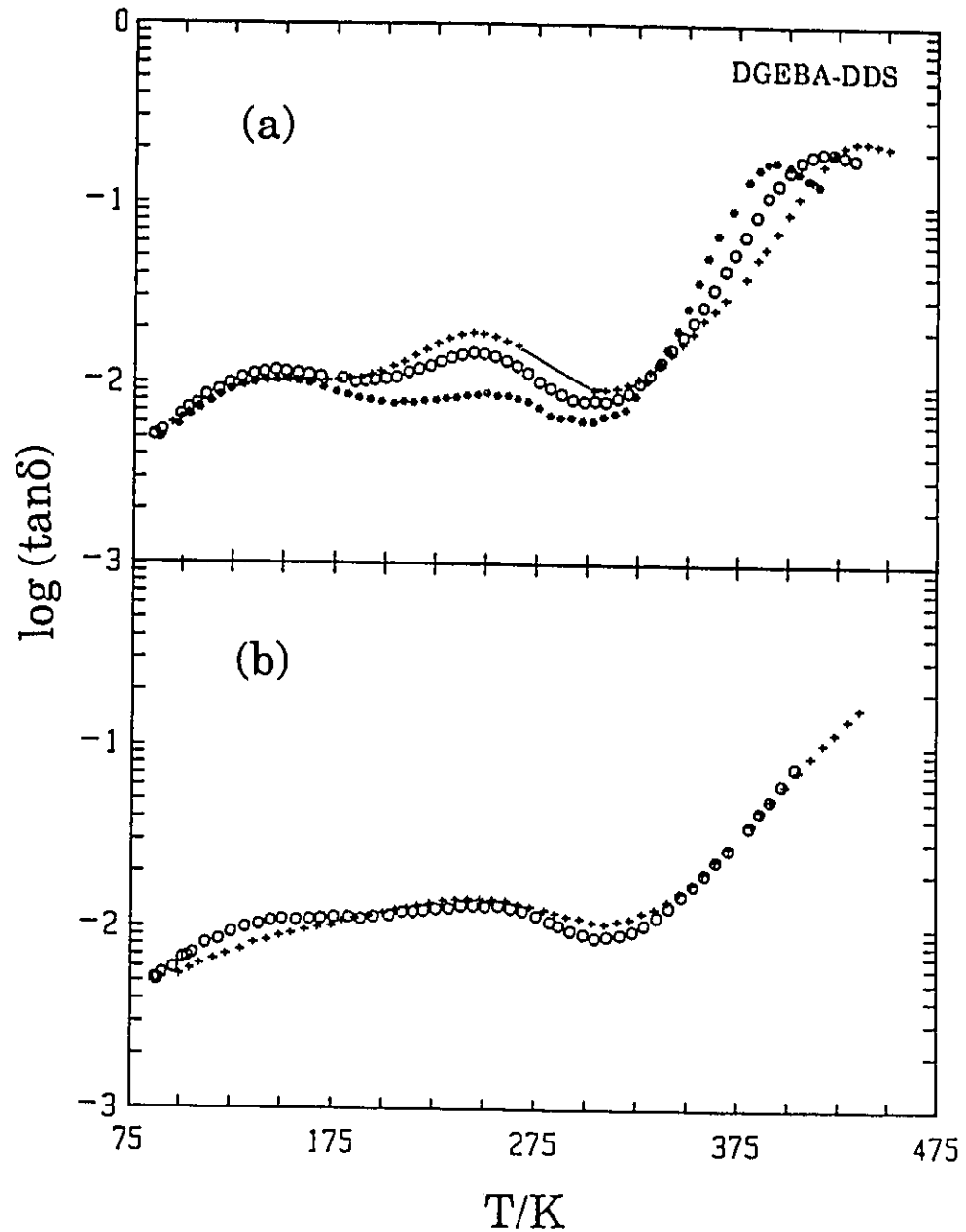


**Figure 5.4:** (a) The dielectric loss tangent plotted against the temperature of the DGEBA-DDS thermoset cured (\*) 1h45 min, (o) 3h30min, and (+) 5h20min at 418K, measured at 1kHz. (b) The dielectric loss tangent plotted against the temperature of the (o) fully cured and (+) aged DGEBA-DDS thermosets.

$\epsilon''$  and  $\tan\delta$  values of the glassy state of the samples were then measured for a fixed frequency of 1kHz from 77K to 350K. The isochrones of  $\epsilon'$ ,  $\epsilon''$  and  $\tan\delta$  of these ungelled, or least cured samples, are shown in Figure 5.5. The height of the  $\beta$  relaxation peak in Figure 5.5 for the ungelled DGEBA-DDM mixture is 0.0045 at 222K, which is nearly 22% of the value of 0.0203 at 249K in Figure 5.1 of the sample cured for 15h at 357K. Similarly, the height of the relaxation peak for the ungelled DGEBA-DDS mixture is 0.0024 at 237K in Figure 5.5, which is nearly 13% of the value of 0.0192 at 243K for the sample cured for 5.5h at 418K in Figure 5.4(a).

The effects of post-curing and physical ageing of the two thermosets on the height of their  $\gamma$  and  $\beta$  relaxation peaks are shown in Figure 5.6, where the appropriate values of  $\tan\delta$  are plotted against the curing and ageing time. The  $\tan\delta$  of the aged samples are shown on the extreme right of Figure 5.6 where the dashed line indicates a region where ageing conditions were uncertain.

## 5.2 DIELECTRIC EFFECTS OF CROSS-LINKING IN THERMOSETS

### 5.2.1 EXPERIMENTAL DETAILS

In order to measure both the temperature dependence of the  $\epsilon'$  and  $\epsilon''$  and the changes in the  $\epsilon'$  and  $\epsilon''$  values over the entire period of curing reaction in the thermoset, the dielectric cell shown in figure 2.3(c) was used. In order to determine the values of dielectric permittivity and loss, the capacitance of the empty cell was measured prior to filling it

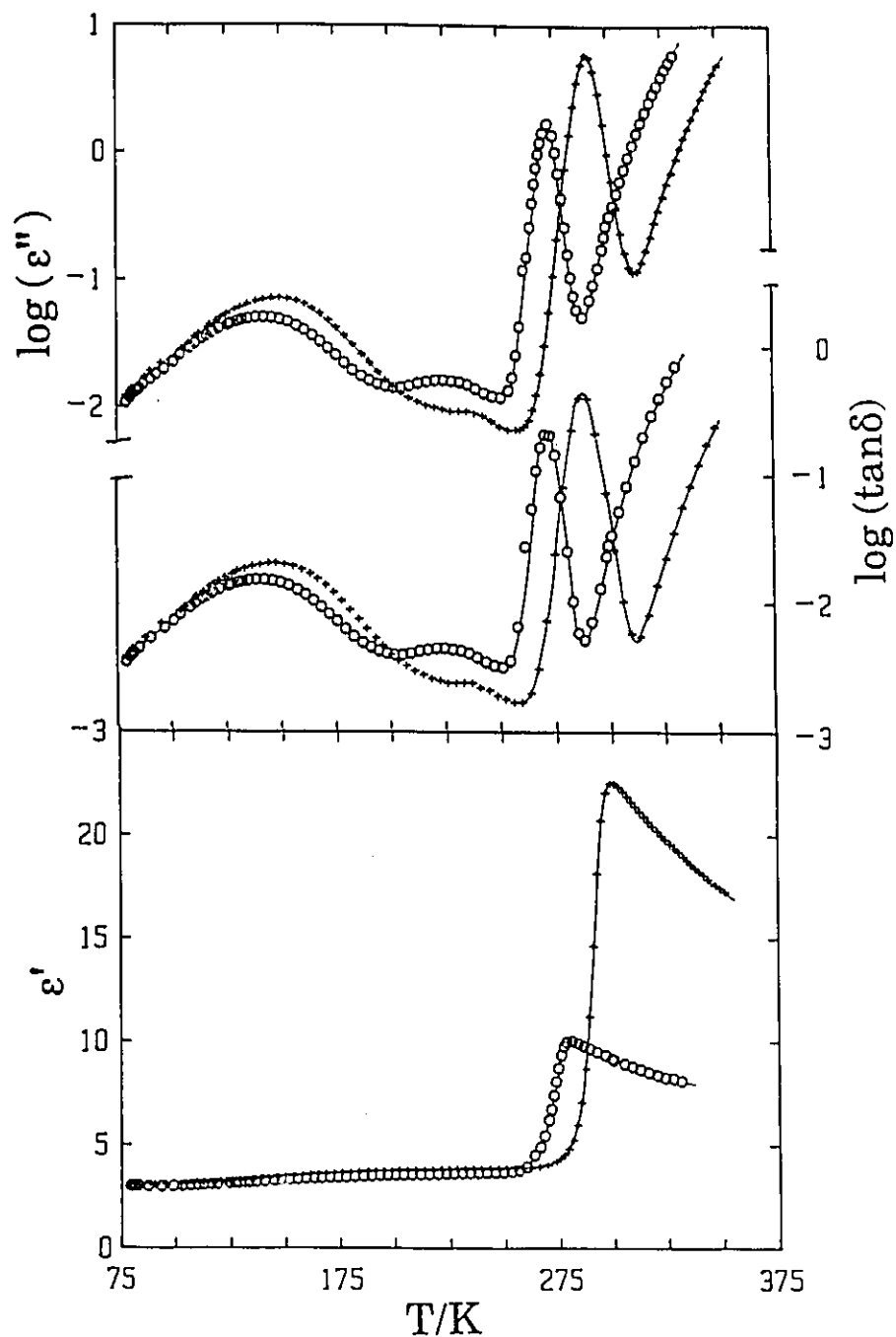


**Figure 5.5:** The dielectric permittivity, loss and loss tangent of the as - prepared mixtures of the (o) DGEBA-DDM and (+) DGEBA-DDS thermosets, measured at 1kHz, plotted against temperature.

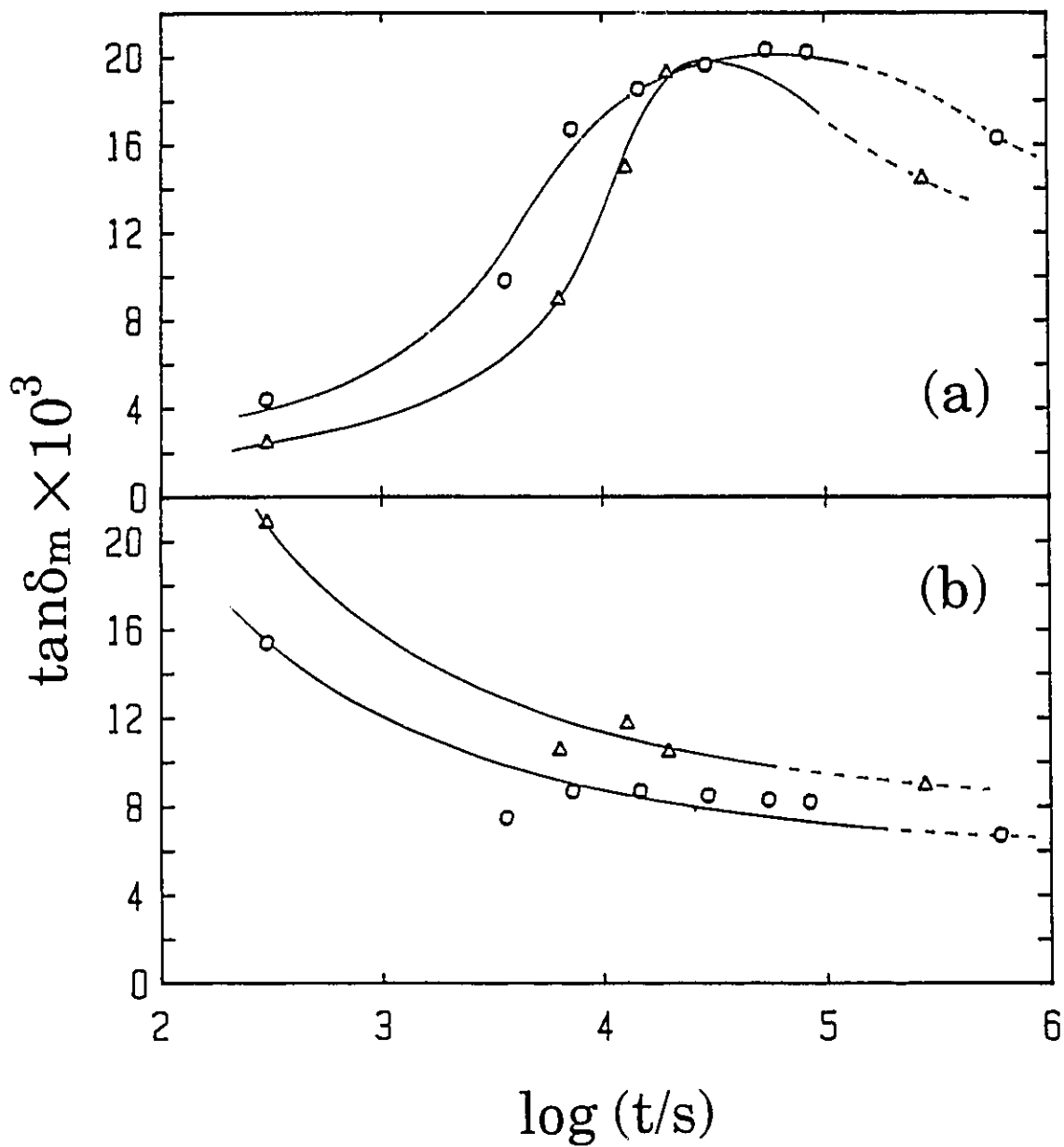


**Figure 5.6:** Plots of  $\tan \delta_{\max}$  for (a) the  $\beta$ -process and (b) the  $\gamma$ -process (at 140K) in the (o) DGEBA-DDM and ( $\Delta$ ) DGEBA-DDS thermosets. The symbols on the far right refer to the aged samples.

with the precursors. The liquid was cooled to 77K and its  $\epsilon'$  and  $\tan\delta$  were measured for a fixed frequency of 1kHz at 1K intervals over the temperature range 90K to the curing temperature  $T_{\text{cure}}$ , during the sample's continuous heating at a rate of 1K/min. The thermal treatment to which the thermosets were subjected is listed in Tables 5.1 to 5.3. In each table, the first row of the data was obtained from measurements made immediately after the dielectric cell containing the liquid precursor was quenched from its mixing temperature to 90K. The dielectric properties of the thermoset were thereafter measured while the assembly was being continuously heated to a preselected  $T_{\text{cure}}$  at which temperature it was isothermally held for an additional, predetermined period of time,  $t_c$ . Values of  $t_c$  and  $T_{\text{cure}}$  for each thermosets are listed in the first column of Tables 5.1 to 5.3. The data obtained from measurements on samples which were not quenched to 77K but were allowed to cool from  $T_{\text{cure}}$  to 298K at an approximate rate of 0.5K/min are marked with an asterisk in the  $(t_c, T_{\text{cure}})$  column of the tables.

### 5.2.2 DGEBA-DDM AND DGEBA-DDS THERMOSETS

Figure 5.7 shows the plots of measured  $\log(\tan\delta)$ ,  $\epsilon'$  and  $\log(\epsilon'')$  against temperature for the DGEBA-DDM thermoset. In this figure, data only for those samples whose  $\alpha$ -relaxation was observed within the temperature range of measurements are plotted. As the curing proceeds, the  $\alpha$ -relaxation peak in Figure 5.7 shifts towards higher temperatures while its height decreases and its width increases. Changes in the features of

TABLE 5.1: The curing and ageing conditions of DGEBA-DDM thermoset and the features of the observed dielectric behaviour.

| $t_{c,}$<br>(s) | $T_{cure}$<br>(K)   | AECT(s)<br>at $T=363$ K | $100 \times \epsilon''_m$ |         |          | $T_m$ (K) |         |          | $\epsilon''_m - \epsilon_\infty$ | $\epsilon_0 - \epsilon''_m$ | $\epsilon_0 - \epsilon_\infty$ |
|-----------------|---------------------|-------------------------|---------------------------|---------|----------|-----------|---------|----------|----------------------------------|-----------------------------|--------------------------------|
|                 |                     |                         | $\gamma$                  | $\beta$ | $\alpha$ | $\gamma$  | $\beta$ | $\alpha$ | $\gamma$                         | $\beta$                     | $\alpha$                       |
| 0               | - <sup>(11)</sup>   | $1.2 \times 10^2$       | 4.63                      | 1.26    | 157      | 142       | 224     | 272      | 0.26                             | 0.08                        | 5.64                           |
| 600,            | 297                 | $1.5 \times 10^2$       | 4.61                      | 1.26    | 153      | 142       | 226     | 272      | 0.25                             | 0.07                        | 5.58                           |
| 900,            | 319 <sup>(2)</sup>  | $5.8 \times 10^2$       | 4.61                      | 1.39    | 133      | 142       | 227     | 277      | 0.25                             | 0.10                        | 5.11                           |
| 300,            | 363 <sup>(3)</sup>  | $2.2 \times 10^3$       | 4.54                      | 2.01    | 80       | 144       | 229     | 298      | 0.26                             | 0.17                        | 3.82                           |
| 600,            | 363 <sup>(4)</sup>  | $6.6 \times 10^3$       | 3.03                      | 5.50    |          | 145       | 242     |          | 0.17                             | 0.32                        |                                |
| 1500,           | 363 <sup>(5)</sup>  | $9.4 \times 10^3$       | 2.87                      | 6.40    |          | 145       | 250     |          | 0.17                             | 0.29                        |                                |
| 2100,           | 363 <sup>(6)</sup>  | $1.5 \times 10^4$       | 2.80                      | 7.08    |          | 251       | 251     |          | 0.16                             | 0.31                        |                                |
| 4500,           | 363                 | $2.1 \times 10^4$       | 2.72                      | 7.41    |          | 254       | 254     |          | 0.16                             | 0.30                        |                                |
| 11700,          | 363 <sup>(7)</sup>  | $3.7 \times 10^4$       | 2.68                      | 7.70    |          | 255       | 255     |          | 0.15                             | 0.31                        |                                |
| 720,            | 403 <sup>(8)</sup>  | $4.7 \times 10^4$       | 2.28                      | 8.88    |          | 263       | 263     |          | 0.12                             | 0.37                        |                                |
| 1080,           | 403 <sup>(9)</sup>  | $7.2 \times 10^4$       | 2.14                      | 10.6    |          | 260       | 260     |          | 0.13                             | 0.43                        |                                |
| 2700,           | 403 <sup>(10)</sup> | $1.05 \times 10^5$      | 2.12                      | 10.5    |          | 261       | 261     |          | 0.12                             | 0.43                        |                                |
| 5400,           | 403 <sup>(11)</sup> | $1.35 \times 10^5$      | 2.12                      | 10.2    |          | 263       | 263     |          | 0.11                             | 0.42                        |                                |
| 21600,          | 403 <sup>(12)</sup> | $2.50 \times 10^5$      | 2.12                      | 9.70    |          | 265       | 265     |          | 0.12                             | 0.39                        |                                |

\* the number in parentheses beside the  $T_{cure}$  value represents the curves in Figures 5.7 to 5.9 .

**TABLE 5.2 :** The curing and ageing conditions of DGEBA-DDS thermoset and the features of the observed dielectric behaviour.

| $t_c$<br>(s) | $T_{\text{cure}}$<br>(K) | AECT(s)<br>at $T=398$ K | $100 \times \epsilon'_m$ |         |          | $T_m$ (K) |         |          | $\epsilon'_m - \epsilon_\infty$ | $\epsilon_0 - \epsilon'_m$ | $\epsilon_0 - \epsilon_\infty$ |
|--------------|--------------------------|-------------------------|--------------------------|---------|----------|-----------|---------|----------|---------------------------------|----------------------------|--------------------------------|
|              |                          |                         | $\gamma$                 | $\beta$ | $\alpha$ | $\gamma$  | $\beta$ | $\alpha$ | $\gamma$                        | $\beta$                    | $\alpha$                       |
| 0            | $-^*(1)$                 | $2.0 \times 10^2$       | 5.32                     | 1.32    | 481      | 148       | 235     | 290      | 0.30                            | 0.07                       | 15.2                           |
| 0,           | 398(2)                   | $1.7 \times 10^3$       | 4.85                     | 1.63    | 399      | 147       | 235     | 292      | 0.27                            | 0.09                       | 13.8                           |
| 180,         | 398(3)                   | $3.5 \times 10^3$       | 4.51                     | 1.83    | 310      | 147       | 235     | 298      | 0.26                            | 0.10                       | 12.0                           |
| 600,         | 389(4)                   | $5.6 \times 10^3$       | 4.09                     | 2.01    | 233      | 147       | 238     | 309      | 0.24                            | 0.10                       | 10.4                           |
| 1800,        | 398(5)                   | $9.0 \times 10^3$       | 3.51                     | 2.77    | 168      | 146       | 245     | 340      | 0.21                            | 0.14                       | 7.72                           |
| 3300,        | 406(6)                   | $1.5 \times 10^4$       | 3.10                     | 3.24    | 146      | 148       | 246     | 369      | 0.20                            | 0.16                       | 6.42                           |
| 2700,        | 419(7)                   | $2.4 \times 10^4$       | 2.81                     | 4.25    | 151      | 151       | 250     |          | 0.18                            | 0.18                       |                                |
| 7200,        | 414*(8)                  | $4.5 \times 10^4$       | 2.43                     | 4.71    | 150      | 150       | 249     |          | 0.15                            | 0.20                       |                                |
| 18000,       | 414*(9)                  | $8.4 \times 10^4$       | 2.24                     | 5.10    | 150      | 150       | 250     |          | 0.13                            | 0.20                       |                                |

\* the number in parentheses beside the  $T_{\text{cure}}$  value represents the curves in Figures 5.10 and 5.11.

**TABLE 5.3:** The curing and ageing conditions of DGEBA (0.3DDM-0.7DDS) thermoset and the features of their observed dielectric behaviour

| $t_c$<br>(s)         | $T_{cure}$<br>(K) | AECT(s)<br>at 363 K | $100 \times \epsilon''_m$ |         |          | $T_m(K)$ |         |          | $\epsilon'_m - \epsilon_\infty$<br>$\gamma$ | $\epsilon_0 - \epsilon'_m$<br>$\beta$ | $\epsilon_0 - \epsilon_\infty$<br>$\alpha$ |
|----------------------|-------------------|---------------------|---------------------------|---------|----------|----------|---------|----------|---------------------------------------------|---------------------------------------|--------------------------------------------|
|                      |                   |                     | $\gamma$                  | $\beta$ | $\alpha$ | $\gamma$ | $\beta$ | $\alpha$ |                                             |                                       |                                            |
| 0,                   | 0(1)*             | $3.2 \times 10^2$   | 5.37                      | 1.42    | 403      | 145      | 223     | 285      | 0.30                                        | 0.11                                  | 12.9                                       |
| 0,                   | 363(2)            | $1.6 \times 10^3$   | 4.91                      | 1.58    | 306      | 147      | 223     | 294      | 0.29                                        | 0.12                                  | 10.8                                       |
| $3.0 \times 10^2$ ,  | 363(3)            | $3.2 \times 10^3$   | 4.86                      | 1.78    | 255      | 147      | 223     | 302      | 0.28                                        | 0.17                                  | 9.9                                        |
| $6.0 \times 10^2$ ,  | 363               | $7.2 \times 10^3$   | 4.45                      | 1.85    | 167      | 144      | 223     | 319      | 0.25                                        | 0.17                                  | 7.8                                        |
| $2.1 \times 10^3$ ,  | 363(4)            | $1.1 \times 10^4$   | 4.14                      | 2.12    | 146      | 145      | 223     | 327      | 0.24                                        | 0.18                                  | 7.1                                        |
| $3.6 \times 10^3$ ,  | 363               | $1.8 \times 10^4$   | 3.74                      | 2.25    | 132      | 146      | 228     | 334      | 0.19                                        | 0.19                                  | 6.5                                        |
| $1.08 \times 10^4$ , | 363(5)            | $3.3 \times 10^4$   | 3.50                      | 2.85    | 114      | 147      | 241     | 356      | 0.21                                        | 0.18                                  | 5.1                                        |
| $2.16 \times 10^4$ , | 363(6)            | $5.8 \times 10^4$   | 3.24                      | 3.60    |          | 151      | 247     |          | 0.21                                        | 0.21                                  |                                            |
| $5.40 \times 10^4$ , | 363(7)            | $1.16 \times 10^5$  | 2.95                      | 4.49    |          | 150      | 247     |          | 0.19                                        | 0.24                                  |                                            |
| $7.92 \times 10^4$ , | 363(8)            | $1.99 \times 10^5$  | 2.77                      | 5.40    |          |          | 251     |          | 0.17                                        | 0.28                                  |                                            |
| $1.19 \times 10^5$ , | 363               | $3.11 \times 10^5$  | 2.70                      | 5.37    |          |          | 252     |          | 0.17                                        | 0.24                                  |                                            |
| $2.88 \times 10^5$ , | 363(9)            | $6.13 \times 10^5$  | 2.68                      | 5.34    |          |          | 252     |          | 0.17                                        | 0.26                                  |                                            |

\* the number in parentheses beside the  $T_{cure}$  value represents the curves in Figures 5.12 and 5.13.

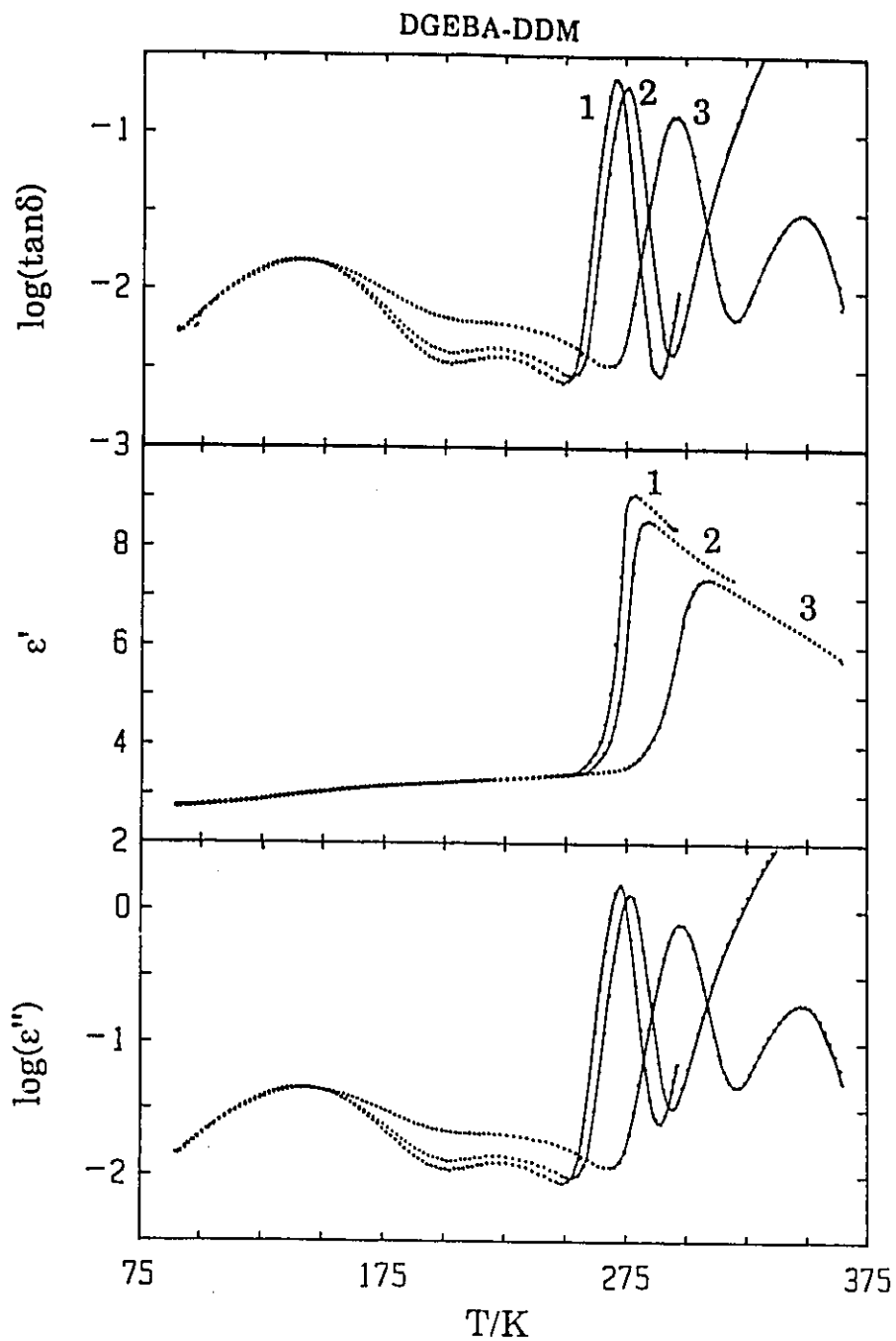


**Figure 5.7:** The dielectric loss tangent, permittivity and loss of the DGEBA-DDM thermoset plotted against the temperature. The times of cure at 363K of the sample for the data labelled 1, 2 and 3 are given in Table 5.1. The curves are numbered in order of increasing extent of cure.

the sub- $T_g$  relaxation peaks with curing time are better resolved in the linear plots of  $\epsilon'$ ,  $\epsilon''$  and  $\tan\delta$  shown in Figure 5.8, where the strength of relaxation, which is related to the peak's height, is seen to increase for the  $\beta$ -relaxation process, and to decrease for the  $\gamma$ -relaxation process. The temperature of cure of the DGEBA-DDM thermoset was then increased from 363K to 403K and the observed changes in the shapes of the sub- $T_g$  relaxations, which subsequently occurred, are shown, for the sake of clarity, on a linear scale in Figure 5.9. In this figure, the height of the  $\beta$ -relaxation peak first increases, reaches a maximum value and then begins to decrease, while that of the  $\gamma$ -relaxation monotonically decreases towards an apparently fixed value.

The effects of curing on the  $\alpha$ -relaxation of the DGEBA-DDS thermoset is shown in Figure 5.10 and the evolution of the sub- $T_g$  relaxation processes with the curing time are shown on a linear scale plot of  $\epsilon'$ ,  $\epsilon''$  and  $\tan\delta$  against temperature in Figure 5.11. The features observed for the DGEBA-DDS thermoset are qualitatively similar to those observed for the DGEBA-DDM thermoset which have been already described. But quantitatively speaking, the heights as well as the temperatures of the three relaxation peaks for the two types of thermosets significantly differ. This difference can be clearly seen in Tables 5.1 and 5.2 where the maximum value of  $\epsilon''$ , or  $\epsilon''_m$ , and the temperatures for the peaks due to the  $\gamma$ -,  $\beta$ - and  $\alpha$ -processes in the two thermosets have been listed. In cases when the  $\gamma$ -relaxation appeared not as a peak but as a

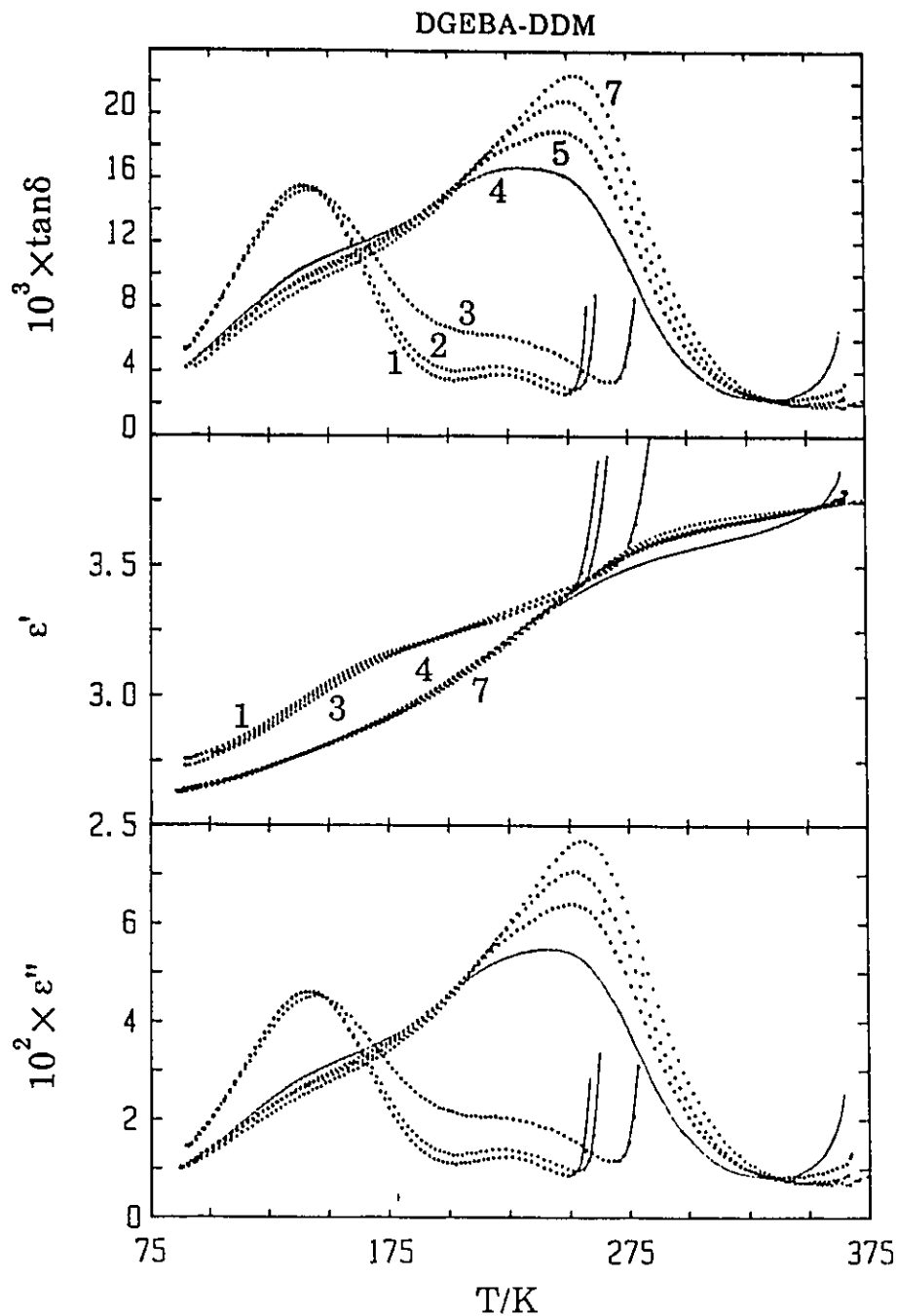


**Figure 5.8:** The dielectric loss tangent, permittivity and loss of the sub- $T_g$  relaxations region of the DGEBA-DDM thermoset plotted against the temperature. The curves are numbered in order of increasing extent of cure and correspond to the thermal histories given in Table 5.1.

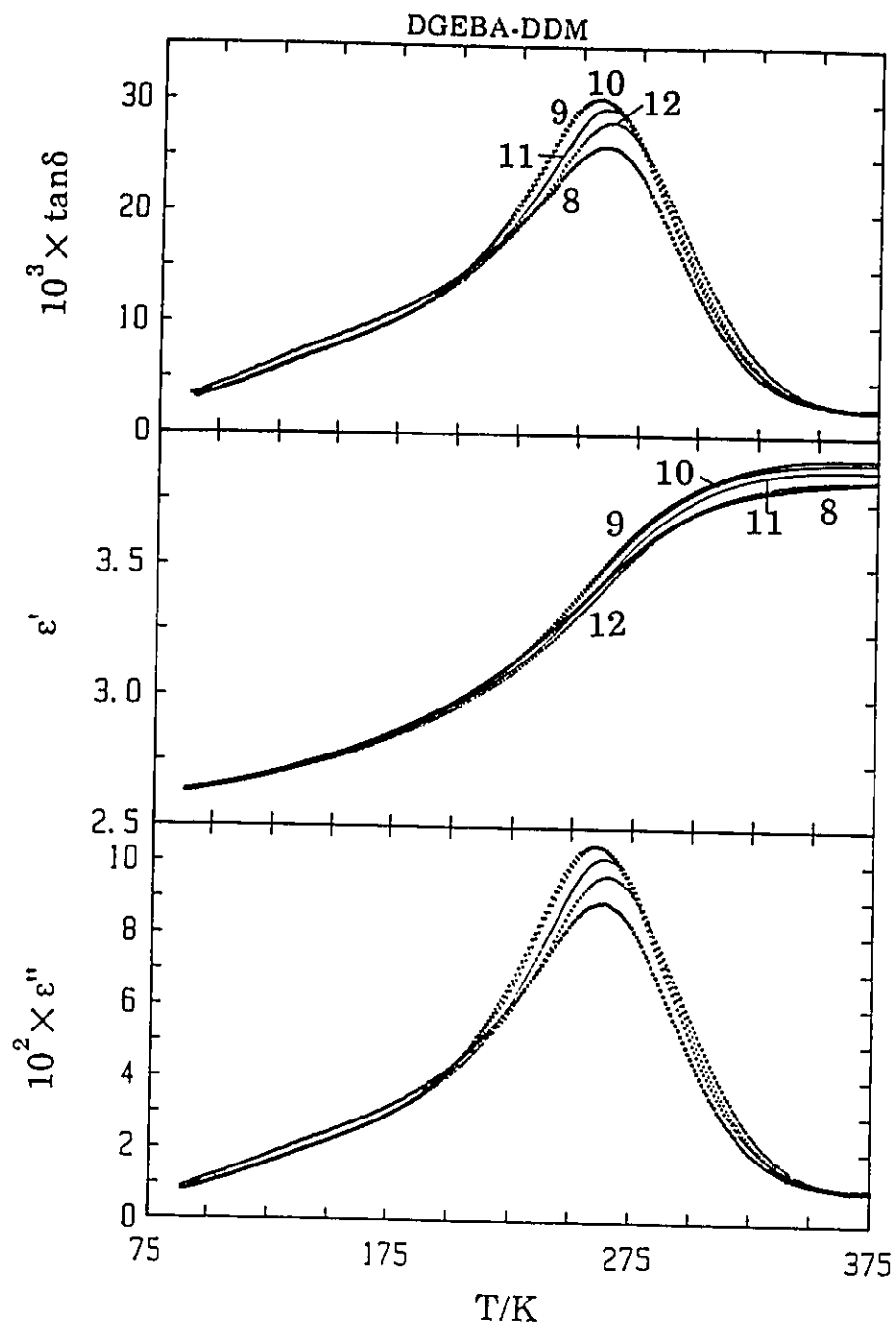


**Figure 5.9:** The dielectric loss tangent, permittivity and loss of the sub- $T_g$  relaxations region of the DGEBA-DDM thermoset plotted against the temperature. The data were obtained after the DGEBA-DDM thermoset was cured at a higher curing temperature of 403K. The curves are numbered in order of increasing extent of cure and correspond to the thermal histories given in Table 5.1.

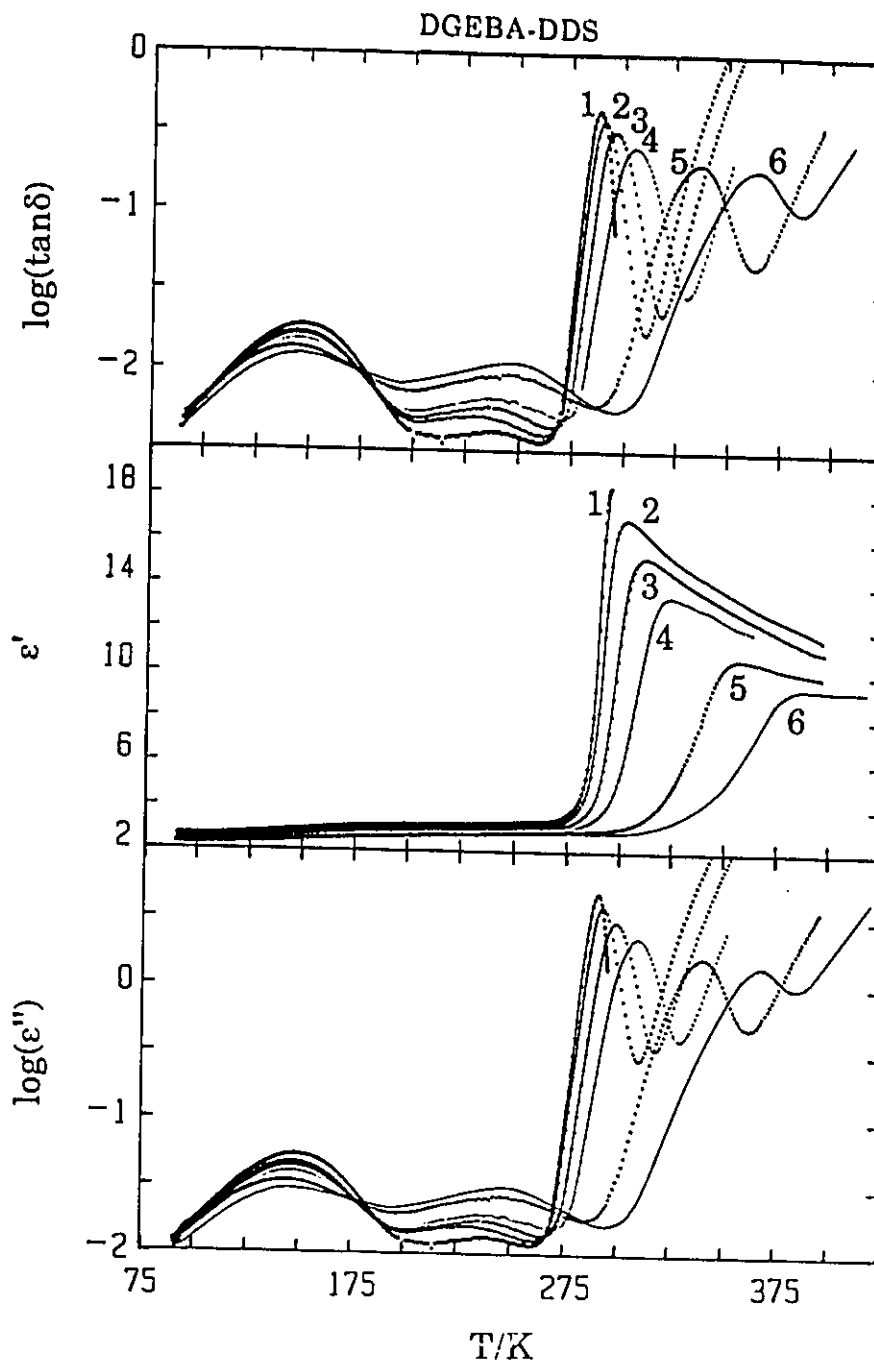


**Figure 5.10:** The dielectric loss tangent, permittivity and loss of the DGEBA-DDS thermoset plotted against the temperature. The times of cure at 398 K for the plots labelled 1 through 6 are given in Table 5.2. The curves are numbered in order of increasing extent of cure.

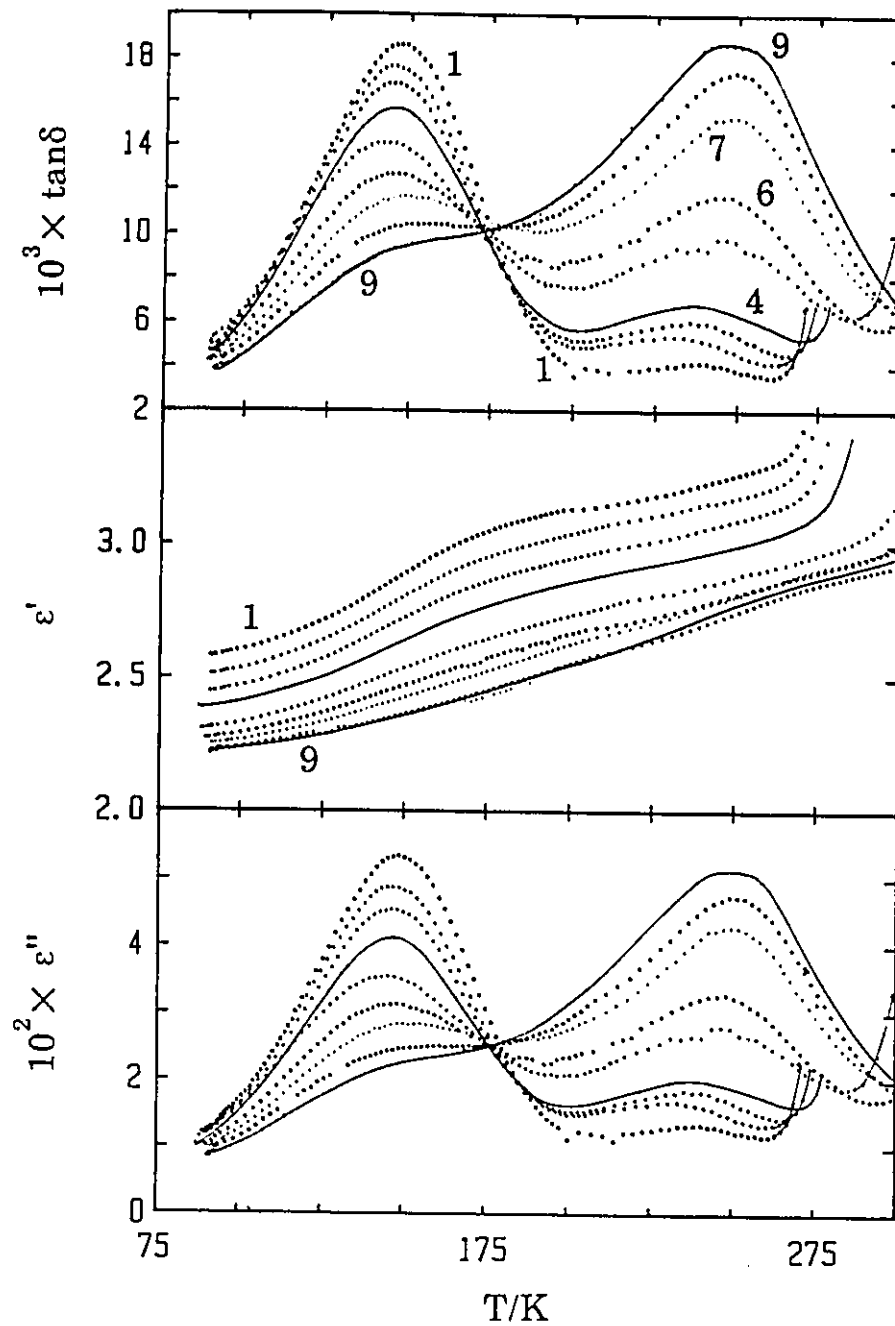


Figure 5.11: The dielectric loss tangent, permittivity and loss of the sub- $T_g$  relaxations region of the DGEBA-DDS thermoset plotted against the temperature. The curves are numbered in order of increasing extent of cure and correspond to the thermal histories given in Table 5.2.

shoulder in the  $\epsilon''$  curve, the  $\epsilon''_m(\gamma)$  value was taken as the  $\epsilon''$  value at the temperature of the  $\gamma$ -peak,  $T_{m\gamma}$ , obtained from the last  $\epsilon''$  curve that did show a peak for the  $\gamma$ -relaxation.

### 5.2.3 DGEBA CURED WITH A MIXTURE OF 70% DDS AND 30% DDM

In order to investigate the effects of each particular diamine on the sub- $T_g$  relaxation of thermosets as it became increasingly more cross-linked, it became necessary to study the effects of cross-linking on the dielectric relaxations of DGEBA cured with a mixture of aromatic amines of different molecular size, dipole moments and rates of chemical reaction. A mixture of 70% DDS and 30% DDM was selected for this investigation since its isothermal dielectric analysis seems to more clearly show the presence of the two diamines as seen in Figure 3.18.

The effects of curing on the  $\alpha$ -relaxation of the DGEBA-(70% DDS, 30% DDM) is shown in Figure 5.12 and the evolution of the sub- $T_g$  relaxation processes with the curing time are shown on the  $\epsilon'$ ,  $\epsilon''$  and  $\tan\delta$  plots in Figure 5.13. The features observed in Figures 5.12 and 5.13 are again qualitatively similar to those observed for the DGEBA-DDM and DGEBA-DDS thermosets. These will be quantitatively analysed in the following chapter. The maximum value of  $\epsilon''$ , or  $\epsilon''_m$ , and the temperatures for the peaks due to the  $\gamma$ -,  $\beta$ - and  $\alpha$ -processes are listed in Table 5.3.

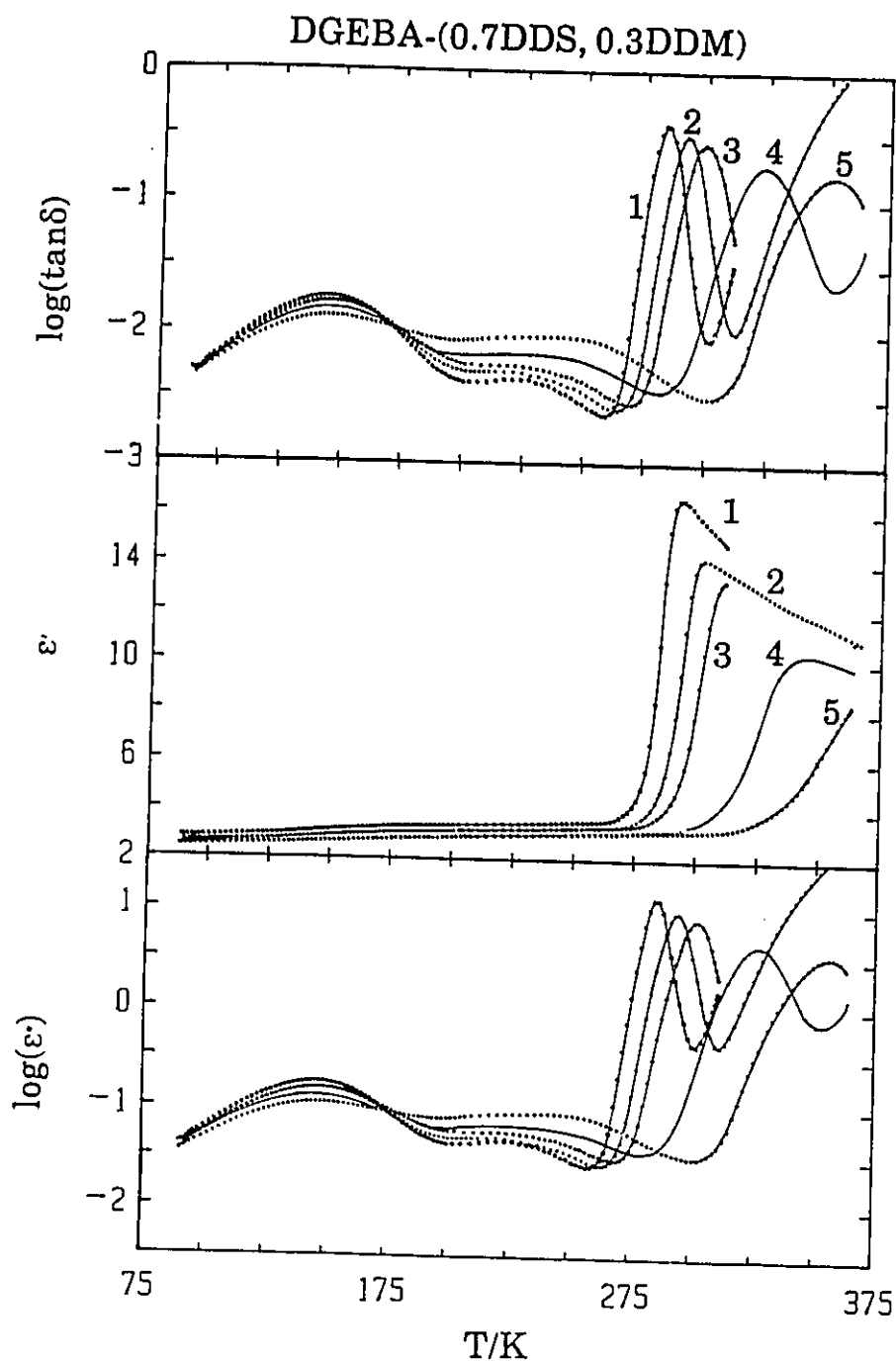


**Figure 5.12:** The dielectric loss tangent, permittivity and loss of the DGEBA-(0.7DDS, 0.3DDM) thermoset plotted against temperature. The increasing times of cure at 363K for the curves labelled 1 through 5 are given in Table 5.3.

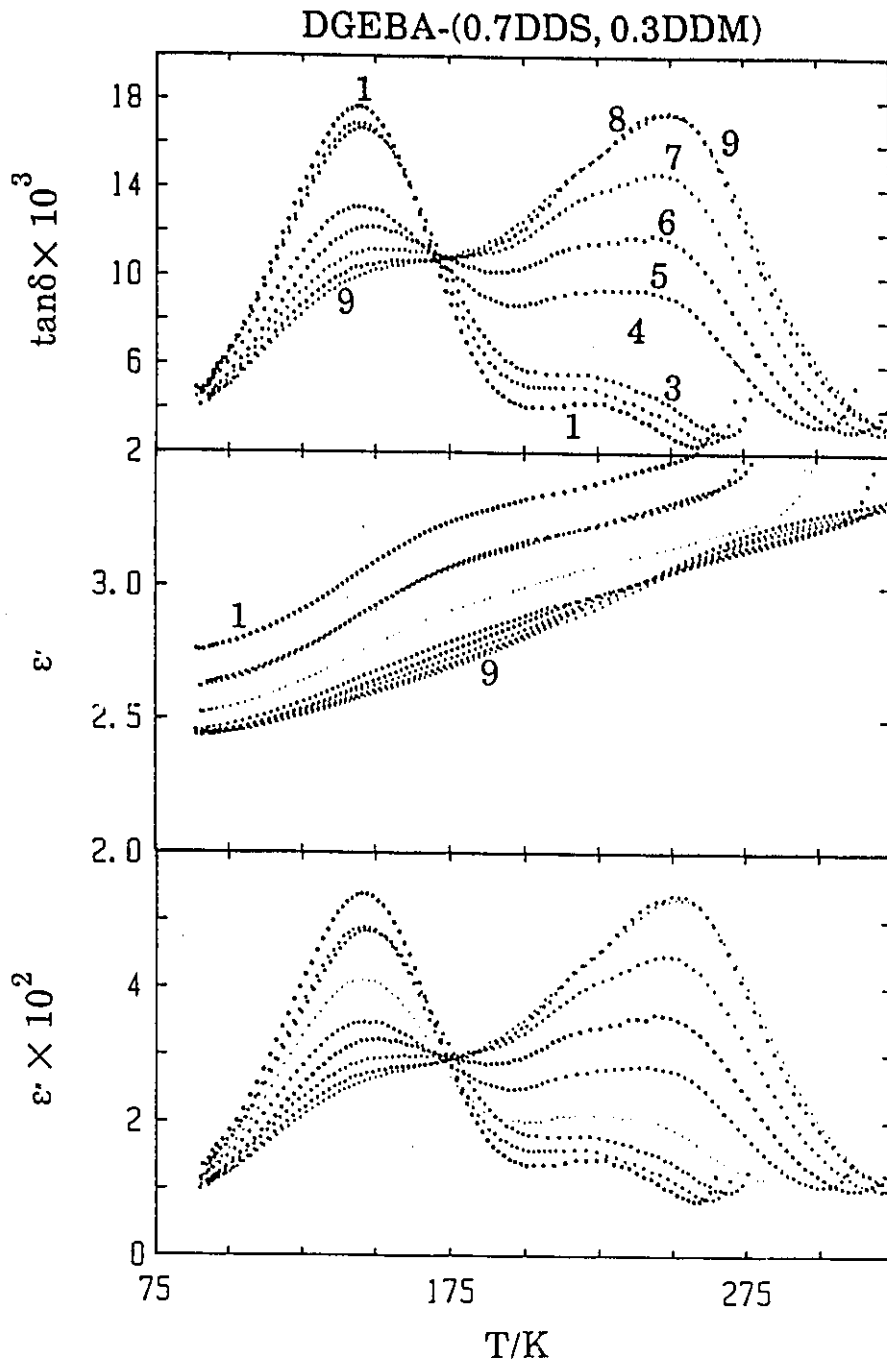


**Figure 5.13:** The dielectric loss tangent, permittivity and loss of the sub- $T_g$  relaxations region of the DGEBA-(0.7DDS, 0.3DDM) thermoset plotted against temperature. The increasing times of cure at 363K for the curves labelled 1 through 9 are given in Table 5.3.

### 5.3 EFFECTS OF COMPOSITION ON THE SUB- $T_g$ RELAXATIONS OF THE DGEBA-DDM THERMOSET

The effects of cross-linking on the sub- $T_g$  relaxations of the stoichiometrically starved and saturated DGEBA-DDM thermosets (molar ratios of 2:0.75 and 2:1.25, respectively) which were prepared by a method described in Section 3.4 were also studied. For this study a different dielectric cell shown in Figure 2.3(d) was used and its geometric capacitance was determined before the measurements. The thermosetting mixtures were cooled to 90K as soon as they were prepared, and their  $\epsilon''$  and  $\tan\delta$  were measured for a fixed frequency of 1 kHz at 1K intervals from 90K to 300K. The temperature dependence of  $\epsilon''$ ,  $\epsilon'$  and  $\tan\delta$  of the as prepared, starved and saturated DGEBA-DDM thermosets are shown in Figure 5.14.

A new stoichiometric DGEBA-DDM mixture was also prepared for comparison and its measured  $\epsilon''$ ,  $\epsilon'$  and  $\tan\delta$  values are also plotted against temperature in Figure 5.14.

Both the stoichiometrically starved and saturated DGEBA-DDM thermosets were subsequently cured at 340.8K and 346.0K, respectively, until their glass transition temperature became higher than their curing temperature. The dielectric sub- $T_g$  relaxations of these thermosets were then measured from 90K to 325K. These were subsequently cured further 15mins at 388.2K and their sub- $T_g$  relaxations were again measured. The procedure of subsequent cure was then repeated with a preselected curing temperature of 403.2K and additional curing times of 0.5, 1, 2, 4, 8 and 16 hours. The detailed thermal

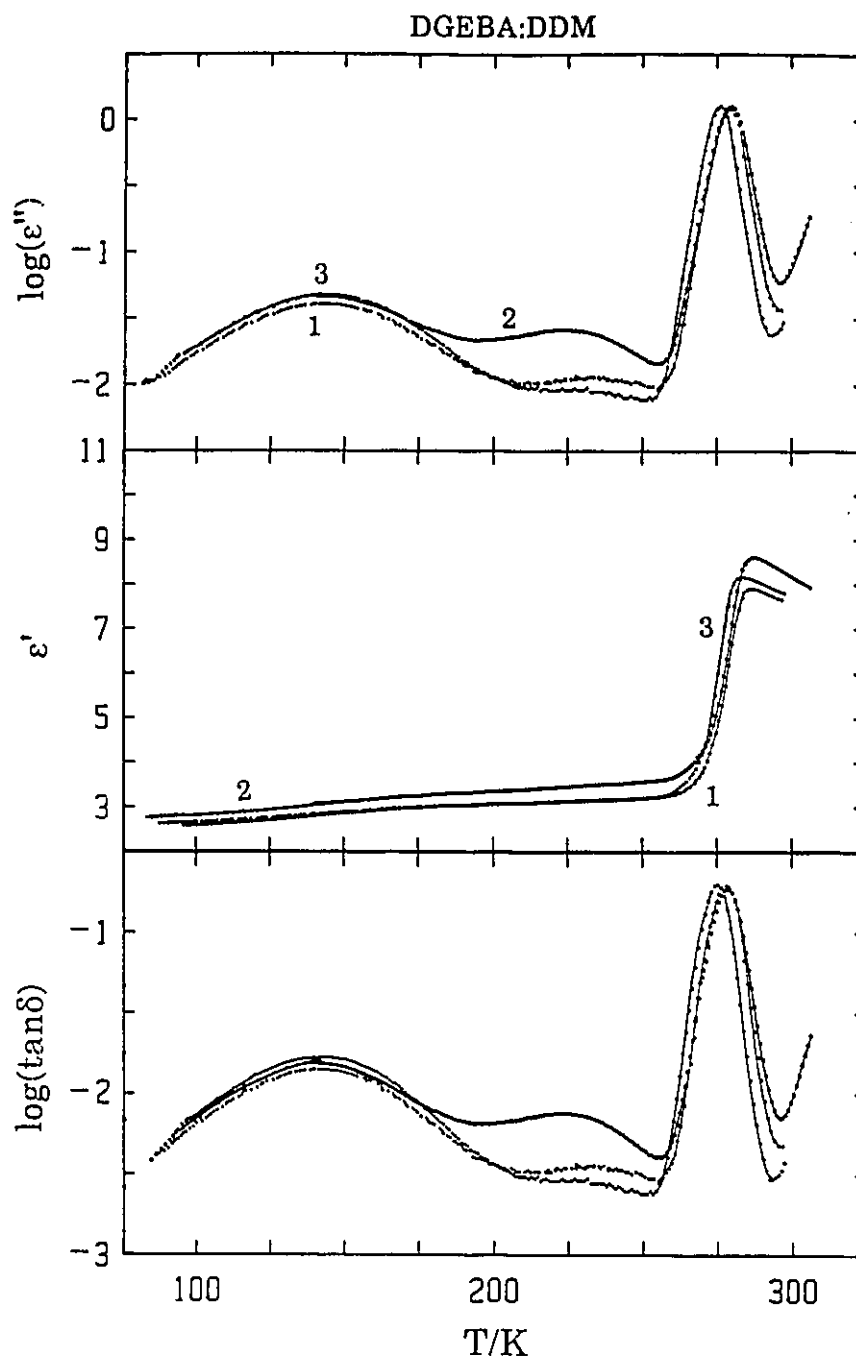


**Figure 5.14:** The dielectric loss, permittivity and loss tangent of the as - prepared DGEBA-DDM mixtures measured at 1kHz are plotted against temperature. Curves labelled 1, 2 and 3 are for the saturated, stoichiometric and starved samples.

history of the thermosets is given in Tables 5.4. The temperature dependence of  $\epsilon''$ ,  $\epsilon'$  and  $\tan\delta$  measured at various states of cure for both the stoichiometrically saturated and starved DGEBA-DDM thermosets are shown in Figures 5.15 and 5.16, respectively. The temperature of the  $\gamma$  and  $\beta$  peaks and the  $\epsilon''$  and  $\epsilon'$  values at these temperatures are listed in Table 5.4(a) and (b) for the saturated and starved DGEBA-DDM thermosets, respectively.

As is seen in Figures 5.15 and 5.16 and Table 5.4, for both non-stoichiometric thermosets, the strength of the  $\gamma$ -relaxation "peak" decreases monotonically with curing towards a limiting value which is higher for the stoichiometrically starved than for the saturated DGEBA-DDM thermoset. The height of the  $\beta$ -relaxation peak initially increases, reaches a limiting high value which is identical in both thermosets, and then decreases. The temperature of the  $\beta$ -relaxation peak increases towards a stable value of 245K and 270K for the stoichiometrically starved and saturated thermosets, respectively. These features of physical ageing effects will be discussed in detail in the following chapter.

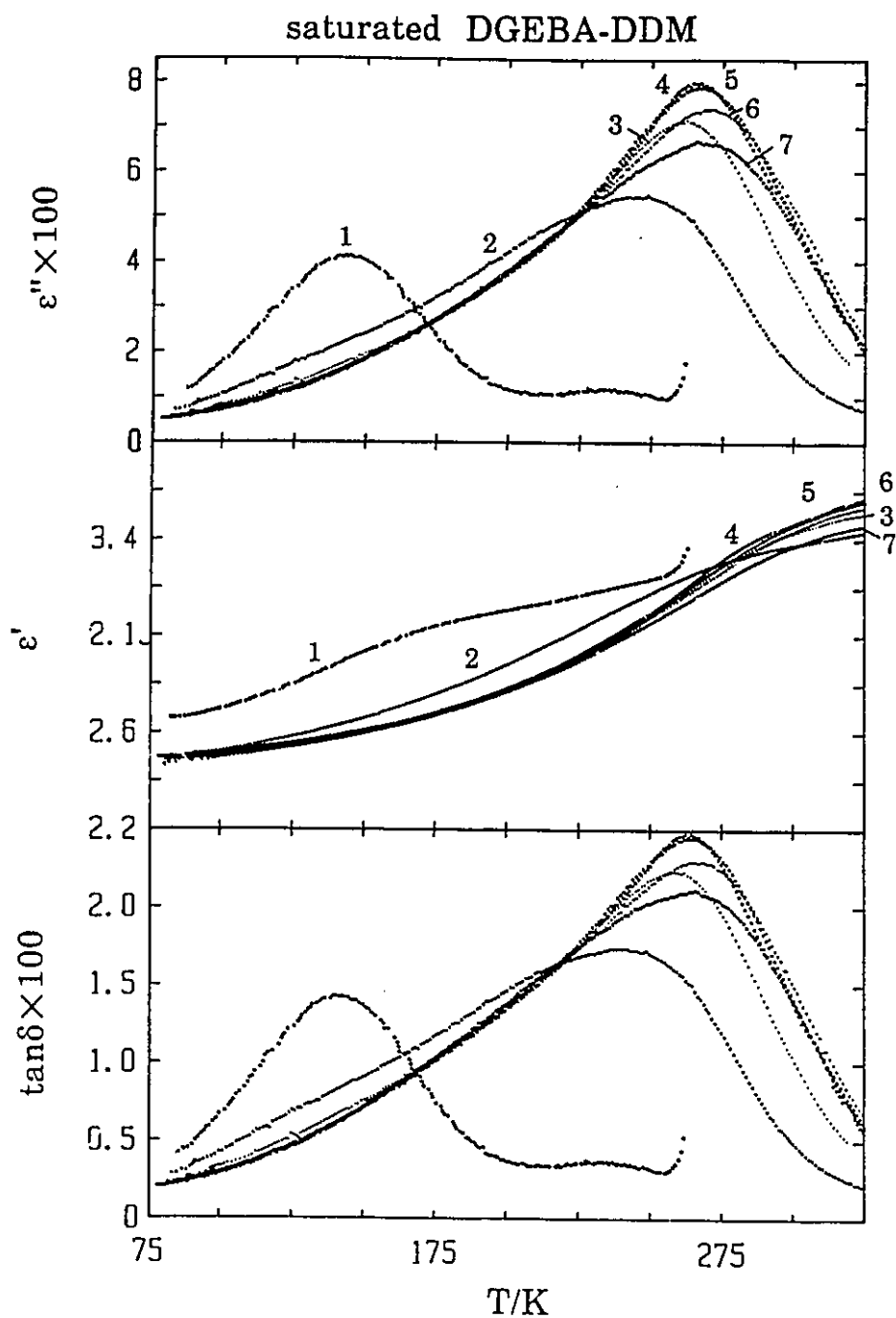


**Figure 5.15:** The dielectric loss, permittivity and loss tangent of the saturated DGEBA-DDM thermoset plotted against temperature. The increasing times of cure at 403K for the curves labelled 1 through 7 are given in Table 5.4.

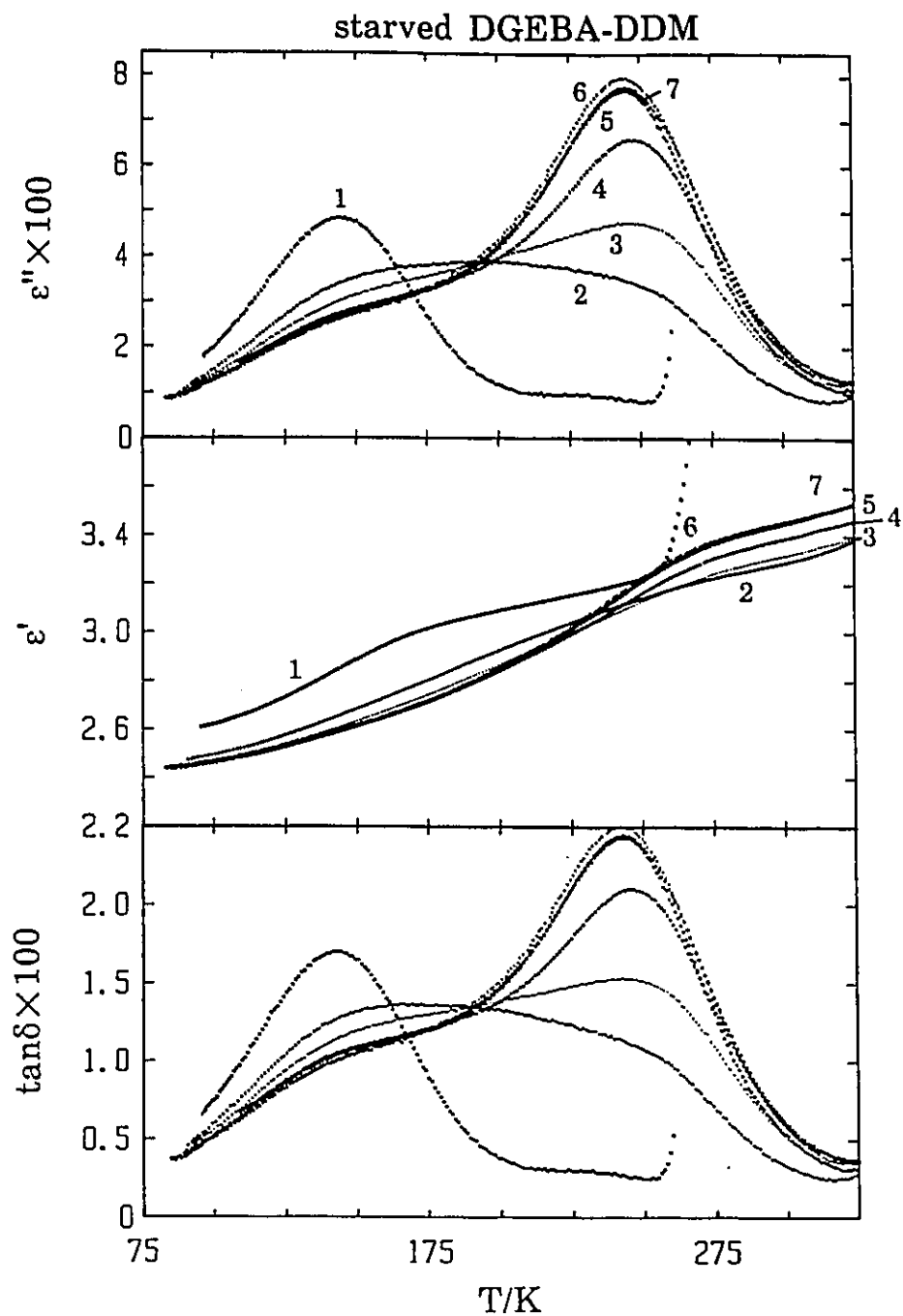


**Figure 5.16:** The dielectric loss, permittivity and loss tangent of the starved DGEBA-DDM thermoset plotted against temperature. The increasing times of cure at 403K for the curves labelled 1 through 7 are given in Table 5.4.

Table 5.4: The curing and ageing conditions of the nonstoichiometric DGEBA-DDM thermosets and the features of the observed dielectric behaviour.

(a) Stoichiometrically saturated sample

| $t_{c'}'$<br>(s) | $T_{cure}$<br>(K) | AECT(s)<br>at 403K | 100 $\gamma$ |         | $x \epsilon''_m$ |         | $T_m$             |                                             | $\epsilon'$ (90K) |  | $\epsilon'_m - \epsilon_\infty$ |  | $\epsilon'_m$<br>$\beta$ |
|------------------|-------------------|--------------------|--------------|---------|------------------|---------|-------------------|---------------------------------------------|-------------------|--|---------------------------------|--|--------------------------|
|                  |                   |                    | $\gamma$     | $\beta$ | $\gamma$         | $\beta$ | $\epsilon'$ (90K) | $\epsilon'_m - \epsilon_\infty$<br>$\gamma$ |                   |  |                                 |  |                          |
| 0                | - (1)*            | $5.40 \times 10^2$ | 4.10         | 1.15    | 142.5            | 25.0    | 2.66              | 0.23                                        | 3.19              |  |                                 |  |                          |
| 25200            | 346.0(2)          | $3.71 \times 10^3$ | 2.28         | 5.44    |                  | 243.0   | 2.51              | 0.13                                        | 3.14              |  |                                 |  |                          |
| 900              | 388.2(3)          | $6.37 \times 10^3$ | 1.83         | 7.15    |                  | 261.0   | 2.48              | 0.11                                        | 3.19              |  |                                 |  |                          |
| 1800             | 403.2(4)          | $8.89 \times 10^3$ | 1.69         | 7.90    |                  | 266.5   | 2.49              | 0.09                                        | 3.22              |  |                                 |  |                          |
| 3600             | 403.2(5)          | $1.30 \times 10^4$ | 1.72         | 7.98    |                  | 266.5   | 2.51              | 0.09                                        | 3.24              |  |                                 |  |                          |
| 7200             | 403.2             | $2.03 \times 10^4$ | 1.71         | 7.77    |                  | 269.5   | 2.50              | 0.09                                        | 3.24              |  |                                 |  |                          |
| 14400            | 403.2(6)          | $3.52 \times 10^4$ | 1.69         | 7.41    |                  | 270.0   | 2.50              | 0.09                                        | 3.23              |  |                                 |  |                          |
| 28800            | 403.2             | $6.45 \times 10^4$ | 1.68         | 7.13    |                  | 270.0   | 2.50              | 0.09                                        | 3.23              |  |                                 |  |                          |
| 57600            | 403.2             | $1.25 \times 10^5$ | 1.71         | 7.13    |                  | 269.5   | 2.50              | 0.09                                        | 3.22              |  |                                 |  |                          |
| 190800           | 403.2(7)          | $3.16 \times 10^5$ | 1.68         | 6.65    |                  | 269.5   | 2.50              | 0.08                                        | 3.20              |  |                                 |  |                          |

(b) Stoichiometrically starved sample

| $t_{c'}'$<br>(s) | $T_{cure}$<br>(K) | AECT(s)<br>at 403K | 100 $\gamma$ |         | $x \epsilon''_m$ |         | $T_m$             |                                             | $\epsilon'$ (90K) |  | $\epsilon'_m - \epsilon_\infty$ |  | $\epsilon'_m$<br>$\beta$ |
|------------------|-------------------|--------------------|--------------|---------|------------------|---------|-------------------|---------------------------------------------|-------------------|--|---------------------------------|--|--------------------------|
|                  |                   |                    | $\gamma$     | $\beta$ | $\gamma$         | $\beta$ | $\epsilon'$ (90K) | $\epsilon'_m - \epsilon_\infty$<br>$\gamma$ |                   |  |                                 |  |                          |
| 0                | - (1)*            | 0                  | 4.81         | 0.92    | 144.             | 227     | 2.60              | 0.25                                        | 3.15              |  |                                 |  |                          |
| 23200            | 340.8(2)          | $2.40 \times 10^3$ | 3.43         | 3.48    |                  |         | 2.48              | 0.19                                        | 3.13              |  |                                 |  |                          |
| 900              | 388.2(3)          | $3.28 \times 10^3$ | 3.03         | 4.76    |                  |         | 2.45              | 0.17                                        | 3.11              |  |                                 |  |                          |
| 1800             | 403.2(4)          | $5.93 \times 10^3$ | 2.77         | 6.63    |                  |         | 2.45              | 0.16                                        | 3.14              |  |                                 |  |                          |
| 3600             | 403.2(5)          | $1.04 \times 10^4$ | 2.73         | 7.78    |                  |         | 2.44              | 0.16                                        | 3.18              |  |                                 |  |                          |
| 7200             | 403.2(6)          | $1.83 \times 10^4$ | 2.72         | 7.99    |                  |         | 2.46              | 0.15                                        | 3.19              |  |                                 |  |                          |
| 14400            | 403.2(7)          | $3.30 \times 10^4$ | 2.62         | 7.72    |                  |         | 2.45              | 0.15                                        | 3.18              |  |                                 |  |                          |

\* the number in parentheses beside the  $T_{cure}$  value represents the curves in Figures 5.15 and 5.16.

## CHAPTER 6

### DIELECTRIC RELAXATION PHENOMENA IN THERMOSETS

#### 6.1 INTRODUCTION

##### 6.1.1 MECHANISMS OF SUB- $T_g$ RELAXATIONS IN POLYMERS

In most physical interpretations of the relaxation process in polymers, a dielectric or mechanical loss peak has usually been assigned to a particular mode of motion in the main chain, a side chain, or a side group in the polymer matrix. This subject has been ably reviewed by McCrum, Read and Williams (1967). But Johari and Goldstein (1970) and Johari (1973) have found that  $\gamma$  and  $\beta$ -relaxations are also observed in glasses made from molecules which have no internal degrees of freedom, i.e., covalent bonds about which thermally activated hindered rotational motions can occur (Johari 1985), in ionic glasses (Mai et al 1987 and 1989), in liquid crystals below their  $T_g$  (Johari 1982), and in polymers without a side group (Johari 1986) or a special mode of segmental motions. These relaxations have characteristics which are indistinguishable from those observed for long, flexible, chain polymers with side groups. therefore ad hoc explanations for such relaxations in amorphous substances are less attractive than general explanations of the occurrence of islands of mobility (Johari 1987) in a rigid matrix. Accordingly, it seems that secondary relaxations in the thermosets generally indicate dipolar motions in local regions which may consist of dissimilar cross-linking densities where dipolar parts of the polymer chain, or hydroxy-ether or epoxy groups, or the

unreacted molecular segments, are loosely packed in an otherwise rigid cross-linked matrix. Therefore, these relaxations are more appropriately interpreted in terms of two effects: (1) the changing number and nature of the existing dipolar segments as the chemical reactions of thermosetting progress and (2) the consequent change in the near-neighbour arrangement, or topology of the chains, as the average chain length increases and the network densifies. These effects are critically examined in this Chapter.

#### 6.1.2 PHYSICAL AGEING EFFECTS IN THERMOSETS

The effects of physical ageing on the sub- $T_g$  relaxations in thermoplastic polymers is currently debated (Struik 1978 and 1987, Johari 1982(a) and (b), Pathmanathan et al 1989, Diaz-Calleja et al 1989), and it seems that the strengths of both the dielectrically and mechanically observed  $\beta$ -relaxations in thermoplastics are affected by their thermal history, i.e., cooling rates, and their isothermal physical ageing, and that the effect vanishes on heating the thermoplastic to  $T > T_g$ . This allows the recovery of the physical properties of a thermoplastic. For thermosets, heating above  $T_g$  does not allow the recovery of the original liquid state because of the consequent occurrence of further curing or partial degradation to which dielectric properties are very sensitive. The original properties of an unaged thermoset cannot therefore be recovered in the same manner as for a thermoplastic. Therefore, the changes observed on physical ageing of

thermosets cannot be studied in the same manner as for the thermoplastics.

As discussed by Johari (1982(a)), changes in the dielectric behaviour of a thermoplastic on physical ageing are caused by at least four processes which are outlined as follows: (1) the decrease in the contribution to the dielectric property from the main or  $\alpha$ -relaxation at the temperature and frequency of the sub- $T_g$  relaxation peak caused by a shift in the main relaxation process to a higher temperature or a lower frequency; (2) a decrease in the strength of the sub- $T_g$  relaxation peak which occurs as a consequence of a reduction in the spatial freedom of motion of particular groups contributing to the relaxation or reduction in their number. This is the case when a decrease in volume is due partially to the collapse of localized high-volume, high-entropy regions which remain in an internal thermodynamic equilibrium in an otherwise macroscopically metastable rigid state of glass; (3) the decrease in the magnitude of the property associated with the main relaxation with increasing number density of molecules; and (4) the decrease in the frequency-independent background loss over which the sub- $T_g$  and  $\alpha$ -relaxation are superposed with a decrease in volume.

All of the above four processes also occur in thermosets, but a fifth process, namely, chemical reactions between the epoxide and the resin, as during the curing, also continues to occur as the limited diffusion of the chain segments causes densification or compaction of thermosets. Therefore, during

the isothermal ageing of a thermoset, the occurrence of all the above mentioned five processes causes a change in its dielectric properties, but the relative importance of each depends upon the frequency for which data are collected, the time and temperature of ageing, and the sensitivity of the dipolar relaxation process to a decrease in its specific volume.

## 6.2 THE CONCEPT OF ACCUMULATED EQUIVALENT CURING TIME

### 6.2.1 DEFINITION

Since a thermoset undergoes curing or cross-linking reactions at all temperatures, howsoever insignificant in their effects, it is important, both from the scientific and technical points of view, to consider the extent of the several effects which are unavoidable in such experiments, namely: (1) the extent of curing that occurs during the period it takes for a thermoset to reach a preselected value of  $T_{\text{cure}}$ , (2) the extent of curing that occurs during the period a thermoset is kept isothermally at  $T_{\text{cure}}$ , (3) the extent of curing that occurs during the period of a thermoset cooling from  $T_{\text{cure}}$  to a much lower temperature, and (4) the curing that occurs during the period it is kept at room or other temperatures for storage in between the measurements. For these reasons, we suggest that the thermal history of a thermoset be represented in terms of an accumulated equivalent curing time, abbreviated as AECT, at a fixed temperature, and propose its use for both theoretical discussion and practical purposes in the general investigations

of thermosets. This concept has a further advantage in that it allows comparisons between the properties of different samples of the same thermoset but with dissimilar thermal histories, although, as it would become clear later, for longer curing times, two samples with the same AECT but dissimilar thermal histories may not have the same dielectric properties.

We define AECT at  $T_1$  as the time period for which a sample would need to be kept isothermally at a temperature  $T_1$  in order for it to reach the same value of its measurable properties, i.e., chemical structure, physical state, or extent of reaction as measured by its dielectric properties here, as that of a sample which is, for example, heated at a rate of 1K/min from 90K to  $T_{cure}$ , isothermally cured at  $T_{cure}$  and thereafter either quenched or allowed to cool slowly in the thermostat, and subjected several times to this procedure. The concept of AECT is valid and useful so long as the curing process is solely governed by the chemical reaction kinetics as would become clear from its theoretical derivation given in the next Section.

### 6.2.2 THEORETICAL BASIS

Kinetic theories of poly-addition reactions of epoxies have been found by Prime (1981), Enns and Gillham (1983) and Barton (1985) to require the use of two kinetic constants whose values depend on the temperature of the curing reaction and obey an Arrhenius rate equation. Therefore, the time period,  $t$ , required for the curing reaction to reach a predefined

extent or chemical and physical state, varies with temperature and may be given by:

$$t(T) = t_0 \exp(E/RT) \quad (6.1)$$

where  $E$  is the activation energy,  $R$  the gas constant and  $t_0$  is the extrapolated value of  $t$  as  $T$  approaches infinity. We assume that the time needed for the dielectric loss of a sample to reach a maximum value during its curing characterizes a certain extent of reaction in the thermoset. Thus, we may write

$$t(T) = t(\epsilon''_m) = t_0 \exp(E/RT) \quad (6.2)$$

As discussed in Section 3.1.1, within the experimental errors, the value of  $E$  we measured remains constant at 45kJ/mole for the DGEBA cured with either DDM or DDS. This value is also in reasonable agreement with the values of 42.8 and 53.0kJ/mole which were obtained by Barton (1973, 1980) from the kinetic studies of the curing of the DGEBA-DDM and DGEBA-DDS thermosets, respectively. We prefer to use our value of 45kJ/mole for further development of the formalism here.

Since the curing reaction occurs at all temperatures, above  $T_g$ , albeit at different rates, the time period  $t(T_1)$ , for achieving a certain extent of cure at temperature  $T_1$  is related by eqn (6.1) to the time period,  $t(T_{cure})$ , for achieving the same extent of cure at  $T_{cure}$  according to

$$t(T_1) = t(T_{cure}) \exp(1/T_1 - 1/T_{cure})E/R \quad (6.3)$$

The advantage of Eqn (6.3) is that it allows us to obtain the AECT corresponding to different curing temperatures, e.g.  $T_1$  here, if the curing time for one curing temperature, e.g.  $T_{cure}$

here, is known.

The AECT can also be determined if, instead of an isothermal cure, a thermoset is cured during its heating at a constant rate. This type of curing is now considered as follows: During the heating from  $T_0$  to  $T_{cure}$  at a constant rate,  $q$ , given in degrees K per sec, the temperature of the system at any time,  $t$ , within the time interval from  $t_0$  (at  $T_0$ ) to  $t_1$  (at  $T_1$ ) is given by:

$$T - T_0 = q (t - t_0). \quad (6.4)$$

Converting the additive and finite time intervals of eqn (6.3) into a continuous change by integration and combining it with eqn (6.4), we write

$$t(T_1) = \int_{t_0}^{t_1} dt (T) \exp(1/T_1 - 1/T) E/R = q^{-1} \exp(E/RT_1) \int_{T_0}^{T_1} \exp(-E/RT) dT \quad (6.5)$$

Since virtually no reaction occurs at  $T_0$  if  $T_0 < T_{g0}$  as is the case in our studies, eqn (6.5) may be rewritten as (Doyle 1961, Ozawa 1965, Coates and Redfern 1964)

$$t(T_1) = (E/qR) \exp(E/RT_1) p(E/RT_1) \quad (6.6)$$

where

$$p(y) = \int_y^{\infty} (e^{-y}/y^2) dy \quad (6.7)$$

Values of  $p$  for different values of  $y$  have been tabulated by Doyle (1961) or they can be conveniently obtained numerically.

The method for determining AECT may now be elucidated as follows: According to eqn (6.6), the state of a thermoset heated from 90K to 363K at a fixed rate of 1K/min is equivalent in the extent of its cure, to that which is achieved after a period of 20 minutes of its isothermal cure at 363K.

Alternatively speaking, cooling a thermoset from 363K to 300K at a rate of 0.5K/min is equivalent, in terms of the extent of its cure, to a 40-minute period of isothermal cure at 363K. These two examples also of course illustrate that the contribution to the curing of thermosets from the heating and cooling cycles in the course of dielectric measurement is far from negligible and that this contribution should be included in the determination of its AECT.

It is important to note at this point that the procedure for determining AECT is implicitly based on the assumption that polyaddition reactions in thermosets are governed by the chemical kinetic behaviour of the reactants. This assumption is strictly valid at the beginning of the curing process, but becomes invalid when the mixture becomes a glass and when the physical (molecular) diffusion mechanisms rather than chemical reactions begin to control the reaction's progress (Peng and Gillham 1985, Williams 1985, Kaiser 1989, Plazek and Frund 1990, Pascault and Williams 1990). Therefore, when the temperature of the cure is changed in order to study the post-curing of thermosets as reported in the case of DGEBA-DDM in figure 5.9, we expect a discontinuity in all of its measured properties when plotted against AECT.

The AECT values were calculated at a designated curing temperature ( $T_c$ ) for all the thermosets studied here and described in Sections 5.2 and 5.3. These calculations were based on their thermal histories and eqns. (6.3) and (6.6) were

used. The values of AECT thus calculated are included in the second column of tables 5.1 to 5.4.

### 6.3 EVOLUTIONS OF THE DIELECTRIC RELAXATION FEATURES

#### 6.3.1 THE RELAXATION PEAK HEIGHT AND TEMPERATURE

The temperature of the  $\alpha$ ,  $\beta$ , and  $\gamma$  relaxation peaks, obtained from Figures 5.7 to 5.11 and tables 5.1 and 5.2, is plotted against the AECT of the DGEBA-DDM thermoset cured at 363K and of DGEBA-DDS cured at 398K in Figure 6.1. For the sake of clarity, the corresponding plot for the DGEBA-(0.7 DDS, 0.3 DDM) thermoset cured at 363K is given separately in Figure 6.2. The temperatures of the  $\gamma$ -,  $\beta$ - and  $\alpha$ -relaxation peaks,  $T_{m,\gamma}$ ,  $T_{m,\beta}$  and  $T_{m,\alpha}$ , respectively, in Figures 6.1 and 6.2 and Tables 5.1 to 5.3 are seen to increase with AECT. This increase is smallest, i.e. less than 5K, for the  $\gamma$ -relaxation and largest, i.e. more than 60K, for the  $\alpha$ -relaxation. For larger values of AECT and when the  $\alpha$  peak is shifted to temperature values higher than  $T_{cure}$ , the value of  $T_{m,\alpha}$  was not determined in order to prevent additional cure or post-cure of the thermoset. Also, as the  $\gamma$ -peak height decreases with increasing AECT, as is seen in Figures 5.6 to 5.11, the  $\gamma$ -relaxation peak begins to appear as a shoulder, in the later part of the cure, and thus the exact  $T_{m,\gamma}$  value could not be determined. Nevertheless, Figures 6.1 and 6.2 do show that both  $T_{m,\gamma}$  and  $T_{m,\beta}$  reach a stable value, which we refer to as  $T_{m,\gamma}(\infty)$  and  $T_{m,\beta}(\infty)$ , respectively, at large AECT values. Values thus determined for  $T_{m,\gamma}(\infty)$  are 145K, 150K and 150K and for

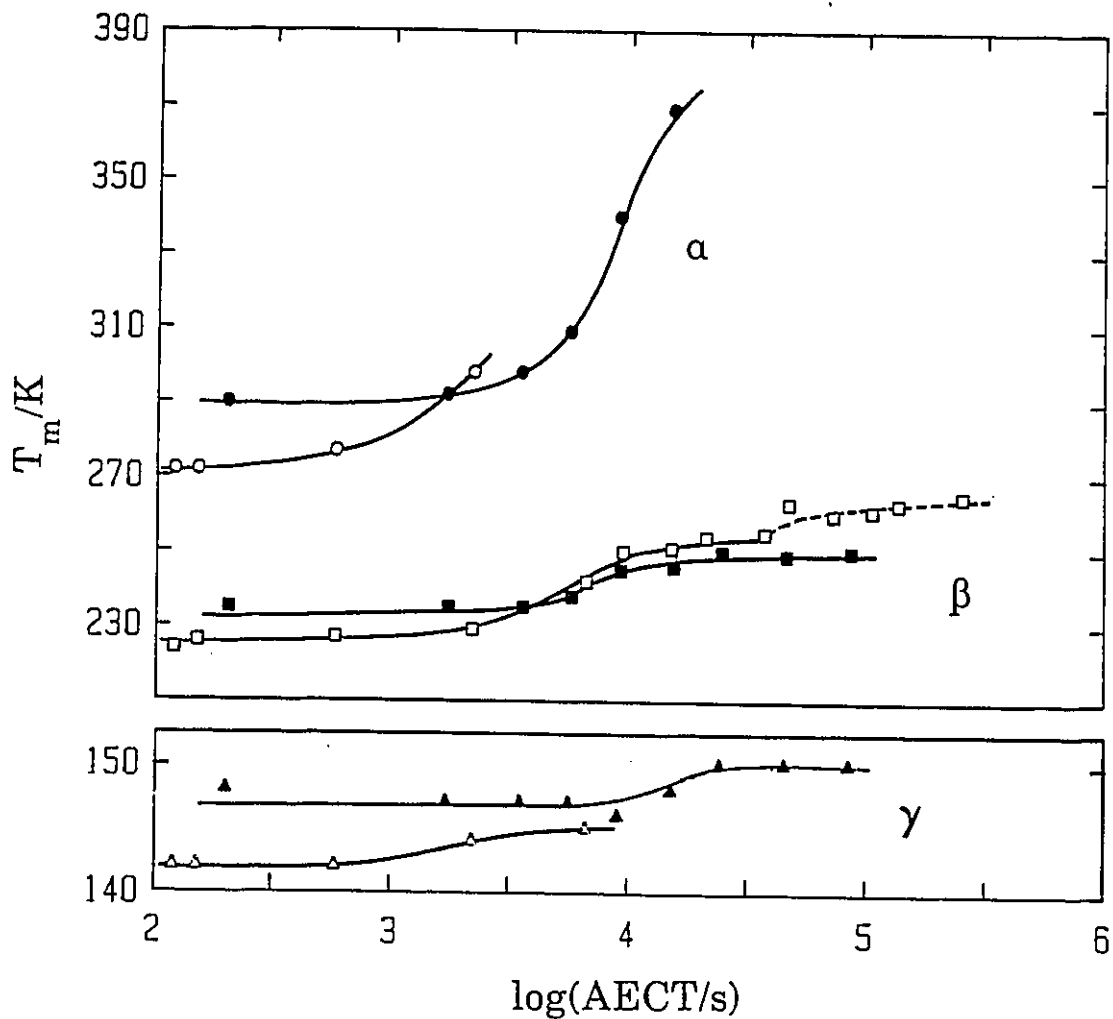


**Figure 6.1:** The temperatures of the  $\gamma$ -,  $\beta$ - and  $\alpha$ -relaxation processes during the curing and post-curing of the DGEBA-DDM and DGEBA-DDS thermosets plotted against the accumulated equivalent curing time. Open symbols are for DGEBA-DDM and filled ones for DGEBA-DDS.

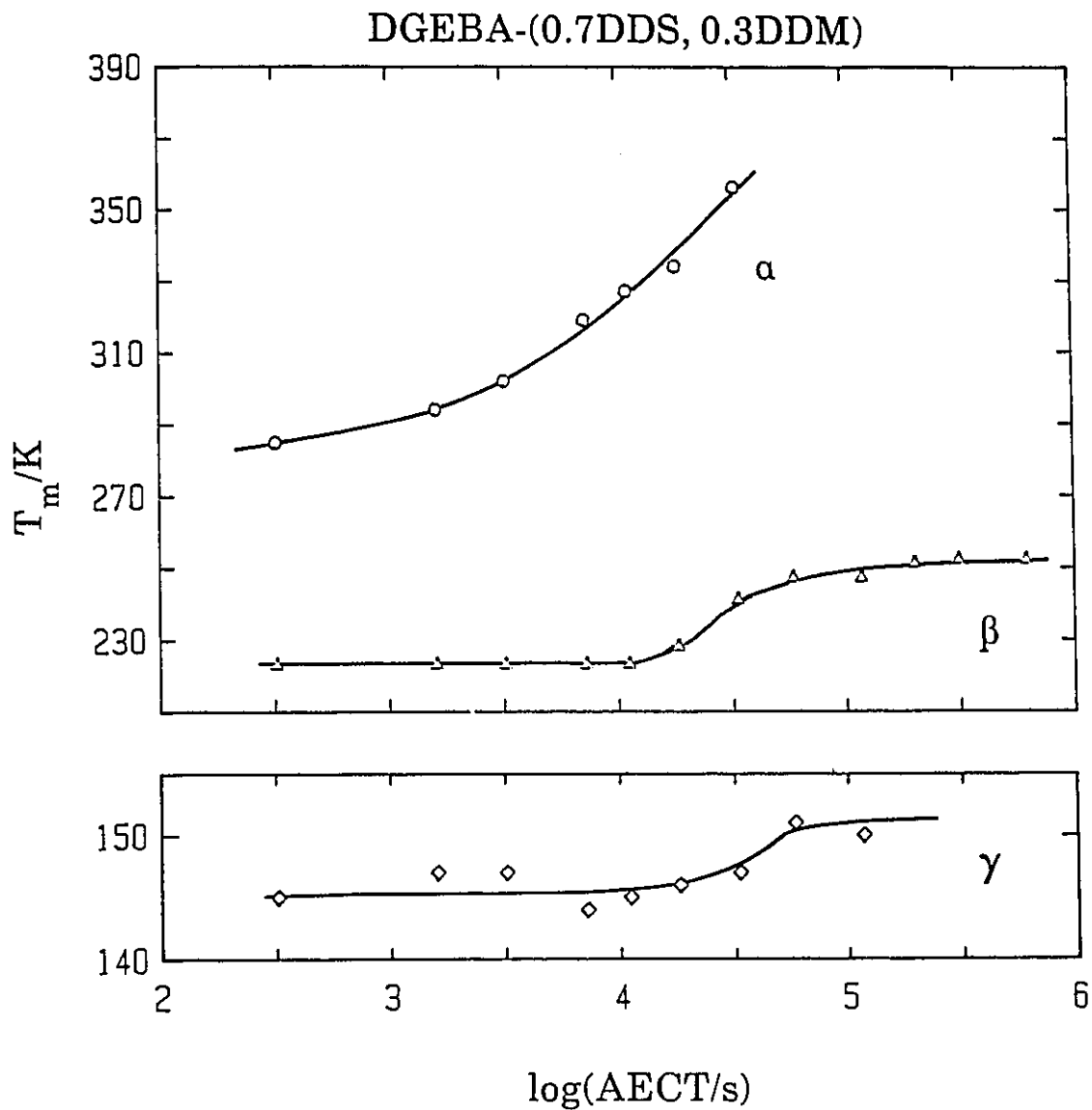


**Figure 6.2:** The temperatures of the  $\gamma$ - $\beta$ - and  $\alpha$ -relaxation processes during the curing of the DGEBA-(0.7DDS, 0.3 DDM) thermoset plotted against the accumulated equivalent curing time.

$T_{m,\beta}(\infty)$  are 255K, 252K and 250K, for the DGEBA-DDM, DGEBA-(0.7 DDS, 0.3 DDM) and DGEBA-DDS thermosets, respectively. When DGEBA-DDM is post-cured at 403K,  $T_{m,\beta}$  is seen in Figure 6.1 and Table 5.1 to increase towards a second value of  $T_{m,\beta}(\infty)$  of 265K.  $T_m(\infty)$  is thus found to depend on the curing temperature selected. The plots in Figures 6.1 and 6.2 also clearly show that curing causes a progressive separation of the  $\alpha$ -relaxation process from the sub- $T_g$  relaxations in a temperature plane.

We now discuss the changes in the strength of the  $\gamma$ ,  $\beta$  and  $\alpha$ -relaxations. The peak value of  $\epsilon''$  which is measured at  $T_{m,\gamma}$ ,  $T_{m,\beta}$  and  $T_{m,\alpha}$ , or  $\epsilon''_{m,\gamma}$ ,  $\epsilon''_{m,\beta}$  and  $\epsilon''_{m,\alpha}$ , respectively, is plotted against the AECT of DGEBA-DDM and DGEBA-DDS in Figure 6.3. The corresponding plot for DGEBA-(0.7 DDS, 0.3 DDM) is shown in Figure 6.4. For larger AECT values, when the  $\gamma$ -relaxation appears only as a shoulder in Figures 5.7 to 5.11,  $\epsilon''_{m,\gamma}$  can be determined only as the  $\epsilon''$  value measured at the  $\gamma$ -peak temperature,  $T_{m,\gamma}(\infty)$ . With an increase in the AECT, the heights of both the  $\gamma$ - and  $\alpha$ -relaxations in the three thermosets monotonically decrease towards a limiting value which we refer to as  $\epsilon''_{m,\gamma}(\infty)$  and  $\epsilon''_{m,\alpha}(\infty)$ . Values of  $\epsilon''_{m,\gamma}(\infty)$  thus determined are  $2.68 \times 10^{-2}$ ,  $2.68 \times 10^{-2}$  and  $2.24 \times 10^{-2}$  for the DGEBA-DDM, DGEBA-(0.7 DDS, 0.3 DDM) and DGEBA-DDS thermosets, respectively. Figure 6.3 further shows that during the post-cure of DGEBA-DDM at 403K,  $\epsilon''_{m,\gamma}$  decreases further towards a second limiting value of  $2.12 \times 10^{-2}$ . Thus, the limiting maximum dielectric loss value  $\epsilon''_m(\infty)$  also depends on the curing temperature.

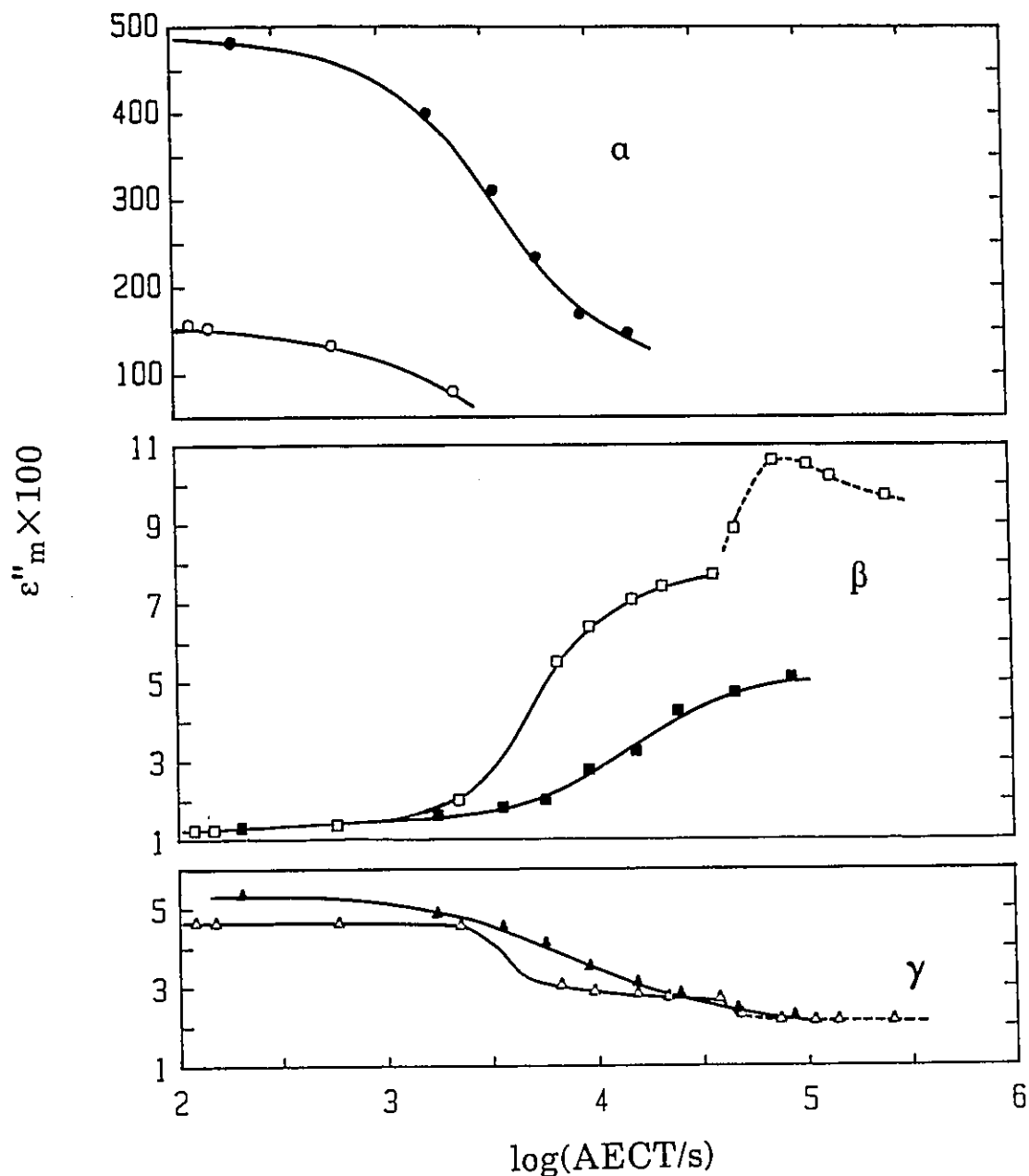


**Figure 6.3:** The  $\epsilon''_m$  value for the  $\gamma$ -,  $\beta$ - and  $\alpha$ -relaxation processes during the curing of the DGEBA-DDM and DGEBA-DDS thermosets plotted against the accumulated equivalent curing time. Open symbols are for DGEBA-DDM and filled ones for DGEBA-DDS.

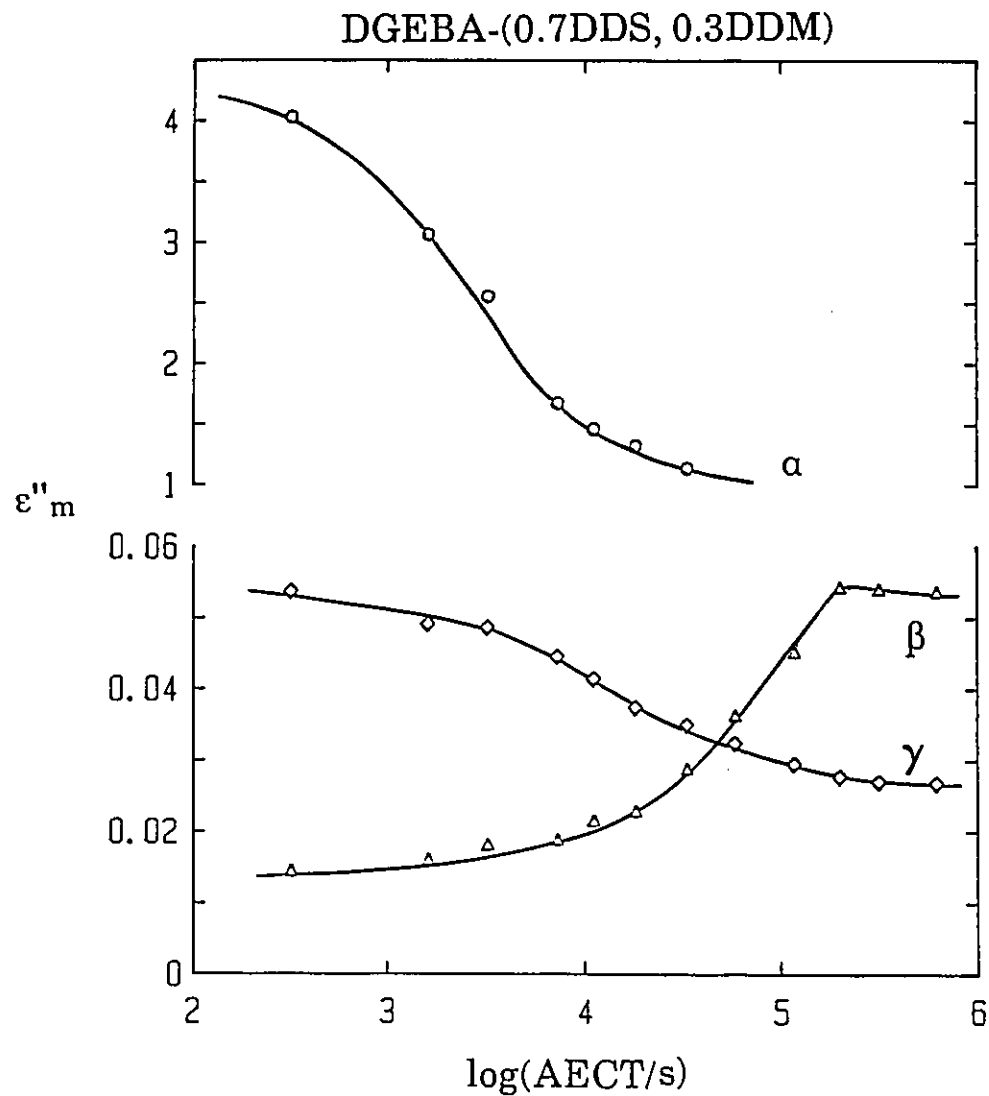


**Figure 6.4:** The temperatures of the  $\gamma$ -,  $\beta$ - and  $\alpha$ -relaxation processes during the curing of the DGEBA-(0.7DDS, 0.3DDM) thermoset plotted against the accumulated equivalent curing time.

We now discuss the strength of the  $\beta$ -relaxation process and its change with AECT. Figures 6.3 and 6.4 and Tables 5.1 to 5.3 show that the strength of the  $\beta$ -relaxation process initially increases with increase in AECT, reaches a maximum value,  $\epsilon''_{m,\beta}(\text{max})$ , and then begins to decrease towards a limiting value,  $\epsilon''_{m,\beta}(\infty)$ . Values of  $\epsilon''_{m,\beta}(\text{max})$  are c.a.  $8 \times 10^{-2}$ ,  $5.4 \times 10^{-2}$  and c.a.  $5.2 \times 10^{-2}$  for DGEBA-DDM, DGEBA-(0.7 DDS, 0.3 DDM) and DGEBA-DDS thermosets, respectively. During the post-cure at 403K of the DGEBA-DDM thermoset shown by dashed line,  $\epsilon''_{m,\beta}$  increases again towards a higher value of  $10.6 \times 10^{-2}$  and then decreases. Thus,  $\epsilon''_{m,\beta}(\text{max})$  also depends on the curing temperature.

### 6.3.2 EFFECT OF SUBSTITUTION OF AMINES ON THE SUB- $T_g$ RELAXATIONS

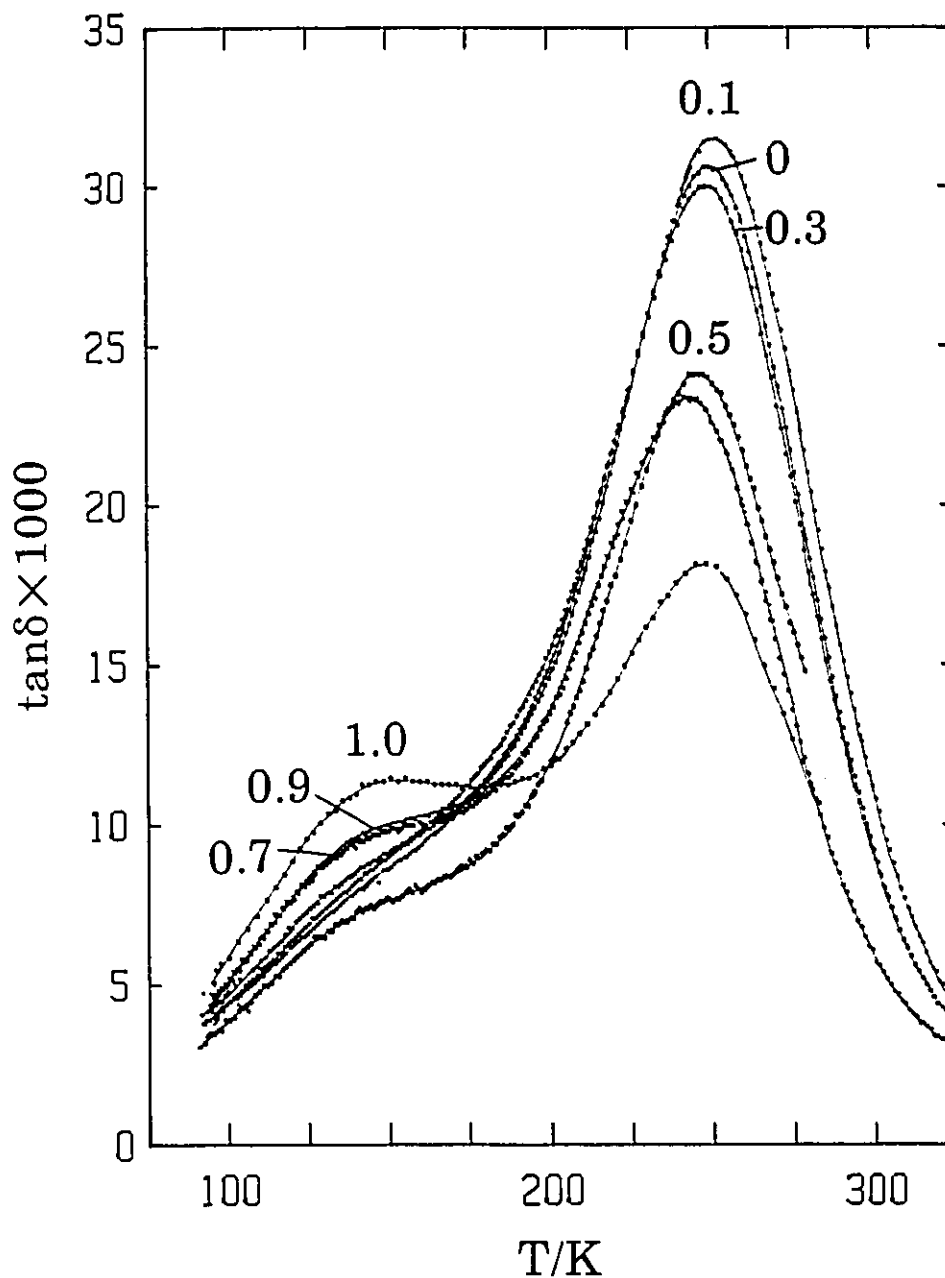
The dielectric behaviour of the DGEBA-based thermosets, when cured isothermally at  $377 \pm 2\text{K}$  for  $m$  number of hours with an amine mixture of DDM and DDS, is already described in Section 3.3. After this study at  $377 \pm 2\text{K}$ , the dielectric cells containing the thermosets were stored at  $298 \pm 2\text{K}$  for  $n$  number of days and their sub- $T_g$  relaxations were again studied. For this purpose, each dielectric cell containing the thermoset was cooled to 90K and thereafter was heated at a rate of 1K/min up to 325K during which its loss tangent and permittivity were measured for a fixed frequency of 1kHz at 1K intervals up to 325K. Numerical values of  $m$  in hours and  $n$  in days are listed in Table 6.1. The  $\tan\delta$  values of the seven thermosets obtained

Table 6.1: Features of the dielectric sub- $T_g$  relaxations of DGEBA-(x DDS, (1-x) DDM) thermosets after their curing for m hours at  $377 \pm 2K$  and n days at 298K.

| x   | m(h) | n(days) | $\epsilon'_m(140)$ | $\epsilon'_m(\beta)$ | $\epsilon'_m(320)$ | $\epsilon''_m(140) \times 10^2$ | $\epsilon''_m(\beta) \times 10^2$ | $T_m(\beta)/K$ | $\tan\delta_m(140) \times 10^2$ | $\tan\delta_m(\beta) \times 10^2$ |
|-----|------|---------|--------------------|----------------------|--------------------|---------------------------------|-----------------------------------|----------------|---------------------------------|-----------------------------------|
| 0   | 49   | 173     | 1.041              | 1.303                | 1.435              | 0.863                           | 3.99                              | 252.0          | .83                             | 3.06                              |
| 0.1 | 96   | 162     | 1.041              | 1.301                | 1.435              | 0.833                           | 4.09                              | 254.5          | .80                             | 3.15                              |
| 0.3 | 49   | 173     | 1.043              | 1.287                | 1.416              | 0.900                           | 3.87                              | 251.2          | .86                             | 3.00                              |
| 0.5 | 45   | 153     | 1.044              | 1.259                | 1.371              | 0.767                           | 3.03                              | 249.0          | .73                             | 2.41                              |
| 0.7 | 47   | 178     | 1.050              | 1.254                | 1.350              | 0.996                           | 2.92                              | 244.5          | .95                             | 2.34                              |
| 0.9 | 69   | 181     | 1.050              | 1.261                | 1.350              | 1.01                            | 2.95                              | 246.0          | .96                             | 2.34                              |
| 1.0 | 75.4 | 182     | 1.060              | 1.240                | 1.339              | 1.16                            | 2.25                              | 249.0          | 1.10                            | 1.81                              |

from these measurements are plotted against the temperature in Figure 6.5, where the shape of the curves are seen to be similar to those in Figures 5.7 to 5.11 obtained for these thermosets.

In order to analyze the features of the sub- $T_g$  relaxation peak as the curing amine DDM is replaced by DDS, the measured  $\epsilon'$  and  $\epsilon''$  values were normalized with respect to the corresponding  $\epsilon'$  value at 90K. These values are represented by subscript N with the temperature given in parenthesis. For example,  $\epsilon'_N(320)$  denotes the value of  $\epsilon'$  measured at 320K divided by  $\epsilon'$  measured at 90K and  $\epsilon''_N(\beta)$ , the value of  $\epsilon''$  measured at  $T_{m,\beta}$  divided by  $\epsilon'$  at 90K, etc. The values of  $\epsilon'_N(140)$ ,  $\epsilon'_N(\beta)$ ,  $\epsilon'_N(320)$ ,  $\epsilon''_N(140)$  and  $\epsilon''_N(\beta)$ , the temperature of the relaxation peak,  $T_{m,\beta}$ , and the height of the  $\tan\delta$  peaks for the  $\beta$  and  $\gamma$ -relaxations are also listed in Table 6.1. All these values are plotted against the mole fraction,  $x$ , of the DDS in the mixed curing amine in Figure 6.6. The figure shows that both the normalized dielectric permittivity and loss measured at  $T_{m,\gamma}$  increase and those measured at  $T_{m,\beta}$  decrease, as a first approximation, linearly with an increase in  $x$ , the mole fraction of DDS. The small deviations from the straight line in Figure 6.6 are likely to be due to the different thermal histories to which the various samples were subjected as described in Table 6.1. The plots in Figure 6.6 further show that the respective sums of  $\epsilon''_N$  and  $\epsilon'_N$  for  $\beta$ - and  $\gamma$ -relaxations decrease with increase in  $x$  suggesting therefore that the decrease in  $\epsilon''_N$  and  $\epsilon'_N$  for the  $\beta$ -relaxation is more than can



**Figure 6.5:** The  $\tan\delta$  for the DGEBA- ( $x$ DDS,  $(1-x)$ DDM) thermosets measured after their curing for  $n$  hours at 377K and ageing for  $m$  days at 298K. The data were obtained for a fixed frequency of 1kHz and are plotted against temperature on a linear scale.

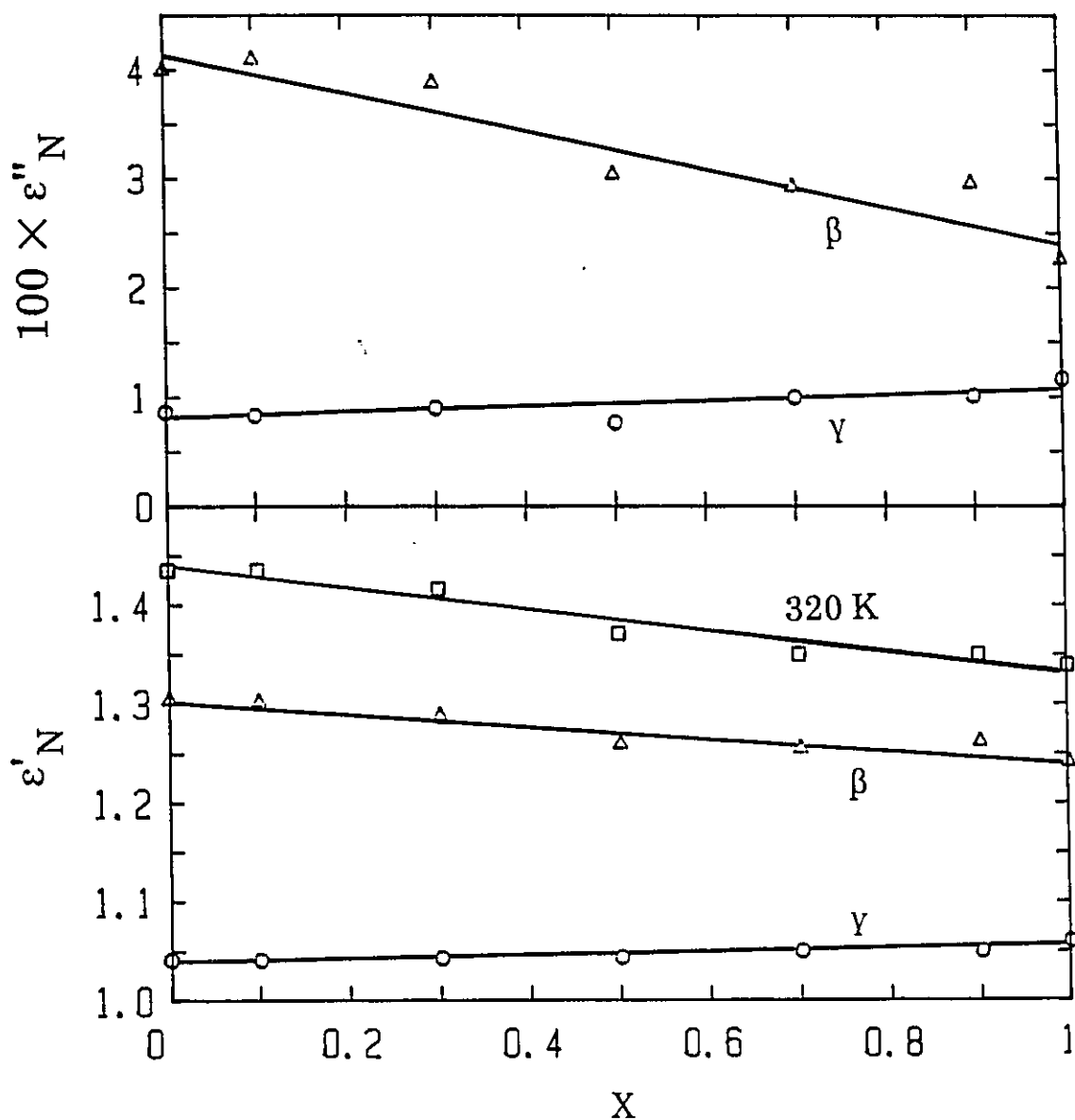


**Figure 6.6:** (a) The normalized heights of the  $\gamma$ - and  $\beta$ - $\alpha$ -relaxation peaks and (b) the corresponding dielectric permittivity,  $\epsilon'$ , plotted against the composition of the curing agent.  $\Delta$  represents the  $\beta$ -process,  $\circ$  the  $\gamma$ -process and  $\square$  the combined magnitudes of the  $\beta$  and  $\gamma$  processes measured at 320K.

be compensated for by the concomitant increase in the  $\epsilon''_{\alpha}$  and  $\epsilon'_{\alpha}$  for the  $\gamma$ -relaxation.

### 6.3.3 EFFECT OF THE THERMOSET'S COMPOSITION

The value of  $T_{m,\beta}$  for the saturated and starved DGEBA-DDM thermoset is plotted against AECT in Figure 6.7(a).  $T_{m,\beta}$  in this figure increases towards an asymptotic value, referred to as  $T_{m,\beta}(\infty)$  here, in both cases but the values of  $T_{m,\beta}$  are larger for the stoichiometrically saturated sample than for the starved sample and  $T_{m,\beta}(\infty)$  is 270K for the saturated sample, which is 15K higher than the corresponding value of 245K observed for the starved sample.

The value of  $\epsilon''$  measured at  $T_{m,\gamma}$  and  $T_{m,\beta}$  is also plotted against AECT for these samples in Figure 6.7(b). In cases when the  $\gamma$ -relaxation appears only as a shoulder,  $\epsilon''_{m,\gamma}$  was taken as the  $\epsilon''$  value at 145K, the  $T_{m,\gamma}(\infty)$  value of DGEBA-DDM cured at 363K given in Section 6.3.1. The trends in the value of  $\epsilon''_{m,\beta}$  for both thermosets are closely similar, and the maximum value,  $\epsilon''_{m,\beta}(\text{max})$ , for both is  $8.00 \times 10^{-2}$ . The curve corresponding to the stoichiometrically starved thermoset is slightly shifted towards longer AECT values. The trends in the value of  $\epsilon''_{m,\gamma}$  are also similar in both thermosets, but the absolute values of  $\epsilon''_{m,\gamma}$  observed for the starved sample are generally higher than those observed for the saturated sample.  $\epsilon''_{m,\gamma}(\infty)$  is  $1.68 \times 10^{-2}$  and  $2.62 \times 10^{-2}$  for the saturated and starved sample, respectively. In a recent study of a stoichiometric mixture of DGEBA and DDM also cured at 403K, Sidebottom and Johari

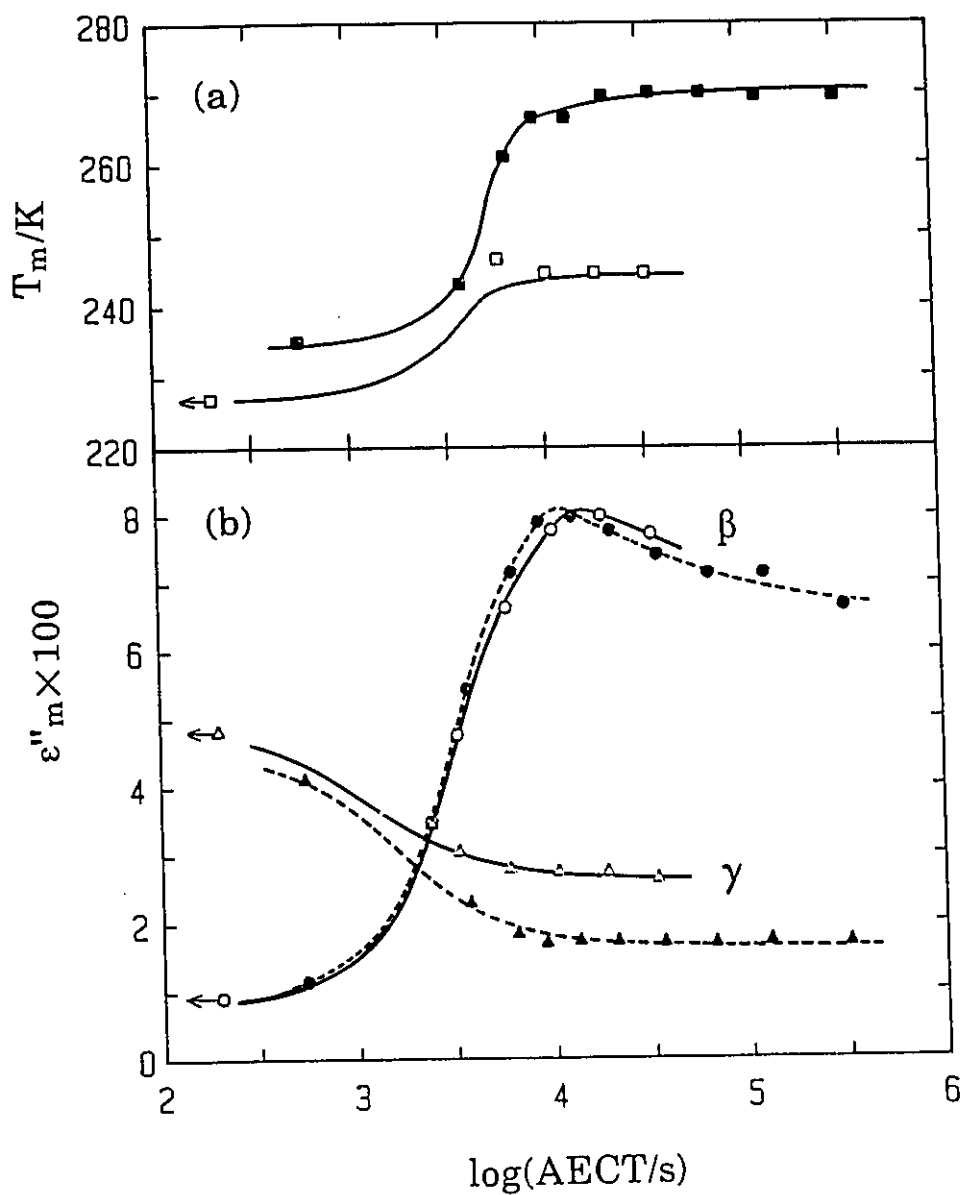


**Figure 6.7:** (a) The temperature of the  $\beta$ -relaxation and (b) the  $\epsilon''_m$  of the  $\gamma$ - and  $\beta$ -relaxation processes during the curing of the DGEBA-DDM thermosets at 403K plotted against accumulated equivalent curing time. Open symbols are for the stoichiometrically starved sample and solid symbols for the stoichiometrically saturated sample.

(submitted) have found a value of  $\epsilon''_{m,\beta}(\max)$  of  $8.62 \times 10^{-2}$ . This value is 7% higher than the value of  $8 \times 10^{-2}$  observed in Figure 6.7 for both the saturated and starved mixture. The value of  $T_{m,\beta}(\infty)$  they measured is 268K (as obtained from their Figure) which is close to the corresponding value of 270K obtained for the stoichiometrically saturated sample. These observations will be discussed further in Section 6.5.

#### 6.4 THE DISTRIBUTION OF RELAXATION TIMES AND CURING EFFECTS

##### 6.4.1. ISOTHERMAL SPECTRA

Information on the nature of the distribution of relaxation times, which partially characterizes the dielectric relaxation of materials, has generally been obtained from an analysis of the frequency dependence of both the dielectric permittivity and loss. For the curing of thermosets this can be studied only when the cross-linking reaction are prohibitively slowed down by quenching the thermoset sample to temperatures far below its glass transition temperature. Thus, only for their sub- $T_g$  relaxations, the distribution parameter can be determined by the use of conventional methods. For the cured thermoset's  $\alpha$ -, or main, relaxation, the conventional procedure for determining the distribution parameter would require raising its temperature above its glass transition temperature, which would allow the curing reactions to occur further and this occurrence would alter the polymer's network topology during the course of the frequency scanning measurements.

Figure 5.2 shows the isothermal spectra for the sub- $T_g$  relaxations of both the fully cured and aged DGEBA-DDM thermoset. It is clear from this figure that the spectra are broad and that the three decades of frequency used here allows only a partial characterization of the sub- $T_g$  relaxations. For example, the  $\beta$ -relaxation peak of the fully cured DGEBA-DDM sample measured at 292.5K is only partly characterized, and the value of its frequency width at half the peak height,  $\Delta$ , which formally speaking, is a measure of the distribution of relaxation times, can not be obtained. The low-frequency part of  $\Delta$ , on the left-hand side of the peak position,  $f_m$ , is equal to about 1.75 decades. Since, for an asymmetric distribution, the low frequency portion of  $\Delta$  is smaller than its high frequency portion, the value of  $\Delta$  for this relaxation peak is estimated to be greater than 3.5 decades. This value is much larger than  $\Delta=1.14$  decades obtained for a single relaxation time process and corresponds to a very broad distribution of relaxation times, with a  $\beta$  parameter value, as given by Moynihan et al (1973), lower than 0.3.

Because of the difficulties of analyzing the complete frequency spectra as discussed above, a method for the analysis of the temperature, rather than the frequency, dependence of  $\epsilon'$  and  $\epsilon''$  was needed. This was developed in order to obtain reliable information on the distribution of relaxation times of a relaxation process, which remains otherwise inaccessible. This method is described as follows:

#### 6.4.2 THEORETICAL FORMALISM

Measurements of the dielectric and mechanical properties of most amorphous materials in the frequency and time domains have been successfully described, as discussed in Section 1.3, in terms of the KWW parameter,  $\beta$ , of the non-exponential relaxation function given in eqn (1.19). This formalism has also been generally found to successfully describe the primary or  $\alpha$ -relaxation process of thermosets during their curing, as described in Chapter 4. Therefore, it is reasonable to assume that this formalism is equally useful for the relaxation processes in thermosets which we now develop for fixed frequency measurements in the temperature domain. The frequency dependence of  $\epsilon^*$  of a substance is given, according to eqns (1.11) and (1.12) by:

$$(\epsilon^*(\omega\tau_0) - \epsilon_\infty) / (\epsilon_0 - \epsilon_\infty) = \int (-d\phi/dt) = N^*(\omega\tau_0) \quad (6.8)$$

where  $\phi$  is the non-exponential relaxation function as defined in eqn (1.19) and  $\tau_0$  is the relaxation time appearing in the definition of  $\phi$  (eqn (1.19)) for a given temperature. The Laplace transform term in eqn (6.8) cannot be easily included for further solution of this equation, and therefore values of  $N^*$  need to be evaluated by another procedure. Alternative procedures were developed by Moynihan et al (1973) and Lindsey and Patterson (1980) and these authors have provided tables of numerical values of  $N^*$  for  $z(=\omega\tau_0)$  in the range  $10^{-3}$  to  $10^4$  which corresponds to the  $\beta$  in the range 0.30 to 1. These values were used here but for values of the parameter  $\beta$  between 0.1 and 0.3, we use the  $z$  dependence of  $N^*$  derived from the formalism

and tables developed by Montroll and Bendler (1984), Dishon et al (1985) and Weiss et al (1985) as described in the Appendix here.

By separating the real and imaginary components of eqn (6.8) we obtain,

$$(\epsilon'(\omega\tau_0) - \epsilon_\infty) / (\epsilon_0 - \epsilon_\infty) = N'(\omega\tau_0) \quad (6.9)$$

and, 
$$\epsilon''(\omega\tau_0) / (\epsilon_0 - \epsilon_\infty) = N''(\omega\tau_0) \quad (6.10)$$

Since  $N^*$  is the normalized value of  $\epsilon^*$  according to eqn (6.8), it follows that as  $(\omega\tau_0)$  increases the value of  $N'$  decreases from one to zero while that of  $N''$  increases from zero, reaches a maximum value,  $N''_m$ , at  $\omega\tau_0 = (\omega\tau_0)_m$ , and then decreases to zero. The values of  $N'$  and  $N''$  used in this work are given in the Appendix. The values of  $z_m = (\omega\tau_0)_m$ ,  $N''_m$  and the  $N''$  peak's width,  $\Delta$ , measured at half its height are all monotonic functions of the value of the parameter  $\beta$  which lies between 0 and unity (Moynihan et al 1973). The values of  $N'_m$  and  $N''_m$  calculated for  $\beta$  values ranging from 0.10 to 0.60 are listed in Table 6.2.

When  $z = z_m$ , eqns (6.9) and (6.10) may be written as:

$$\epsilon'_m - \epsilon_\infty = (\epsilon_0 - \epsilon_\infty) N'_m \quad (6.11)$$

$$\epsilon''_m = (\epsilon_0 - \epsilon_\infty) N''_m \quad (6.12)$$

where  $\epsilon'_m$  and  $\epsilon''_m$  are the values of  $\epsilon'$  and  $\epsilon''$  at  $z = z_m$ .  $\epsilon'_m$  and  $\epsilon''_m$  are usually experimentally accessible but  $N'_m$  and  $N''_m$  are defined by an adequate choice of the value of  $\beta$  according to Table 6.2. Thus, when in an experiment only  $\epsilon_0$  (or  $\epsilon_\infty$ ) can be measured, eqns (6.11) and (6.12) can be used to determine the values of both  $\beta$  and  $\epsilon_\infty$  (or  $\epsilon_0$ ), and the dielectric strength of the relaxation,  $\Delta\epsilon = \epsilon_0 - \epsilon_\infty$ , can be calculated. Eqns (6.11)

**TABLE 6.2:** Parameters used for determining the KWW parameter for sub- $T_g$  relaxations.

| $\beta$ | $N'_m$                | $N'_m$ | $N'_m/N'_m$ | $N'_m/(1-N'_m)$ |
|---------|-----------------------|--------|-------------|-----------------|
| 0.60    | 0.323                 | 0.57   | 0.59        | 0.75            |
| 0.55    | 0.298                 | 0.60   | 0.50        | 0.74            |
| 0.50    | 0.273                 | 0.62   | 0.44        | 0.72            |
| 0.45    | 0.248                 | 0.62   | 0.40        | 0.65            |
| 0.40    | 0.222                 | 0.62   | 0.36        | 0.58            |
| 0.35    | 0.196                 | 0.62   | 0.32        | 0.52            |
| 0.30    | 0.169                 | 0.62   | 0.27        | 0.44            |
| 0.25    | 0.142                 | 0.62   | 0.23        | 0.37            |
| 0.20    | 0.114                 | 0.62   | 0.18        | 0.30            |
| 0.18    | 0.103                 | 0.63   | 0.16        | 0.28            |
| 0.15    | 0.086                 | 0.63   | 0.14        | 0.23            |
| 0.10    | $\frac{0}{k}$<br>0.58 | 0.63   | 0.09        | 0.16            |

and (6.12) are thus particularly useful in these cases where the presence of a second sub- $T_g$  relaxation process prevents one from experimentally determining  $\epsilon_o$  (or  $\epsilon_o'$ ), but where the values of  $\epsilon'_m$  and  $\epsilon''_m$  are still relatively unaffected by its proximity.

The equations derived in the previous section are strictly applicable for measurements made in the frequency- and time-domains, where  $\tau_o$  is a constant. Nevertheless, the quantity  $z = \omega\tau_o$  decreases as  $\tau_o$  decreases with an increase in the temperature, in a fixed frequency measurement.  $\omega\tau_o$  is related to the peak frequency,  $f_m$ , according to (Moynihan et al 1973, Lindsey and Patterson 1980, Mangion and Johari 1988):

$$\tau_o = \lambda / 2\pi f_m \quad (6.13)$$

with,

$$\lambda = z_m \exp(\log(z_m) \times \ln(10)) \quad (6.14)$$

where the value of  $\log(z_m)$  varies with  $\beta$  according to the data given in the table provided by Lindsey and Patterson (1980). Thus, if the parameter  $\beta$  is assumed to remain relatively constant with a change in temperature,  $\lambda$  would remain constant, and, since  $f_m$  has been found to vary with temperature according to an Arrhenius relationship in eqn (5.1), the value of  $\tau_o$  would vary with temperature according to:

$$\tau_o(T) = \tau = \tau_o \exp(E/RT) \quad (6.15)$$

where  $\tau_o = \lambda / 2\pi f_o$  and  $f_o$  is the pre-exponential factor in eqn. (5.1).

The  $\epsilon_o$  of most amorphous polymers changes with temperature by only as much as the optical refractive index and infrared absorptivity change, as has been reviewed by McCGrum et al

(1967), and since these changes are negligibly small,  $\epsilon_0$  may be assumed to remain constant over the temperature range of the sub- $T_g$  relaxation process. We further assume that the change in  $\Delta\epsilon$  over the corresponding temperature range has negligible effects on our calculations. This assumption is admittedly poor, but within the attainable accuracy from such data it is useful here. Eqn (6.15) can then be combined with eqn (6.8) to obtain the temperature dependence of  $\epsilon^*$  for a fixed measurement frequency,  $\omega_0$ . Angell and coworkers (Hodge and Angell 1978, Liu et al 1986, Liu and Angell 1986) implicitly made the same assumptions when they plotted the dielectric loss tangent data measured for a fixed frequency against the reciprocal temperature. They then converted the value of the half-width of the peak thus obtained into a value of the parameter  $\beta$  also according to a table given by Moynihan et al (1973). We recognize that this conversion is possible only when an accurate value of the activation energy in eqn (6.15) is known or if there exist isothermal data, obtained on the same material for various frequencies, which can serve as a calibrating curve (as in Angell's work). Angell and coworker's method for the evaluation of the  $\beta$  parameter is obviously less useful in our studies for two reasons: namely, (1) the two sub- $T_g$  relaxation peaks are too close to each other to enable us to determine accurately, their half-widths, even when plots are made in a reciprocal temperature plane, and (2), accurate values of the activation energy for the  $\gamma$ ,  $\beta$  and  $\alpha$  processes in our studies are unknown. Therefore, the formalism developed in

the following is more suitable for our data measured for a fixed frequency with changing temperature.

Dividing eqn (6.12) by eqn (6.11) gives

$$\epsilon_m'' / (\epsilon_m' - \epsilon_\infty) = N_m'' / N_m' \quad (6.16)$$

or equivalently,

$$\epsilon_m'' / (\epsilon_0 - \epsilon_m') = N_m'' / (1 - N_m') \quad (6.17)$$

The numerical values of the ratios on the right hand side of eqns (6.16) and (6.17), have been listed in Table 6.2, for the various values of the  $\beta$  parameter ranging from 0.1 to 0.6. Thus, the magnitude of the experimentally determined value of  $\epsilon_m'' / (\epsilon_m' - \epsilon_\infty)$ , or  $\epsilon_m'' / (\epsilon_0 - \epsilon_m')$ , becomes an approximate but reliable measure of the distribution of relaxation times parameter,  $\beta$ , for a relaxation process.

#### 6.4.3 DATA ANALYSIS

We now use the above-given procedure to analyze the distribution of relaxation times for the sub- $T_g$  relaxations. The value of the low-frequency (or high-temperature) limiting dielectric permittivity,  $\epsilon_\infty$ , of the low temperature, or  $\gamma$ -, process of the thermosets cannot be obtained experimentally, mainly because, as seen in Figures 5.7 to 5.11, the contributions from the  $\beta$ -relaxation process become significant on the high temperature side of the  $\gamma$ -relaxation peak. Nevertheless, its high-frequency (or low-temperature) limiting dielectric permittivity,  $\epsilon_0$ , can be measured and this value was taken as the value of  $\epsilon'$  at 90K. The values of  $(\epsilon_m' - \epsilon_\infty)$  for the  $\gamma$ -relaxation process of various thermosets were thus measured

from the plots in Figures 5.7 to 5.11 and these values are given in Tables 5.1 to 5.4.

Turning now to an analysis for the  $\beta$ -relaxation process, Figures 5.7 to 5.11 show that neither its  $\epsilon_0$  nor  $\epsilon_\infty$  value can be readily determined from our measurements. This is so because the  $\alpha$ -relaxation process at higher temperatures and the  $\gamma$ -relaxation process at lower temperatures contribute to  $\epsilon^*$  for the  $\beta$ -relaxation process. Therefore, the value of  $\epsilon_0$  for the  $\beta$  relaxation process was taken as equal to the value of  $\epsilon'$  at a temperature where  $\epsilon''$  reached a minimum value between the  $\beta$  and  $\alpha$ -relaxation peak. We realize that this is a poor approximation particularly for the early period during the cure, i.e. when the temperatures of the  $\beta$ - and  $\alpha$ -relaxation processes are close to each other, and that its validity becomes increasingly more justified when substantial curing has occurred and the two relaxation processes become progressively separated. Nevertheless, it is deemed here as a reliable procedure particularly within the limits of long curing time and therefore has been used for our analysis. The value of  $(\epsilon_0 - \epsilon_m')$  for the  $\beta$ -relaxation process thus determined from the data in Figures 5.7 to 5.11 are also listed in Tables 5.1 to 5.4.

In order to demonstrate the validity of the above method for analyzing the sub- $T_g$   $\epsilon^*$  data measured for a fixed frequency of 1 kHz, the  $\epsilon'$  and  $\epsilon''$  values for the DGEBA-DDS thermoset measured after an AECT of 15ks at 398K, which were shown as plot number 6 in Figure 5.11, were fitted to the following

equations:

$$\epsilon'(T) = \epsilon_{\infty} + \Delta\epsilon_{\gamma}N'_{\gamma}(\omega_0\tau_{\gamma}) + \Delta\epsilon_{\beta}N'_{\beta}(\omega_0\tau_{\beta}) \quad (6.18)$$

$$\epsilon''(T) = \Delta\epsilon_{\gamma}N''_{\gamma}(\omega_0\tau_{\gamma}) + \Delta\epsilon_{\beta}N''_{\beta}(\omega_0\tau_{\beta}), \quad (6.19)$$

where  $\tau_{\gamma}$  and  $\tau_{\beta}$  vary with temperature according to the general eqn (6.15). The values of  $E$  and  $\tau_0$  needed to fit the data are 28.5 and 102kJ/mole, and  $3.8 \times 10^{-15}$ s and  $2.0 \times 10^{-26}$ s, respectively, for  $\gamma$  and  $\beta$  relaxation processes, respectively. Also, the  $\beta$  and  $\Delta\epsilon$  values used are 0.17 and 0.14, and 0.31 and 0.364, respectively, for the  $\gamma$  and  $\beta$ -relaxation processes, respectively, and  $\epsilon_{\infty} = 2.27$ . The measured and calculated  $\epsilon'$  and  $\epsilon''$  data are plotted against temperature in Figure 6.8. We realize that the value of 102kJ/mole used in our calculation is higher than that, generally reported for the  $\beta$ -relaxation processes in other polymers and is 20% higher than the value of 80.3kJ/mole determined from the temperature dependence of the DGEBA-DDM  $\beta$ -peak's frequency as described in Section 5.1.2. Nevertheless, the fit of the experimental data to our calculation as seen in Figure 6.8 is reasonable enough to show that the  $\epsilon'$  and  $\epsilon''$  values can be adequately described by the non-exponential relaxation function formalism and that the method developed here for such an analysis is satisfactory.

The above given analysis is obviously unnecessary for the  $\alpha$ -relaxation process because its half-width is much lower, and the sensitivity of its relaxation rate to temperature much greater, than that of the sub- $T_g$  relaxations. Therefore, for the  $\alpha$ -relaxation, both the  $\epsilon_0$  and  $\epsilon_{\infty}$  can be unambiguously determined from Figures 5.8, 5.10 and 5.12 and these values are

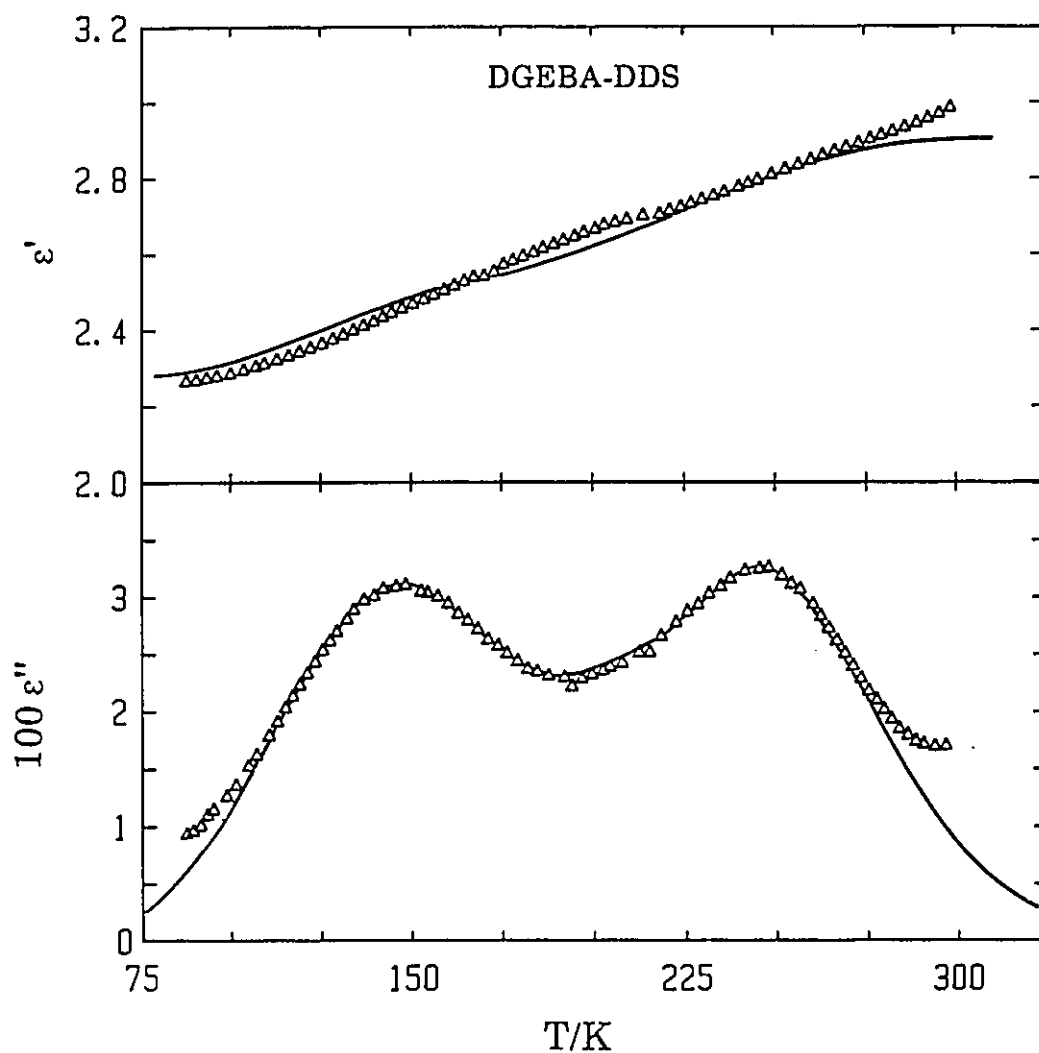


**Figure 6.8:** Fitting of a non-exponential decay function to the  $\gamma$ - and  $\beta$ -relaxation peaks of plot 6 in Figures 5.10 and 5.11 corresponding to the DGEBA-DDS thermoset cured 15ks (AECT) at 398K.

listed in Tables 5.1 to 5.3 for further discussion in the next section. The ratio  $\epsilon''_m/(\epsilon'_o - \epsilon'_o)$  which is equal to  $N''_m$  according to eqn (6.12) can therefore be directly obtained and in turn used for determining the value of  $\beta$  reasonably accurately without data fitting of the type used for sub- $T_g$  relaxations.

#### 6.4.4 RESULTS AND DISCUSSION

As just mentioned, both  $\epsilon''_m$  and  $\Delta\epsilon$  for the  $\alpha$ -relaxation process could be measured, and the plot of  $(\epsilon''_m/\Delta\epsilon)$  against AECT is shown in Figure 6.9 for both the DGEBA-DDM and DGEBA-DDS thermosets and in Figure 6.10 for the DGEBA-(0.7 DDS, 0.3 DDM) thermoset. The ratio  $\epsilon''_m/\Delta\epsilon$  decreases from the initial values of 0.28, 0.31 and 0.32 towards an asymptotic value of 0.20, 0.21 and 0.22 as the curing of DGEBA mixed with DDM, (0.7 DDS, 0.3 DDM), and DDS, respectively, proceeds. From Table 6.2 and eqn (6.12), these values correspond to a decrease in the parameter  $\beta$  from an initial value of 0.51, 0.57 and 0.59, respectively, to an asymptotic value of 0.36, 0.38 and 0.40, respectively.

The decrease of the parameter  $\beta$  for the  $\alpha$ -relaxation process, which is observed early in the cure of all the three thermosets, is a characteristic behaviour of the network-forming polymers as the number of cross-links in them increases. The value of  $\beta$  seems to reach a limiting value, for example when the AECT becomes greater than 10ks during the cure of DGEBA-(0.7 DDS, 0.3 DDM) thermoset at 363K. In the isothermal curing experiment of the same thermoset at a 14K

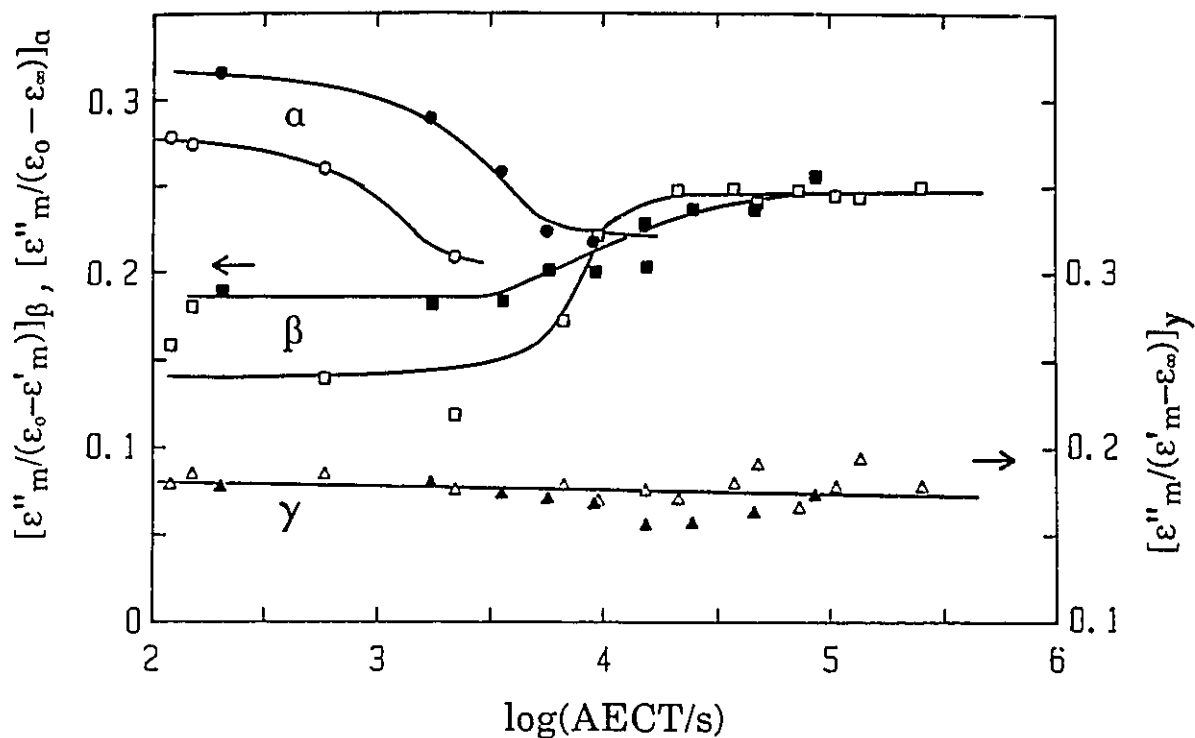


**Figure 6.9:** The  $(\epsilon''_m / (\epsilon'_m - \epsilon_\infty))$  or  $(\epsilon''_m / (\epsilon_0 - \epsilon'_m))$  ratios for the sub- $T_g$  relaxations and the  $\epsilon''_m / \epsilon'_m$  ratio for the  $\alpha$ -relaxation process in the DGEBA-DDM (open symbols) and DGEBA-DDS (solid symbol) thermosets plotted against the accumulated equivalent curing time.  $\Delta$  is for the  $\gamma$ -process,  $\square$  for the  $\beta$ -process and  $\circ$  for the  $\alpha$ -process.

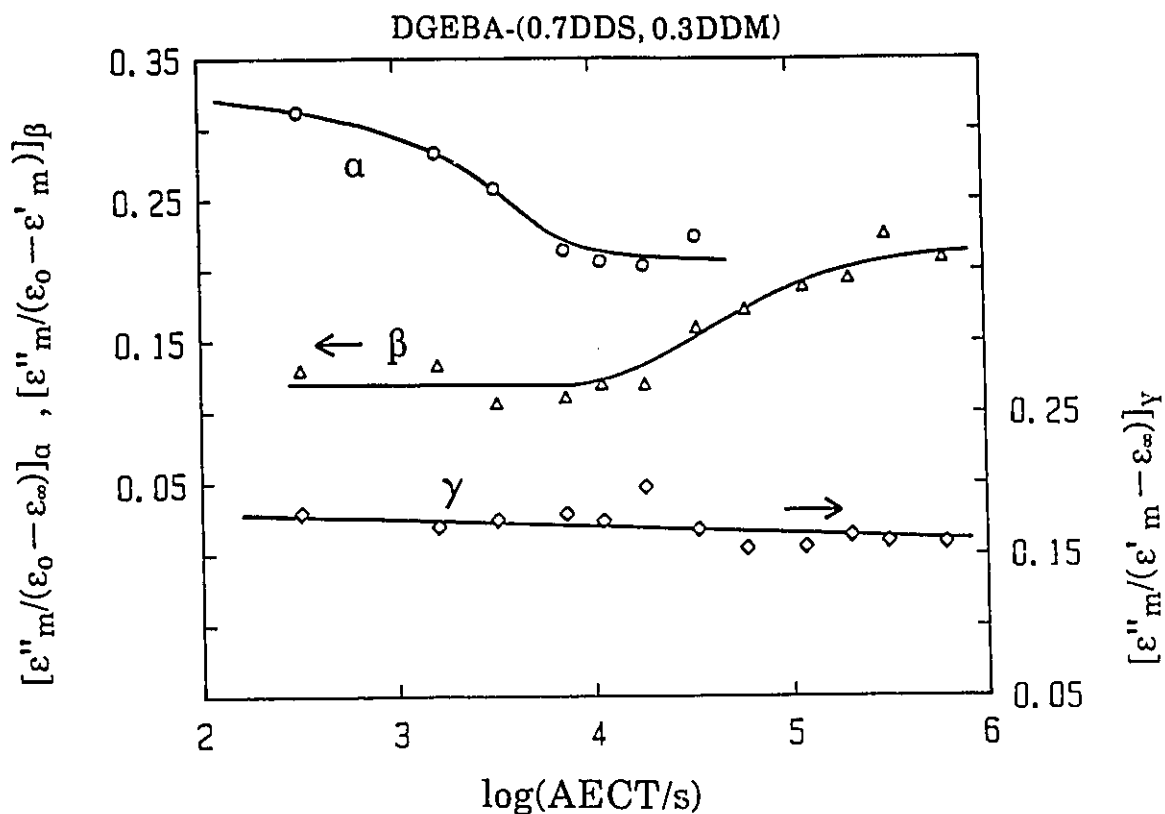


**Figure 6.10:** The values of  $\epsilon''_m / (\epsilon'_m - \epsilon_\omega)$  for the  $\gamma$ -,  $\epsilon''_m / (\epsilon_0 - \epsilon'_m)$  for the  $\beta$ - and  $\epsilon''_m / (\epsilon'_m - \epsilon_\omega)$  for the  $\alpha$ -relaxation processes plotted against time for the curing of the DGEBA-(0.7DDS,0.3DDM) thermoset.  $\diamond$  is for the  $\gamma$ -process,  $\Delta$  for the  $\beta$ -process and  $\circ$  for the  $\alpha$ -process.

higher temperature of 377K in Figures 3.18 and 3.24, this limiting value of  $\beta$  is expected to be reached in less than 10ks. Since the minimum in  $\epsilon''$  during the isothermal cure has occurred at 20ks, as seen in Figure 3.18, the  $\beta$ -value for the relaxation has reached its limiting value before the dielectric relaxation peak appears. This justifies further our assumption of a constant value of  $\beta$  we have used in the formalism for the curing parameter  $\gamma$ , in Section 4.1. The limiting values of  $\beta$  of 0.38 and 0.40 for the DGEBA-(0.7 DDS, 0.3 DDM) and DGEBA-DDS thermoset, respectively, derived from Figure 6.10 are also intriguingly similar to the values of 0.38 and 0.38 of the parameter  $\gamma$  which were independently obtained from the data analyzed in Chapter 4 and listed in Table 4.3, thereby providing support for the concept and the analysis developed in this work.

The ratio  $\epsilon''_m/(\epsilon'_m - \epsilon'_\infty)$  measured for the  $\gamma$ -process is also plotted in Figures 6.9 and 6.10. Its value is seen to decrease from 0.18 to 0.16 for all the three thermosets, which, from eqn (6.16) and table 6.2, corresponds to a decrease in the  $\beta$  parameter from 0.20 to 0.18. The ratio  $\epsilon''_m/(\epsilon'_0 - \epsilon'_m)$  measured for the  $\beta$ -process is also plotted in Figures 6.9 and 6.10. Its value increases towards a limiting value of 0.245 for both DGEBA-DDM and DGEBA-DDS thermosets and 0.215 for the DGEBA-(0.7 DDS, 0.3 DDM) thermoset. The anomalous increase in the value of  $\epsilon''_m/(\epsilon'_0 - \epsilon'_m)$  early in the cure may be explained as follows. For short AECT as seen in Figures 5.7, 5.11 and 5.13, the  $\beta$  and  $\gamma$  peaks are in close proximity, and the height of the  $\gamma$ -

relaxation is much greater than that of the  $\beta$ -relaxation process. The proximity of the two relaxation processes, while not affecting the  $\epsilon'_{m,\gamma}$  value, does affect the value of  $\epsilon'_{m,\beta}$ , which causes inaccuracies in the determination of the  $\epsilon''_m/(\epsilon'_0 - \epsilon'_m)$  ratio for the  $\beta$  process early in the cure. Thus, only later in the cure, when the  $\beta$  and  $\gamma$  peaks become sufficiently separated, this ratio can be determined with sufficient accuracy. Therefore, this ratio of  $\epsilon''_m/(\epsilon'_0 - \epsilon'_m)$  is less meaningful early in the cure but becomes useful later in the cure, although their values during the entire period of cure have been included in Figures 6.9 and 6.10 for the sake of completion. From this ratio only the final values of  $\beta$  can be obtained by using eqn (6.17) and Table 6.2. These values are 0.16 for both DGEBA-DDM and DGEBA-DDS thermosets and 0.14 for DGEBA-(0.7 DDS, 0.3 DDM) thermoset.

## 6.5 MECHANISMS OF DIELECTRIC RELAXATIONS IN THERMOSETS

### 6.5.1 THE MAIN OR $\alpha$ -RELAXATION

We now review some of the important observations of this Chapter as follows. The height of the  $\epsilon''$  peak for the  $\alpha$ -process seen in Figures 6.3 and 6.4, or equivalently  $(\epsilon'_0 - \epsilon'_\infty)$  given in Tables 5.1 to 5.3, rapidly decreases as curing occurs and approaches a limiting value later during the cure. The initial decrease is probably caused mainly by a decrease in the dipole moment per unit monomer, as is known to occur during the chain-growth for most polymeric substances. It may also be partly caused by the effective removal of free dipolar, end

groups of the reactants i.e.  $\text{-NH}_2$ ,  $\text{-NH}$ , epoxy, during the curing process. The approach of  $\epsilon''_m$  to a constant value later in the cure indicates that, once the network is formed at the gel point, a further increase in the density of cross-links does not significantly affect the micro Brownian motions of chain segments that show up as the primary relaxation.

Figures 6.1 and 6.2 show that the separation between the  $\beta$  and  $\alpha$  peaks increase with both the growth of polymer chain and increase in the number of crosslinks. A similar increase in the separation of  $\beta$  and  $\alpha$  peaks has also been observed with an increase in the molecular weight or chain length of poly(propylene oxide), which has neither a side chain nor a side group (Pathmanathan and Johari 1988). These observations imply that the rate of the  $\beta$  relaxation is less affected by the growth of a polymer chain or of a polymer network than is the rate of the  $\alpha$  relaxation.

Finally, both the initial and limiting values of  $\epsilon''_m$  are much higher for the DGEBA-DDS thermoset than for the DGEBA-DDM thermoset. This indicates that the DDS molecule has a larger dipole moment than the DDM molecule.

#### 6.5.2 THE $\beta$ -RELAXATION

Figures 6.3, 6.4, 6.7 and 6.8 show that the strength of the  $\beta$ -relaxation process in the thermosets studied here increases by a factor of about 5 to 10 during the curing process. Since curing produces  $\text{-OH}$  groups which undergo relatively less hindered reorientation, and  $\text{C-N-C}$  linkages

which are not entirely rigid, the  $\beta$ -relaxation appears at first sight, to be assignable to the local motion of these dipolar groups. This interpretation is in accord with the previous suggestions made by Keenan et al (1979) and Ochi et al (1982) which have been already reviewed in Section 1.4.3. Nevertheless, our further considerations given as follows, show that the occurrence of the  $\beta$ -relaxation is not entirely attributable to these group motions. First, we find that the strength of the  $\beta$ -relaxation process, or equivalently the height of its peak, which according to the interpretation above is expected to only depend on the extent of the reaction and to remain invariant with respect to one's choice of diamine as a curing agent, instead, depends as seen in Figures 6.3, 6.4 and 6.6, on the choice of the curing agent and the size of the reacted diamine molecule. Second, further studies of the effects of curing on the strength of the  $\beta$ -relaxation in the DGEBA-DDM thermoset by Sidebottom and Johari (submitted) show that the increase in the height of the  $\beta$  relaxation peak theoretically calculated on the basis of an increase in the -OH groups by using the Onsager (1936) and Kirkwood (1939) equations is three times higher than the observed increase. Both observations suggest that the motion of these groups alone is insufficient as an explanation for the  $\beta$ -process.

We believe that, there is merit in considering these effects in general physical terms without assigning a particular mode of group or molecular motion for each process. Intuitively speaking, the probability of efficient packing in

a thermoset is expected to progressively diminish as the reaction becomes diffusion-controlled and as the internal viscosity of the gel increases with an increase in the chain length and the cross-link density. This would allow the occurrence of regions with a greater variance of packing density thereby producing a larger number of defect sites (Cavaillé, Perez and Johari 1989) which contain particular dipolar side groups or chain segments. The observed increase in the strength of the  $\beta$ -peak may in this interpretation be partly associated with an increase in chain length during the curing, which decreases the efficiency of packing and would depend upon the steric hindrance for the rotation of the main chain segment, and through this steric hindrance on the type and size of the crosslinking amine.

We now discuss the effect of the curing amine on the strength of the  $\beta$ -relaxation process. Figures 6.3, 6.4 and 6.6 show that the strength of the  $\beta$ -process in the DGEBA-DDM thermoset is significantly larger than that in the DGEBA-DDS thermoset. This would seem to be in contradiction with our previous suggestion for the main relaxation that the DDS molecule has a higher dipole moment than the DDM molecule and therefore for the same angular motion contributes more to the primary relaxation. But since the sub- $T_g$  relaxations are caused by the motions in local regions of the otherwise rigid molecular structure, it is probable that the motion of the dipolar segment of the diamine that contributes to the  $\beta$ -relaxation is more restricted in the reacted states of the DDS,

than in that of the DDM. This may rationalize the observation of a lower height of the  $\beta$ -relaxation in the DGEBA-DDS thermoset than in the DGEBA-DDM thermoset.

The change in the temperature of the  $\beta$ -relaxation process in a fixed frequency measurement indicates a change in the relaxation rate of the dipoles involved. An increase of this temperature indicates a slowing of the rate and vice-versa. Figures 6.1, 6.2 and 6.7 show that this temperature increases towards a limiting value,  $T_m(\infty)$ , with an increase in AECT. Additionally, when, in particular, the DGEBA-DDM thermoset is post-cured at a higher curing temperature and thereby the extent of the cross-linking reaction is increased,  $T_m$  increases further towards a yet higher value of  $T_m(\infty)$  of 265K. The effect of the extent of reaction on  $T_m(\infty)$  can be clearly seen in the corresponding results for the starved and saturated thermosets. Figure 6.7(a) shows that the  $T_m(\infty)$  value corresponding to the starved DGEBA-DDM thermoset is about 13K lower than that for the stoichiometric sample and 15K lower than that for the saturated sample. Therefore, these combined observations lead us to conclude that the relaxation rate for the  $\beta$ -process decreases as curing proceeds. There is therefore, a resemblance between the dependence of the rate of the  $\beta$  and  $\alpha$  processes on the extent of reaction.

It is now instructive to investigate the effect of the curing amine on the relaxation rate of the  $\beta$ -process. The  $T_m(\infty)$  value of DGEBA-DDM thermoset is 5K higher than that of DGEBA-DDS thermoset as seen in Figure 6.1. Again, it means

that the relaxation rate in the DGEBA-DDM thermoset is lower than in the DGEBA-DDS thermoset. In order to rationalize this observation, we recall that the DGEBA-DDM molecule is more flexible than the DGEBA-DDS molecule and further, that the former is smaller than the latter. One expects therefore that the DGEBA-DDS cross-links are associated with relatively large free volume which allows greater spatial freedom for the local motion of the dipolar segments.

### 6.5.3 THE $\gamma$ -RELAXATION

The strength of the  $\gamma$ -relaxation is seen in figures 6.3, 6.4 and 6.7 to decrease by a factor of about 5 approaching a limiting value, during the curing of the thermosets. On post-curing, it decreases further towards a lower limiting value as also seen in Figure 6.3. Correspondingly, the ultimate value of  $\epsilon''_{m,\gamma}$  of the starved DGEBA-DDM thermoset is 50% higher than that of the saturated sample which is expected to have been more fully reacted. Hence, the  $\gamma$ -peak would be more appropriately attributed to the local motions of those dipoles that are a part of the unreacted components during the curing of thermosets. These dipoles may be parts of the DGEBA polymer chain including the unreacted epoxy groups, or free amino-diphenyls, an explanation which is consistent with the previously proposed attribution by Ochi et al (1982) of the mechanically observed  $\gamma$ -process to the local motion of polymer segments consisting of at least four carbon atoms.

The initial value of the  $\gamma$ -peak height is higher for the DGEBA-DDS thermoset than for the DGEBA-DDM thermoset. This observation is also consistent with our previous finding in Section 6.5.1 that the free DDS molecule has a larger dipole moment than the DDM molecule.

#### 6.5.4 PHYSICAL AGEING EFFECTS

As discussed in Sections 6.5.2 and 6.5.3, the decrease in the height of the  $\gamma$ -peak and the initial increase in that of the  $\beta$ -peak is a reflection of further curing in the two thermosets, which controls the change in the measured  $\epsilon''_m$  of the sub- $T_g$  relaxation. Physical ageing or structural relaxation decreases  $\epsilon''_m$  and, near the maximum value of  $\epsilon''_m(\beta)$  in Figures 6.3, 6.4 6.7 and 6.8, the two effects cancel each other. For still longer times of cure, the physical ageing effect dominates, and the decrease in the strength of the  $\gamma$ - and  $\beta$ -relaxations in the thermosets studied at long AECT values becomes qualitatively similar to the decrease seen during ageing of thermoplastics. It is important to note that in contrast with thermoplastics, where physical ageing effects are observable only over a limited range of temperatures below  $T_g$ , in thermosets, the physical ageing effects are observable over a wide range of temperatures between  $T_{g0}$  and  $T_{g\infty}$ , because the  $T_g$  of a thermoset is lower, the lower the temperature of its cure.

## CHAPTER 7

### CONCLUSIONS

Two aspects of the behaviour of the dielectric and Brillouin scattering properties of thermosets during their cure have been studied. In the first aspect, the curing kinetics of the thermosets have been measured by dielectric spectroscopy and Brillouin scattering measurements. The results showed that the dielectric properties are mainly determined by two effects, namely: (1) a large decrease in the dc conduction at the beginning of the cure and (2) the dipolar relaxation process later in the cure.

The complex plane plot of the electrical modulus correspondingly has the shape of two arcs. The short time arc characterizes a conductivity relaxation phenomenon and was fitted to a semi-circle. Therefore, the dc conduction process in liquid thermosets follows a single or Maxwell's relaxation time formalism. The value of the dc conductivity was determined from dielectric loss data and its decrease with the curing time was fitted to the power law used in the description of critical phenomena. The dc conductivity formally approaches zero at the gelation of the thermoset. An empirical equation based on an exponential decrease of conductivity with curing time towards a singularity also fits the dc conductivity data. This may account for the decrease in the conductivity observed at temperatures at which vitrification occurs prior to gelation during the curing, and where the decrease in the

mobility of ions is due to the increase in viscosity leading to vitrification.

As the curing approaches completion the complex plane plots of the dielectric permittivity acquire the shape of an arc which is skewed at both the limiting short and long-time intercepts. The evolution of the dielectric features of thermosets during their curing is thus phenomenologically similar to the evolution of the dielectric features of physically and chemically stable dipolar liquids and solids with increasing frequency of measurements at constant temperature or decreasing temperature at a constant frequency. This is a consequence of the invariance of the dielectric equations with respect to either the frequency or the relaxation time and demonstrates that the cross-linking of thermosets causes the relaxation time to monotonically increase.

The shape of the Cole-Cole plots of dielectric permittivity was fitted to a stretched exponential functional form,  $\phi(t) = \exp-(t/\tau_{\text{cure}})^\gamma$ , with the values of  $\gamma$  between 0.2 and 0.4. This equation implies that the isothermal spectra of dielectric permittivity at any instant of cure is given by  $(\epsilon^* - \epsilon_\infty) / (\epsilon_0 - \epsilon_\infty) \hat{=} (-d\phi/dt)$  where  $\phi(t) = \exp-(t/\tau)^\beta$ , where  $\beta$  is the Kohlrausch-Williams-Watts parameter in chemically stable phases and  $\hat{=}$  represents a one sided Laplace transform. The value of  $\gamma$  remains constant over the time range during which the dipolar relaxation process is observed. Its values monotonically decreases with increasing temperature of the cure and tends

towards a limiting value characteristic of a thermoset at higher temperatures. Thus, the temperature dependences of  $\gamma$  and  $\beta$  are found to show opposite trends. We propose that  $\gamma$  be regarded as a curing parameter for the vitrification of a thermoset precursor.

The complex dielectric permittivity which was measured during the curing process was in turn used to calculate the dependence of the dipolar relaxation time on the curing time of the thermoset. The logarithmic plots showing this dependence have the shape of an elongated S. The time of cure at which the relaxation rate reaches a fixed value is directly proportional to the exponential of the reciprocal of the curing temperature with parameters that are characteristic of the curing kinetics of a thermoset.

The non-monotonic trend observed in the various features of the dielectric properties of DGEBA-based thermosets cured with mixed amines, with one amine being replaced by the other, is caused by the large difference in the kinetics of the cross-linking reactions of DGEBA with each pure amine.

Brillouin light scattering studies have in addition shown that the initially broad Brillouin peak becomes narrow as cross-linking occurs and is shifted towards higher frequencies. Correspondingly, the hypersonic velocity increases and its attenuation decreases with curing. Both the velocity of sound and its attenuation show a stepwise change during the process of cross-linking. This stepwise change occurs at the time of gelation and is inversely related to the curing temperature.

The time required to reach physically identical states in Brillouin scattering at different temperatures follows an Arrhenius equation with values of the activation energy which are comparable to the corresponding values obtained from dielectric measurements. The changes observed in both Brillouin and dielectric properties are a reflection of the physical properties determined by the rates of chemical reactions. These physical properties in turn determine the rates of chemical reactions which in turn determine the physical properties and so on, until the reaction formally reaches completion.

In the second aspect, the sub- $T_g$  and main relaxation processes of the thermosets were measured by dielectric spectrometry and their dependence on the curing time was investigated. Amongst the two sub- $T_g$  relaxation processes, the low temperature, or  $\gamma$ , process is initially prominent and its strength decreases towards a limiting value on curing. The strength of the high temperature, or  $\beta$ , process initially increases, reaches a maximum value and then decreases on further curing. The mechanisms for the  $\gamma$  relaxation process involve motions of dipolar entities that are consumed during the curing reaction but, those for the  $\beta$ -relaxation process involve motions of dipolar entities that are formed.

Ageing of thermosets affects their dielectric behaviour for different reasons. The predominant amongst them is the chemical reactions at the early period of cure. This causes the strength of the  $\beta$ -relaxation to increase and its rate to

decrease. At long curing times, structural relaxation becomes predominant and, consequently, the strength of the  $\beta$ -relaxation decreases, as is generally observed for thermoplastics and other amorphous solids.

A concept of accumulated equivalent curing time is introduced and shown to be more useful than the isothermal curing time itself for the investigation of the cure of a thermoset. It is theoretically justified on the basis of their chemical kinetics. A procedure for obtaining the distribution of relaxation times, or the Kohlrausch-Williams-Watts or KWW parameter, from limited dielectric data is developed. The procedure leads to the finding that, while the KWW parameter for the sub- $T_g$  relaxation process remains constant during the curing, post-curing and physical ageing of thermosets, that for the main or primary relaxation process monotonically decreases and reaches a limiting value before vitrification occurs.

## APPENDIX

### METHODOLOGY FOR OBTAINING THE THEORETICAL $N^*$ VARIATION

The Laplace transform term on the right side of eqn (1.12) which was used for calculating the normalized complex permittivity,  $N^*$ , may be expressed in terms of stable law distribution used in the probability theories (Levy 1937, Fella 1966), as:

$$N' = 1 - \pi z V_\beta(z) = (\epsilon'(z) - \epsilon_\infty) / (\epsilon_0 - \epsilon_\infty) \quad (\text{A.1})$$

$$N'' = \pi z Q_\beta(z) = \epsilon''(z) / (\epsilon_0 - \epsilon_\infty) \quad (\text{A.2})$$

where  $z = \omega\tau$ ,  $\beta$  is the exponent in the expression for the stretched exponential of eqn (1.19), and  $V_\beta(z)$  and  $Q_\beta(z)$  are stable distribution functions:

$$V_\beta(z) = (1/\pi) \int_0^\infty \exp(-u^\beta) \sin(zu) du \quad (\text{A.3})$$

$$Q_\beta(z) = (1/\pi) \int_0^\infty \exp(-u^\beta) \cos(zu) du \quad (\text{A.4})$$

Tables of the numerical values of  $V_\beta(z)$  and  $Q_\beta(z)$  are given by Dishon et al (1985) for  $z$  values in the range 0.001 to 2500 and  $\beta$  values from 0.01 to 2.0. Using these values, and eqns (A.1) and (A.2),  $N^*$  was evaluated for  $\log(z)$  values from -3.0 to 3.2, and  $\beta$  between 0 and 1. This covers almost the full range of possible value for the KWW parameter  $\beta$  ( $0 < \beta \leq 1$ ), and most of the experimental range of the  $\log z$  values. The values of  $V_\beta(z)$  and  $Q_\beta(z)$ , corresponding to  $\beta$ , or  $\log z$  values, which were not available in the tables of Dishon et al (1985) were approximated by a linear interpolation procedure.

In our fitting of the isochronal dielectric permittivity data over a wide range of temperatures shown in Figure 6.8 of Section 6.4.3, a much larger range of  $\log z$  values is required,

particularly where  $\beta \leq 0.40$  and  $N'$  and  $N''$  have not yet reached their asymptotic behaviour at the limiting  $\log z$  values of  $-3.0$  and  $3.2$ . For  $\beta \leq 0.25$ , Montroll and Bendler (1984) showed that  $Q_\beta(z)$  could be accurately calculated using an analytical expression given in eqn (37) of their paper for  $z$  values  $\geq 0.1$ . The expression was found to be accurate within 1% for  $\log z$  ranging from  $-3.0$  to  $3.2$  and was used to extend our table of  $N''$  for  $\log z$  ranging from  $-8$  to  $16$ . The extension of the  $N'$  tables was less crucial, since the tabulated  $N'$  variation already covered more than 70% of its total change for  $\beta = 0.15$ . Hence, a linear extrapolation procedure gave us a satisfactory approximation of the  $N'$  variation outside the tabulated range, and its plausibility is evident in Figure 6.8. The table of  $N^*$  thus obtained is given in the following pages.

The values of  $1-N'$  and  $N''$  are given as a function of  $\log(z=\omega\tau)$  for  $\beta$  values between 0.10 and 0.25.

| $\log(z) \backslash \beta$ | $1-N'$ |       |       |       | $N''$ |       |       |       |
|----------------------------|--------|-------|-------|-------|-------|-------|-------|-------|
|                            | 0.25   | 0.20  | 0.15  | 0.10  | 0.25  | 0.20  | 0.15  | 0.10  |
| -8.0                       | 0.005  | 0.028 | 0.083 | 0.148 | 0.018 | 0.000 | 0.000 | 0.001 |
| -7.8                       | 0.005  | 0.028 | 0.083 | 0.148 | 0.018 | 0.000 | 0.000 | 0.001 |
| -7.6                       | 0.005  | 0.028 | 0.083 | 0.148 | 0.018 | 0.000 | 0.000 | 0.001 |
| -7.4                       | 0.005  | 0.028 | 0.083 | 0.148 | 0.018 | 0.000 | 0.000 | 0.001 |
| -7.2                       | 0.005  | 0.028 | 0.083 | 0.148 | 0.018 | 0.000 | 0.000 | 0.002 |
| -7.0                       | 0.005  | 0.028 | 0.083 | 0.148 | 0.018 | 0.000 | 0.000 | 0.002 |
| -6.8                       | 0.005  | 0.028 | 0.083 | 0.148 | 0.018 | 0.000 | 0.000 | 0.002 |
| -6.4                       | 0.005  | 0.028 | 0.083 | 0.148 | 0.018 | 0.000 | 0.001 | 0.003 |
| -6.2                       | 0.005  | 0.028 | 0.083 | 0.148 | 0.018 | 0.000 | 0.001 | 0.003 |
| -6.0                       | 0.005  | 0.028 | 0.083 | 0.148 | 0.018 | 0.000 | 0.001 | 0.004 |
| -5.8                       | 0.005  | 0.028 | 0.083 | 0.148 | 0.018 | 0.000 | 0.002 | 0.005 |
| -5.6                       | 0.005  | 0.028 | 0.083 | 0.148 | 0.018 | 0.000 | 0.002 | 0.006 |
| -5.4                       | 0.005  | 0.028 | 0.083 | 0.148 | 0.018 | 0.001 | 0.003 | 0.008 |
| -5.2                       | 0.005  | 0.028 | 0.083 | 0.148 | 0.018 | 0.001 | 0.005 | 0.010 |
| -5.0                       | 0.005  | 0.028 | 0.083 | 0.148 | 0.018 | 0.001 | 0.006 | 0.012 |
| -4.8                       | 0.005  | 0.028 | 0.083 | 0.148 | 0.018 | 0.002 | 0.008 | 0.014 |
| -4.6                       | 0.005  | 0.028 | 0.083 | 0.148 | 0.018 | 0.003 | 0.010 | 0.016 |
| -4.4                       | 0.005  | 0.028 | 0.083 | 0.148 | 0.018 | 0.004 | 0.013 | 0.019 |
| -4.2                       | 0.005  | 0.028 | 0.083 | 0.148 | 0.018 | 0.006 | 0.016 | 0.021 |
| -4.0                       | 0.005  | 0.028 | 0.083 | 0.148 | 0.018 | 0.008 | 0.019 | 0.024 |
| -3.8                       | 0.005  | 0.028 | 0.083 | 0.148 | 0.018 | 0.011 | 0.023 | 0.027 |
| -3.6                       | 0.005  | 0.028 | 0.083 | 0.148 | 0.018 | 0.015 | 0.027 | 0.030 |
| -3.4                       | 0.005  | 0.028 | 0.083 | 0.148 | 0.018 | 0.020 | 0.032 | 0.033 |
| -3.2                       | 0.005  | 0.028 | 0.083 | 0.148 | 0.018 | 0.026 | 0.036 | 0.036 |
| -3.0                       | 0.005  | 0.028 | 0.083 | 0.148 | 0.018 | 0.033 | 0.041 | 0.039 |
| -2.8                       | 0.010  | 0.040 | 0.096 | 0.163 | 0.023 | 0.040 | 0.045 | 0.042 |
| -2.6                       | 0.020  | 0.056 | 0.110 | 0.177 | 0.033 | 0.048 | 0.049 | 0.045 |
| -2.4                       | 0.031  | 0.074 | 0.125 | 0.192 | 0.042 | 0.056 | 0.053 | 0.048 |
| -2.2                       | 0.045  | 0.082 | 0.143 | 0.207 | 0.053 | 0.067 | 0.058 | 0.050 |
| -2.0                       | 0.065  | 0.102 | 0.162 | 0.223 | 0.065 | 0.073 | 0.063 | 0.052 |
| -1.8                       | 0.085  | 0.125 | 0.182 | 0.240 | 0.077 | 0.082 | 0.068 | 0.054 |
| -1.6                       | 0.110  | 0.151 | 0.203 | 0.255 | 0.090 | 0.089 | 0.072 | 0.055 |
| -1.4                       | 0.138  | 0.178 | 0.225 | 0.271 | 0.102 | 0.096 | 0.075 | 0.055 |
| -1.2                       | 0.171  | 0.208 | 0.248 | 0.288 | 0.113 | 0.101 | 0.079 | 0.056 |
| -1.0                       | 0.208  | 0.240 | 0.272 | 0.304 | 0.123 | 0.106 | 0.081 | 0.057 |
| -0.8                       | 0.248  | 0.274 | 0.298 | 0.323 | 0.132 | 0.110 | 0.084 | 0.057 |
| -0.6                       | 0.289  | 0.307 | 0.322 | 0.338 | 0.137 | 0.112 | 0.085 | 0.057 |
| -0.4                       | 0.332  | 0.341 | 0.348 | 0.355 | 0.140 | 0.114 | 0.086 | 0.058 |
| -0.2                       | 0.376  | 0.376 | 0.374 | 0.372 | 0.142 | 0.114 | 0.086 | 0.058 |

The values of  $1-N'$  and  $N''$  are given as a function of  $\log(z=wr)$  for  $\beta$  values between 0.10 and 0.25 (continued).

| $\log(z) \backslash \beta$ | $1-N'$ |       |       |       | $N''$ |       |       |       |
|----------------------------|--------|-------|-------|-------|-------|-------|-------|-------|
|                            | 0.25   | 0.20  | 0.15  | 0.10  | 0.25  | 0.20  | 0.15  | 0.10  |
| 0.0                        | 0.420  | 0.410 | 0.399 | 0.389 | 0.141 | 0.114 | 0.086 | 0.057 |
| 0.2                        | 0.464  | 0.446 | 0.427 | 0.408 | 0.139 | 0.113 | 0.085 | 0.057 |
| 0.4                        | 0.504  | 0.477 | 0.450 | 0.423 | 0.134 | 0.110 | 0.084 | 0.057 |
| 0.6                        | 0.544  | 0.510 | 0.475 | 0.440 | 0.129 | 0.107 | 0.082 | 0.057 |
| 0.8                        | 0.581  | 0.542 | 0.500 | 0.457 | 0.122 | 0.104 | 0.080 | 0.056 |
| 1.0                        | 0.617  | 0.572 | 0.522 | 0.473 | 0.116 | 0.100 | 0.078 | 0.056 |
| 1.2                        | 0.653  | 0.604 | 0.548 | 0.492 | 0.109 | 0.097 | 0.076 | 0.055 |
| 1.4                        | 0.681  | 0.629 | 0.567 | 0.505 | 0.101 | 0.092 | 0.073 | 0.054 |
| 1.6                        | 0.709  | 0.655 | 0.588 | 0.521 | 0.094 | 0.088 | 0.070 | 0.053 |
| 1.8                        | 0.736  | 0.681 | 0.609 | 0.537 | 0.087 | 0.083 | 0.068 | 0.052 |
| 2.0                        | 0.760  | 0.704 | 0.628 | 0.552 | 0.080 | 0.078 | 0.065 | 0.052 |
| 2.2                        | 0.786  | 0.730 | 0.650 | 0.570 | 0.074 | 0.074 | 0.063 | 0.051 |
| 2.4                        | 0.802  | 0.747 | 0.665 | 0.582 | 0.067 | 0.069 | 0.059 | 0.050 |
| 2.6                        | 0.821  | 0.767 | 0.681 | 0.596 | 0.062 | 0.065 | 0.057 | 0.049 |
| 2.8                        | 0.840  | 0.785 | 0.698 | 0.610 | 0.056 | 0.061 | 0.054 | 0.047 |
| 3.0                        | 0.853  | 0.802 | 0.713 | 0.624 | 0.051 | 0.057 | 0.051 | 0.046 |
| 3.2                        | 0.871  | 0.826 | 0.731 | 0.641 | 0.047 | 0.053 | 0.049 | 0.045 |
| 3.4                        | 0.888  | 0.843 | 0.752 | 0.660 | 0.043 | 0.049 | 0.047 | 0.044 |
| 3.6                        | 0.908  | 0.859 | 0.772 | 0.680 | 0.039 | 0.045 | 0.045 | 0.043 |
| 3.8                        | 0.923  | 0.874 | 0.789 | 0.700 | 0.035 | 0.042 | 0.043 | 0.042 |
| 4.0                        | 0.934  | 0.888 | 0.807 | 0.718 | 0.032 | 0.039 | 0.041 | 0.041 |
| 4.2                        | 0.943  | 0.901 | 0.823 | 0.733 | 0.029 | 0.036 | 0.039 | 0.040 |
| 4.4                        | 0.952  | 0.913 | 0.838 | 0.750 | 0.026 | 0.033 | 0.037 | 0.038 |
| 4.6                        | 0.959  | 0.921 | 0.848 | 0.767 | 0.023 | 0.031 | 0.035 | 0.037 |
| 4.8                        | 0.964  | 0.931 | 0.861 | 0.780 | 0.021 | 0.028 | 0.033 | 0.036 |
| 5.0                        | 0.969  | 0.940 | 0.874 | 0.795 | 0.019 | 0.026 | 0.031 | 0.035 |
| 5.2                        | 0.973  | 0.948 | 0.887 | 0.810 | 0.017 | 0.024 | 0.029 | 0.034 |
| 5.4                        | 0.977  | 0.955 | 0.899 | 0.824 | 0.015 | 0.022 | 0.027 | 0.033 |
| 5.6                        | 0.980  | 0.961 | 0.908 | 0.838 | 0.013 | 0.020 | 0.026 | 0.032 |
| 5.8                        | 0.983  | 0.966 | 0.916 | 0.852 | 0.012 | 0.018 | 0.024 | 0.031 |
| 6.0                        | 0.986  | 0.970 | 0.924 | 0.865 | 0.011 | 0.017 | 0.022 | 0.030 |
| 6.2                        | 0.988  | 0.974 | 0.935 | 0.877 | 0.010 | 0.016 | 0.021 | 0.028 |
| 6.4                        | 0.990  | 0.977 | 0.943 | 0.889 | 0.009 | 0.014 | 0.020 | 0.027 |
| 6.6                        | 0.992  | 0.980 | 0.950 | 0.900 | 0.008 | 0.013 | 0.018 | 0.026 |
| 6.8                        | 0.993  | 0.983 | 0.957 | 0.909 | 0.007 | 0.012 | 0.017 | 0.026 |
| 7.0                        | 0.994  | 0.986 | 0.962 | 0.918 | 0.006 | 0.011 | 0.016 | 0.025 |
| 7.2                        | 0.995  | 0.988 | 0.966 | 0.926 | 0.005 | 0.010 | 0.015 | 0.024 |
| 7.4                        | 0.995  | 0.990 | 0.970 | 0.934 | 0.005 | 0.009 | 0.014 | 0.023 |
| 7.6                        | 0.996  | 0.991 | 0.974 | 0.940 | 0.004 | 0.008 | 0.013 | 0.022 |
| 7.8                        | 0.996  | 0.992 | 0.977 | 0.946 | 0.004 | 0.008 | 0.012 | 0.021 |

The values of  $1-N'$  and  $N''$  are given as a function of  $\log(z=wr)$  for  $\beta$  values between 0.10 and 0.25 (continued).

| $\log(z) \backslash \beta$ | $1-N'$ |       |       |       | $N''$ |       |       |       |
|----------------------------|--------|-------|-------|-------|-------|-------|-------|-------|
|                            | 0.25   | 0.20  | 0.15  | 0.10  | 0.25  | 0.20  | 0.15  | 0.10  |
| 8.0                        | 0.997  | 0.993 | 0.980 | 0.952 | 0.003 | 0.007 | 0.011 | 0.020 |
| 8.2                        | 0.997  | 0.994 | 0.982 | 0.957 | 0.003 | 0.006 | 0.010 | 0.020 |
| 8.4                        | 0.997  | 0.994 | 0.984 | 0.961 | 0.003 | 0.006 | 0.009 | 0.019 |
| 8.6                        | 0.998  | 0.995 | 0.987 | 0.966 | 0.002 | 0.005 | 0.009 | 0.018 |
| 8.8                        | 0.998  | 0.995 | 0.989 | 0.970 | 0.002 | 0.005 | 0.008 | 0.017 |
| 9.0                        | 0.998  | 0.996 | 0.990 | 0.973 | 0.002 | 0.004 | 0.007 | 0.017 |
| 9.2                        | 0.998  | 0.996 | 0.990 | 0.973 | 0.002 | 0.004 | 0.007 | 0.016 |
| 9.4                        | 0.998  | 0.996 | 0.990 | 0.973 | 0.002 | 0.004 | 0.006 | 0.015 |
| 9.6                        | 0.998  | 0.996 | 0.990 | 0.973 | 0.002 | 0.003 | 0.006 | 0.015 |
| 9.8                        | 0.998  | 0.996 | 0.990 | 0.973 | 0.002 | 0.003 | 0.006 | 0.014 |
| 10.0                       | 0.998  | 0.996 | 0.990 | 0.973 | 0.002 | 0.003 | 0.005 | 0.014 |
| 10.2                       | 0.998  | 0.996 | 0.990 | 0.973 | 0.002 | 0.003 | 0.005 | 0.013 |
| 10.4                       | 0.998  | 0.996 | 0.990 | 0.973 | 0.002 | 0.002 | 0.005 | 0.012 |
| 10.6                       | 0.998  | 0.996 | 0.990 | 0.973 | 0.002 | 0.002 | 0.004 | 0.012 |
| 10.8                       | 0.998  | 0.996 | 0.990 | 0.973 | 0.002 | 0.002 | 0.004 | 0.011 |
| 11.0                       | 0.998  | 0.996 | 0.990 | 0.973 | 0.002 | 0.002 | 0.004 | 0.011 |
| 11.2                       | 0.998  | 0.996 | 0.990 | 0.973 | 0.002 | 0.002 | 0.003 | 0.011 |
| 11.4                       | 0.998  | 0.996 | 0.990 | 0.973 | 0.002 | 0.001 | 0.003 | 0.010 |
| 11.6                       | 0.998  | 0.996 | 0.990 | 0.973 | 0.002 | 0.001 | 0.003 | 0.010 |
| 11.8                       | 0.998  | 0.996 | 0.990 | 0.973 | 0.002 | 0.001 | 0.003 | 0.009 |
| 12.0                       | 0.998  | 0.996 | 0.990 | 0.973 | 0.002 | 0.001 | 0.003 | 0.009 |
| 12.2                       | 0.998  | 0.996 | 0.990 | 0.973 | 0.002 | 0.001 | 0.002 | 0.009 |
| 12.4                       | 0.998  | 0.996 | 0.990 | 0.973 | 0.002 | 0.001 | 0.002 | 0.008 |
| 12.6                       | 0.998  | 0.996 | 0.990 | 0.973 | 0.002 | 0.001 | 0.002 | 0.008 |
| 12.8                       | 0.998  | 0.996 | 0.990 | 0.973 | 0.002 | 0.001 | 0.002 | 0.007 |
| 13.0                       | 0.998  | 0.996 | 0.990 | 0.973 | 0.002 | 0.001 | 0.002 | 0.007 |
| 13.2                       | 0.998  | 0.996 | 0.990 | 0.973 | 0.002 | 0.001 | 0.002 | 0.007 |
| 13.4                       | 0.998  | 0.996 | 0.990 | 0.973 | 0.002 | 0.001 | 0.002 | 0.007 |
| 13.6                       | 0.998  | 0.996 | 0.990 | 0.973 | 0.002 | 0.001 | 0.002 | 0.006 |
| 13.8                       | 0.998  | 0.996 | 0.990 | 0.973 | 0.002 | 0.001 | 0.001 | 0.006 |
| 14.0                       | 0.998  | 0.996 | 0.990 | 0.973 | 0.002 | 0.000 | 0.001 | 0.006 |
| 14.2                       | 0.998  | 0.996 | 0.990 | 0.973 | 0.002 | 0.000 | 0.001 | 0.006 |
| 14.4                       | 0.998  | 0.996 | 0.990 | 0.973 | 0.002 | 0.000 | 0.001 | 0.005 |
| 14.6                       | 0.998  | 0.996 | 0.990 | 0.973 | 0.002 | 0.000 | 0.001 | 0.005 |
| 14.8                       | 0.998  | 0.996 | 0.990 | 0.973 | 0.002 | 0.000 | 0.001 | 0.005 |
| 15.0                       | 0.998  | 0.996 | 0.990 | 0.973 | 0.002 | 0.000 | 0.001 | 0.005 |
| 15.2                       | 0.998  | 0.996 | 0.990 | 0.973 | 0.002 | 0.000 | 0.001 | 0.004 |
| 15.4                       | 0.998  | 0.996 | 0.990 | 0.973 | 0.002 | 0.000 | 0.001 | 0.004 |
| 15.6                       | 0.998  | 0.996 | 0.990 | 0.973 | 0.002 | 0.000 | 0.001 | 0.004 |
| 15.8                       | 0.998  | 0.996 | 0.990 | 0.973 | 0.002 | 0.000 | 0.001 | 0.004 |
| 16.0                       | 0.998  | 0.996 | 0.990 | 0.973 | 0.002 | 0.000 | 0.001 | 0.004 |

The values of  $1-N'$  and  $N''$  are given as a function of  $\log(z=\omega\tau)$  for  $\beta$  values between 0.25 and 0.45.

| $\log(z) \backslash \beta$ | $1-N'$ |       |       |       | $N''$ |       |       |       |
|----------------------------|--------|-------|-------|-------|-------|-------|-------|-------|
|                            | 0.45   | 0.40  | 0.35  | 0.30  | 0.45  | 0.40  | 0.35  | 0.30  |
| -3.0                       | 0.000  | 0.000 | 0.000 | 0.001 | 0.002 | 0.003 | 0.005 | 0.009 |
| -2.8                       | 0.000  | 0.000 | 0.001 | 0.002 | 0.004 | 0.005 | 0.008 | 0.014 |
| -2.6                       | 0.000  | 0.000 | 0.001 | 0.005 | 0.006 | 0.008 | 0.012 | 0.020 |
| -2.4                       | 0.000  | 0.001 | 0.003 | 0.009 | 0.010 | 0.013 | 0.019 | 0.030 |
| -2.2                       | 0.001  | 0.002 | 0.006 | 0.017 | 0.016 | 0.020 | 0.029 | 0.041 |
| -2.0                       | 0.002  | 0.005 | 0.012 | 0.029 | 0.024 | 0.032 | 0.042 | 0.056 |
| -1.8                       | 0.006  | 0.011 | 0.023 | 0.045 | 0.038 | 0.047 | 0.060 | 0.072 |
| -1.6                       | 0.012  | 0.023 | 0.041 | 0.068 | 0.057 | 0.069 | 0.081 | 0.090 |
| -1.4                       | 0.026  | 0.043 | 0.067 | 0.098 | 0.084 | 0.095 | 0.104 | 0.108 |
| -1.2                       | 0.051  | 0.073 | 0.101 | 0.134 | 0.118 | 0.125 | 0.128 | 0.125 |
| -1.0                       | 0.090  | 0.116 | 0.145 | 0.176 | 0.154 | 0.155 | 0.150 | 0.141 |
| -0.8                       | 0.144  | 0.170 | 0.196 | 0.222 | 0.189 | 0.181 | 0.169 | 0.153 |
| -0.6                       | 0.212  | 0.233 | 0.253 | 0.272 | 0.220 | 0.203 | 0.184 | 0.162 |
| -0.4                       | 0.291  | 0.303 | 0.314 | 0.324 | 0.239 | 0.217 | 0.192 | 0.167 |
| -0.2                       | 0.374  | 0.376 | 0.377 | 0.377 | 0.247 | 0.222 | 0.196 | 0.169 |
| 0.0                        | 0.457  | 0.448 | 0.439 | 0.430 | 0.246 | 0.220 | 0.194 | 0.168 |
| 0.2                        | 0.536  | 0.518 | 0.500 | 0.481 | 0.234 | 0.212 | 0.188 | 0.164 |
| 0.4                        | 0.607  | 0.582 | 0.556 | 0.530 | 0.217 | 0.199 | 0.179 | 0.158 |
| 0.6                        | 0.672  | 0.641 | 0.610 | 0.577 | 0.196 | 0.183 | 0.168 | 0.150 |
| 0.8                        | 0.727  | 0.693 | 0.658 | 0.621 | 0.174 | 0.165 | 0.154 | 0.141 |
| 1.0                        | 0.774  | 0.740 | 0.702 | 0.661 | 0.152 | 0.148 | 0.141 | 0.131 |
| 1.2                        | 0.814  | 0.780 | 0.741 | 0.699 | 0.130 | 0.130 | 0.127 | 0.121 |
| 1.4                        | 0.847  | 0.814 | 0.776 | 0.732 | 0.111 | 0.113 | 0.114 | 0.110 |
| 1.6                        | 0.875  | 0.844 | 0.806 | 0.763 | 0.094 | 0.098 | 0.101 | 0.101 |
| 1.8                        | 0.898  | 0.869 | 0.833 | 0.790 | 0.078 | 0.084 | 0.089 | 0.091 |
| 2.0                        | 0.917  | 0.890 | 0.857 | 0.815 | 0.065 | 0.072 | 0.078 | 0.082 |
| 2.2                        | 0.932  | 0.908 | 0.877 | 0.838 | 0.054 | 0.061 | 0.068 | 0.073 |
| 2.4                        | 0.945  | 0.923 | 0.894 | 0.857 | 0.045 | 0.052 | 0.059 | 0.065 |
| 2.6                        | 0.955  | 0.936 | 0.910 | 0.874 | 0.037 | 0.044 | 0.051 | 0.058 |
| 2.8                        | 0.963  | 0.946 | 0.923 | 0.890 | 0.030 | 0.037 | 0.045 | 0.052 |
| 3.0                        | 0.970  | 0.955 | 0.934 | 0.904 | 0.025 | 0.031 | 0.039 | 0.046 |
| 3.2                        | 0.976  | 0.963 | 0.944 | 0.916 | 0.020 | 0.026 | 0.033 | 0.040 |
| 3.4                        | 0.980  | 0.969 | 0.952 | 0.926 | 0.016 | 0.022 | 0.028 | 0.035 |
| 3.6                        | 0.984  | 0.974 | 0.958 | 0.935 | 0.013 | 0.018 | 0.024 | 0.031 |
| 3.8                        | 0.987  | 0.978 | 0.964 | 0.943 | 0.011 | 0.016 | 0.021 | 0.028 |
| 4.0                        | 0.989  | 0.982 | 0.970 | 0.951 | 0.009 | 0.013 | 0.019 | 0.025 |
| 4.2                        | 0.989  | 0.982 | 0.970 | 0.951 | 0.009 | 0.013 | 0.019 | 0.021 |

The values of  $1-N'$  and  $N''$  are given as a function of  $\log(z=wr)$  for  $\beta$  values between 0.25 and 0.45 (continued).

| $\log(z) \backslash \beta$ | $1-N'$ |       |       |       | $N''$ |       |       |       |
|----------------------------|--------|-------|-------|-------|-------|-------|-------|-------|
|                            | 0.45   | 0.40  | 0.35  | 0.30  | 0.45  | 0.40  | 0.35  | 0.30  |
| 4.4                        | 0.989  | 0.982 | 0.970 | 0.951 | 0.009 | 0.013 | 0.019 | 0.019 |
| 4.6                        | 0.989  | 0.982 | 0.970 | 0.951 | 0.009 | 0.013 | 0.019 | 0.016 |
| 4.8                        | 0.989  | 0.982 | 0.970 | 0.951 | 0.009 | 0.013 | 0.019 | 0.014 |
| 5.0                        | 0.989  | 0.982 | 0.970 | 0.951 | 0.009 | 0.013 | 0.019 | 0.013 |
| 5.2                        | 0.989  | 0.982 | 0.970 | 0.951 | 0.009 | 0.013 | 0.019 | 0.011 |
| 5.4                        | 0.989  | 0.982 | 0.970 | 0.951 | 0.009 | 0.013 | 0.019 | 0.010 |
| 5.6                        | 0.989  | 0.982 | 0.970 | 0.951 | 0.009 | 0.013 | 0.019 | 0.008 |
| 5.8                        | 0.989  | 0.982 | 0.970 | 0.951 | 0.009 | 0.013 | 0.019 | 0.007 |
| 6.0                        | 0.989  | 0.982 | 0.970 | 0.951 | 0.009 | 0.013 | 0.019 | 0.006 |
| 6.2                        | 0.989  | 0.982 | 0.970 | 0.951 | 0.009 | 0.013 | 0.019 | 0.006 |
| 6.4                        | 0.989  | 0.982 | 0.970 | 0.951 | 0.009 | 0.013 | 0.019 | 0.005 |
| 6.6                        | 0.989  | 0.982 | 0.970 | 0.951 | 0.009 | 0.013 | 0.019 | 0.004 |
| 6.8                        | 0.989  | 0.982 | 0.970 | 0.951 | 0.009 | 0.013 | 0.019 | 0.004 |
| 7.0                        | 0.989  | 0.982 | 0.970 | 0.951 | 0.009 | 0.013 | 0.019 | 0.003 |
| 7.2                        | 0.989  | 0.982 | 0.970 | 0.951 | 0.009 | 0.013 | 0.019 | 0.003 |
| 7.4                        | 0.989  | 0.982 | 0.970 | 0.951 | 0.009 | 0.013 | 0.019 | 0.002 |
| 7.6                        | 0.989  | 0.982 | 0.970 | 0.951 | 0.009 | 0.013 | 0.019 | 0.002 |
| 7.8                        | 0.989  | 0.982 | 0.970 | 0.951 | 0.009 | 0.013 | 0.019 | 0.002 |
| 8.0                        | 0.989  | 0.982 | 0.970 | 0.951 | 0.009 | 0.013 | 0.019 | 0.002 |
| 8.2                        | 0.989  | 0.982 | 0.970 | 0.951 | 0.009 | 0.013 | 0.019 | 0.001 |
| 8.4                        | 0.989  | 0.982 | 0.970 | 0.951 | 0.009 | 0.013 | 0.019 | 0.001 |
| 8.6                        | 0.989  | 0.982 | 0.970 | 0.951 | 0.009 | 0.013 | 0.019 | 0.001 |
| 8.8                        | 0.989  | 0.982 | 0.970 | 0.951 | 0.009 | 0.013 | 0.019 | 0.001 |
| 9.0                        | 0.989  | 0.982 | 0.970 | 0.951 | 0.009 | 0.013 | 0.019 | 0.001 |

## BIBLIOGRAPHY

- Acitelli, M.A., Prime, R.B. and Sacher, E., 1971, *Polymer* **12**, 335.
- Aherne, J.P., Enns, J.B., Doyle, M.J. and Gillham, J.K., 1982, *Am. Chem. Soc. Div. Org. Coat. Plast. Chem. Prepr.* **46**, 574.
- Anderson, P.W., 1986, *Ann. N.Y. Acad. Sci.* **484**, 288.
- Angell, C.A., 1986, *Solid State Ionics* **18/19**, 72.
- Aronhime, M.T., Gillham, J.K., 1986, *Adv. Polym. Sci.* **78**, 83.
- Barton, J.M., 1973, *Makrom. Chem.* **171**, 247.
- Barton, J.M., 1980, *Polymer* **21**, 603.
- Barton, J.M., 1985, *Adv. Polym. Sci.* **72**, 111.
- Bidstrup, S.A., Sheppard, Jr., N.F. and Senturia, S.D., 1989, *Polym. Eng. Sci.* **29**, 325.
- Blyakhman, Y.H., Borisova, T.I. and Levitskaya, T.M., 1970 (a), *Polym. Sci. USSR* **12**, 1756.
- Blyakhman, Y.H., Borisova, T.I. and Levitskaya, T.M., 1970 (b), *Polym. Sci. USSR* **12**, 2602.
- Bockris, J.O'M., Reddy, A.K.N., 1970, *Modern electrochemistry*, Volume 1, Section 4.4, NY, Plenum Press.
- Boese, D., Meier, G., Kremer, F., Hagenah, J.-U. and Fischer, E.W., 1989, *Macromolecules* **22**, 4416.
- Borjesson, L., Martin, S.W., Torell, L.M. and Angell, C.A., 1986, *Solid State Ionics* **18/19**, 141 and 431.
- Byrne, C.A., Hagnauer, G.L., Schneider, N.S. and Lenz, R.W., 1980, *Polymer Composites* **1**, 71.

- Cavaill , J.-Y., Johari, G.P. and Mikolajczak, G., 1987, *Polymer* **28**, 1841.
- Cavaill , J.-Y., Perez, J. and Johari, G.P., 1989, *Phys. Rev.* **B39**, 2411.
- Chai, C.K. and McCrum, N.G., 1980, *Polymer* **21**, 706.
- Chan, L.C., Nae, H.N. and Gillham, J.K., 1984, *J. Appl. Polym. Sci.* **29**, 3307.
- Chern, C.-S. and Poehlein, G.W., 1987, *Polym. Eng. Sci.* **27**, 788.
- Choy, I.-C. and Plazek, D.J., 1986, *J. Polym. Sci: Polym. Phys. Edn.* **24**, 1303.
- Coates, A.W. and Redfern, J.P., 1964, *Nature* **201**, 68.
- Cole, K.S. and Cole, R.H., 1941, *J. Chem. Phys.* **9**, 341.
- Cole, R.H. and Gross, P.M., 1949, *Rev. Sci. Instr.* **20**, 252.
- Cole, R.H., 1989, private communication.
- Curie, P.J., 1888, *Annales de Chimie Physique* **17**, 385.
- Dannenberg, H., 1959, *SPE J.*, 875.
- Davidson, D.W., and Cole, R.H., 1950, *J. Chem. Phys.* **18**, 1417.
- Davidson, D.W., and Cole, R.H., 1951, *J. Chem. Phys.* **19**, 1484.
- Davidson, D.W., 1961, *Canadian Journal of Chemistry* **39**, 571.
- Day, D.R., 1986, *Polym. Eng. Sci.* **26** 362.
- Debye, P., 1929, Polar molecules, Chem. Catalog., NY.
- De Genne, P.G., *J. Phys. (Paris)* **37**, L1.
- Delmonte, J., 1959, *J. Appl. Polym. Sci.* **2**, 108.
- Diaz-Calleja, R., Ribes-Greus, A. and Gomez-Ribelles, J.L., 1989, *Polymer* **30**, 1433.

- Dishon, M., Weiss, G.H., and Bendler, J.T., 1985, J. Res. Natl. Bur. Stand. **90**, 27.
- Dobas, I., Eichler, J. and Klaban, J., 1975, Coll. Czechos. Chem. Commum. **40**, 2989.
- Doi, A., 1988, Solid State Ionics **31**, 227.
- Doyle, C.D., 1961, J. Appl. Polym. Sci. **5**, 285.
- Dusek, K., and Bleha, M., 1977, J. Polym. Sci: Polym. Chem. Ed. **15**, 2393.
- Dusek, K., 1985, Adv. Polym. Sci. **78**, 1.
- Dusi, M.R., May, C.A. and Seferis, J.C., 1983, in Chemorheology of Thermosetting Polymers (May, C.A., Ed.), ACS Symp. ser. **227**, 301.
- Elliott, S.R. and Owens, A.P., 1989, Phil. Mag. B **60**, 777.
- Enns, J.B. and Gillham, J.K., 1983(a), in Polymer Characterization, Spectroscopy, Chromatographic and Physical Instrumental Methods, (Craver, C.D., Ed.), Adv. in Chem. series **203**, 27.
- Enns, J.B. and Gillham, J.K., 1983(b), J. Appl. Polym. Sci. **28**, 2567.
- Fava, R.A. and Horsfield, A.E., 1968, Brit. J. Appl. Phys. series 2, **1**, 117.
- Feller, W., 1966, in An Introduction to Probability Theory and its Applications, vol. II, Wiley, N.Y.
- Ferry, J.D., 1980, Viscoelastic Properties of Polymers, J. Wiley & Sons, NY, Third Edn.
- Frohlich, H., 1949, Theory of dielectrics, Oxford University Press, Oxford.

- Gillham, J.K., 1986, *Polym. Eng. Sci.* **26**, 1429.
- Gotro, J. and Yandrasits, M., 1989, *Polym. Eng. Sci.* **29**, 278.
- Grant, R.J., Hodge, I.M., Ingram, M.D. and West, A.R., 1977, *Nature* **266**, 42.
- Hamon, B.V., 1952, *Proc. IEEE* **99** pt. II, 291.
- Haran, E.N., Gringras, H. and Katz, D., 1965, *J. Appl. Polym. Sci.* **9**, 3505.
- Harran, D. and Laudouard, A., 1985, *Rheol. Acta* **24**, 596.
- Harran, D. and Laudouard, A., 1986, *J. Appl. Polym. Sci.* **32**, 6043.
- Harran, D., Grenier-Loustalot, M.F. and Monge, P., 1988, *Eur. Polym. J.* **24**, 225.
- Havriliak, S. and Negami, S., 1966, *J. Polym. Sci.: part C* **14**, 99.
- Hodge, I.M., Ingram, M.D. and West, A.R., 1975, *Electroanal. Chem. Interfac. Electrochem.* **58**, 429.
- Hodge, I.M., Ingram, M.D. and West, A.R., 1976, *J. Electroanal. Chem.* **74**, 125.
- Hodge, I.M. and Angell, C.A., 1978, *J. Phys. Chem.* **82**, 1761.
- Hopkinson, J., 1877, *Phil. Trans. Roy. Soc.* **167**, 599.
- Hu, Z., 1988, Spectroscopy of Disordered Materials, Ph.D. Thesis, McMaster University.
- Huguenin, F.G.A.E. and Klein, M.T., 1985, *Ind. Eng. Chem. Prod. Res. Dev.* **24**, 166.
- Huraux, C. and Sellaimia, A., 1973, *Compte Rendu de l'Academie des Sciences de Paris* **227B**, 497 and 691.
- Johari, G.P. and Dannhauser, W., 1969, *J. Chem. Phys.* **50**, 1862.

- Johari, G.P. and Goldstein, M., 1970, J. Chem. Phys. **53**, 2372.
- Johari, G.P. and Smyth, C.P., 1972, J. Chem. Phys. **56**, 4411.
- Johari, G.P., 1973, J. Chem. Phys. **58**, 1766.
- Johari, G.P., 1982(a), J. Chem. Phys. **77**, 4619.
- Johari, G.P., 1982(b), in Plastic Deformation in Amorphous and Semicrystalline Materials, Les Editions de Physique, Les Ulis, France. Les Houches Lectures, p. 109.
- Johari, G.P., 1985, J. Chim. Physique (Fr.) **82**, 282.
- Johari, G.P., 1986, Polymer **27**, 866.
- Johari, G.P., 1987, in Molecular Dynamics and Relaxation Phenomena in Glasses, Dorfmueller, T., and Williams, G., Eds., Springer-Verlag, Heidelberg, Lecture Notes on Physics, p. 90.
- Johari, G.P. and Pathmanathan, K., 1988, Phys. Chem. Glasses **29**, 219.
- Kaiser, T., 1989, Prog. Polym. Sci. **14**, 373.
- Keenan, J.D., Seferis, J.C. and Quinlivan, J.T., 1979, J. Appl. Polym. Sci. **24**, 2375.
- Kirkwood, J.G., 1939, J. Chem. Phys. **7**, 911.
- Kohlrausch, R., 1854, Ann. Phys. (leipzig) **91**, 179.
- Kranbuehl, D.E., Delos, S., Yi, E., Mayer, J., Hou. T. and Winfree, W., 1985, Proceedings of the 30th SAMPE Symposium, p. 638.
- Kranbuehl, D.E., Delos, S., Hoff. M., Haverty, P., Freeman, W., Hoffman, R. and Godfrey, J., 1989, Polym. Eng. Sci. **29**, 285.
- Lane, J.W. and Seferis, J.C., 1986, Polym. Eng. Sci. **26**, 346.

- Lane, J.W., Seferis, J.C. and Bachmann, M.A., 1986, *J. Appl. Polym. Sci.* **31**, 1155.
- Lane, J.W., Khattak, R.K. and Dusi, M.R., 1989, *Polym. Eng. Sci.* **29**, 339.
- Lawless, G.W., 1980, *Polym. Eng. Sci.* **20**, 546.
- LeMay, J.D., Swetlin, B.J. and Kelley, F.N., 1984, in Characterization of highly cross-linked polymers. Am. Chem. Soc. Symp. Series **243**, Labana, S.S. and Dickie, R.S. Eds., Am. Chem. Soc., Washington DC, p. 65.
- LeMay, J.D. and Kelley, F.N., 1986, *Adv. Polym. Sci.* **78**, 115.
- Levy, P., 1937, Théorie de L'addition des Variables Aléatoires. Gauthier-Villars, Paris.
- Lindsey, C.P. and Patterson, G.D., 1980, *J. Chem. Phys.* **73**, 3348.
- Lipshitz, S.D. and Mascoko, C.W., 1976, *Polym. Eng. Sci.* **16**, 803.
- Liu, C. and Angell, C.A., 1986, *J. Non-Cryst. Sol.* **83**, 162.
- Liu, C., Sundar, H.G.K. and Angell, C.A., 1986, *Solid State Ionics*, **18/19**, 442.
- Lynch, A.C., 1957, *Proc. Inst. Elec. Engrs. (London)* **104**, pt B. 363.
- Macedo, P.B., Moynihan, C.T. and Bose, R., 1972, *Phys. Chem. Glasses* **13**, 171.
- Mai, C., Asseiro, A., Johari, G.P., Etienne, S. and Abbas, K., 1987, *J. Non-Cryst. Solids* **93**, 35.
- Mai, C., Poulain, M., Asseiro, A.M. and Johari, G.P., 1989, *J. Non-Cryst. Solids* **113**, 94.

- Mangion, M.B.M., 1987, Fast-ionic Conduction in Silver Iodide-Silver Phosphate Glasses. M.Sc. Thesis, McMaster University.
- Mangion, M.B.M., and Johari, G.P., 1988, Phys. Chem. Glasses **29**, 225.
- Mangion, M.B.M. and Johari, G.P., 1990, J. Polym. Sci: Polym. Phys. Ed. **28**, 71.
- Mangion, M.B.M. and Johari, G.P., 1990, J. Polym. Sci: Polym. Phys. Ed. in press.
- Mangion, M.B.M. and Johari, G.P., 1990 Macromolecules, in press.
- Maxwell, J.C., 1867, Philos. Trans. R. Soc. (London) **157**, 52.
- McCrum, N.G., Read, B.E. and Williams, G., 1967, Anelastic and Dielectric effects in Polymeric Solids, Wiley.
- Mijovic, J. and Lee, C.H., 1990, J. Appl. Polym. Sci. **38**, 2155.
- Mikolajczak, C., Cavaille, J.-Y. and Johari, G.P., 1987, Polymer **28**, 2023.
- Montroll, E.W. and Bendler, J.T., 1984, J. Stat. Phys. **34**, 129.
- Moynihan, C.T., Boesch, L.P. and Laberge, N.L., 1973, Phys. Chem. Glasses **14**, 122.
- Nass, K.A. and Seferis, J.C., 1989, Polym. Eng. Sci. **29**, 315.
- Ochi, M., Okazaki, M. and Shimbo, M., 1982, J. Polym. Sci: Polym. Phys. Ed. **20**, 689.
- Ochi, M., Shimbo, M., Saga, M. and Takashima, N., 1986, J. Polym. Sci.: Polym. Phys. Ed. **24**, 2185.
- Ochi, M., Yoshizumi, M. and Shimbo, M., 1987, J. Polym. Sci.: Polym. Phys. Ed. **25**, 1817.

- Oleinik, E.F., 1985, *Adv. Polym. Sci.* **80**, 49.
- Onsager, L., 1936, *J. Am. Chem. Soc.* **58**, 1486.
- Ozawa, T., 1965, *Bull. Chem. Soc. Jpn.* **38**, 1881.
- Pascault, J.P. and Williams, R.J.J., 1990, *J. Polym. Sci.: Polym. Phys. Ed.* **28**, 85.
- Pathmanathan, K. and Johari, G.P., 1988, *Polymer* **29**, 303.
- Pathmanathan, K., Cavaille, J.-Y. and Johari, G.P., 1989, *J. Polym. Sci.: Polym. Phys. Ed.* **27**, 1519.
- Pathmanathan, K. and Johari, G.P., 1990 *Phil. Mag. B*, in press.
- Patterson, G.D., 1980, *CRC Crit. Rev. Solid State Mater. Sci.* **9**, 373.
- Peng, X. and Gillham, J.K., 1985, *J. Appl. Polym. Sci.*, **30**, 4685.
- Plazek, D.J., O'Rourke, V.M., and Choy, I.-C., 1981, Air Force Office of Scientific Research Contract F49620-83-0032 Report.
- Plazek, D.J. and Frund, Jr., J., 1990. *J. Polym. Sci.: Polym. Phys. Ed.*, **28**, 431.
- Prime, R.B., 1981, in Thermal Characterization of Polymeric Materials (Turi, E.A., Ed.). Academic Press, New York, p.435.
- Riew, C.K. and Gillham, J.K., Eds, 1985, Rubber-Modified Thermoset Resins, Adv. Chem. Ser. n°208, ACS, Washington, DC.
- Roller, M.B., 1986, *Poly. Eng. Sci.* **26**, 432.

- Sandercock, J.R., 1982, in Light Scattering in Solids III, M. Gardonna and G. Guntherodt Eds., Springer-Verlag, Berlin, p. 173.
- Senturia, S.D. and Sheppard, Jr., N.F., 1986, *Adv. Polym. Sci.* **80**, 1.
- Shechter, L., Wynstra, J. and Kurkjy, R.P., 1956, *Ind. Eng. Chem.* **48**, 94.
- Sheldon, R.P., 1982, Composite Polymeric Materials, Appl. Sci. Publishers, England.
- Sheppard, Jr., N.F., Garverick, S.L., Day, D.R. and Senturia, S.D., 1981, *Proceedings of the 26th SAMPE Symposium*, p. 65.
- Sheppard, Jr., N.F., Coln. M.C.W. and Senturia, S.D., 1984, *Proceedings of the 29th SAMPE Symposium*, p.1243.
- Sheppard, Jr., N.F., Senturia, S.D., 1985, *SPE Tech. Papers* **31**, 321.
- Sheppard, Jr., N.F., Senturia, S.D., 1986, *Polym. Eng. Sci.* **26**, 354.
- Shimbo, M., Ochi, M. and Iesako, M., 1984, *J. Polym. Sci.: Polym. Phys. Ed.* **22**, 1461.
- Sidebottom, D.L. and Johari, G.P., submitted, *J. Phys. Chem.*
- Smyth, C.P., 1955, Dielectric Behaviour and Structure, McGraw-Hill, NY.
- Soualmia, A., Huraux, C., Leaux, B., 1982, *Makromol. Chem.* **183**, 1803.
- Sourour, S. and Kamal, M.R., 1976, *Thermochimica Acta* **14**, 41.
- Stauffer, D., 1976. *J. Chem. Soc. Faraday Trans. II* **72**, 1354.

- Stauffer, D., Coniglio A. and Adam, M., 1982, *Adv. Polym. Sci.* **44**, 103.
- Struik, L.C.E., 1978, Physical Ageing in Amorphous Polymers and other Materials, Elsevier Amsterdam.
- Struik, L.C.E., 1987, *Polymer* **28**, 57.
- Sundstrom, D.W. and Burkert, S.J., 1981, *Polym. Eng. Sci.* **21**, 1108.
- Tajima, Y.A. and Crozier, D., 1983, *Polym. Eng. Sci.* **23**, 186.
- Thompson, A.M., 1956, *Proc. Inst. Elec. Engrs. (London)* **103**, pt. B, 704.
- Vanderwal, J., Mudare, S.M. and Walton, D., 1981, *Opt. Commun.* **37**, 33.
- Wagner, K.W., 1913, *Ann. der Physik* **40**, 817.
- Weiss, G.H., Bendler, J.T. and Dishon, M. 1985, *J. Chem. Phys.* **83**, 1424.
- Whitehead, J.B. and Banos, A., 1932, *Trans. AIEE* **51**, 392.
- Williams, G. and Watts, D.C., 1970, *Trans. Faraday Society* **66**, 80.
- Williams, C., 1984, in Molecular Liquids, Dynamics and Interactions, Barnes, A.J., Orville-Thomas, W.J., and Yarwood, J., Eds., Dordrecht:Reidel, p. 239.
- Williams, R.J.J., 1985, in Development in Plastics Technology, Vol. 2 (Whelan, A. and Craft, J.L., Eds.), Elsevier, London, p.339.
- Yager, W.A., 1936, *Physics* **7**, 434.